Characterizing soil organic nitrogen using advanced molecular analytical techniques

A Dissertation Submitted to the College of Graduate Studies and Research in Partial Fulfillment of the Requirements for the Degree of

Doctor of Philosophy

in the

Department of Soil Science

University of Saskatchewan

Saskatoon, Saskatchewan, Canada

by

Adam Gillespie

Permission to Use

In presenting this thesis in partial fulfillment of the requirements for a Postgraduate degree from the University of Saskatchewan, I agree that the Libraries of this University may make it freely available for inspection. I further agree that permission for copying of this thesis in any manner, in whole or in part, for scholarly purposes may be granted by the professor or professors who supervised my thesis work or, in their absence, by the Head of the Department or the Dean of the College in which my thesis work was done. It is understood that any copying, publication, or use of this thesis or parts thereof for financial gain shall not be allowed without my written permission. It is also understood that due recognition shall be given to me and to the University of Saskatchewan in any scholarly use which may be made of any material in my thesis. Requests for permission to copy or to make other use of material in this thesis in whole or part should be addressed to:

Head of the Department of Soil Science
51 Campus Dr.
University of Saskatchewan
Saskatoon, Saskatchewan
Canada, S7N 5A8

Abstract

Soil organic N (SON) comprises 90% of all N in surface soils, yet as much as half remains in forms which are chemically unknown or, at best, poorly understood. Analytical methods such has pyrolysis field-ionization mass spectrometry (Py-FIMS) and ^{15}N cross polarization magic-angle spinning nuclear magnetic resonance (CPMAS-NMR) spectroscopy are widely used for the characterization of SON; however, these methods have limitations which contribute to the gaps in our understanding of SON chemistry. For example, Py-FIMS may produce heat-induced secondary compounds, and ^{15}N-NMR may lack sensitivity and resolution for experiments at natural ^{15}N abundance. X-ray absorption near edge structure (XANES) spectroscopy probes the bonding environment of individual elements. The application of this technique to complex environmental samples such as soil is still in its infancy, but early studies suggest that this technique may help resolve SON molecular structure. This dissertation sought to develop and apply synchrotron-based N and C K-edge XANES spectroscopy to the study of soil and soil extracts to determine the structures in which SON is bound. In these studies, Py-FIMS was coupled with XANES as a corroboratory technique.

Initial methodological development resulted in a calibration method whereby N_2 gas generated in ammonium-containing salts was used to calibrate a soft X-ray beamline at the N K-edge. Although XANES can produce secondary compound artifacts, contrary to early assertions that it is a non-destructive technique, it was shown in a second study that beam-induced decomposition can be minimized by moving the beam to a fresh spot between scans.

Three applied studies exploring SON composition were conducted. These studies followed a spatial gradient ranging from the landscape scale, through a rhizosphere study, and ended with a study of glomalin-related soil protein (GRSP). Glomalin-related soil protein is a persistent soil glycoprotein of arbuscular

mycorrhizal origin (AMF) implicated in aggregation and long-term C and N storage. Nitrogen and C K-edge XANES and Py-FIMS were used in all studies, and GRSP was further characterized using proteomics techniques.

Soil organic N composition was largely controlled by topographic position, and to a lesser degree, by cultivation. Divergent (i.e., water shedding) positions were enriched in carbohydrates and low molecular weight lignins, whereas convergent, depressional and level positions showed enrichment in lipid-type compounds. These differences were attributed to tillage-induced redistribution of soil, and water movement from upper to lower slope positions. Nitrogen XANES revealed a unique form of organic N, identified as N-bonded aromatics, particularly in the divergent positions.

Rhizosphere soil was enriched in higher molecular weight lipid-type materials and depleted in low molecular weight polar compounds. This was attributed to increased input of fresh plant material and higher microbial turnover in the rhizosphere. Nitrogen-bonded aromatics also were detected in the rhizosphere.

The GRSP extracts were characterized as mostly proteinaceous, but also contained many co-extracted, non-protein compounds. Despite being previously described as a glycoprotein, only weak carbohydrate signals were observed. Proteomics-based assessment of GRSP showed no homology to any proteins of AMF origin, instead showing homology with thioredoxin and with heat-stable soil proteins. This may be because protein databases do not yet contain glomalin-related sequences, or that glomalin is homologous to non-AMF soil proteins.

This dissertation demonstrated that N XANES is a sensitive and novel method for characterizing SON, and can be used complementarily with other analytical techniques such as Py-FIMS and proteomics. The continued development of XANES will provide a useful tool for SOM research into the future.

Acknowledgements

This entire process would not have been possible without the support of my wife, Karène Paquin. Lorsque je serai vieux et que tu seras vieille, Lorsque mes cheveux blonds seront des cheveux blancs, Au mois de mai, dans le jardin qui s'ensoleille, Nous irons réchauffer nos vieux membres tremblants.

Deepest gratitude to my supervisors Drs. Fran Walley and Richard Farrell for providing the opportunity to work on this project, for their financial support, and for their guidance throughout my Ph.D. I would also like to thank my supervisory committee, Drs. Diane Knight, Derek Peak, Andrew Ross, Robert Blyth and Jim Germida for their advice and counsel throughout this project. Thanks also to Dr. Daniel Olk for his contributions as an external examiner.

I would like to thank Tom Regier (Canadian Light Source Inc.) for all his contributions with the synchrotron work. Also thanks to Steve Ambrose, Uma Aryal, Doug Olsen and Randy Purves (NRC-Plant Biology Institute) for their expertise, facilities and participation in the proteomics analyses. Many thanks to Peter Leinweber, Kai-Uwe Eckhardt, Gerald Jandl, Jens Kruse, André Schlichting and Rolf Beese at Universität Rostock Institute for Land Use in Germany for Py-FIMS work and for their partnership throughout this journey into the world of XANES. I'm grateful for all the assistance in the lab and the friendships throughout this ordeal, Christian, Melissa, Holly, Lori, Ailsa, Darin, Mark and Bobbi, and to all those willing to spend time on the beamline.

This work was supported by the Natural Sciences and Engineering Research Council (NSERC) and industrial and government partners, through the Green Crop Networks (GCN)

Research Network. XANES analyses were performed at the Canadian Light Source facility, a national scientific user facility supported by the Natural Sciences and Engineering Research Council, National Research Council, the Canadian Institutions of Health Research and other federal government agencies. I also acknowledge financial support through the College of Agriculture Deans Scholarship, support for travel to Germany through the College of Agriculture Education Enhancement Fund and through the German Academic Exchange Service (DAAD - Deutscher Akademischer Austausch Dienst).

Contents

List of Tables

List of Figures

List of Abbreviations

ACN	Acetonitrile
Ambic	Ammonium bicarbonate
AMF	Arbuscular mycorrhizal fungi
BLAST	Basic Local Alignment Search Tool
CP-MAS	Cross polarization-magic angle spinning
CLS	Canadian Light Source
DOM	Dissolved organic matter
DTT	Dithiothreitol
ELISA	Enzyme-linked immunosorbent assay
ESCA	Electron spectroscopy for chemical analysis
FLY	Fluorescence yield
Gly	Glycine
Gly-Gly	Glycyl-glycine
GRSP	Glomalin-related soil protein
Met	Methionine
Met-Met	Methionyl-methionine
m/z	mass:charge
NEXAFS	Near-edge x-ray absorption fine structure
NMR	Nuclear magnetic resonance
NMS	Non-metric multidimensional scaling
PAGE	Polyacrylamide gel electrophoresis
PHP	Pyroglutamyl-histidyl-proline amide
Py-FIMS	Pyrolysis field ionization mass spectrometry
SDS-PAGE	Sodium dodecyl sulphate-polyacrylamide gel electrophoresis
SGM	Spherical grating monochromator
SOC	Soil organic carbon
SOM	Soil organic matter
SON	Soil organic mitrogen
SPIDER	Saturation-pulse induced dipolar exchange with recoupling
STXM	Scanning transmission X-ray microscopy
TEY	Total electron yield
TII	Total ion intensity
XANES	X-ray absorption near edge structure
XAS	X-ray absorption spectroscopy
XPS	X-ray photoelectron spectroscopy

Chapter 1

Introduction

Organically bound N comprises more than 90% of the N in most surface soils (Bremner, 1965; Stevenson, 1982; Olk, 2008b). These compounds are both a source and sink for N in the global N cycle, providing substrates for microbial formation of mineral N (NH_4^+ and NO_3^-). While essential for plant production, excess N application leads to environmental problems including groundwater contamination, acidic deposition, and production of N_2O, a potent greenhouse gas (Vitousek et al., 1997; Galloway and Cowling, 2002; Galloway et al., 2003; Schindler et al., 2006; Robertson and Vitousek, 2009). Despite decades of research, 30-50% of the soil organic N pool remains in chemical forms which are unknown, or at best are only poorly understood, indicating an enormous gap in the knowledge base (Stevenson, 1982; Olk, 2008b). Undoubtedly, identifying the chemical forms of this 'unknown N' will be essential to achieving a better understanding of N-cycling and storage.

There is wide consensus that amide and peptide N predominate in soil organic matter, whereas estimates on the types and amounts of heterocyclic-N are contested (Olk, 2008b). Controversy surrounding the understanding of soil organic N chemistry arises from conflicting data provided by a diverse range of analytical techniques. Among the various analytical approaches used are wet chemical acid hydrolysis (Stevenson, 1982), pyrolysis-mass-spectrometry (Py-MS) (Schulten and Schnitzer, 1998), and ^{15}N-CPMAS NMR (Preston, 1996a). While each technique has advanced our understanding of SON composition, each also has been fundamentally criticized. Firstly, there are uncertainties surrounding the effectiveness and

products released through acid hydrolysis (Stevenson, 1982, 1994). Secondly, there is evidence for the formation of secondary compounds from pyrolysis heating (Knicker et al., 2005; Olk, 2008b). Finally, poor sensitivity toward lower abundant forms of organic N using ^{15}N-NMR has been demonstrated (Smernik and Baldock, 2005; Olk, 2008b).

Synchrotron-based X-ray absorption near-edge structure (XANES) spectroscopy is a promising technique which offers an isotope-independent, purportedly non-destructive (Myneni, 2002; Vairavamurthy and Wang, 2002) assessment of SON chemistry in whole field soils (Leinweber et al., 2007). X-ray absorption spectroscopy provides information on the binding chemistry of compounds by probing the electronic structure (Stöhr, 1992). Each element absorbs X-rays at unique energies, which allows chemical analyses of specific elements in complex media, rendering this technique especially valuable for environmental samples (Myneni, 2002). For soil organic matter, probing at the N and C K-edges is most relevant, and these techniques have been applied in this dissertation.

Proteomics is a technique which specifically characterizes proteins (Bastida et al., 2009). Although SON is dominated by protein-N, very little is known about the proteins themselves. One candidate for study is glomalin, a purportedly widespread glycoprotein of AMF origin which is highly persistent and may be an important long-term pool of organic C and N sequestration (Wright et al., 1996; Treseder and Turner, 2007). This protein is operationally defined (as glomalin-related soil protein - GRSP) through an autoclaving extraction and AMF-specific immunoreactive assay (Wright et al., 1996; Wright and Upadhyaya, 1996), and has not as yet been conclusively identified or characterized.

The overall goal of this PhD dissertation project was to use synchrotron-based XANES techniques and mass-spectrometric-based proteomics in conjunction with established pyrolysis field-ionization mass-spectrometry (Py-FIMS) to determine the structures in which organic nitrogen is bound. The project is focused on developing, and applying these techniques to whole soil samples and soil fractions and exploring how SOM structures are affected by landscape, rhizosphere processes and extraction techniques.

This dissertation is structured in nine chapters. Following an introduction (Chapter 1) and a literature review (Chapter 2), are two studies addressing methodological questions. Chapter 3 presents a simple method of calibrating a soft X-ray beamline at the N K-edge using N_2 gas released by beam-induced decomposition of ammonium-containing salts. Chapter 4 presents a study using X-ray photoelectron spectroscopy (XPS) to providing a time series assessment of amino acid and peptide degradation under the X-ray beam.

The three next chapters describe experiments characterizing whole soils and soil extracts using XANES, Py-FIMS and proteomics. The sequence of chapters follows a spatial gradient starting at the field scale, moving to the rhizosphere scale, and ending with an assessment of an operationally extracted pool. Chapter 5 demonstrates a study where XANES and Py-FIMS were used to explore the impact of topography on the organic N and C chemistry in whole soils. Chapter 6 applies XANES and Py-FIMS at a finer scale, investigating the complexities of organic N and C in the rhizosphere of *Pisum sativum*. Chapter 7 focuses on the characterization of GRSP using XANES, Py-FIMS, and proteomics. This study investigated the bulk chemistry of the operationally-defined GRSP extract, and attempts to characterize the protein(s) within GRSP.

Over the course of this research, there was substantial progress in the development and refinement of XANES data collection and handling. This included ongoing beamline improvements, and methods of handling of XANES data. Most notable were improvements in the handling of C K-edge data, where refinement of normalization procedures improved through the course of the program of study. Chapters in this dissertation were arranged according to content rather than strict chronology. Chapter 6 (rhizosphere study) was written, and published, before Chapters 5 and 7 (landscape and glomalin studies); thus, to follow the improvement in spectral quality and data handling that evolved over the course of this dissertation project, the reader should view the spectra in the order Chapters 6, 5 and 7.

The dissertation ends with a synthesis, overall conclusion, critical evaluation of methods and directions for future research (Chapter 8), and a list of references (Chapter 9).

Chapter 2

Literature Review

2.1 Importance of nitrogen in the biosphere

Nitrogen is essential for plant growth, but is often the most limiting nutrient. Nitrogen is abundant, with dinitrogen gas (N_2) comprising 78% of the atmosphere. However, the triple-bonded N_2 is essentially inert, and biologically unavailable to most organisms. The biosphere thus exists in an environment of available nitrogen scarcity, because molecular N_2 first must be cleaved and fixed into reactive forms before incorporation into living biomass (Stevenson and Cole, 1999; Smil, 2001; Voroney and Derry, 2008). The entry of N into the biosphere is through the process of dinitrogen fixation, where N_2 from the atmosphere is converted to ammonia by the nitrogenase enzyme found in some prokaryotic organisms. Indeed, biological N fixation by free-living organisms and through the legume-rhizobium symbiosis was the main input of fixed N into the biosphere until the development of chemical fertilizer (Posgate, 1998; Voroney and Derry, 2008; Fani and Fondi, 2009). Farmers in preindustrial times realized the benefits of cultivating legumes and have included N_2-fixing pulses in rotation with cereals and other crops since the earliest agrarian civilizations (Smil, 2001). Post-industrially, farming and indeed, humanity, have undergone rapid and fundamental changes with the discovery of the Haber-Bosch process, where atmospheric N is fixed at industrial scales into ammonia by combining $N_2(g)$ with $H_2(g)$ at high temperatures and pressures:

$$N_2(g) + 3H_2(g) \rightleftharpoons 2NH_3(g) \textit{ magnetite catalyst } (\Delta H = \text{-}92.4 \text{ kJ}\cdot\text{mol}^{-1})$$

The first industrial ammonia plant was built in Germany in 1910 (Aldrich, 1980) marking the beginning of the modern fertilizer industry and of modern fertilizer-based agriculture. Since that time, it is estimated that humanity has doubled the amount of fixed N in the terrestrial ecosystem (Vitousek et al., 1997), and that approximately 40% of all people alive today have derived their N nutrition from the Haber-Bosch process (Crews and Peoples, 2004).

The ability for humanity to fix N provided a more secure food supply for a growing population and allowed societies to diversify away from farming. At the same time, this drastic increase in fixed N has had widespread environmental consequences. Nitrous oxide (N_2O), produced through nitrification and denitrification reactions, is a potent greenhouse gas and a contributor to stratospheric ozone depletion (Vitousek et al., 1997; Galloway et al., 2003). Other gaseous oxides of N, nitrogen dioxide and nitric oxide (NO_2, NO), participate in photochemical reactions that produce ground level ozone, causing problems with urban air quality (Vitousek et al., 1997; Galloway et al., 2003). Reactive N is also redistributed over large areas through volatilization and deposition, leaching, and runoff of surface waters (Galloway and Cowling, 2002). These deposition processes affect N-budgets in areas (sometimes pristine or unmanaged) far from the initial point of application, and may alter plant species composition and organic matter turnover rates (Aldrich, 1980; Vitousek et al., 1997). Acidification (from HNO_3) and basification (from NH_4^+) are other serious problems resulting from deposition (Vitousek et al., 1997; Schindler et al., 2006; Robertson and Vitousek, 2009). The range of environmental consequences of excess reactive N in the terrestrial biosphere is rendered more poignant when realized against the consequences of a secure food supply and the needs of human nutrition. Management of fixed N is thus essential to balance food production for a growing population with the need to protect the environment from problems associated with excess N in terrestrial and aquatic ecosystems (Robertson and Vitousek, 2009).

Nitrogen is important in biological systems because it can occur in oxidation states ranging from -3 to +5; N can thus carry energy by participating in electron transfer reactions. Nitrogen can also form double and triple bonds through orbital hybridization, allowing it to incorporate into organic molecules. This bonding flexibility allows N-containing compounds to bind with structural carbon atoms, and provide function (along with phosphorous and sulphur) to biomolecules. Nitrogen-containing macromolecules are essential to biological systems; proteins, DNA nucleotides, vitamins, alkaloids, chitin and chlorophyll all contain N. In soils, the fate of N-containing molecules is debated, with some researchers arguing for physical protection as a method of stabilization (Kleber et al., 2007; Simpson et al., 2007; Marschner et al., 2008; von Lützow et al., 2008) while others argue in favour of chemical transformation of soil organic N (SON) into humic materials, the structures of which are still largely speculative (Schnitzer and Khan, 1972; Stevenson, 1994; Schulten and Schnitzer, 1998; Jokic et al., 2004b). (See Appendix A for structures of organic nitrogen-containing molecules identified in soils.) This controversy arises largely through conflicting assessments of SON using available analytical methods. As a consequence, understanding the structures, distributions and transformations of N-containing compounds is essential to a better understanding of the possible environmental impact of excess N in the biosphere. New analytical approaches may yield new insights into the nature an fate of SON.

2.2 The nitrogen cycle

Figure 2.1 shows a simplified version of major N transformations in soil. While it is helpful to visualize N cycling, a diagram such as this oversimplifies the reality of how N moves through the biosphere. Indeed, this implies that N atoms move in a linear fashion through the different organic and inorganic pools; however, any given N atom will randomly move between pools and forms (Stevenson and Cole, 1999). Once N has been fixed into organic forms, the first step for N release into the soil system is through depolymerization (Schimel

and Bennett, 2004; Näsholm et al., 2009) and subsequent ammonification or mineralization (Marschner, 1995; Stevenson and Cole, 1999). It is widely accepted that microbes release NH_3 by enzymatic degradation of N-containing compounds (Ladd and Jackson, 1982; Myrold and Bottomley, 2008). Mineralized N is released as ammonium (NH_4^+) ions into a competitive system with a variety of possible fates; microbial assimilation, plant uptake, and the redox pathways of nitrification/denitrification. The classical approach to plant N nutrition has been that ammonium and organic N are quickly assimilated by microbes, and that N available to plants comes as a result of net mineralization beyond microbial needs and through nitrification

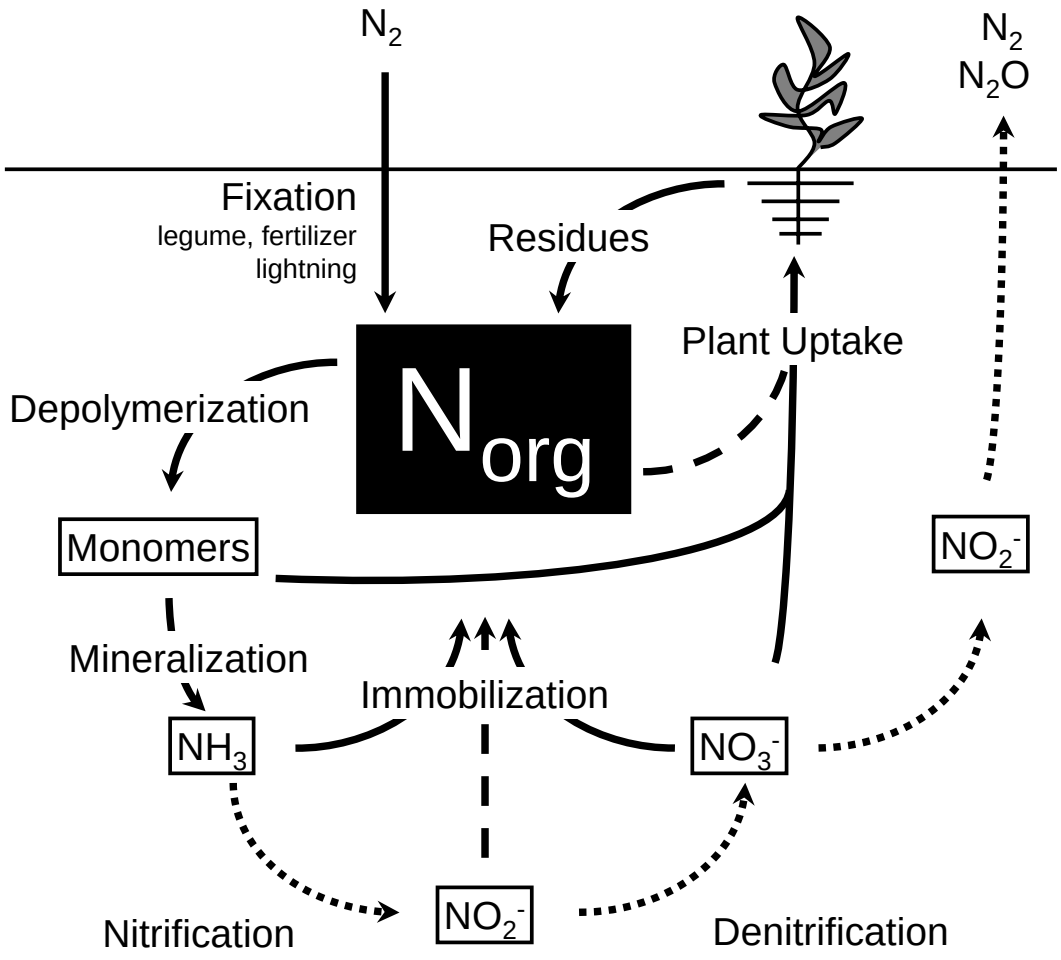

Fig. 2.1. Simplified schematic of the nitrogen cycle in soil from the point of view of organic N. Main N fluxes into and out of organic N pool shown with solid arrows, inorganic N transformations shown with dotted arrows, and contentious fluxes shown with dashed arrows.

processes (Marschner, 1995; Sylvia et al., 2005). The main bottleneck for N supply and plant productivity is thus the depolymerization and subsequent mineralization of organic N from the organic N pool. In recent years, however, a 'paradigm shift' in the understanding of plant N uptake has occurred. This new evidence shows that plants can take up ammonium (Jackson et al., 2008) and low molecular weight organic N directly (Schimel and Bennett, 2004; Badalucco and Nannipieri, 2007). Proteins (Paungfoo-Lonhienne et al., 2008), particularly in N-limited and unmanaged environments (Näsholm et al., 2009; Rennenberg et al., 2009), may also be assimilated. Nonetheless, in Figure 2.1, the organic N pool is show as a black box, largely because the forms, structures, fluxes and transformations so important to N-mineralization and plant nutrition are still largely unknown.

2.3 Soil organic nitrogen: an analytical controversy

In surface soils, organically-bound N comprises approximately 90% of the total N (Bremner, 1965; Stevenson, 1982; Olk, 2008b). Despite decades of research, 30-50% of the soil organic N pool is bound in chemical forms that remain unknown or, at best, are only poorly understood (Stevenson, 1994; Olk, 2008b). This indicates an enormous gap in the knowledge base. Consider the following quotations taken from comprehensive reviews of soil organic N published over the span of 43 years:

> "Many theories have been advanced concerning the nature of the organic soil nitrogen which has not been identified ... However, there is very little evidence to support these theories, and the chemical nature of about half of the organic nitrogen in soils remains obscure" (Bremner, 1965, p.97).

> "The importance of this organic N from the standpoint of soil fertility has long been recognized, and our knowledge concerning the nature and chemical composition of the organic N is extensive. Nevertheless, approximately one half of the soil organic

> N has not been adequately characterized, and little is known of the chemical bonds linking nitrogenous constituents to other soil components"(Stevenson, 1982, p.67).
>
> "Elucidation of the chemical structure of soil organic N has progressed slowly, due to technological limitations, incomplete understanding of the binding of nitrogenous molecules and of the macromolecular structure of SOM, and the absence of an organic N fractionation that is meaningful for all soils" (Olk, 2008b, p.57).

Identifying the composition of unknown soil N is thus a long-standing challenge in soil chemistry, and identifying the chemical forms of this 'unknown N' is an essential first step in achieving a better, more thorough understanding of N-cycling and storage.

The main challenges toward understanding the full range of N-containing compounds in soils are analytical in nature. Many techniques adopted from the fields of pure analytical chemistry have been applied to the characterization of soil and soil organic matter. These techniques generally fall under one of three families: fractionation and quantification with wet chemical methods; depolymerization and molecular characterization; and atomic/functional group characterization.

2.3.1 Wet chemistry - hydrolysis

The conventional method used to describe soil organic N has for many years been acid hydrolysis followed by chemical fractionation (Stevenson, 1982; Feng et al., 2008). Table 2.1, reproduced from (Stevenson, 1982), shows the pools into which organic N is fractionated, along with the reagents and methods used to classify these different hydrolyzate fractions. This method shows amino acid-N as the most abundant form of organic N in soils, and also detects small quantities of amino sugar-N. Inorganic N, measured as NH_3, is also a large part of N in soils, and the remaining N is in unknown forms which are either non-hydrolyzable or

Table 2.1. Classical fractionation soil N based on acid hydrolysis.†

Form	Definition and method	% of soil N‡
Acid-insoluble N	N remaining in soil residue following acid hydrolysis; usually obtained by difference (total soil N – hydrolyzable N).	20-35
NH_3-N	Ammonia recovered from hydrolyzate by steam distillation with MgO.	20-35
Amino acid N	Usually determined by the ninhydrin-CO_2 or ninhydrin-NH_3 methods; recent workers have favoured the latter.	30-45
Amino sugar N	Steam distillation with phosphate-borate buffer at pH 11.2 and correction for NH_3-N; colourimetric methods are also available.	5-10
Hydrolyzable unknown N	Hydrolyzable N not accounted for as NH_3, amino acids or amino sugars; part of this N occurs as non-α-amino N in arginine, tryptophan, lysine, histidine and proline.	10-20

†Reproduced with permission (see Appendix B) from Stevenson (1982); also reproduced in Stevenson and Cole (1999), Olk (2008a), and Olk (2008b).

‡In each method, the NH_3 liberated by steam distillation is collected in a H_3BO_3-indicator solution and determined by titration with standard (0.0025 M) H_2SO_4.

unidentified. Essentially, fractions are operationally separated using steam distillation in the presence of different reagents, and quantified using colourimetric reactions. Many variants are reported in the literature with respect to acid concentration, temperature, and length of hydrolysis time, rendering it difficult to compare results between studies (Bremner, 1965; Kowalenko, 1978; Stevenson, 1982, 1996). The main criticisms of this technique are that the initial hydrolysis reactions, and subsequent steam distillation steps, introduce artifacts. Amino acid-N is underestimated because of degradation of some amino acids to NH_4^+ in the hydrolysis step (Bremner, 1965; Badalucco and Kuikman, 2001). This, along with extraction of interlayer NH_4^+, which is normally unavailable to plants, combines to yield an overestimation of NH_3-N (Stevenson, 1982). Amino sugar-N in turn, is underestimated because of incomplete conversions during the distillation process and because an artificially high value for NH_3-N is subtracted (Mulvaney and Khan, 2001). A second criticism is that this classical fractionation has not successfully correlated these fractions to measures of agronomic significance, such as crop yield, or fertilizer recommendations (Stevenson, 1982; Olk, 2008b). Thirdly, distillation reagents are selected to fractionate specific compounds, which require prior assumptions of what compounds are likely to be found. This method targets known pools, and by design, omits information on unknown pools. Finally, this method is unable to assign functionality to 50% of the N in most soils, leading researchers to seek other techniques to characterize SON. Nevertheless, a large body of research into SON has been published using hydrolysis, and the findings that SON is primarily bound in amino acids and peptides is still widely accepted (Catroux and Schnitzer, 1987; Leinweber and Schulten, 1998; Nannipieri and Paul, 2009).

2.3.2 Analytical Pyrolysis

Pyrolysis refers to applications whereby complex organic samples are thermally decomposed in the absence of oxygen. Absorbed heat energy causes physical cleavage of weaker chemical bonds, and volatilizes the decomposition products, making this technique ideal for characterizing complex and polymeric substances such as soil organic matter (Sorge

et al., 1994; Schnitzer and Schulten, 1995; Schulten, 1996; Schnitzer et al., 2006). Volatilized pyrolysis products are then identified using mass spectrometry, either with prior separation of compounds by gas chromatography, or by employing a temperature ramp in the pyrolysis procedure, whereby volatilization temperature provides diagnostic information complementary to the measured mass (Schulten, 1996). One technique of particular value to SOM characterization is pyrolysis field-ionization mass-spectrometry (Py-FIMS), where soft electric field ionization is used to yield the molecular masses of the decomposition products with little fragmentation (Schulten, 1996). This allows the detection of higher molecular weight monomers from soil samples which would otherwise be fragmented using a harder ionization technique such as electron impact ionization. Pyrolysis techniques thus provide information about soil organic matter structures at the molecular level.

The strength of Py-FIMS lies in the ability to monitor many mass-to-charge (m/z) signals, and assign them to precursor compounds. Assignment of m/z signals comes from extensive study of natural substances, including soils and soil fractions, microbial mucilages and plant materials (Haider and Schulten, 1985; Hempfling et al., 1991; Schulten, 1996; Wilcken et al., 1997). Natural polymeric materials such as lignin, proteins and cellulose release characteristic families of monomers with unique m/z signals. These m/z signals correspond to individual compounds found in natural materials, which can also be grouped and treated as compound classes (see Appendix C). This technique has been successfully applied to humic substances (Haider and Schulten, 1985), dissolved organic matter (DOM) (Kuzyakov et al., 2003; Melnitchouck et al., 2005), organic-mineral particle-size and aggregate fractions (Leinweber and Schulten, 1999; Schulten and Leinweber, 2000) and whole soil samples (Sorge et al., 1994; Schnitzer and Schulten, 1995; Schulten and Sorge, 1995; Gregorich et al., 1996; Wilcken et al., 1997; Schnitzer et al., 2006; Leinweber et al., 2009).

Data from pyrolysis techniques support evidence from hydrolysis experiments that amino acid and amide-N are the most abundant forms of organic N in soils (Schulten et al., 1997). The novel information revealed by pyrolysis-based studies was the presence of heterocyclic

N-containing compounds in various environmental and whole soil samples (Schnitzer and Schulten, 1995; Schulten et al., 1995, 1997; Jokic et al., 2004b). Heterocyclic N is part of many molecules important to biological systems, including the nucleotides of DNA and the porphyrin molecule in chlorophyll; consequently it is conceivable that these materials should also exist in soil. It is well-known, however, that thermal decomposition causes bond rearrangements, and that heterocyclic N compounds can be formed from certain amino acid precursors (Boon and De Leeuw, 1987; Schulten and Schnitzer, 1998), and from plant and microbial substances (i.e., non-humic materials in soils) (Schulten and Sorge, 1995; Nierop and Van Bergen, 2002; Olk, 2008b). This problem of precursor assignment is the main criticism of pyrolysis techniques (Burdon, 2001; Olk, 2008b). Even so, spectra obtained through pyrolysis still provide a fingerprint of SOM compounds, which can be used to compare treatments and gain a stronger understanding of the composition of SOM.

2.3.3 Nuclear magnetic resonance (NMR)

Nuclear magnetic resonance (NMR) spectroscopy is a useful technique for the characterization of SOM because it provides information regarding the chemical nature of certain elements in a sample. The principle of NMR is that nuclei, when aligned in a magnetic field, can absorb electromagnetic radiation in the radio frequency range. The absorption depends on the nuclear spin, and this varies with the type of bond present; NMR thus provides information at the atomic scale. Silverstein et al. (2005) and Simpson and Preston (2008) provide technical overviews of NMR. Great insights into the structures of SOM have come with the development of ^{13}C-NMR (Baldock et al., 1992; Preston, 1996b,a; Kögel-Knabner, 1997, 2000; Preston, 2001; Schnitzer, 2001; Simpson, 2001). Research into N structures using NMR, however, has proven more challenging. The most abundant isotope of nitrogen, ^{14}N, while accessible to NMR, has a large quadrupole moment, which broadens the resulting signal and renders high resolution NMR impossible (Silverstein et al., 2005). The other stable N isotope, ^{15}N, is accessible, but suffers from sensitivity problems because of a small and

negative gyromagnetic ratio (Knicker et al., 1993; Silverstein et al., 2005). More importantly, detection limits become a serious problem because of the low natural abundance of ^{15}N (0.336 atom % for ^{15}N; Junk and Svec, 1958) coupled with low concentrations of total N in soils (Smernik and Baldock, 2005).

In soils, amide-N, found in the amide bond of proteins and acetylated amino sugars, is by far the highest proportion of organic N detected using ^{15}N-NMR. In most studies, amide-N accounts for over 80% of total organic N (e.g., Knicker et al., 1993; Knicker and Lüdemann, 1995; Mahieu et al., 2000; DiCosty et al., 2003). Signals for heterocyclic-N compounds are rarely recorded in soils, even in studies where ^{15}N labeled materials were incubated for up to 630 d (Knicker and Lüdemann, 1995). The lack of these signals in spectra of mineral soils may be attributed to an overlap with the amide peak, or to the result of multiple smaller signals distributed across many different types of N-heterocycles (Schulten and Schnitzer, 1998; Smernik and Baldock, 2005). More problematic is a fundamental criticism of the NMR sensitivity to heterocyclic N in general. Specifically, the cross polarization (CP) technique is most often used, and operates by transferring polarization from ^{1}H nuclei to the ^{15}N nuclei (Simpson and Preston, 2008). This increases sensitivity, allowing collection of spectra at a practical time scale. The problem is that heterocyclic-N compounds do not have protonated N (see Appendix A). This means that protonated N forms (such as amide) will have a faster polarization transfer, thus biasing the signal transfer away from non-protonated N. This same phenomenon is observed in CP studies using ^{13}C-NMR, where aromatic and carbonyl carbon are underrepresented (Smernik et al., 2004). Indeed, Smernik and Baldock (2005) used spin counting to determine that signals from caffeine, a non-protonated N-heterocycle, accounted for only 20% of the signal from an equivalent amount of amide-N in gliadin, a wheat protein. They argued that these results show that characteristics inherent in CP ^{15}N-NMR may be underestimating, or even omitting, N-heterocyclic signals in environmental samples.

Heterocyclic-N has been observed, however, in studies on fire affected soils, where charring was attributed to heterocyclic-N formation (Knicker and Skjemstad, 2000), and in highly

humified samples where enrichment occurred through long-term microbial turnover (Mahieu et al., 2000). Interestingly, both these NMR studies detected heterocyclic N only in physically or chemically stable fractions. Knicker and Skjemstad (2000) removed unprotected organic material using UV radiation, and Mahieu et al. (2000) differentiated between mobile humic acids and calcium-bound humic acids using a fractionation technique described by Olk (2006). The authors thus imply a link between heterocyclic-N formation and stability through long-term humification (Mahieu et al., 2000) and burning (Knicker and Skjemstad, 2000). Although the authors of these papers argue that ^{15}N-NMR is, in fact, capable of detecting heterocyclic N if it is present, Mahieu et al. (2000) do not specify specific types of heterocyclic-N, and Knicker and Skjemstad (2000) describe results only for pyrrolic-N (see Appendix A). Pyrrolic-N is protonated, which would impart higher sensitivity when using a CP-NMR technique, which still leaves the question of unprotonated heterocyclic-N (i.e., pyridinic) detection limits unanswered. Also, Knicker and Skjemstad (2000) drew connections between their observations of heterocyclic-N in charred material and the production of heterocyclic-N through pyrolysis, suggesting that estimates of heterocyclic-N observed using analytical pyrolysis may be inflated.

A new technique, termed saturation-pulse induced dipolar exchange with recoupling (SPIDER), is a method that selects for ^{13}C that is bonded to ^{14}N (Schmidt-Rohr and Mao, 2002). This technique has been applied to humic acid samples and to submerged triple-cropped rice soils and revealed significant amounts of pyridinic N, with large amounts (up to 30%) detected as anilide-N (Schmidt-Rohr et al., 2004; Olk et al., 2006). Some of these same soils were investigated using conventional CP ^{15}N-NMR (Mahieu et al., 2000), and it was concluded that amide signals originally detected using conventional techniques were more likely attributable to anilide-N.

2.3.4 X-ray absorption spectroscopy (XAS)

Ambiguities and criticisms of existing methods of characterizing SON reveal that there is still a pressing need for corroborating analytical methods. Synchrotron-based X-ray absorption near-edge structure (XANES) spectroscopy is an emerging technique applicable to the study of SON, and offers complementary information to ^{15}N-NMR and Py-FIMS. The ability to probe N and C speciation of soil samples *in situ* with soft X-rays offers a unique, purportedly non-destructive (Vairavamurthy and Wang, 2002) opportunity to characterize SON in field soils and other environmental samples (Myneni, 2002). Original studies of humic acids and petroleum products using X-ray photoemission spectroscopy showed a dominance of amide structures with contributions from pyrrolic and pyridinic structures (Kelemen et al., 2002; Abe and Watanabe, 2004; Abe et al., 2005). Vairavamurthy and Wang (2002) used N K-edge XANES to characterize marine sediments and humic acids and found heterocyclic- and amide-N as the dominant forms. Wetland soils were studied by Jokic et al. (2004a), who also found small amounts of heterocyclic pyridinic- and pyrrolic-N in addition to large amounts of amide functionality. These studies relied on small libraries of reference compounds, and as such may limit the interpretations of spectra obtained for whole soils. Leinweber et al. (2007) conducted a comprehensive study whereby a spectra library was constructed for many compounds and N functionalities expected to be found in environmental samples. These included DNA nucleotides, nitriles, and inorganic N-containing compounds (Figure 2.2). In addition to showing the potential for beam damage to peptide-N, this dataset also showed potential overlap for some features, including those for amide-N and the NH moiety in DNA nucleotides.

These potential overlaps may be addressed by characterizing samples with C K-edge XANES. Organic N must be bound to C, and so an exploration of C functionality in a sample will provide insight into the overall structure of organic N. Carbon K-edge studies have been performed on soils and sediments (Jokic et al., 2003; Solomon et al., 2005), soil extracts (Christl and Kretzschmar, 2007), synthetic systems (Hardie et al., 2007), and whole soils

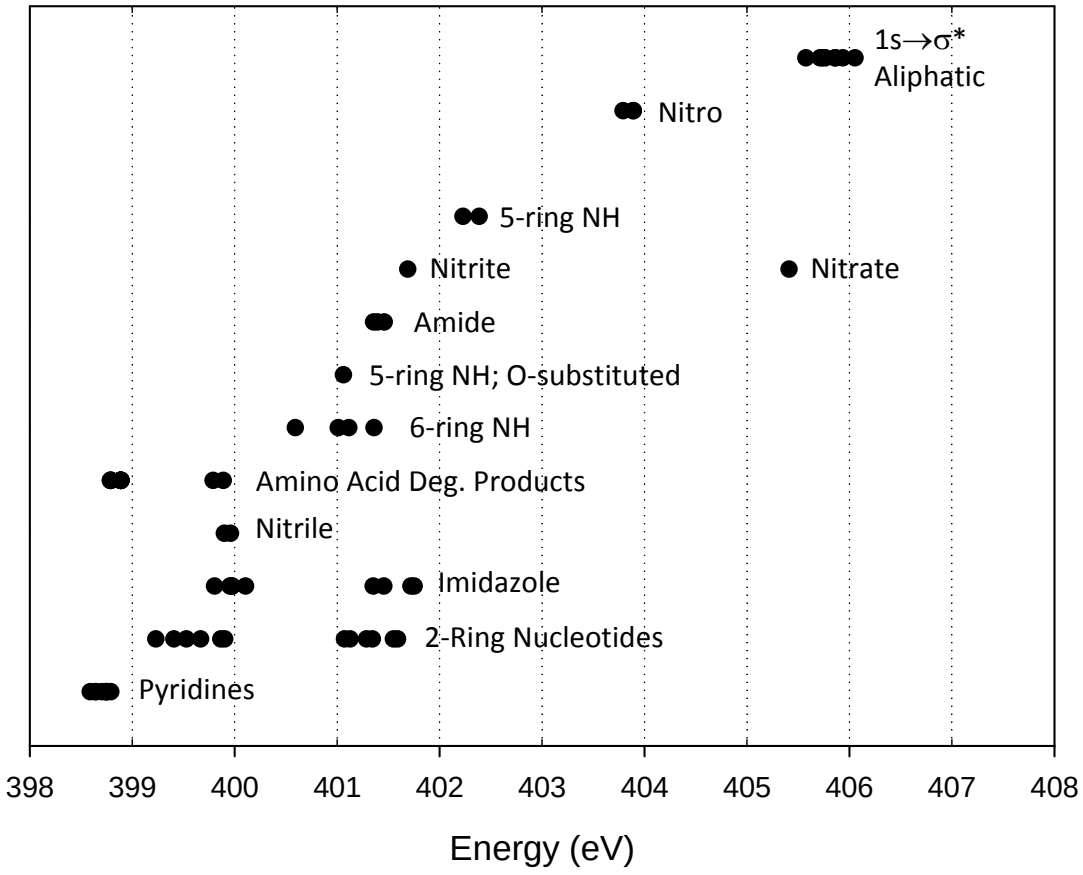

Fig. 2.2. Summary of characteristic XANES resonances for N-containing reference compounds. Adapted from Leinweber et al. (2007)

(Leinweber et al., 2009). Moreover, they have been coupled with the imaging technique of scanning transmission X-ray microscopy (STXM) to elucidate the spatial distribution of C-containing moieties at the nanoscale (Lehmann et al., 2005, 2008; Kinyangi et al., 2006).

2.4 Glomalin: a special case of protein-N

Assessments of SON composition using various techniques all report that proteins, peptides and amino acids comprise the most abundant forms of SON (e.g., Stevenson, 1994; Stevenson and Cole, 1999; Olk, 2008b; Nannipieri and Paul, 2009). This fraction of SON is often characterized by hydrolysis with a strong acid, followed by colourimetric quantification using

the ninhydrin reagent (Stevenson, 1982; Knicker and Skjemstad, 2000; Chantigny et al., 2008) or by chromatographic separation of individual amino acids (Bremner, 1965; Schnitzer and Khan, 1972; Stevenson, 1982, 1994). Studies characterizing intact proteins from soils are less common, focusing mainly on assaying enzyme activities (Skujins, 1967; Boyd and Mortland, 1990; Tabatabai, 1994; Badalucco and Nannipieri, 2007); however, study of non-catalytic proteins is in its infancy (Bastida et al., 2009).

One such soil protein may be glomalin, a putative glycoprotein produced by arbuscular mycorrhizal fungi (AMF) (Wright and Upadhyaya, 1996; Wright et al., 1998; Bolliger et al., 2008). Glomalin is produced in the cell walls of AMF hyphae, and deposited in soil after hyphal death (Driver et al., 2005). Glomalin is reportedly hydrophobic and has been linked with aggregate stability (Wright and Upadhyaya, 1998; Rillig, 2004). This protein is produced in copious amounts (mg g^{-1} soil) and is also persistent in the environment, with an estimated residence time of 6 to 42 y (Rillig et al., 2001). The discovery of glomalin has thus generated great interest in the soil ecological community because slow turnover coupled with large quantities of this material implies that it may be a significant long term sink for C and N in terrestrial systems (Wright et al., 1996; Rillig et al., 2001; Lovelock et al., 2004; Treseder and Turner, 2007).

2.4.1 Glomalin is operationally defined

Many fractions of SOM are often operationally defined. These include, for example, humic substances (Schnitzer and Khan, 1972; Stevenson, 1994; Anderson and Schoenau, 2008), density fractions (Gregorich and Beare, 2008), and the classical distillation fractionations of N (see Table 2.1; Bremner, 1965; Stevenson, 1982, 1996). Operational definitions seek to separate or isolate components of SOM based on particular characteristics. While it is generally understood that operationally fractionated pools are not pure, it is presumed that they are dominated by a specific group of compounds (Nichols and Wright, 2006). Glomalin is operationally defined as the material released from soil after autoclaving in citrate buffer

(Wright and Upadhyaya, 1996; Wright et al., 2006). This material is then quantified using either the Bradford total protein assay (Bradford, 1976), or an enzyme-linked immunosorbant assay (ELISA), with MAb32B11 antibodies generated against spores of *Glomus intraradices* (Wright et al., 1996; Rosier et al., 2006). The Bradford total protein assay method is a simple, non-specific quantification method where Coomassie Brilliant Blue dye changes from red to blue when complexed with protein residues (Bradford, 1976). Problems with this detection method for the quantification of glomalin stem from cross-reactivity of the dye with polyphenols, tannins and nucleotides, all which apparently are co-extracted in glomalin (Nichols and Wright, 2006; Schindler et al., 2007; Whiffen et al., 2007). Because the Bradford assay can be performed without specialized equipment, it is likely to find widespread use. This has negative consequences, because it is likely contributing to overestimations of glomalin stocks if cross-reacting impurities or non-glomalin proteins are present in the glomalin extract (Roberts and Jones, 2008).

Because this material is operationally defined, Rillig (2004) argued that the term 'glomalin' should be reserved only for the gene product, and proposed the term 'glomalin-related soil protein' (GRSP) as a means to distinguish the gene product from the operational extract. In addition, Rillig (2004) and Rosier et al. (2006) also recommended differentiating between Bradford-reactive and immunoreactive GRSP as a means of reinforcing that the specificity of each detection method yielded differing results. This nomenclature reflects the acknowledgement that the operationally extracted material is, at best, poorly characterized and that the structure and molecular characterization of glomalin-proper is still unclear (Rosier et al., 2006).

2.4.2 Characterizing glomalin-related soil protein

Analytical characterization of bulk GRSP is limited to an NMR characterization, which showed that this material more closely resembles humic acid rather than protein (Schindler et al., 2007). Bolliger et al. (2008) sought to evaluate the purity of the GRSP extract using

sodium dodecyl sulfate-polyacrylamide gel electrophoresis (SDS-PAGE) combined with a suite of visualization methods including western blot, lectin affinity and crossed immuno- and lectin affinity electrophoresis (CIE-CLAE). The authors concluded that GRSP is in fact a single glycosylated protein based on its reactivity to the glomalin-defining antibody, and on CIE-CLAE evidence (which showed a single, diffuse precipitate arc, indicative of a single protein). This report was made despite evidence presented showing PAGE gels with multiple bands reactive to silver stain, western blot and lectin blot. In addition, the authors indicate that the diffused character of the precipitate arc in the CIE-CLAE gel suggested multiple isoforms of a single protein coupled with heavy glycosylation.

Indeed, early attempts at partial characterization of glomalin focused on the glycan domain. Glomalin was determined to be a glycoprotein because it exhibited a strong binding affinity for lectin. This was followed by a study which used capillary electrophoresis to characterize the *N*-linked oligosaccharides released from AMF cultures and from GRSP using enzymatic deglycosylation (Wright et al., 1998). This study found that a single glycan group was released from AMF cultures, and that several different glygan groups were released from GRSP extracts, of which dominant soil glycan possessed the same retention time as that observed from AMF.

A study focusing on the protein portion of glomalin identified it as a homolog of a stress protein, namely heat-shock protein 60 (Hsp60, Gadkar and Rillig, 2006). In this study, a protein isolated from an *in vitro* mycorrhizal culture of *G. intraradices* was sequenced, and found to have homology to Hsp60. A sequence encoding the Hsp60 gene from a *G. intraradices* library was used to encode the protein, which was reactive to the glomalin-defining antibody MAb32B11. The qualification (and quantification) of glomalin in most studies relies on the material's immunoreactivity against the MAb32B11 antibody (e.g., Driver et al., 2005; Gadkar and Rillig, 2006; Rosier et al., 2006; Schindler et al., 2007; Bolliger et al., 2008). The monoclonal antibody is developed by immunizing a mouse against crushed *G. intraradices* spores (Wright et al., 1987, 1996), culturing multiple hybridoma from recovered spleen cells,

and determining which hybridoma has the strongest immunoreactive response toward the target isolate spores (Wright et al., 1996). In this case, Wright et al. (1996) named their hybridoma 32B11 which was the most reactive to a range of AMF fungi, and did not cross react with other, non-AMF fungi (Rillig and Mummey, 2006). The link between AMF and glomalin has thus been made by satisfying two criteria: autoclave stability and a positive reaction against the MAb32B11 antibody generated against spores of *G. intraradices*. The binding site of the 32B11 antibody is not yet known; however evidence that it reacts with Hsp60 produced *in vitro* (Gadkar and Rillig, 2006) and that it changes in reactivity with multiple autoclave cycles (Janos et al., 2008) suggests that it is on the protein domain, and that the site is sensitive to denaturation. While it has been shown that the MAb32B11 antibody is specific to AMF-derived protein (Wright et al., 1996), one would assume that the antibody would be reactive to any of a number of proteins found in AMF spores (Xavier et al., 2000). This suggests that the current methods of detection are rather indirect, and perhaps a more directed, protein-centric approach to glomalin characterization should be explored.

2.4.3 Proteomics as a soil analytical tool

Proteomics comprises a suite of techniques developed for the isolation, characterization and identification of proteins (Ogunseitan, 2006; Solaiman et al., 2007; Bastida et al., 2009). In this multistep procedure, protein mixtures are separated based on their molecular weight using SDS-PAGE, and visualized using a staining technique (commonly using Coomassie Blue dye or colloidal silver staining). Bands of interest are then excised, and subjected to proteolytic digestion, commonly using the trypsin enzyme. Individual peptides are then sequenced using tandem mass spectrometry, and these sequences are compared to a database to identify, or find homology to, a known protein. The concept of using metaproteomics for the characterization of soil proteins is an emerging tool for characterizing soil biology (Solaiman et al., 2007; Bastida et al., 2009). Like metagenomics, where the collective DNA

from many organism is used to describe soil processes, metaproteomics focus on characterizing the collective proteins as a way of elucidating gene functionality (Maron et al., 2007; Bastida et al., 2009; Nannipieri and Paul, 2009). This technique is being applied to study protein profiles in AMF (Xavier et al., 2000; Dumas-Gaudot et al., 2004), dissolved organic carbon (Schulze et al., 2005), contaminated soil (Benndorf et al., 2007), and forest soil (Masciandaro et al., 2008).

While this technique shows great promise, there exist challenges to its implementation. First, proteins are isolated using SDS-PAGE, which requires removal of interfering compounds such as humic substances and nucleotides, which are common in soil (Bastida et al., 2009). This requires systematic evaluations of extraction and purification methods specific to soils. Secondly, unlike DNA, proteins cannot be amplified to increase detection limits (Bastida et al., 2009). This means that extraction protocols may require consideration of an enrichment step. Finally, proteomics relies on the completeness of the database, which for soil microorganisms remains poorly covered (Bastida et al., 2009).

Currently, the most direct structural information on the structure and/or function of glomalin comes from the study published by Gadkar and Rillig (2006), which found homology between a MAb31B11-reactive protein isolated from AMF and Hsp60. No studies exist, however, which seek to characterize the protein(s) which are extracted in GRSP. At this point, little information exists on the actual protein structure, or on other protein (and non-protein) impurities in the GRSP extract. Applying metaproteomics to the study of GRSP may validate the connection between glomalin and AMF, and would also allow a direct understanding of the composition, and ecological significance of the material comprising GRSP.

2.5 Synchrotron-based X-ray absorption spectroscopy

2.5.1 The synchrotron facility

The construction and use of synchrotron radiation has been described in detail in Winick (1994), Peatman (1997), and Sham and Rivers (2002). Presented here is an overview of the synchrotron setup and the phenomenon of X-ray absorption relevant to studies of soils (see also Ginder-Vogel and Sparks, 2010). A synchrotron produces high-intensity photons that can be used to probe the chemical, physical, and biological properties of matter. Electrons, when traveling at relativistic speeds (i.e., almost the speed of light) will emit radiation when they are accelerated by a force perpendicular to their velocity (Elder et al., 1947; Sham and Rivers, 2002). Early synchrotron experiments were parasitic off machines designed for high-energy particle physics, where circular particle accelerators were being used and synchrotron radiation was considered a nuisance because it was a waste of energy from the system (Winick, 1994). It was discovered, however, that this radiation had specific and desirable properties, namely high brightness, collimation (directionality), and polarization, and could be used as a high-intensity light source for a range of spectroscopic studies (Winick, 1994; Peatman, 1997).

In a modern synchrotron, electrons are generated and accelerated by a linear accelerator. This is followed by a second acceleration step whereby electrons are brought to relativistic speeds using a booster ring (Winick, 1994). These electrons are then fed into a storage ring, and it is here that synchrotron radiation is generated for experimental use. The storage ring is a polygon, and each corner is fitted with a dipole magnet (Figure 2.3A). As relativistic electrons travel around the ring, they are accelerated at each corner by the dipole magnet (also called a "bending magnet") and directed along the next straight section (Figure 2.3B). Each corner around the ring produces synchrotron radiation, and thus may support an experimental station, or beamline (Winick, 1994).

Modern third generation synchrotrons are designed to increase flux (brightness) by

including insertion devices, known as wigglers and undulators. These devices are installed into the straight sections of the storage ring, between the bending magnets. These devices are arrays of multiple magnet pairs, arranged in alternating polarity (Figure 2.4). When an electron beam enters an insertion device, the beam oscillates between the poles, and follows a sinusoidal path with a period equal in length to the distance between two like magnetic poles. This system produces a photon release each time the beam is diverted, thus mimicking multiple bending magnets, and providing a substantial increase in photon flux compared to a bending magnet (Peatman, 1997). Wigglers and undulators differ in how the repeated magnet periods relate to the wavelength of energy transmitted through them. Wigglers use fewer, larger, magnets so that the electrons passing through undergo a large angular deflection, producing a beam with a wide, continuous, incoherent spread of radiation. Undulators are built so that the magnetic periods are shorter, and are equal to the wavelength of photons desired for the experiment (Winick, 1994; Sham and Rivers, 2002). As electrons move through the undulator, out-of-phase photons that are produced will cancel out

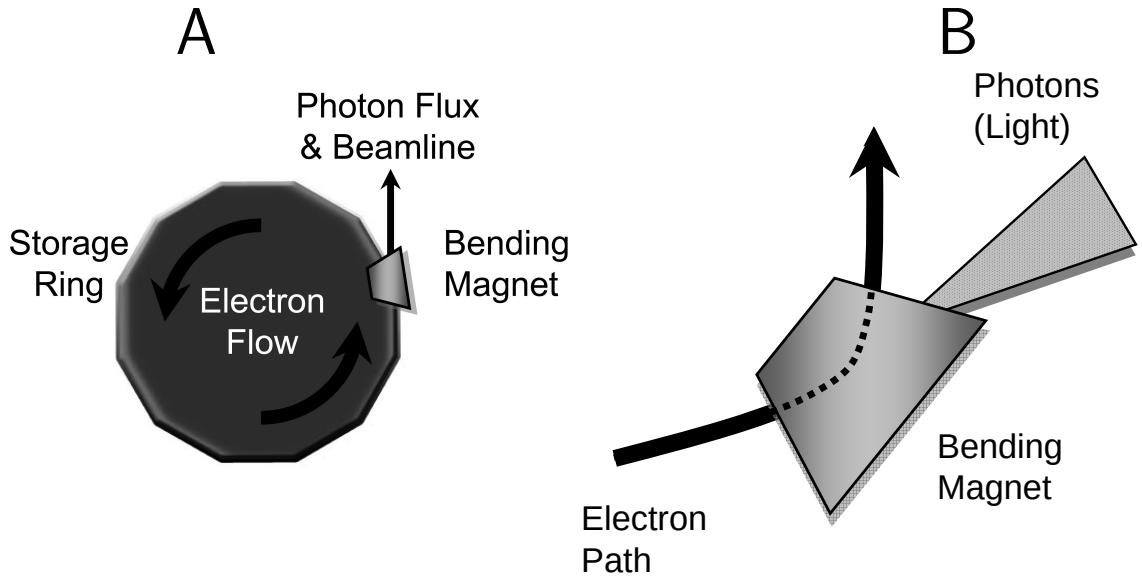

Fig. 2.3. Schematic of (A) Electron path and position of bending magnets on a synchrotron storage ring and (B) photon production as the electron beam is accelerated by a dipolar bending magnet.

through destructive interference. The result is a highly brilliant and quasi-monochromatic beam that is delivered to the optics of the beamline (Sham and Rivers, 2002). The undulator thus offers a degree of tunability to the delivered radiation, which is related to the distance between the top and bottom array of magnets (undulator gap). Because of this, the upper magnet array is motor-driven, and the undulator gap is varied so as to track along with a monochromator, which further selects radiation energy, to achieve the maximum flux to the sample of a particular energy.

In general, beamlines contain similar components, including shutters to protect the ring vacuum, and mirrors to divert and focus the beam onto the sample. For the user, the two most important components are the monochromator and the endstation. Monochromators are devices that select the energy of the radiation that will be delivered to the sample. These devices are diffraction-based, and, according to Bragg's Law ($n\lambda = 2d \sin\theta$), deliver a

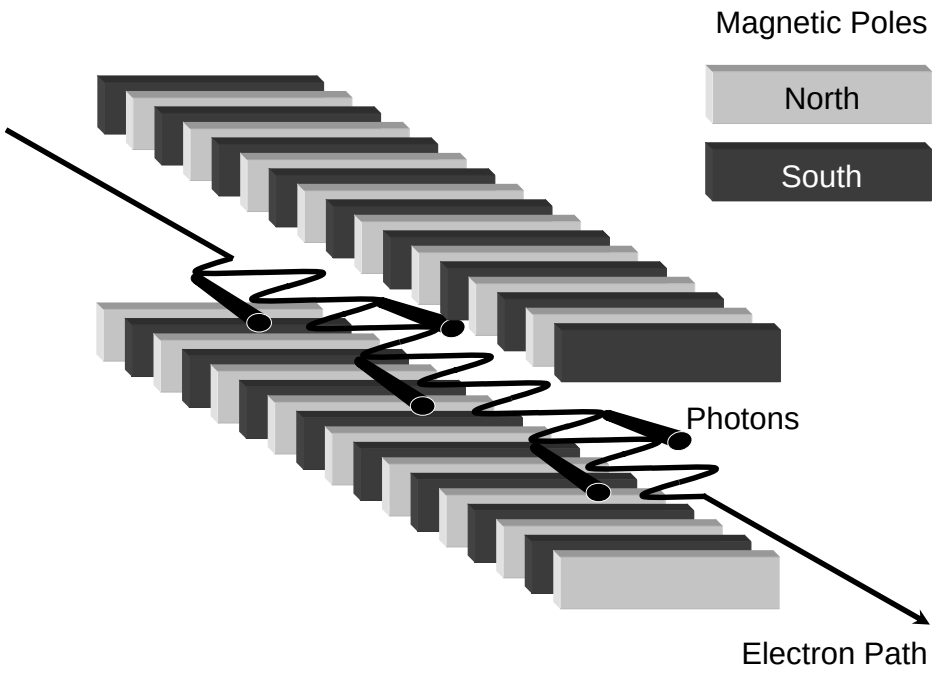

Fig. 2.4. Electron flow and production of high intensity photon flux from an insertion device (undulator or wiggler).

highly-resolved, narrow band of photon energies to the sample by altering the angle of the monochromator with respect to the incoming beam (Peatman, 1997). The monochromator is thus one of the most important components of a synchrotron beamline, because it allows fine control over the photons delivered to the sample, and thus has the potential to produce a highly resolved spectrum.

The endstation is where the sample is presented to the beam, and where the data is collected. The endstation is application specific, and in theory, can be exchanged depending on the experiment. Examples of endstations include X-ray photoemission chambers, X-ray absorption chambers, scanning-transmission X-ray microscopes (STXM), and photoemission electron microscopes (PEEM). Soft X-rays, which do not penetrate air, are used for experiments at the N and C K-edges. Moreover, air is 78% N_2, which will overwhelm any signal produced from N in a sample unless it is excluded. The prime requirement of a soft X-ray endstation, therefore, is that it be kept under high vacuum. The endstation also houses the detection apparatus. Detectors are designed to record the outcomes of the X-ray absorption process.

2.5.2 The X-ray absorption process

The technique of X-ray absorption spectroscopy (XAS) is an element-specific probe of the electron structure of a material. This means that XAS can detect specific bonds and functional groups in a sample (Stöhr, 1992). Every electron shell of every element in the periodic table absorbs at a unique X-ray energy. This phenomenon is referred to as the absorption edge. The power of XAS thus lies in the ability to probe the chemistry of specific elements of interest in complex samples by exploring electron structures. Since electronic structure explains different bonding and speciation arrangements of an element, the resulting spectral shifts provide a fingerprint of the elemental chemistry in the sample.

2.5.3 Experiments using X-ray absorption

2.5.3.1 X-ray photoemission spectroscopy (XPS)

The first studies to use X-rays to characterize chemical structures were performed by Dr. Kai Siegbahn in Uppsala, Sweden using X-ray photoelectron spectroscopy (XPS), or electron spectroscopy for chemical analysis (ESCA) (Siegbahn et al., 1967; Siegbahn, 1990; Briggs, 1998; Ratner and Castner, 2009). In this technique, the incident photon energy is fixed, and the kinetic energies of emitted electrons are measured. The kinetic energy is related to the binding energy of the electron, by the equation $E_B = h\nu - E_K - \phi$, where E_B = binding energy, h = Planck's constant, ν = photon frequency, E_K = kinetic energy, ϕ = work function (which is the minimum energy needed to remove an electron from a solid) (Hrbek, 2002; Ratner and Castner, 2009). The ejection of a photoelectron requires the input of energy greater than the ionization potential (or binding energy + work function) of the particular electron (Figure 2.5). These electron binding energies are sensitive to the charge distribution of the valence electrons, imparting chemical bonding information related to the element (Siegbahn, 1990; Hrbek, 2002; Ratner and Castner, 2009). An example of an XPS spectrum of a soil is shown in Figure 2.6.

2.5.3.2 X-ray absorption near-edge structure (XANES) spectroscopy

X-ray absorption near-edge structure (XANES) spectroscopy differs from XPS in that the incident photon energy is varied, and the amount of absorbed photons is measured. The final result of an electron excitation event is dependent on the energy of the incident photon, where the electron need not be completely ejected from an atom after interaction with a photon. Figure 2.7 shows four possible outcomes for an excited electron: (1) $h\nu < E_B$: no photon absorption; (2) $h\nu = E_B$: resonance - a well defined final state where the electron is not removed, and has a high probability of occurring; (3) $h\nu > E_B$, $h\nu < E_B + \phi$: absorption, but electron not removed; (4) $h\nu > E_B + \phi$: electron removed, same as XPS.

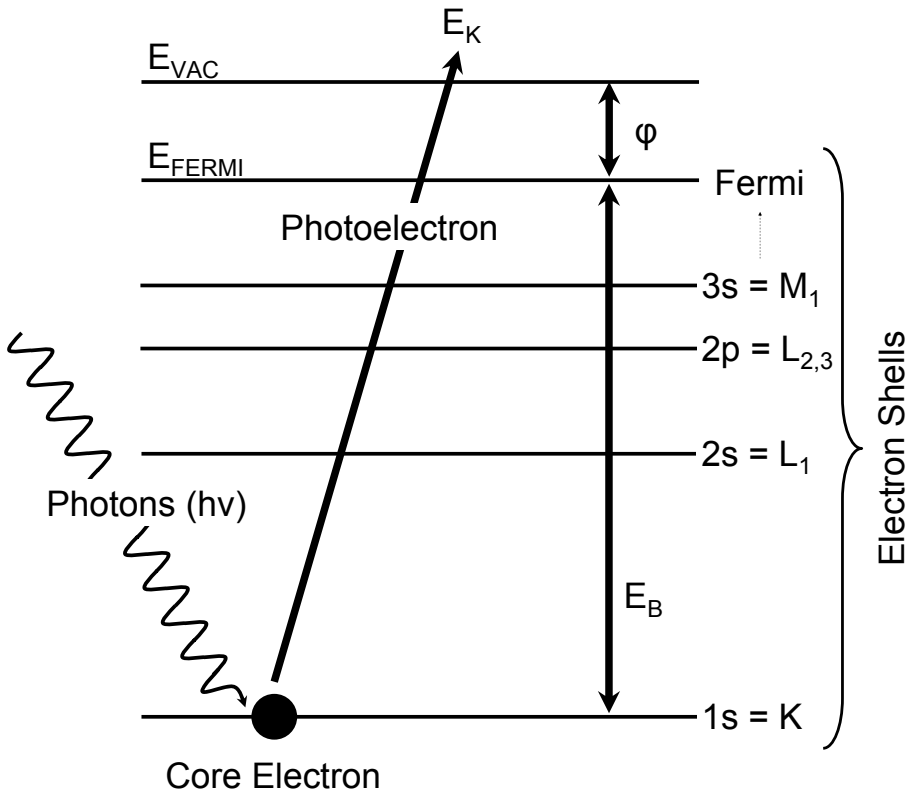

Fig. 2.5. Schematic of the X-ray absorption process in X-ray photoelectron spectroscopy. An incident photon excites a core electron, removing the electron into the continuum. E_B = binding energy, h = Planck's constant, ν = photon frequency, E_K = kinetic energy, $\mathbf{E}_{FERMI}$ = position of zero binding energy, $\mathbf{E}_{VAC}$ = energy of an isolated electron at rest, ϕ = work function, which is the energy required to remove electron from a solid (the difference between $\mathbf{E}_{FERMI}$ and $\mathbf{E}_{VAC}$). Two common nomenclatures for labelling electron shells are included here: Atomic Notation (1s, 2s, 2p, 3s, etc.) and X-ray Notation (K, $\mathbf{L}_1$, $\mathbf{L}_{2,3}$, $\mathbf{M}_1$, etc.)

In a XANES experiment, outcomes 2 and 3 are of particular interest. Here, different the electron can be promoted to specific resonant final states by tuning the photon energy to the electron transition energy. These final states correspond to unfilled molecular orbitals, which reflect the local bonding structure of the element (Stöhr, 1992; Myneni, 2002; Sham and Rivers, 2002). Patterns in the XANES spectra can provide a fingerprint of the elemental chemistry in the sample. Figure 2.8 shows a schematic of a wide XANES scan across a range

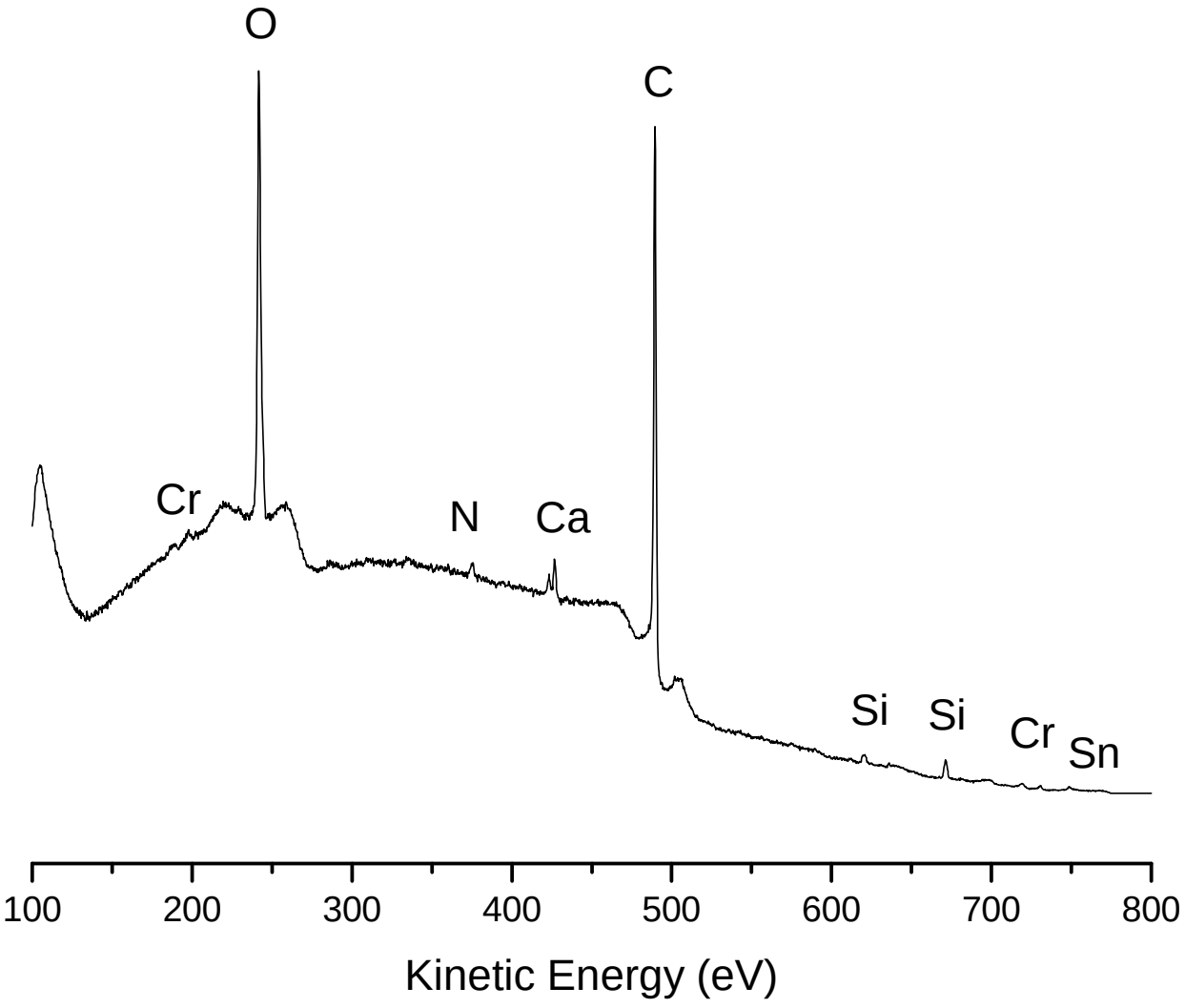

Fig. 2.6. Example of X-ray photoelectron spectrum of a soil.

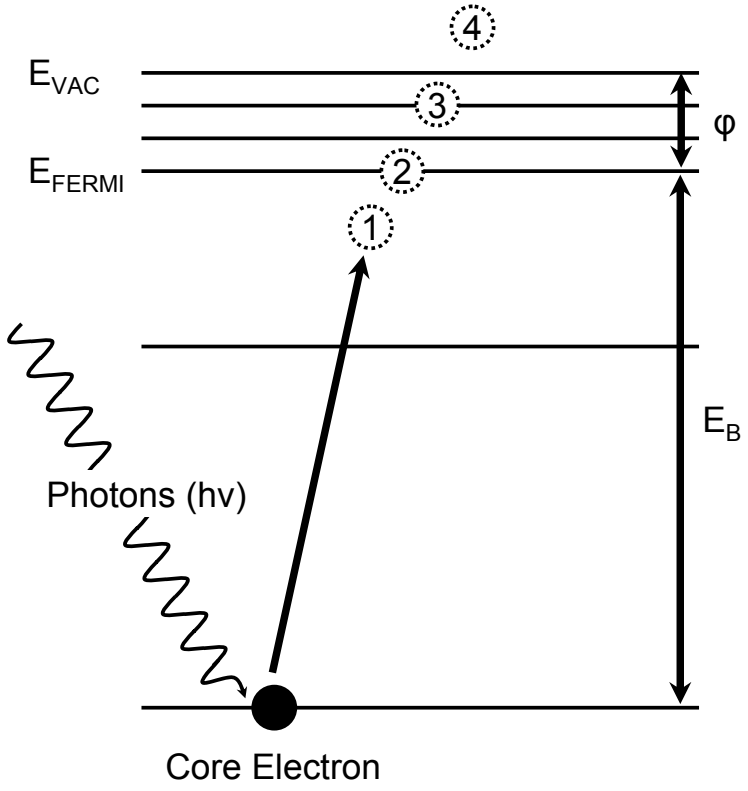

Fig. 2.7. **Schematic of the X-ray absorption near-edge structure process. An incident photon excites a core electron, resulting in several outcomes depending on the photon energy. E_B = binding energy, h = Planck's constant, ν = photon frequency, E_K = kinetic energy, ϕ = work function (which is the minimum energy needed to remove an electron from a solid). (1) h$\nu < E_B$ - no absorption; (2) h$\nu = E_B$: resonance - a well defined final state where the electron is not removed; (3) h$\nu > E_B$, h$\nu < E_B + \phi$: absorption, but electron not removed; (4) h$\nu > E_B + \phi$: electron removed, same as XPS.**

of photon energies and absorption edges.

The K-edges for N and C fall in the soft X-ray region, which cannot pass through samples deeper than *ca.* 100 nm (Myneni, 2002). Measuring X-ray absorption therefore cannot be accomplished simply by measuring transmittance. Instead, two surrogate methods of measurement may be used: fluorescence yield and total electron yield.

Electron promotion leaves an electron core hole, which is filled through the relaxation of another electron from a higher energy shell (Ratner and Castner, 2009). This electron must lose energy to do this, and does so in one of two competing secondary de-excitation processes. The first is a radiative process, where the energy is lost as a fluorescence photon (Figure 2.9). The second process is non-radiative, where the energy is lost through the emission of an Auger (pron: Oh-zhay) electron (Figure 2.10) (Stöhr, 1992; Sham and Rivers, 2002). Fluorescence yield (FLY) and Auger electron emission, measured as the drain current from the sample (total electron yield, TEY), both are proportional to the number of electron core holes created, and are thus proportional to the number of photons absorbed. These phenomena can therefore be used as surrogate measurements of X-ray absorption. Both processes are recorded simultaneously in a XANES experiment, and they provide complementary data with respect to the probing depth (Stöhr, 1992). The mean free path for electrons escaping the surface is <10 nm (Frazer et al., 2003), whereas fluorescence yield has an estimated escape

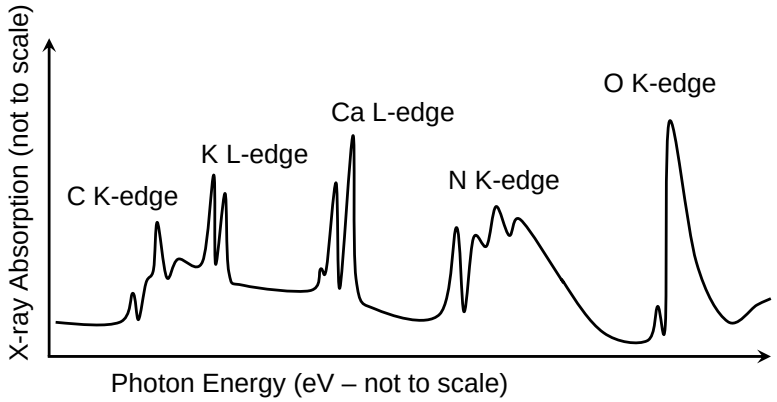

Fig. 2.8. Example of a XANES spectrum

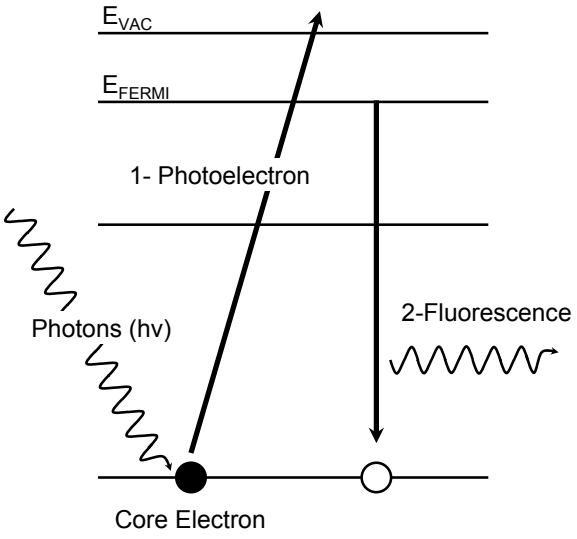

Fig. 2.9. Schematic of fluorescence photon release through relaxation process after X-ray-induced photoelectron removal.

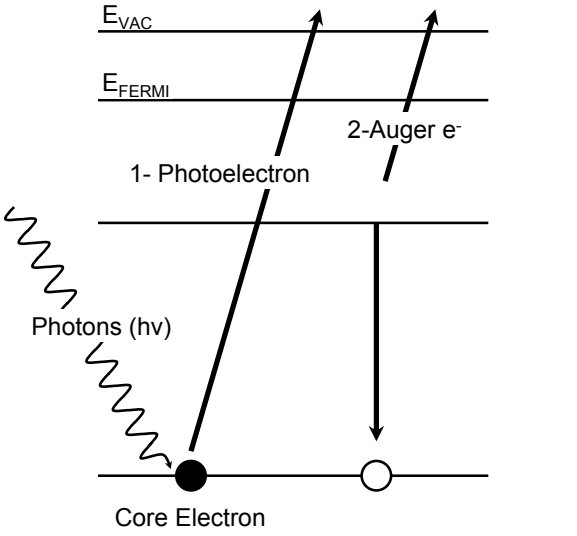

Fig. 2.10. Schematic of Auger electron release through relaxation process after X-ray-induced photoelectron removal. Process is competitive with fluorescence.

depth of 70-100 nm (Katsikini et al., 1997). TEY is thus a surface-sensitive detection method, whereas FLY probes more of the bulk material.

As mentioned above, the spectral features observed in a XANES scan correspond with unfilled molecular orbitals. When two atoms are brought together into a chemical compound, their atomic orbitals blend together, and form delocalized molecular orbitals (Stöhr, 1992; Myneni, 2002). These transitions to unoccupied orbitals still leave a core hole that must be filled, which is done so either by fluorescence or electron emission.The detection of fluorescence or electron emission in a XANES experiment are thus measurements of unoccupied π^* and σ^* antibonding orbitals, which reflects the electronic configuration, giving insight into the local bonding structure of the molecule (Stöhr, 1992; Myneni, 2002; Sham and Rivers, 2002).

2.6 Novel Approaches Toward Characterizing SON

Understanding the forms and chemistry of organic N in soil is crucial to understanding N cycling at the global scale. Despite many years of study, considerable controversy remains surrounding organic N chemistry, largely due to analytical limitations inherent in the available methods. The challenge is to develop and adopt new and relevant technologies from analytical chemistry and biochemistry and apply them to the characterization of organic N.

Advantages in analytical techniques such as synchrotron-based XANES, pyrolysis mass spectrometry and proteomics present new opportunities to further our basic understanding of SON. Complementary, multipronged approaches may be the answer to elucidating the fundamental structures in which SON is bound, thus providing insight into the cycling, persistence, agronomic significance and global environmental distribution of N-containing compounds.

Chapter 3

Calibration method at the N *K*-edge using interstitial nitrogen gas in solid- state nitrogen-containing inorganic compounds[†]

Abstract

The standard method of soft X-ray beamline calibration at the N K-edge uses the $\nu = 0$ peak transition of gas-phase N_2. Interstitial N_2 gas trapped or formed within widely-available solid-state ammonium- and amine-containing salts can be used for this purpose, bypassing gas-phase measurements. Evidence from non nitrogen-containing compounds (KH_2PO_4) and from He-purged ammonium salts suggest that production of N_2 gas is through beam-induced decomposition. Compounds with nitrate or nitrite as anions produce coincident features and are not suitable for this calibration method.

3.1 Introduction

The ideal method for energy calibration of soft X-ray analysis at the nitrogen K-edge is the measurement of the vibrational peak positions of gas-phase N_2 with an in-line mounted gas cell. The vibrational manifold of the 1s $\rightarrow \pi^*$ transition is well known from electron

[†]This work has been published in Gillespie, A.W., F.L. Walley, R.E. Farrell, T.Z. Regier, and R.I.R. Blyth. 2008. Calibration method at the N K-edge using interstitial nitrogen gas in solid-state nitrogen-containing inorganic compounds. J. Synch. Rad. 15:532-534. Minor modifications have been made for consistency in formatting.

spectroscopy, and the $\nu = 0$ peak has an energy of 400.8 eV (Sodhi and Brion, 1984; Schwarzkopf et al., 1999). Not all beamlines have facilities for gas-phase measurements, however, and in beamtime shifts where solid-state measurements are planned, setup and use of the gas cell can be unwieldy and time-consuming.

Characteristic N_2 molecular vibrations in nitrogen-containing salts were observed during an investigation of natural reference compounds (Leinweber et al., 2007). As well, trapped N_2 gas has been reported in the characterization of N_2^+-bombarded alumina (Holgado et al., 2003), and of compound semiconductors (Ruck et al., 2004; Petravic et al., 2006). The objective of this study was to conduct an assessment of suitable inorganic compounds that can be used for a simple, alternative calibration method at the N K-edge using high-resolution scans over energies corresponding to N_2 gas.

3.2 Materials and Methods

3.2.1 Reference compounds

The inorganic, N-containing salts used as reference compounds are listed in Table 3.1. All reference compounds were pulverized with a mortar and pestle, affixed to double-sided conductive carbon tape (SGE, Toronto, ON) and mounted onto stainless steel sample discs. In addition, hydroxylamine hydrochloride and ammonium sulfate were dissolved in deionized water, purged with ultra-high purity helium, evaporated under helium to remove existing N_2 gas, and pulverized and mounted as described above. Gas-phase photoabsorption N_2 measurements were obtained using a double ionization gas cell with a 10 cm active pathlength in each chamber (Yates et al., 2000) for comparison to N_2 vibrations measured in solid-state samples.

Table 3.1. Names, formulae, CAS (Chemical Abstracts Service) and suppliers for compounds used in this study.

Compound	Formula	CAS #	Supplier
Ammonium chloride	NH_4Cl	12125-02-9	AnalaR
Ammonium phosphate, Dibasic	$(NH_4)_2HPO_4$	7783-28-0	BDH
Ammonium phosphate, Monobasic	$(NH_4)H_2PO_4$	7722-76-1	EMD
Ammonium sulfate	$(NH_4)_2SO_4$	7783-20-2	Fisher
Ammonium nitrate	NH_4NO_3	6484-52-2	Sigma-Aldrich
Hydroxylamine hydrochloride	$NH_2OH{\cdot}HCl$	5470-11-1	Chemservice
Potassium nitrate	KNO_3	7757-79-1	EMD
Sodium nitrite	$NaNO_2$	7632-00-0	Sigma-Aldrich
Potassium dihydrogen phosphate†	KH_2PO_4	7778-77-0	Baker

†ultra high purity (99.8%)

3.2.2 N *K*-edge XANES

Nitrogen K-edge X-ray absorption near edge structure (XANES) spectra were collected using the Spherical Grating Monochromator (SGM) beamline 11ID-1 at the Canadian Light Source (CLS), Saskatoon, SK, Canada. This facility delivers 10^{11} photons s^{-1} at the N K-edge with a resolving power (E/ΔE) greater than 10,000 (Regier et al., 2007a,b). Fluorescence yield (FLY) data were recorded using a two-stage multichannel plate detector that was operated in parallel with total electron yield (TEY) data collection through measurement of the drain current from the sample. High-resolution scans were taken using a step size of Δ0.01 eV over the expected range for N_2 gas, and of Δ0.1 eV for the remainder of the scan. Spectra were normalized to the incident flux using an in-line Au mesh which was refreshed by evaporation *in situ* prior to data collection. Data processing was done using the Athena software package (Version 0.8.050) (Ravel and Newville, 2005). Data from at least two scans were averaged, and background corrected by a linear regression fit through the pre-edge region followed by normalization to an edge step of one.

3.3 Results and Discussion

Figure 3.1 shows FLY data of N K-edge XANES scans for the inorganic N-containing compounds studied, with panel A illustrating the energy region surrounding the vibronic structure of N_2 gas in detail, and panel B showing the full scan. Nitrogen gas vibronic structure is clearly evident in the reduced N- (i.e., ammonium- or amine-) containing salts that do not have an oxidized N anion. The $\nu = 0$ transition occurs at the same peak position in the solid phase as it does in the gas phase (Figure 3.1A). The data of show no significant shift in the peak position until the peak width broadens by over 100 meV, by which time a significant change in the overall shape has occurred. Provided there is a valley between the second and third peaks, we quantitatively estimate the accuracy to be within 100 meV. Peak widths, however, vary due to lifetime reduction through solid state mechanisms. This change correlates with the crystal lattice constant, and thus with confinement of N_2 gas within the solid phase. This has been discussed in detail with respect to compound semiconductors by Petravic et al. (2006).

The presence of nitrate (NO_3^-) or nitrite (NO_2^-) produces a feature at 401.7 eV, which is coincident with 1s $\rightarrow \pi^*$ of N_2 gas, rendering these compounds less useful for calibration purposes. Although observed previously (Leinweber et al., 2007), this feature remains unidentified. It should be noted, however, that this feature was not observed in previously published analyses of KNO_3 (Vinogradov and Akimov, 1998; Rodrigues et al., 2007), suggesting that it may be a product of beam-induced decomposition. If this is the case, it is not likely to be decomposing to nitrous oxide (N_2O) or nitrogen dioxide (NO_2), as this feature does not match previously published spectra for these oxides of N (Adachi and Kosugi, 1995; Gejo et al., 2003). Decomposition to NO, however, is observed here in NH_4NO_3, with vibrations corresponding to published results (Remmers et al., 1993; Adachi and Kosugi, 1995; Yates et al., 2000).

Certainly, atmospheric N_2 trapped within the solid phase would explain the occurrence of this feature; implying that the use of any inorganic salt would suffice as a calibration

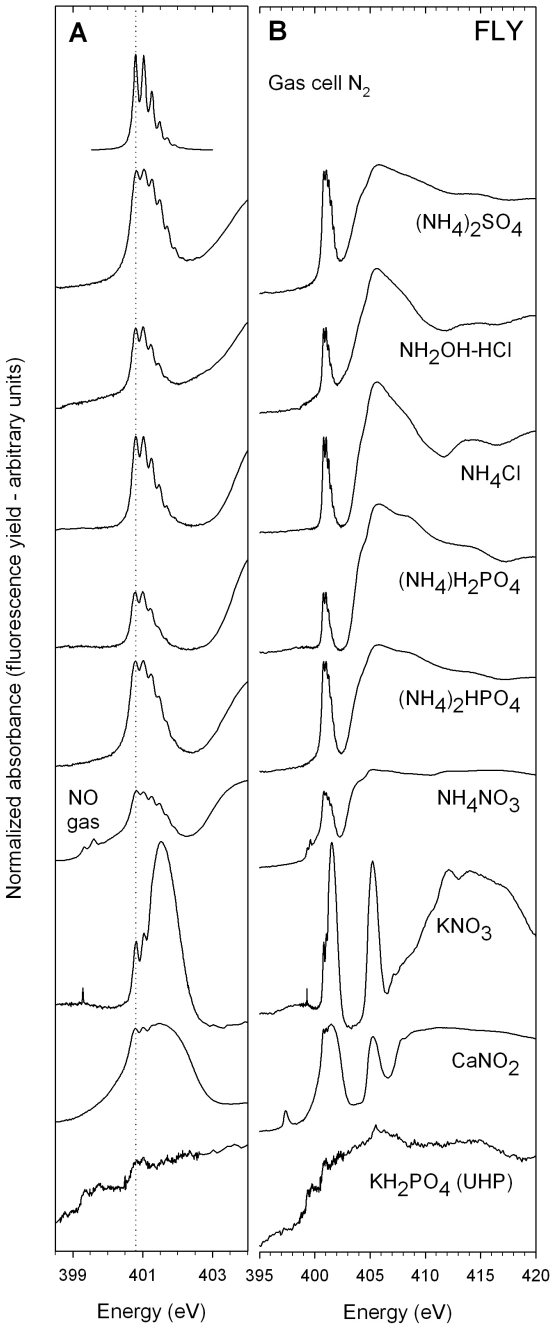

Fig. 3.1. Nitrogen *K*-edge fluorescence yield (FLY) spectra showing N_2 gas in the solid state of inorganic salts used in this study. Panel A shows detail of high-resolution section, and panel B shows the full N *K*-edge scan. Dotted line corresponds to 400.8 eV, which is the $\nu = 0$ peak for the vibrational manifold of the $1s \rightarrow \pi^*$ transition for N_2 gas (Sodhi and Brion, 1984; Schwarzkopf et al., 1999).

material. However, spectra obtained for N-free, ultrapure potassium phosphate (dibasic) showed no evidence of N_2 gas vibrational structure (Figure 3.1). In addition, we analyzed ammonium sulfate and hydroxylamine hydrochloride that had been dissolved, purged of N_2 and recrystallized under an ultra-high purity helium atmosphere. These scans showed the presence of N_2 gas, matching those obtained for the unprocessed salts (data not shown). While it is beyond the scope of this paper to determine the mechanism of entrapment or production of interstitial N_2, these results suggest that it is derived from decomposition of the ammonium moiety. Indeed, for calibration purposes, the salt must contain ammonium- or amine-N to be of use.

Total electron yield (TEY) spectra for selected scans are shown in Figure 3.2, with panel A illustrating the region encompassing N_2 gas within the full scan pictured in panel B. Scans for all the ammonium-containing salts, except NH_4NO_3, showed similar characteristics; thus only data for $(NH_4)_2SO_4$ is presented here as a representative scan. The N_2 gas vibronic feature is suppressed in all TEY scans for all substances, and is absent from NH_4NO_3 and KNO_3. Total electron yield (with an estimated penetration depth <10 nm) is more surface sensitive than FLY (with an estimated penetration depth of 70-100nm) (Katsikini et al., 1997; Frazer et al., 2003). This suggests that the N_2 gas originates (i.e., is entrapped or produced) below the surface layer, and that any N_2 at/near the surface is removed in the vacuum chamber. Therefore, as a calibration method, TEY provides a less useful measure of absorption when compared to FLY. Total electron yield data also revealed a stronger feature at 401.7 eV seen in KNO_3 and $CaNO_2$, indicating that if this is a decomposition product, then the mechanism of its formation is surface-sensitive.

3.4 Conclusions

Interstitial N_2 gas contained within solid-state inorganic ammonium- and amine-containing salts can be used to quickly and accurately calibrate soft X-ray beamlines at the N K-edge

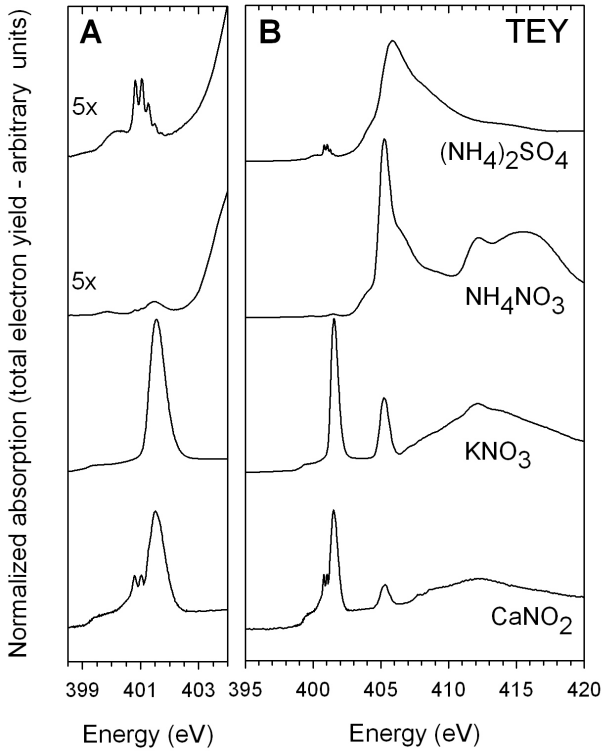

Fig. 3.2. Nitrogen *K*-edge total electron yield (TEY) spectra showing suppressed N_2 gas detection. Panel A shows detail of high-resolution section, and panel B shows the full N *K*-edge scan. Spectrum for ammonium sulfate is representative for all spectra of ammonium- and amine- containing salts.

without the need for gas-cell measurements. Dinitrogen gas contained within these solids may be generated via beam-induced decomposition. Other, as yet unknown compounds may be produced if the anion is an oxidized N moiety such as nitrate or nitrite. Characteristic N_2 molecular features are observed more strongly with FLY, indicating formation/presence within the bulk material.

Chapter 4

Time-scale assessment of amino acid and peptide degradation using synchrotron-based photoemission spectroscopy

Abstract

XANES spectroscopy provides a unique and powerful approach to analysing peptides, proteins and amino acids in environmental samples. Once considered non-destructive, development of this method through the evaluation of reference compounds has shown degradation of these substances through beam exposure over time, particularly on high flux undulator beamlines. The rate of degradation may be occurring more quickly than that which can be observed at the timescale of a typical XANES scan at the C and N K-edges (*ca.* 7 min). Photoemission scans across binding energies for C 1s and N 1s can be performed quickly (75-180 s), and thus provides a tool to examine the rapidity of decomposition. Presented here is a time-resolved study of simple peptides containing histidine, glycine, methionine and arginine to evaluate the decomposition rates and possible products from beam exposure of these proteinaceous substances. Results showed that irradiation increased the conductivity (i.e., removed differential charging) of these insulating organic compounds. Irradiation also produced a secondary set of compounds for which charging was lifted completely, suggesting physical damage as well as chemical changes to the amino acid/peptide material. In addition, different chemical changes were observed in the 'insulating' compounds compared to the

'conducting' products. Finally, peptides containing methionine and histidine were more sensitive, with physical and chemical changes occurring within 10 min, whereas glycine and arginine-containing compounds were more stable. XANES scans of sensitive material must therefore be monitored for beam damage that may occur before completion of the first scan.

4.1 Introduction

Synchrotron-based X-ray absorption spectroscopy provides a unique and powerful approach to the characterization of organic material in environmental samples. In particular, N and C K-edge XANES spectroscopy has been successfully used to characterize N-bonding environments in soils and sediments (Myneni, 2002; Vairavamurthy and Wang, 2002; Jokic et al., 2003, 2004a; Solomon et al., 2005; Kinyangi et al., 2006; Leinweber et al., 2007, 2009). Once purported as a non-destructive method (Vairavamurthy and Wang, 2002), XANES studies have shown degradation and transformation of some reference compounds through beam exposure over time, particularly when using high photon flux undulator beamlines (Coffey et al., 2002; Ascone et al., 2003; Kade et al., 2007; Leinweber et al., 2007; Cody et al., 2009; Schäfer et al., 2009; Wang et al., 2009). Amino acids and peptides appear to be highly susceptible to X-ray damage (Bozack et al., 1994; Kade et al., 2007; Leinweber et al., 2007; Wilks et al., 2009), which is of concern for analyses of soil and environmental samples where protein and amide N predominates (Schulten and Schnitzer, 1998; Olk, 2008b). While it is clear that X-ray exposure induces chemical changes in proteins and amino acids, (Zubavichus et al., 2004a,b; Kade et al., 2007; Wilks et al., 2009; Zubavichus et al., 2009), the question remains as to whether degradation reactions are occurring more quickly than the time required to acquire a single spectrum.

A typical XANES scan on the spherical grating monochromator (SGM) beamline at the Canadian Light Source (CLS) lasts *ca.* 7 min, where the analysis time is limited by

optical system movements. Another option available to assess X-ray absorption is to use the complementary technique of X-ray photoemission spectroscopy (XPS). This technique uses a different detector mounted on the beamline which measures the kinetic energy of electrons emitted from the sample during irradiation (Siegbahn, 1990; Briggs, 1998; Ratner and Castner, 2009). Kinetic energy can be measured more quickly across binding energies for N 1s and C 1s (75-180 s) than a typical XANES scan, and thus provides a tool to examine the speed of decomposition at higher temporal resolution.

Kinetic energy is related to the binding energy of a core electron by:

$$E_B = h\nu - E_K - \phi \qquad \text{[Eq. 4.1]}$$

Where E_B = binding energy, $h\nu$ = incident photon energy, E_K = kinetic energy, ϕ = work function (which is the minimum energy needed to remove an electron from a solid) (Hrbek, 2002; Ratner and Castner, 2009). The electron binding energies are, like XANES, unique to the individual elements. They also are sensitive to the charge distribution of the valence electrons, yielding information pertaining to the chemical bonding of the element (Siegbahn, 1990; Hrbek, 2002; Ratner and Castner, 2009).

Presented here is a study of soft X-ray irradiation effects on proteinaceous materials over time using XPS. The model substances selected include amino acids (methionine, arginine), simple peptides (methionyl-methionine, glycyl-glycine, pyroglutamyl-histidyl-proline amide) and non-peptides (2,3-pyrazinedicarboxylic acid, guanine) for comparison to non-protein materials. This study was undertaken by recording time-resolved XPS scans across E_K equivalent to the N 1s and C 1s binding energies, to evaluate and compare the decomposition rates and possible products from beam exposure of these proteinaceous substances.

4.2 Materials and Methods

4.2.1 Reference compounds

Methionine (met; CAS#: 7005-18-7); arginine (arg; CAS#: 74-79-3); methionyl-methionine (met-met; CAS #: 7349-78-2); glycylglycine (gly-gly; CAS#: 61499-00-1); pyroglutamyl-histidyl-proline amide (PHP; CAS#: 24305-27-9); 2,3-pyrazinedicarboxylic acid (PZDA; CAS#: 89-01-0) and guanine (CAS#: 73-40-5) were obtained from Sigma-Aldrich (Mississauga, ON). Compounds were powdered in a mortar and pestle and affixed to a sample plate using double-sided conductive carbon tape (SGE, Toronto, ON), after which they were pumped to ultra-high vacuum in the XPS chamber for *ca.* 24 h.

4.2.2 XPS

X-ray photoelectron spectra were collected using a Scienta SES100 photoemission analyzer (VG Scienta Inc., Newburyport MA) using the Spherical Grating Monochromator (SGM) beamline 11ID-1 at the Canadian Light Source (CLS), Saskatoon, SK, Canada. This beamline delivers 10^{11} photons s^{-1} at the N K-edge with a resolving power (E/ΔE) better than 10,000 (Regier et al., 2007a,b). The monochromator and undulator were set to provide an incident photon flux of 600 eV with a slit opening of 50 μm. Without shifting the beam from the original incident spot on the sample, single XPS spectra were consecutively recorded across E_K corresponding to the N 1s and C 1s binding energies while recording each start time. Each scan lasted between 75-180 s, depending on the E_K range required to capture the N 1s and C 1s regions, and was recorded in a separate data file.

Curve fitting was carried out on the t=22 min spectrum of met-met to determine possible degradation products using fityk (ver. 0.8.6). Voigt lineshapes, which are convolutions of Gaussian and Lorentzian curves, were used in the deconvolution (Briggs, 1998; Ratner and Castner, 2009). For insulating samples such as amino acids (and other polymers), the E_B may be calculated based on an internal reference for the C 1s of saturated hydrocarbons,

where $E_B = 285.00eV$. In this study, E_B for peaks resulting from beam decomposition were calculated relative to the C 1s for the graphitic C tape substrate where $E_B = 284.70eV$. Carbon 1s peak assignments were made using values calculated from Briggs (1998) and presented in Appendix D.1. Nitrogen 1s assignments were estimated from data presented in Nordberg et al. (1968), Zubavichus et al. (2004a,b, 2005a), Plekan et al. (2007) and Zhang et al. (2009).

4.3 Results and Discussion

4.3.1 XPS

Successive scans for met and met-met are shown in Figure 4.1, with N spectra plotted on the left and C on the right. These results were plotted as E_K rather than the conventional method of presenting XPS data (as E_B) to show the changes in differential charging on the sample over time. When electrons from within an insulating material do not balance emitted photoelectrons, a positive charge builds up at the material surface (Briggs, 1998; Gregoratti et al., 2009). This creates a positive charge at the surface, which slows the emitted electron (i.e., decreases E_K), resulting in an apparent increase in E_B (Gregoratti et al., 2009; Ratner and Castner, 2009). This phenomenon is referred to as 'charging'. This apparent shift in E_B is actually due to a changing value for the work function of the electron (ϕ) in Equation 4.1. In Figure 4.1, both met and met-met show single peaks for N and C XPS scans at time = 0 min. Charging appears to be lessened from the sample over time, with shifts in these N and C peaks toward higher kinetic energies, indicating changes to ϕ, and thus changes to the charging characteristics of the sample. The distance (i.e., ΔE_K) between C and N peaks also remains constant over the course of the experiment, indicating that charging is responsible for the shift, and not the development of chemical changes in the material.

New peaks, representing different C and N functionalities (at *ca.* $E_K = 310$ eV and 195 eV, respectively), appear within minutes of radiation incidence. These new peaks do not

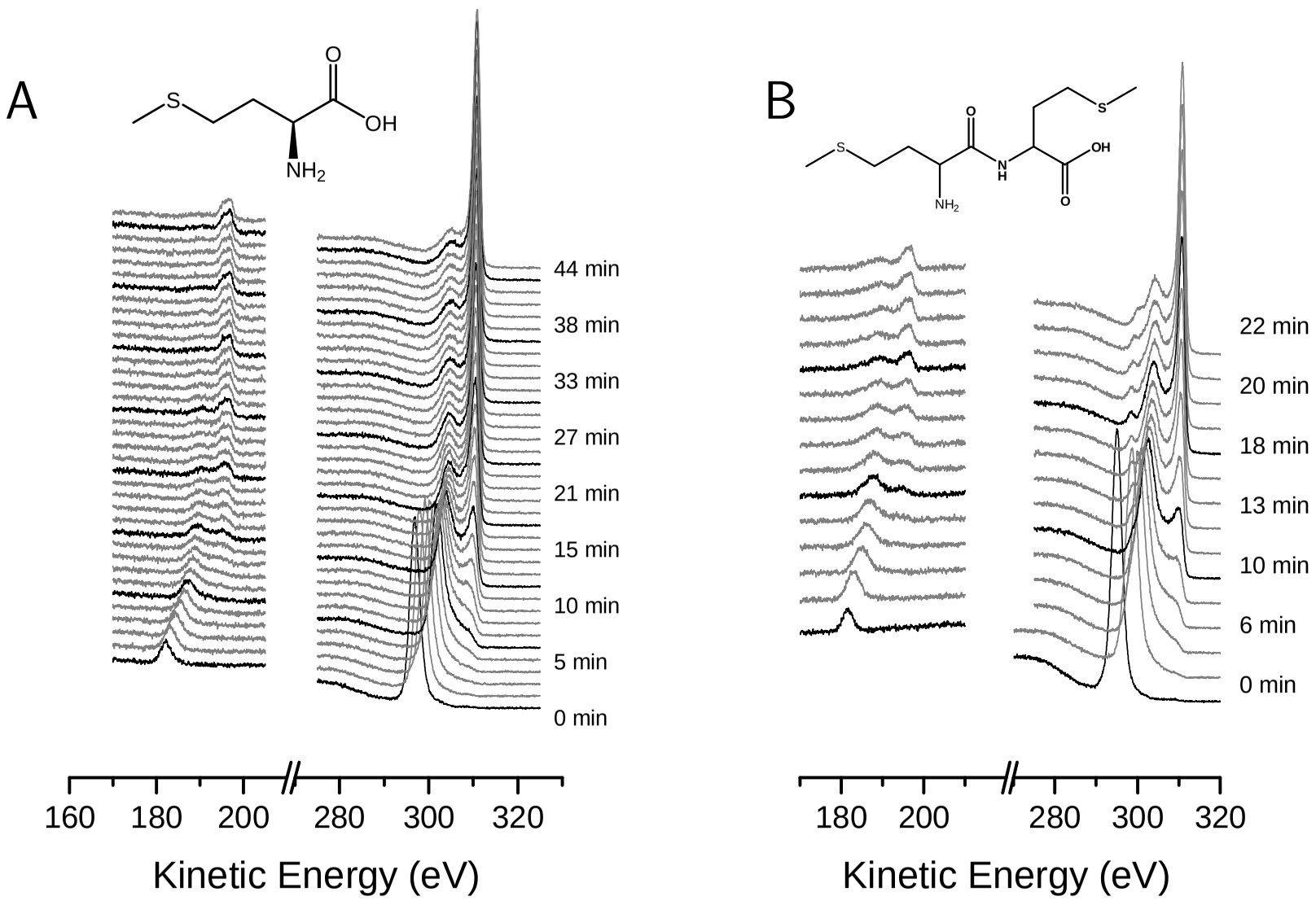

Fig. 4.1. X-ray photoemission spectra of methionine (A) and methionyl-methionine (B) recorded consecutively at the original incident spot. All spectra recorded at 600 eV incident energy with slit openings of 50 μm. Nitrogen spectra at left, carbon at right. Plotted as kinetic energy to demonstrate charging changes over time.

experience shifts due to charging, indicating closer contact with the graphite substrate and suggesting physical fragmentation and removal of material. Indeed, the initial peak heights decrease with subsequent scans along with an increase in height of the newly-formed peaks (Figure 4.1). XPS is well known as a surface-sensitive analytical method (Siegbahn, 1990; Briggs, 1998; Hrbek, 2002; Ratner and Castner, 2009), and although photons may be able to penetrate the bulk material, the mean free path for electrons to escape elastically (i.e., without losing energy) is shallow (<10Å; Hrbek, 2002). Removal and fragmentation of these amino acids thus allows progressive exposure of the C tape substrate, introducing graphitic C (at *ca.*E_K = 310 eV) into the XPS spectrum.

Chemical changes to the structure of met and met-met are also taking place as a result of irradiation. Figure 4.2 shows the deconvoluted spectrum of met-met after a 22 min exposure. After deconvolution, the assignment of C and N functionalities to each peak was not possible when using a single reference C 1s peak with the lowest E_K (peak 5). This is because the peak positions farthest from the C 1s peak occurred at binding energies that were higher than those corresponding to C functionalities that were possible in this sample (e.g., no compounds exist for $E_B > 290.4$ eV, see Appendix D.1). The deconvolution procedure instead revealed that irradiation of this dipeptide mounted on conductive C tape produced a bimodal system, each cluster with its own conduction regime and photoreaction products. Group A (Figure 4.2, peaks 1-4) comprises compounds derived from the original amino acid/peptide material, and group B (peaks 5-9) comprises a secondary set of compounds, where charging has been removed completely. When converting E_K to E_B, peak 1 was used as the reference for group A, where C 1s $_{C-C}$ = 285.00 eV, and peak 5 was used for the reference for group B, where C 1s $_{C=C}$ = 284.7 for the graphitic carbon substrate (Briggs, 1998). Progressive exposure of the substrate indicates that physical degradation, in addition to chemical changes, of the material is occurring with beam exposure.

The N 1s lineshape starts (0 min) as a dominant peak with a binding energy of 400.2 eV (See Figures 4.1B and 4.2). At the end of the experiment (22 min exposure), the bimodal

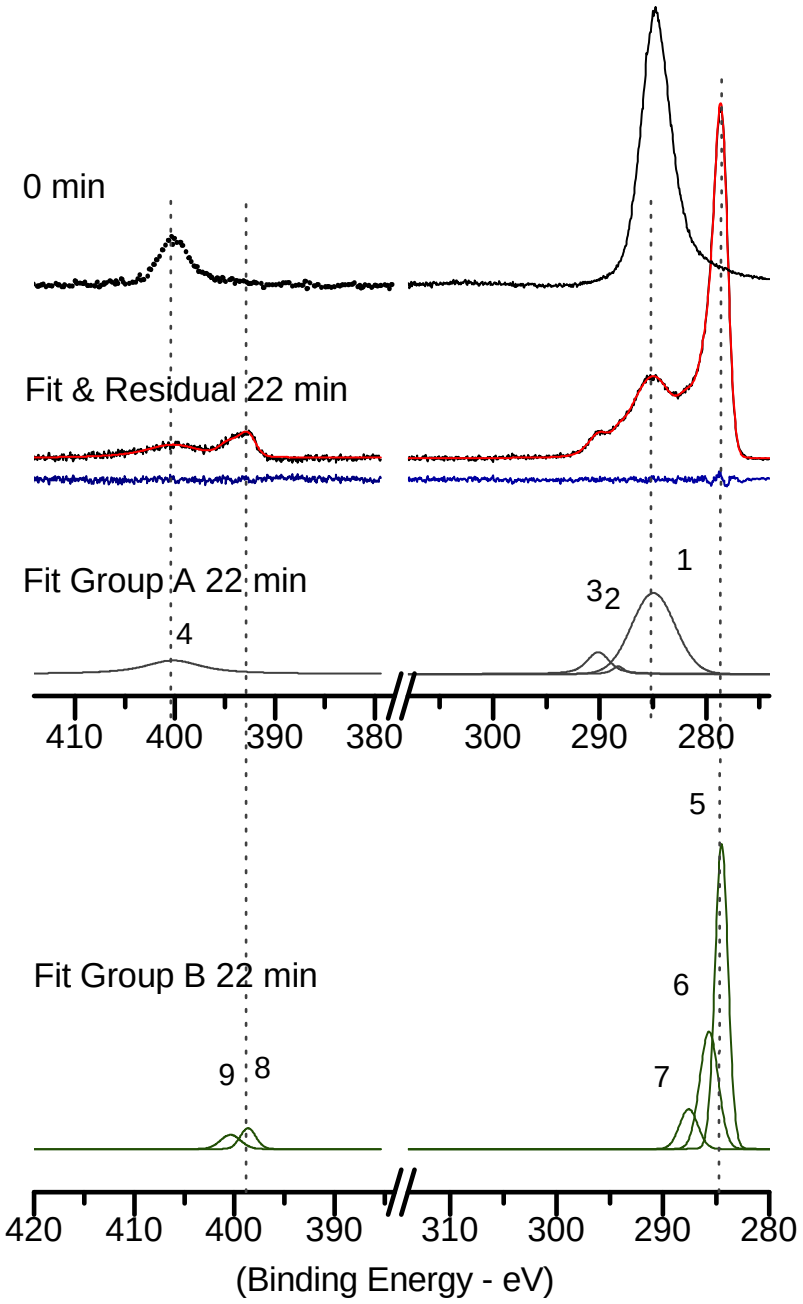

Fig. 4.2. N 1s (left) and C 1s (right) XPS spectra of methionyl-methionine at 0 min irradiation (C 1s peak adjusted to 285.00 eV) and deconvolution of XPS of met-met after 22 min radiation exposure. Irradiation creates two sets of peaks (A and B). Binding energies relative to C 1s binding energy for saturated hydrocarbons (Group A; charging) or graphite from carbon tape (Group B; charging lifted). Peaks numbered as: (1) 285.0 eV, C–C (C 1s reference); (2) 288.3 eV, N–C=O (peptide); (3) 290.2 eV, C–CO_3 (carbonate) (4) 400.2 eV, -NH_3^+ / -NH_2; (5) 284.7 eV, C=C (reference); (6) 285.9 eV, C-N<; (7) 287.8 eV, N–C–O; (8) 398.9 eV, NH_2; (9) 400.6 eV, NH_3^+.

N 1s lineshape is seen, with a single peak remaining at 400.2 eV (referenced to group A) and two new peaks generated at 398.9 eV and 400.6 eV (referenced to group B). Studies of amino acid decomposition also show a dominant initial peak, assigned as protonated amine ($–NH_3^+$), followed by the development of a second peak at a lower binding energy, assigned as unprotonated amine ($–NH_2$) (Bozack et al., 1994; Zubavichus et al., 2004a,b). This is the result of progressive irradiative deprotonation of the $–NH_3^+$ moiety; in this experiment, however, the observed phenomenon of deprotonation is only observed in the material for which charging has been removed. This shows an interaction between the mechanisms of physical and chemical decomposition of met-met due to irradiation.

The C 1s lineshape also starts as a single peak (Figures 4.1B and 4.2), and develops into a complex bimodal spectrum. In this case, group A progressively shows peptide (N-C=O) functionality (peak 2) and a highly oxygenated peak corresponding closely in E_B to organic carbonate (Appendix D.1). The E_B for group B, in contrast, correspond closely with C-N (peak 6) and saturated N-C-O bonds (peak 7). Again, like the development of the N 1s spectra, there are distinct patterns of chemical differentiation under irradiation in the group of compounds which are insulating (group A) as compared to the group for which charging has been removed (group B). Zubavichus et al. (2004a) have outlined several mechanisms for chemical degradation of amino acids, including dehydrogenation (deprotonation), decarboxylation, dehydration, deamination and desulphurization. One or more of these destructive processes appear to be occurring in the present study; however, there also appears to be the development of new compounds, such as organic carbonates. This indicates that these amino acid systems undergo extensive rearrangement of chemical bonds under irradiation (Wilks et al., 2009).

Similar patterns of charging and subsequent bimodal spectral development are observed in analyses of gly-gly and PHP (Figure 4.3). Again, the N 1s and C 1s lineshapes begin as single peaks, and immediately drift toward higher kinetic energies as a result of charge removal. The development of secondary compounds is also evident, with N 1s changes following the

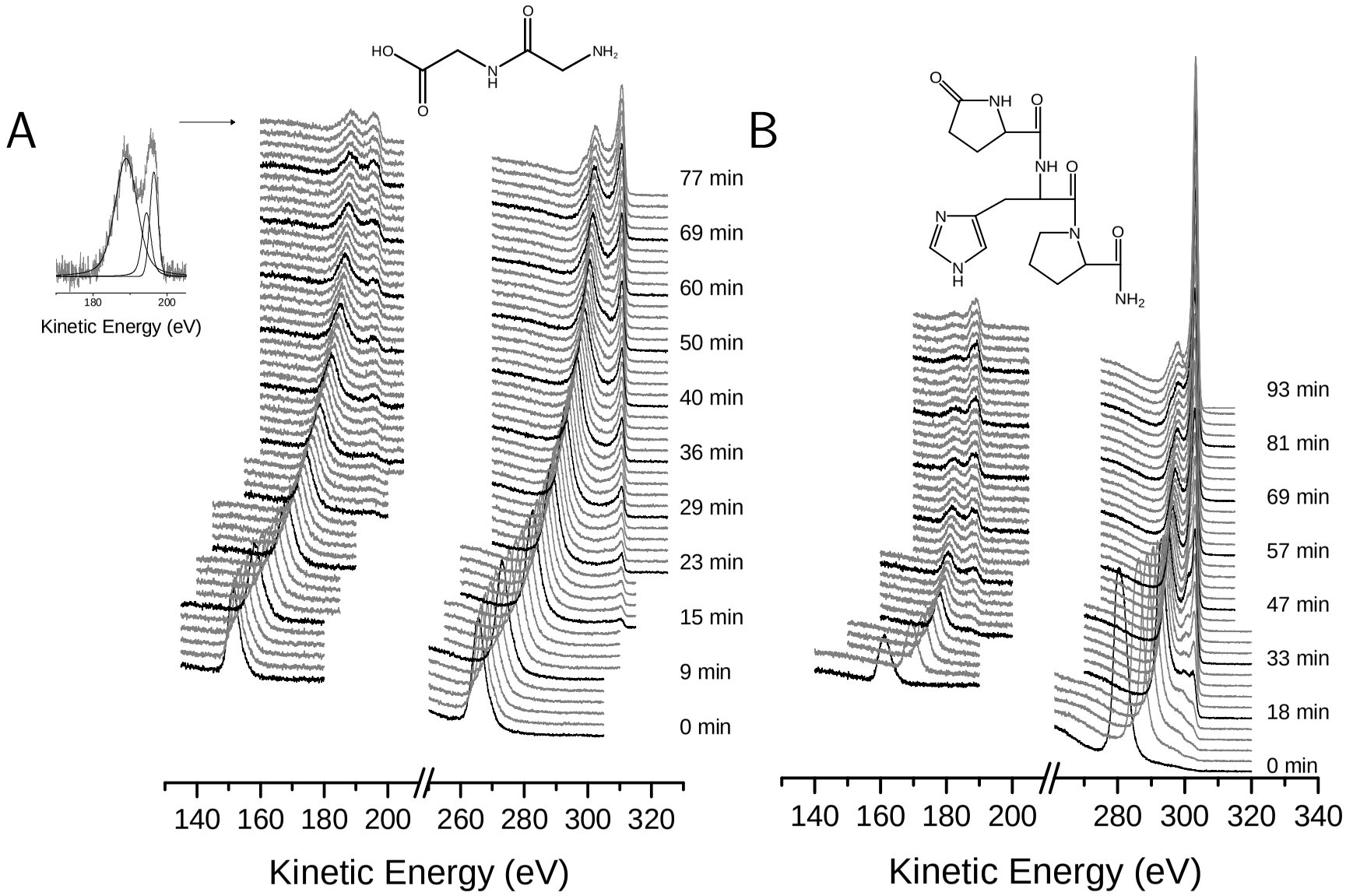

Fig. 4.3. X-ray photoemission spectra of glycyl-glycine (A) and pyroglutamyl-hisitidyl-proline amide (B) recorded consecutively at the original incident spot. All spectra recorded at 600 eV incident energy with slit openings of 50 μm. Nitrogen spectra at left, carbon at right. Plotted as kinetic energy to demonstrate charging changes over time.

same pattern observed in met and met-met (i.e., deprotonation of $-NH_3^+$ is only observed for the material from which charging has been lifted - see inset). The same pattern of C 1s changes is also observed, with charge lifting occurring on the original material, physical deterioration of the sample resulting in the development of a secondary set of compounds, and the development of chemical changes in both sets of compounds over time.

This contrasts with the data for arg (Figure 4.4), where the onset of charging is slower, and the appearance of secondary compounds is slow. Chemical changes of N are occurring; however, in this case, the deprotonation of $-NH_3^+$ is occurring in the original material (see inset). This indicates that different amino acids and peptides have vastly different degradation characteristics under soft X-ray irradiation.

Finally, two compounds were evaluated for which radiation damage was not observed in the evaluation of reference compounds (Leinweber et al., 2007). Figure 4.5 shows the time-resolved XPS for heterocyclic N-containing PZDA and heterocyclic N- and amine-containing guanine. For these compounds, physical degradation was slow, and chemical degradation was not observed over the course of the experiment. Indeed, amino acids are comparatively much more sensitive to soft X-ray irradiation than these heterocyclic and amine-containing compounds.

4.3.2 Time-scale degradation assessment

There exists concern that radiation damage occurs in XANES scans of peptides before the completion of the first spectral collection (Zubavichus et al., 2004a,b; Leinweber et al., 2007). In this study, met and met-met (Figure 4.1) are most sensitive to degradation, with quick formation of photodegradation products (< 10min) and the disappearance of original N-compounds within 30 min. These data show that this methylated thiol-containing amino acid is highly susceptible to radiation damage, and that the concern reported in Leinweber et al. (2007) that initial XANES scans of methionine may be damaged before its completion is justified. This contrasts the data of Zubavichus et al. (2004a), where the thiol-containing

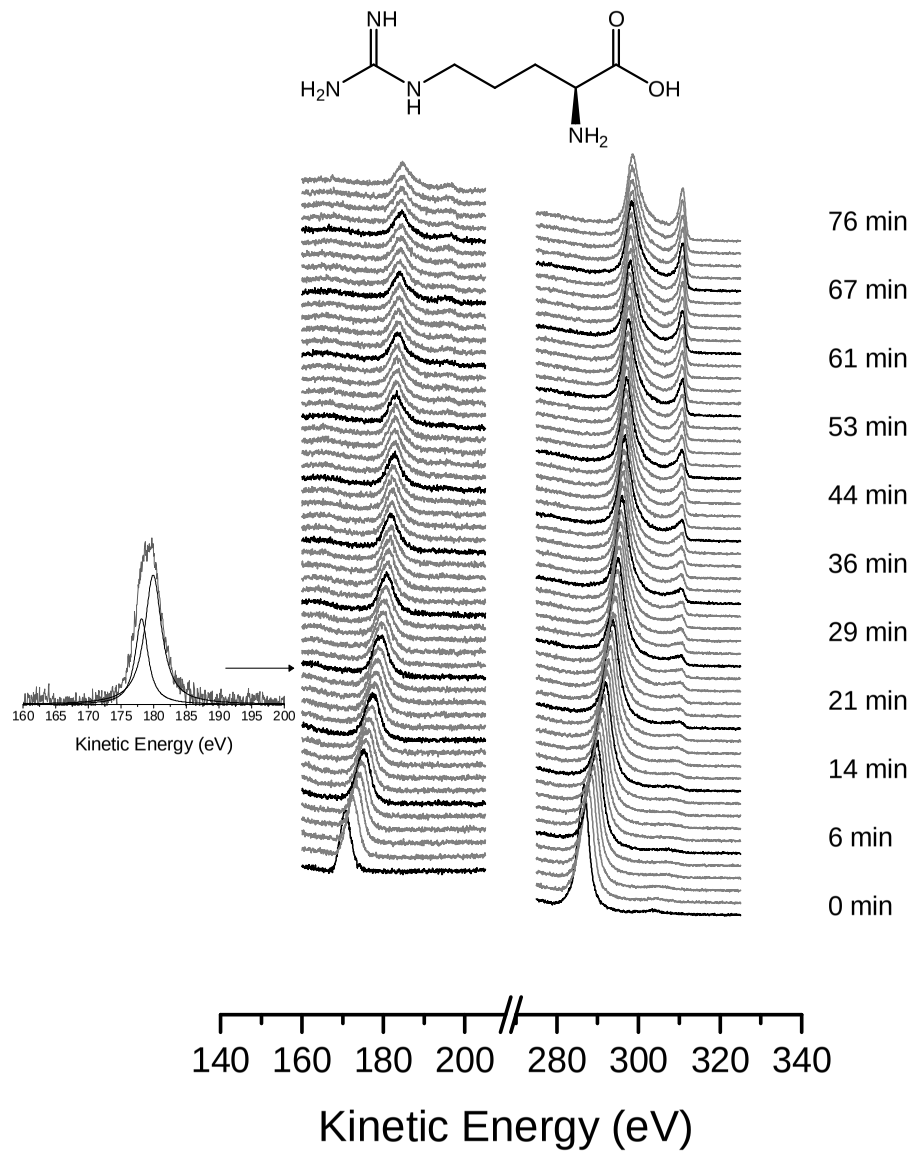

Fig. 4.4. X-ray photoemission spectra of arginine recorded consecutively at the original incident spot. All spectra recorded at 600 eV incident energy with slit openings of 50 μm. Nitrogen spectra at left, carbon at right. Plotted as kinetic energy to demonstrate charging changes over time.

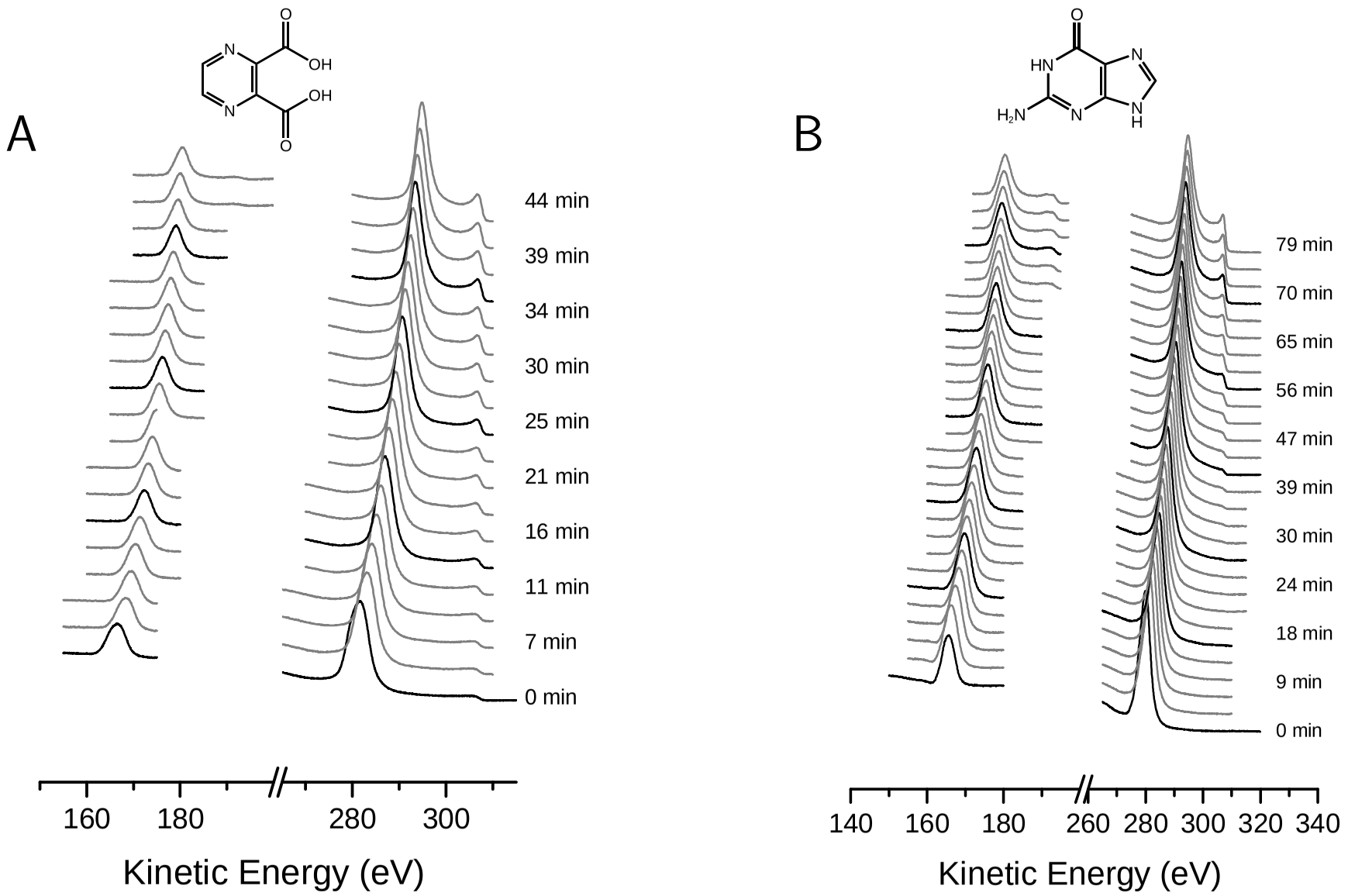

Fig. 4.5. X-ray photoemission spectra of 2,3-pyrazine dicarboxylic acid (A) and guanine (B) recorded consecutively at the original incident spot. All spectra recorded at 600 eV incident energy with slit openings of 50 μm. Nitrogen spectra at left, carbon at right. Plotted as kinetic energy to demonstrate charging changes over time.

cysteine is reported to be more stable than other functionalized amino acids (alanine, serine and aspartic acid). It is possible that demethylation of the methiol group occurred, and consequently led to a more reactive system.

Pyroglutamyl histidyl proline amide also displays rapid onset of degradation products, although not as quickly as for the met-containing compounds. This tripeptide contains histidine, which is also susceptible to beam damage (Zubavichus et al., 2005b). Glycyl-glycine and arginine are more stable, and are slow in their development of secondary compounds. As seen in other studies, this shows that functional group side chains of amino acids differ greatly in their susceptibility to damage by X-ray irradiation. In addition, there is a consistent difference between degradation products formed by simple peptides, where new carbon functionalities develop at slightly lower K_E, (i.e., peak 2 in Figure 4.2) which are absent in single amino acid scans. This lower K_E peak has been identified as the signal for N-C=O, which likely represents degradation products of the closely-related peptide bond.

Overall, it appears that the sensitivity of amino acids and peptides degradation under soft X-ray irradiation varies greatly, and that the most sensitive compounds (e.g., sulfur-containing met and met-met) degrade within the time-scale of a standard XANES scan. The other compounds are less sensitive, are stable beyond 7 min, and do not appear to be significantly changed within the first XANES scan. Caution must thus be exercised when performing experiments to minimize dose and exposure time, and to ensure that fresh spots are irradiated when multiple scans are desired from a single sample.

4.4 Conclusions

Quick, consecutive scans of amino acids and peptides show time (dose)-dependant changes in C and N functionality within minutes. Charging is evident on original material; however new compounds formed show no changes in charging. Chemical and physical changes can occur in the sample through beam exposure, and a bimodal series of compounds related to

their grounding status develops over time. Implications for XANES experiments are that beam damage is occurring over the time-scale of a standard undulator scan only for the most sensitive compounds. Less sensitive compounds do not appear to be damaged in the first scan; however multiple scans on the same spot will result in damage to amino acid and peptide material. Subsequent soil analyses using XANES will thus be carried out at a fresh sample spot for each scan.

Chapter 5

Landscape position and management regime affect the molecular composition of soil organic N and C

Abstract

Quantity and quality of soil organic N and C are strongly influenced by variations in landscape position and management practices such as cultivation. In this study, we used synchrotron-based N and C K-edge XANES spectroscopy and Py-FIMS to explore N and C chemistry between soils obtained from different landscape positions along a hummocky transect and from locations under different management practices. A distinct landscape pattern in SOM functionality was observed, but only a small effect of management (i.e., cultivated vs. uncultivated) was detected. Normally thought as labile, both carbohydrates and low molecular weight aromatics apparently were stabilized in divergent (i.e., water shedding) slope positions, while lipids were enriched in depressional areas. Tillage incorporation was likely responsible for the enrichment of older, microbially altered carbohydrates and lignins at divergent positions. A novel application of non-metric multidimensional scaling ordination to XANES data revealed increased heterocyclic-N with cultivation. XANES data also showed the presence of unique, oxidized N-bonded aromatics which predominated at calcareous shoulder slope positions. These types of organic N compounds are rarely reported in the literature except for samples obtained in acidic or anaerobic environments.

5.1 Introduction

Soil properties exhibit spatial variability across landscapes. For example, hummocky terrains typically show pronounced differences in soil characteristics at different topographic positions (Verity and Anderson, 1990). These differences have been linked to tillage-induced translocation of soils (Gregorich and Anderson, 1985; Pennock and Dejong, 1990; Pennock et al., 1994) and to water redistribution toward downslope positions (Verity and Anderson, 1990). Hummocky landscapes can be divided into landscape segments based on three-dimensional topographic data of gradient and curvature (Pennock et al., 1987, 1992; Pennock and Corre, 2001). Field locations which fit the criteria for a particular landscape element experience similar drainage regimes, and thus show similar soil properties. For example, landscape-scale elements have demonstrated control over such soil properties as organic C quantity (Landi et al., 2004), N mineralization (Walley et al., 1996), denitrification (Pennock et al., 1992; van Kessel et al., 1993) and microbial community composition (Ma et al., 2008). Land management also strongly affects this same range of soil properties (Breuer et al., 2006), with conversion of cultivated land to grassland or wetland areas having a significant impact on C and N dynamics (Bedard-Haughn et al., 2006; Breuer et al., 2006).

Soil organic N (SON) comprises approximately 90% of total N; however, up to half of organic N exists in forms that are either unknown or poorly understood (Bremner, 1965; Stevenson, 1982, 1994; Olk, 2008b). Microbial mineralization of organic N is a significant source of plant N uptake, and the rates of mineralization of different N-containing compounds are likely to vary. Understanding the relative contributions of different N-containing compounds to the overall composition of organic matter (OM) is thus important to understanding soil N cycling. Since landscape position and land use affect organic C and total N, they also may influence the composition of soil organic matter (SOM); however, we are unaware of studies specifically linking landscape position and management information with OM speciation.

Organic matter may be characterized spectroscopically using ^{13}C-and ^{15}N-solid-state cross-

polarization magic angle spinning nuclear magnetic resonance (CP-MAS-NMR, Baldock et al., 1992; Knicker et al., 1996; Simpson, 2001), and classified into functional groups based on spectral features corresponding to specific compound classes. Soil organic matter is also characterized using analytical pyrolysis coupled with mass spectrometry, where whole soils are thermally degraded in the absence of oxygen, and the volatilized monomeric products characterized using mass spectrometry (Balesdent and Mariotti, 1996; Schulten, 1996; Schulten and Schnitzer, 1998). A continuing debate surrounds the use of these techniques because of low sensitivity inherent to CP-MAS ^{15}N-NMR (Smernik and Baldock, 2005) and the possible formation of artifacts during pyrolysis of soils (Knicker and Lüdemann, 1995; Nierop and Van Bergen, 2002). Recently, the application of synchrotron-based X-ray absorption near-edge structure (XANES) spectroscopy has been explored as a sensitive method to assess the complex nature of C and N in soils (Myneni, 2002; Vairavamurthy and Wang, 2002; Jokic et al., 2004a; Leinweber et al., 2007). This technique uses monochromatic X-rays to select the binding energy of a specific element, and probes the electron structure of that particular element in the sample. Slight differences in the X-ray absorptivity between the various binding arrangements of N and C can be used to fingerprint the overall chemical bonding environment in a soil sample. In this way, XANES may be a valuable tool for the characterization of soil N and C.

In this study, we use synchrotron-based N and C K-edge XANES and pyrolysis field-ionization mass spectrometry (Py-FIMS) to compare N and C functionalities among soils obtained from a cultivated hummocky landscape and from adjacent uncultivated areas. We also explore the use of multivariate ordination to gain insight into dominant trends influenced by landscape and site management and to visualize differences between the SOM composition of these soils.

5.2 Materials and Methods

5.2.1 Study materials

Soils were collected from distinct landscape positions in a hummocky toposequence located at the St. Denis National Wildlife Area, (SDNWA - 52°12′ N, 106°5′ W) *ca.* 40 km east of Saskatoon, SK. This research site was established and characterized as a component of another research program, and is described in detail in Yates et al. (2006). Briefly, this site is located in the Dark Brown soil zone on a hummocky till terrain with a relative elevation difference of *ca.* 5.5 m and slopes ranging from 10 to 15%. The parent material comprises a mixture of glacio-lacustrine sediments and unsorted calcareous till, with soil textures ranging from loam at the highest elevations to silt loams in depressional positions. Samples were collected from a continuously cultivated area (57+ yr, Leinweber et al., 2009) encompassing a range of landform elements, which were initially classified using topographic data processed by algorithms described in Pennock et al. (1987, 1992). Samples from uncultivated wetland areas within the SDNWA, from unbroken native grassland (N1) and from 20 yr bromgrass (B1) sites immediately adjacent to the research area were also collected. Samples were obtained from the 0 to 15 cm depth and stored at -20 °C until analysis. The total C and total N contents were determined by the combustion method using a LECO CNS-2000; organic C was determined using a LECO Carbonator model CR-12 at 840 °C (Wang and Anderson, 1998). Particle size analysis was performed using the hydrometer method as described by Kroetsch and Wang (2008) after sample pretreatment with $1M$ HCl to remove carbonates and with 30% hydrogen peroxide (H_2O_2) to remove organic matter. Basic soil characteristics are reported in Figure 5.1.

5.2.2 C and N *K*-edge XANES

Soils were air-dried and pulverized using a ball-mill; subsamples (*ca.* 1 mg) were pressed onto freshly scraped indium metal (Sigma-Aldrich, Mississauga, ON, Canada) that was

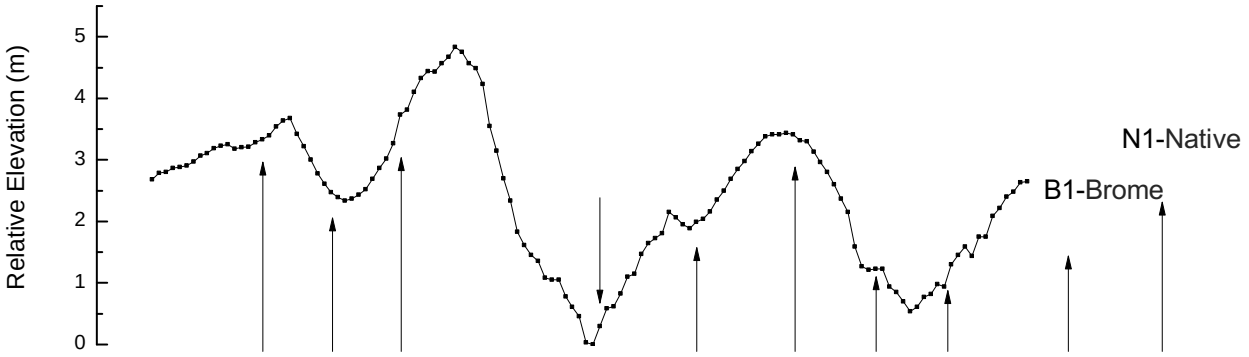

		17	27	37	66	80	94	106	116	B1	N1
Desc.		DSH †	CFS	DBS	LFS	LFS	DSH	Wet	Wet	LBr	LNat
OC‡	$g \cdot kg^{-1}$	15.14	23.41	9.81	23.69	31.55	8.47	28.92	25.52	28.72	22.08
TotC	|	17.70	26.05	27.13	26.37	33.87	37.63	30.50	26.70	30.13	23.57
TotN	|	1.87	2.67	0.93	2.62	3.53	0.82	3.11	2.74	3.03	2.46
OC/N	-	8.05	8.75	8.17	9.03	8.94	7.48	9.29	9.32	9.49	8.99
Sand	%	41.8	35.2	56.9	48.0	40.3	55.4	37.5	45.0	51.4	49.5
Silt	|	41.1	49.5	17.2	34.4	45.7	23.1	47.7	42.8	32.2	39.3
Clay	|	17.1	15.3	25.9	17.6	13.9	21.6	14.9	12.2	16.4	11.2
Class		L §	L	SCL	L	L	SCL	L	L	L	L

†DSH - Divergent Shoulder; CFS - Convergent Footslope; DBS - Divergent Backslope; LFS - Level Footslope; Wet - Wetland; LBr - Level Bromegrass; LNat - Level Native Prairie
‡OC = organic carbon
§L - Loam; SCL - Sandy Clay Loam

Fig. 5.1. Elevation plot, landform descriptions and agronomic characteristics of soils from St. Denis site.

affixed to a steel sample disc using double-sided conductive carbon tape (SGE, Toronto, ON, Canada). Carbon and N K-edge XANES spectra were collected using the Spherical Grating Monochromator (SGM) beamline 11ID-1 at the Canadian Light Source (CLS), Saskatoon, SK, Canada. At the time of the experiment, this beamline delivered 10^{11} photons s^{-1} at the N K-edge with a resolving power (E/ΔE) better than 10,000 (Regier et al., 2007a,b). The exit slit was set at 50 μm and fluorescence yield (FLY) data and total electron yield (TEY) were collected simultaneously. A two stage microchannel plate detector was used to collect FLY data, and TEY was determined by measuring the drain current from the sample.

For calibration at the N K-edge, an absorption spectrum for N_2 was measured using ammonium sulfate as described in Chapter 3. The vibrational manifold of the N 1s $\rightarrow \pi^*$

transition has an energy of 400.8 eV for the $\nu = 0$ peak. Assignment of the N spectral features to N functions was based on published analysis of reference compounds (Leinweber et al., 2007). For calibration at the C K-edge, a solid-state absorption spectrum for glutaric acid (dicarboxylic acid) was measured. The C 1s $\rightarrow \pi^*_{C=O}$ transition has an energy of 288.6 eV (Kim et al., 2003). Carbon spectra were processed using a double normalization technique. First, the difference was calculated between the raw C sample spectrum and a reference spectrum from a freshly sputtered gold surface after matching the pre-edge curvatures by adjusting the gain and offset of the sample spectrum. Second, normalization to the incident flux (I_0) to account for attenuation of the photon beam by C on the optical components was carried out using a spectrum obtained from a freshly-evaporated gold mesh positioned upstream from the sample chamber. Carbon features were assigned based on a review of the literature (Myneni, 2002; Urquhart and Ade, 2002; Hardie et al., 2007).

Data processing was performed using the aXis 2000 (Hitchcock et al., 2005) and Athena (Ver. 0.8.050, Ravel and Newville, 2005) software packages. Data for N and C K-edges were averaged from a minimum of two scans, and background corrected by a linear regression fit through the pre-edge region followed by normalization to an edge step of one.

5.2.3 Py-FIMS

Soils were dried, pulverized with a mortar and pestle, transferred to quartz capsules and pyrolyzed at temperatures ranging from 110 °C to 700 °C in steps of 20 °C in the direct inlet of a Finnigan MAT 731 mass spectrometer (Finnigan MAT, Bremen, Germany). Over the full temperature range, 91 scans were recorded for masses ranging from 15 to 900 m/z, and ion intensities were normalized on a sample weight basis (i.e., ion counts per mg soil). These were combined to produce a single thermogram of total ion intensity (TII) and a single summed and averaged mass spectrum. A detailed description of the Py-FIMS method and the statistical treatment of TII and weight normalization is given by Sorge et al. (1993a).

5.2.4 Data handling

Differences between soils were explored using non-metric multidimensional scaling (NMS) ordination using PC-ORD (ver. 5.10). NMS is an ordination method suitable for ecological data because it does not rely on assumptions of normality or linear relationships between variables (McCune et al., 2002). X-ray absorption data used in NMS were generated by deconvoluting normalized spectra using fityk (http://www.unipress.waw.pl/fityk/, ver. 0.8.6). After fitting a background arctan function (parameterized as: $f(x) = a1 \times \arctan((x - a2) \times a3) + a4$; Rovezzi et al., 2009), a series of Lorentzian curves were fitted to the spectral features. Nitrogen XANES spectra were fitted with six curves corresponding to pyridines, nitrilic and aromatic N in 5-membered rings (pyrazolic), proteins, pyrroles, N-bonded aromatics and aliphatic/sigma features. Carbon XANES curves were fitted with eight curves corresponding to aromatic, substituted aromatic, aliphatic, amide, carboxylic, carbohydrate, carbonate and sigma features. While included in the fitting procedure, inorganic C (carbonate) features were not included in the ordination analysis. NMS ordinations using Sorenson (Bray-Curtis) distance measures were performed using integrated variable area counts in the first matrix. The second matrix, which generates vectors showing relationships between variables and ordination scores, contained these same area counts, plus additional topographic data (gradient, profile, specific dispersal area, specific catchment area), and soil characterization data (total C, total N, total organic C).

The Py-FIMS data were also subjected to NMS ordination; however, Py-FIMS data were first explored using Wilks' lambda feature selection. The Wilks' lambda scores (F-statistics comparing the variance within specific landscape positions to the overall variance) were calculated for each individual m/z normalized to TII. For this dataset, 80% of m/z had Wilks' lambda scores which were significant ($p \leq 0.05$). All m/z were therefore retained for visualization using NMS, and the top 100 m/z were retained for analysis of variance (ANOVA) to determine significant position effects. ANOVA and Wilks' lambda calculations were performed using SPSS (ver. 16.0).

5.3 Results

5.3.1 XANES

Carbon K-edge spectra for the St. Denis soils are presented in Figure 5.2. Resonances corresponding to C types have been identified (Myneni, 2002; Urquhart and Ade, 2002; Hardie et al., 2007) as: (1) aromatic C at 285.2 eV; (2) N-substituted aromatic at 286.8 eV; (3) phenolic at 287.1 eV; (4) aliphatic at 287.5 eV; (5) amide at 288.1 eV; (6) carboxylic at 288.6 eV; (7) carbohydrate hydroxyl at 289.6 eV; and (8) carbonate at 290.5 eV.

Inorganic carbonate signals predominated in the divergent position soils (Figure 5.2). This was expected because these soils were derived from calcareous parent material and upper slope positions experience reduced water infiltration and leaching. Aromatic C signals were consistent in the convergent, level and footslope positions, except for in the native soil, where aromatic C showed a weak signal. In the divergent soil spectra, the aromatic peak varied greatly. All soils displayed strong carboxylic peaks at *ca.* 288.6 eV. A feature representing amide carbon occured as a shoulder at *ca.* 288.1 eV, and was more prominent in the uncultivated (wetland, bromegrass, and native) samples. Substituted aromatic peaks at *ca.* 287.1 eV were consistent among the level and convergent soils, and showed weaker signals in the divergent and wetland soils. The aliphatic signal at *ca.* 287.5 eV did not show a consistent relationship with respect to landscape position.

Nitrogen K-edge spectra for the St. Denis soils are presented in Figure 5.3. The dominant features of the N K-edge spectra include: (1) aromatic N in 6-membered rings (pyridines, pyrazines) at 398.7 eV, (2) nitrilic, and aromatic N in 5-membered rings (pyrazolic) at 400.0 eV, (3) amide (protein) at 401.1 eV, (4) inorganic nitrite at 401.7 eV, (5) N with unpaired electrons in 5-membered rings (pyrrolic) at 402.5 eV, (6) N-bonded aromatic at 403.5 eV, (7) inorganic nitrate at 405.8 eV, and (8) alkyl-N and the 1s$\rightarrow \sigma^*$ transition at 406.2 eV.

The types and amounts of N in whole soils showed strong patterns related to landscape position and management. Most notably, divergent position, native prairie, and level position

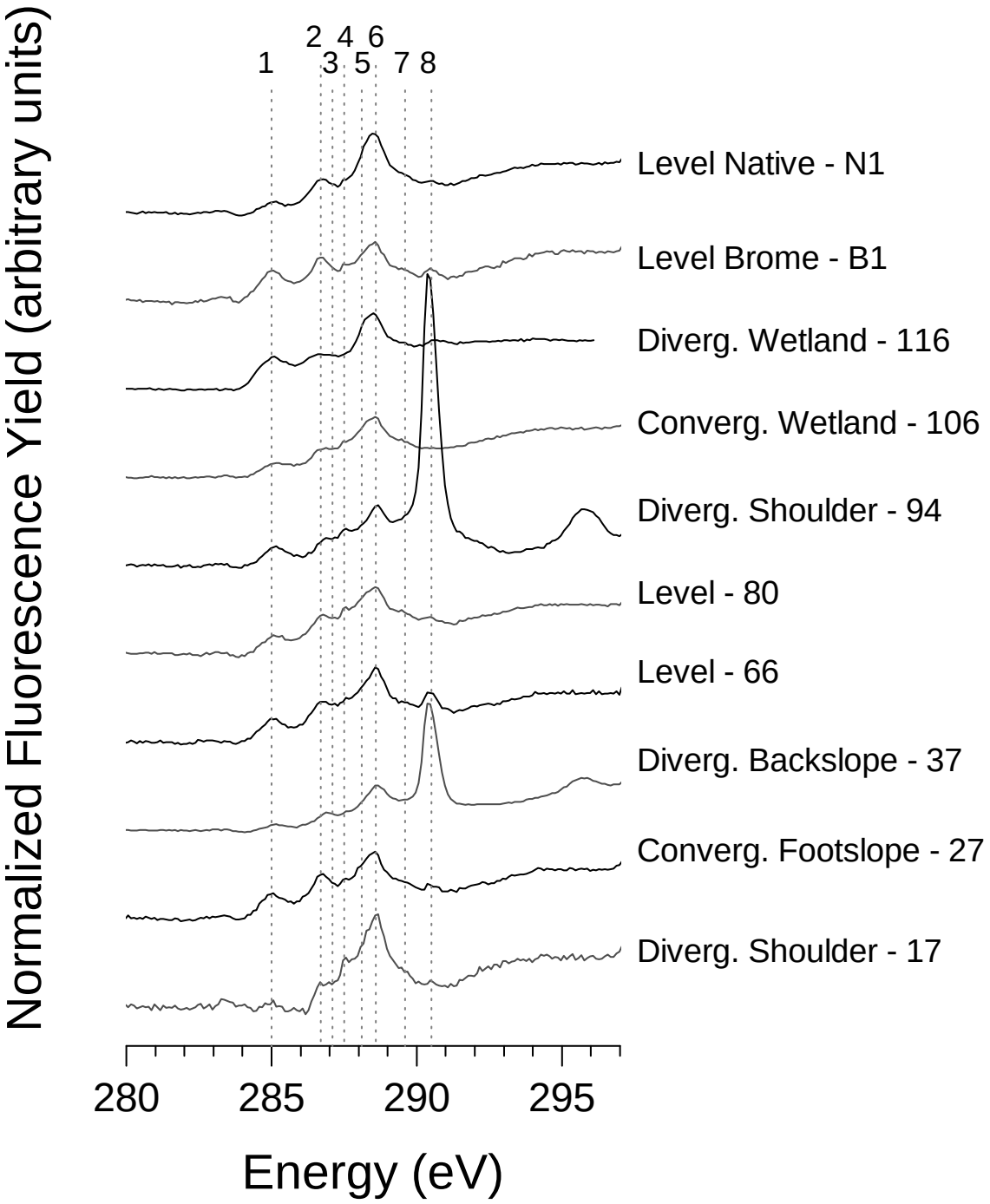

Fig. 5.2. Normalized fluorescence yield of C *K*-edge XANES scans of soils obtained from St. Denis National Wildlife Area. Features numbered as: (1) 285.2 eV, aromatic; (2) 286.8 eV, N-substituted aromatic; (3) 287.1 eV, phenolic; (4) 287.5 eV, aliphatic; (5) 288.1 eV, amide; (6) 288.6 eV, carboxylic; (7) 289.6 eV, carbohydrate hydroxyl; and (8) 290.5 eV, carbonate.

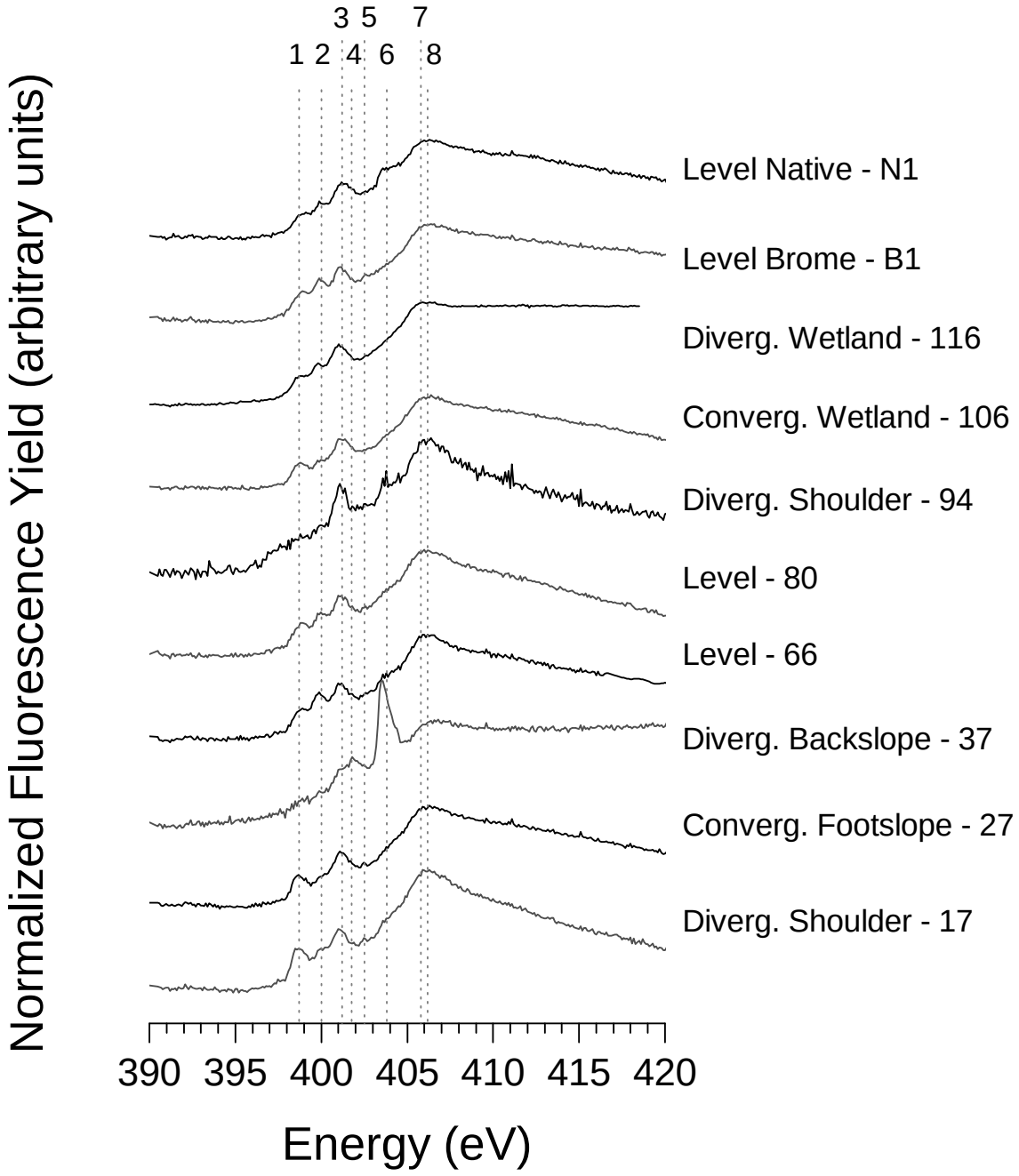

Fig. 5.3. Normalized fluorescence yield of N *K*-edge XANES scans of soils obtained from St. Denis National Wildlife Area. Features numbered as: (1) 398.7 eV: aromatic N in 6-membered rings (pyridines, pyrazines); (2) 400.0 eV: nitrilic & aromatic N in 5-membered rings (pyrazolic); (3) 401.1 eV: amide (protein); (4) 401.7 eV: inorganic nitrite; (5) 402.5 eV: N with unpaired electrons in 5-membered rings (pyrrolic); (6) 403.5 eV: N-bonded aromatic; (7) 405.8 eV: inorganic nitrate; and (8) 406.2 eV: alkyl-N and the 1s$\rightarrow \sigma^*$ feature.

soils showed nitroaromatic and anilide functionalities. These N-bonded aromatics are not widely discussed in the literature, and have been reported only for anaerobic or acidic soils (Stevenson, 1994; Schmidt-Rohr et al., 2004; Olk et al., 2006; Schmidt and Matzner, 2009). The N-bonded aromatic functionality was expressed to a lesser degree in soils from other positions or management types. Pyridinic and pyrrolic functionalities were evident in the spectra for all soils except those from the divergent positions. All soils also showed strong signals for amide-N, which is in consensus with many studies reporting that amide-N is the predominant form of organic N in soils (Stevenson, 1982; Schulten and Schnitzer, 1998; Kögel-Knabner, 2006; Olk, 2008b).

Multivariate ordination methods allowed the visualization and comparison of treatment effect (in this case, landscape position and land use) through an ordination plot, and extracts factors that have the largest influence on the distribution of the points in the ordination. Variables for multivariate analysis were obtained by curve fitting to the normalized C and N K-edge XANES spectra (Figure 5.4). NMS ordinations generated from the area counts corresponding to C XANES are presented in Figure 5.5. Both axes combined to explain 91% of the variation in the data, and the stress value of 12.283 indicates an acceptable ordination has been achieved (i.e., < 20, McCune et al., 2002). Clustering was observed among the divergent soils, the level soils, and the wetland/convergent soils. Uncultivated bromegrass and native prairie, however, did not separate from the cultivated level soils. This indicates that soil organic C composition, as observed using XANES, is predominantly influenced by terrain and hydrology and less by land use. Vectors overlaid on the ordination plots represent the strength and direction of correlation between variables and the ordination distribution. Variables that were correlated with the ordination with $r^2 \geq 0.4$ were total organic C, carbohydrate content, sigma-type features, whereas substituted aromatic compounds were correlated at $r^2 = 0.25$. Carbohydrate content increased in soils moving downslope, along with total C. Sigma features, though important in discriminating between organic matter content of these different soils, are difficult to assign. That is, sigma features are poorly understood, and in

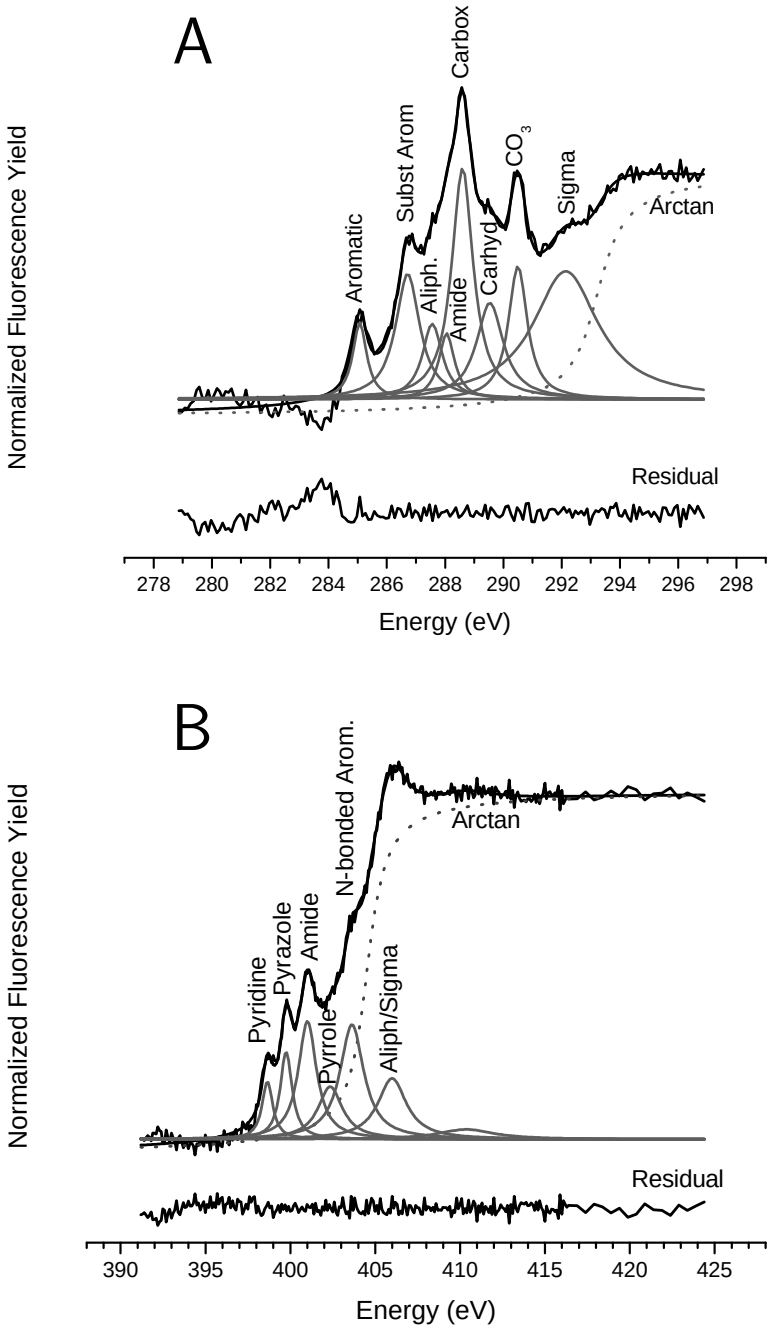

Fig. 5.4. Representative deconvolutions of (A) C *K*-edge XANES spectra and (B) N *K*-edge XANES spectra used in non-metric multidimensional scaling analysis. Original spectra, from soil 66 in Figures 5.2 and 5.3, were further processed to yield a flat post-edge region for proper arctan fitting.

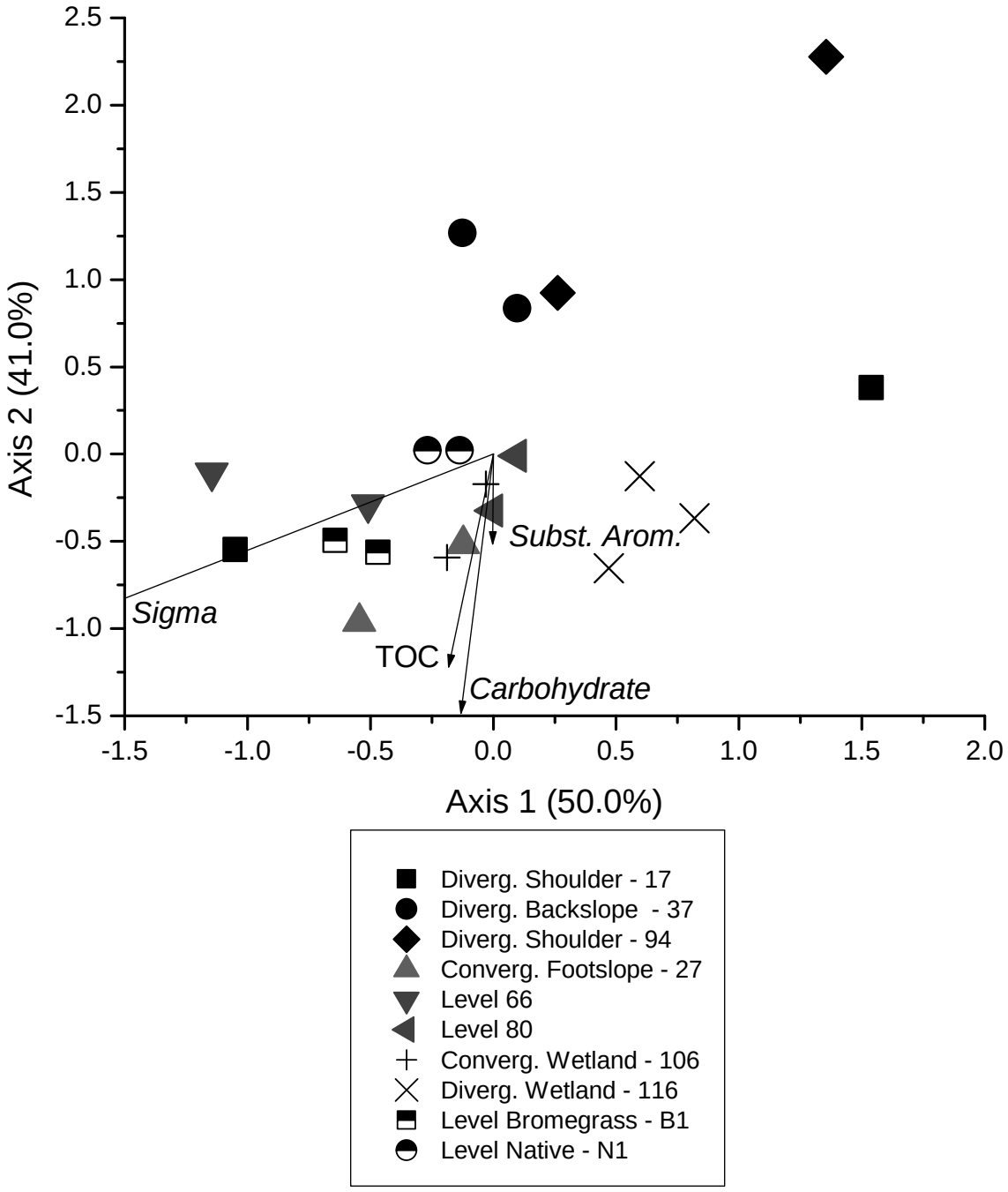

Fig. 5.5. Non-metric multidimensional scaling analysis of C *K*-edge XANES features from soils obtained across landscape elements. Multidimensional analysis performed using peak areas from deconvoluted XANES spectra. Vectors correspond to environmental factors which correlate with ordination at $r^2 > 0.40$, except substituted aromatic vector, which correlates at r^2=0.25. Peaks included in ordination were: aromatic (285 eV), N-substituted aromatic (286.8 eV), aliphatic (287.5 eV), amide (288.1 eV), carboxylic (288.6 eV), carbohydrate hydroxyl (289.6 eV), and 1s$\rightarrow \sigma$* feature (292.5 eV).

complex samples such as soil, a wide variety of compounds contribute to this feature (Stöhr, 1992).

Examining the ordination plots for the XANES N functionalities (Figure 5.6), there was also strong clustering among the soils recovered from similar landscape positions. The stress value for this ordination is 9.513, indicating that an acceptable distribution of the data had been achieved (i.e., < 20, McCune et al., 2002), and the two axes accounted for 95.4% of the total variation in the data. Similar to the ordination for the C data, soils from divergent positions clustered together, as did the soils from wetlands and convergent slope positions. Also, as with the C data, bromegrass and native grass management areas clustered with their cultivated level slope counterparts, indicating that landscape position had a stronger controlling effect on organic N composition than did management. Unlike the C ordination, many of the variables contributed significantly ($r^2 \geq 0.40$) to the distribution of points in the ordination. N-bonded aromatics were most prominent in the divergent soils, and decreased in prominence from the level to the wetland soils.

5.3.2 Py-FIMS

The mass spectra and thermograms of total ion intensity from the Py-FIMS analyses of transect soils are presented in Figures 5.7 to 5.9. These spectra were dominated by signals identified as carbohydrates (m/z 82, 96, 110), peptides (m/z 58, 67, 70), phenols and lignin monomers (m/z 124, 150, 194, 208, 210), and a homologous series of alkenes (m/z 252, 266, 280, 294, 308, 322, 336, 350). Py-FIMS spectra can be evaluated by grouping characteristic biomarker m/z signals into compound classes (Schulten, 1996), and subsequently subjected to ANOVA. The results of this compound class evaluation are shown in Table 5.1. Divergent position soils had the highest relative abundance of carbohydrates and peptides, while the depressional positions had the highest relative amounts of lignin dimers, lipids, sterols and suberins. Thermograms plot the amount of thermally volatilized material against pyrolysis temperature, and provide an assessment of organic matter chemical stability and biodegra-

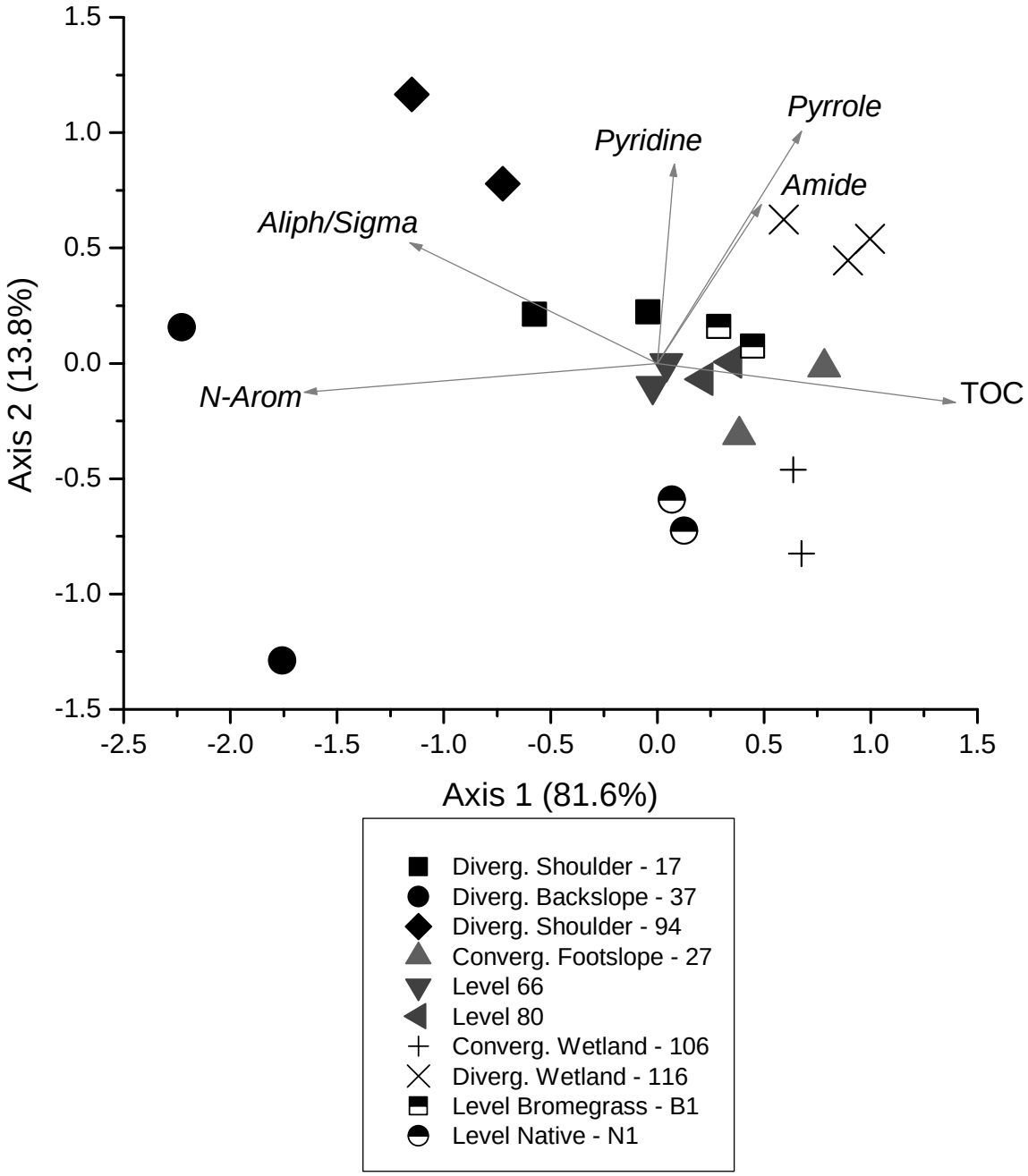

Fig. 5.6. Non-metric multidimensional scaling analysis of N *K*-edge XANES features from soils obtained across landscape elements. Multidimensional analysis performed using peak areas from deconvoluted XANES spectra. Vectors correspond to environmental factors which correlate with ordination at $r^2 > 0.40$. Peaks included in ordination were: pyridinic-N (398.7 eV), nitrilic & aromatic N in 5-membered rings (pyrazolic) (400.0 eV), amide (401.1 eV), pyrrolic (402.5 eV), N-bonded aromatic (403.5 eV), and alkyl-N and the 1s→ σ* feature (406.2 eV).

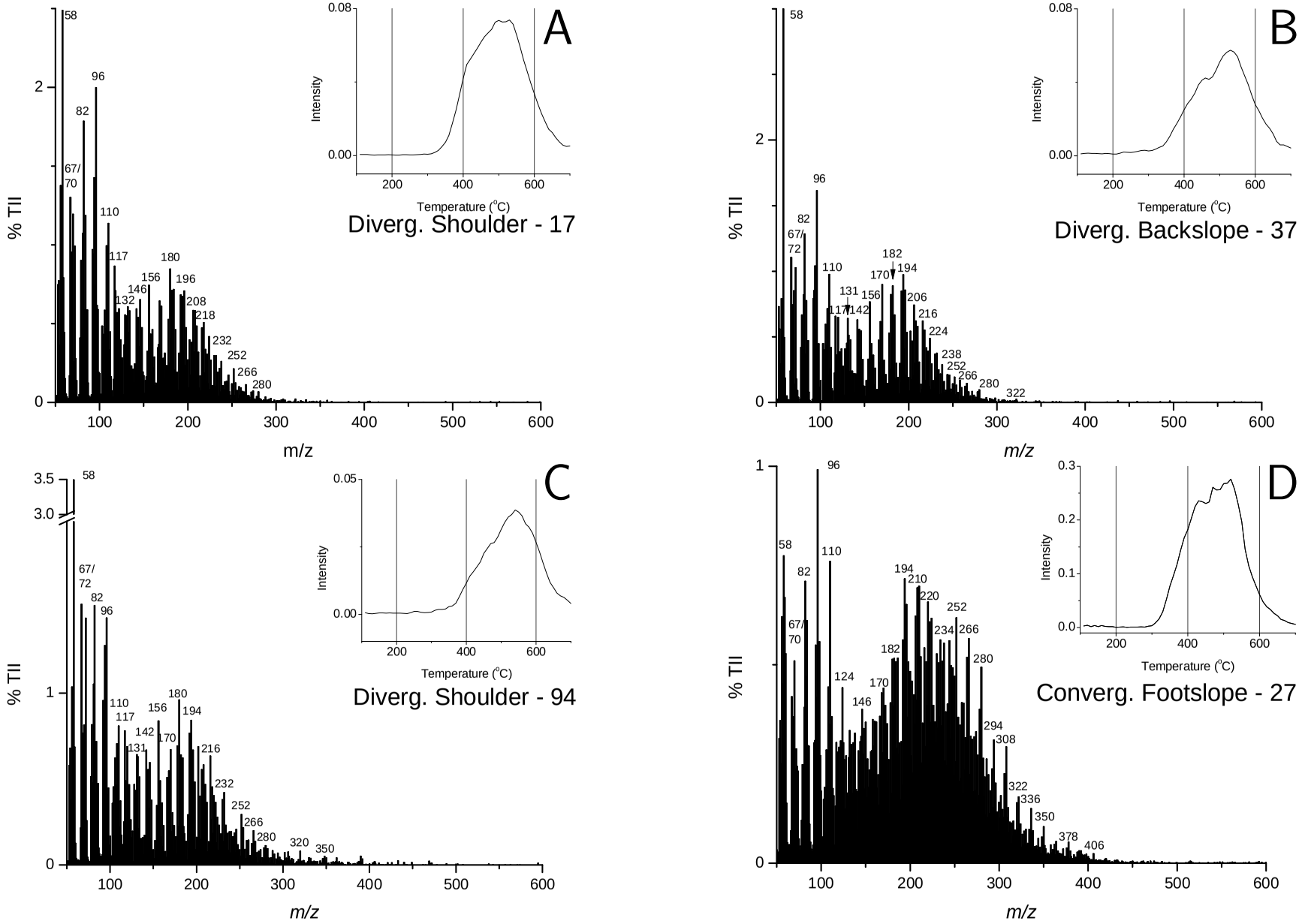

Fig. 5.7. **Summed and averaged pyrolysis field ionization mass spectra and thermograms of total ion intensity (TII, upper right) of divergent and convergent soils obtained across landscape elements.**

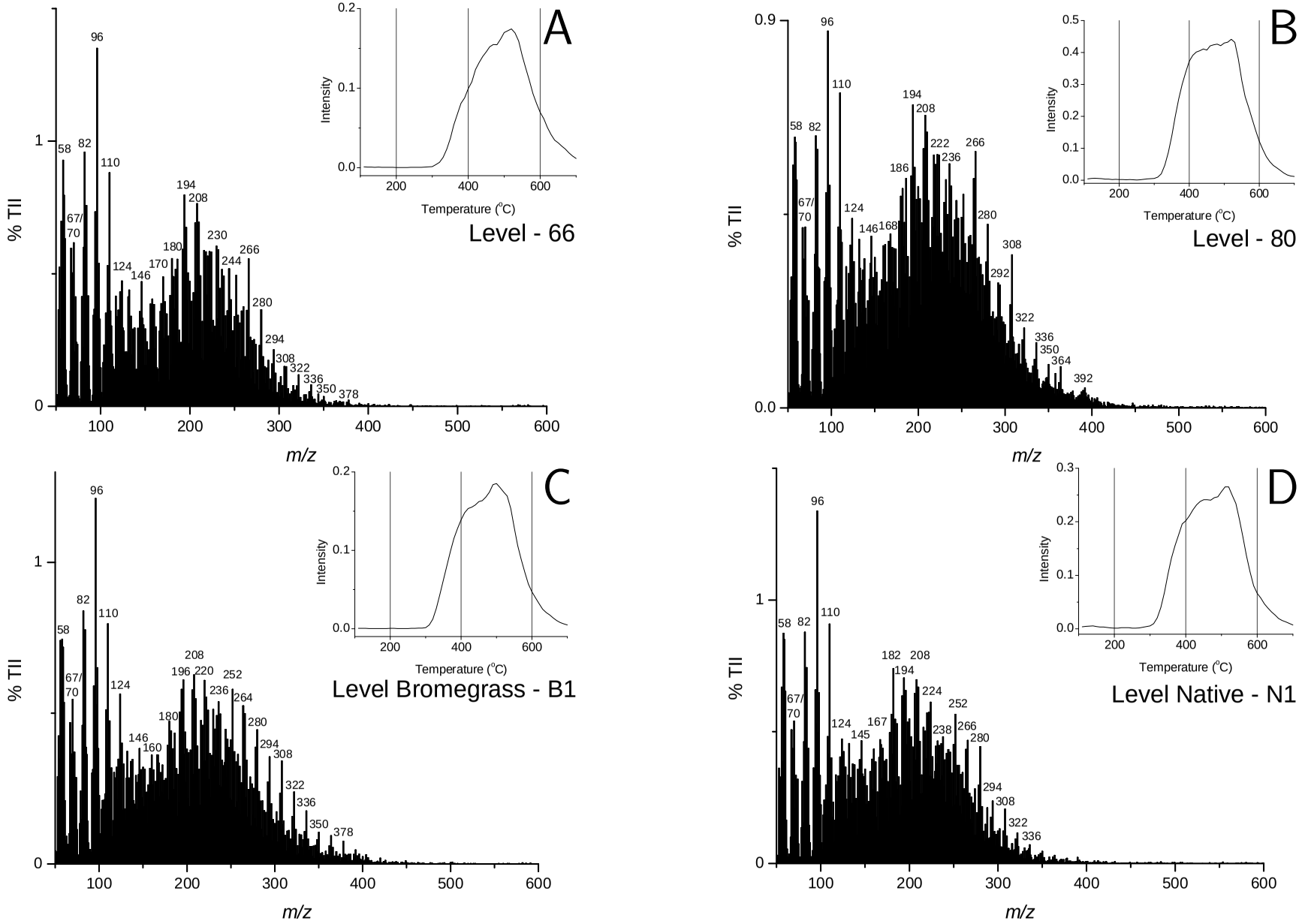

Fig. 5.8. Summed and averaged pyrolysis field ionization mass spectra and thermograms of total ion intensity (TII, upper right) of level cultivated and uncultivated soils obtained across landscape elements.

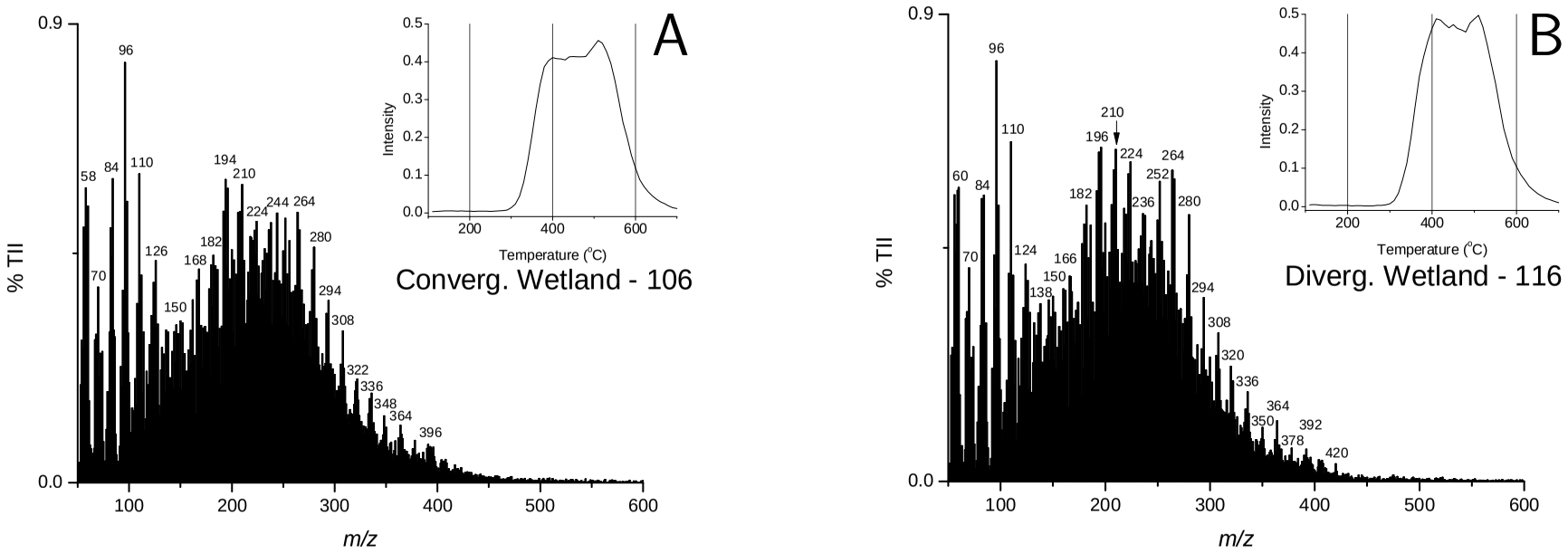

Fig. 5.9. Summed and averaged pyrolysis field ionization mass spectra and thermograms of total ion intensity (TII, upper right) of wetland soils obtained across landscape elements.

Table 5.1. Compound class groupings of marker signals from pyrolysis field-ionization mass spectrometry (Py-FIMS) of soils from St. Denis site.

Loc	Landform	Carb	Phen Lignin	Lignin Dimer	Lipid	Alkyl Arom.	N-Hetero	Sterol	Pept.	Subrn	Volat Mtl
		% Total Ion Intensity (TII)									%
17	Divergent Shoulder	10.4a†	11.6	0.5d	1.7b	10.5	8.9	0.0d	5.5a	0.0b	10.3ab
27	Convergent Footslope	6.2bcd	9.6	3.5abc	4.8a	10.3	7.8	0.3bcd	3.6b	0.0b	13.4a
37	Divergent Backslope	8.4abc	11.3	0.6d	2.2b	11.1	7.3	0.0d	3.9ab	0.0b	8.1b
66	Level Footslope	7.4bcd	9.9	2.4c	4.0a	10.1	8.2	0.1cd	4.1ab	0.0b	10.6ab
80	Level Footslope	6.1cd	9.5	3.7ab	4.9a	9.8	8.3	0.4bc	3.7b	0.0b	9.9ab
94	Divergent Shoulder	8.6ab	10.8	0.9d	2.5b	11.0	8.0	0.1cd	4.1ab	0.0b	8.1b
106	Convergent Wetland	5.9cd	8.5	3.8ab	5.4a	9.2	7.4	0.6a	3.5b	0.1a	10.9ab
116	Divergent Wetland	5.9d	9.3	3.9a	5.1a	9.6	8.0	0.5ab	3.5b	0.1b	9.3ab
B1	Brome Level Footslope	7.3bcd	9.2	3.2abc	4.4a	9.2	8.1	0.3bc	4.5ab	0.0b	13.0ab
N1	Native Level Footslope	7.8bcd	10.5	2.6bc	3.8a	10.2	8.8	0.1cd	4.2ab	0.0b	9.1ab

†Values with same letter are not significantly different at $p \leq 0.05$

dation potential (Schulten and Leinweber, 1999; Leinweber et al., 2009). Thermograms with peaks at higher temperatures thus indicate soils with a higher OM stability. The thermograms, plotted as insets in Figures 5.7 to 5.9, show mono-, di-, and multimodal peaks. Thermograms for divergent slope soils yielded curves with single peaks between *ca.* 500 °C and 600 °C (Figure 5.7A,B,C). Level cultivated and uncultivated soils also showed intense peaks at *ca.* 500 °C, and also showed a smaller peak at *ca.* 400 °C (Figure 5.7D and Figure 5.8A through D). Wetland soils produced multimodal thermograms, with strong peaks at *ca.* 400 °C and 500 °C (Figure 5.9A and B). This indicates that landscape position influenced the stability of organic matter, with increasing stability displayed at divergent landscape positions. Thermograms for the carbohydrate compound class were obtained by plotting the summed and averaged carbohydrate *m/z* signals (Figure 5.10). The thermogram onset temperatures at the divergent positions were higher and showed a single principal volatilization peak at a higher temperature (*ca.* 525 °C) whereas the predominant volatilization temperature at the convergent, level and depressional positions peaks were at a lower pyrolysis temperature (*ca.* 350-375 °C).

The extent of carbohydrate and lignin degradation at different landscape positions was estimated using product:substrate ratios for hemicellulose and vanillin. Biomarkers corresponding to *m/z* for xylose (a hemicellulose monomer, *m/z* 132), xylan (a hemicellulose polymer, *m/z* 114), vanillic acid (a lignin metabolite, *m/z* 168) and for vanillin (a lignin monomer, *m/z* 152) were extracted from the Py-FIMS spectra. Product:substrate ratios (i.e., xylose:xylan and vanillic acid:vanillin) are plotted in Figure 5.11, where increasing transformation of carbohydrates and lignins has occurred in samples lying at larger values in the X and Y axes. Convergent, level, and depressional positions showed relatively lower ratios of product compared to divergent positions, meaning that carbohydrates and lignins are preserved in their original form at depressions, but are increasingly depolymerized/oxidized at the slope tops.

Multivariate ordination feature selection was carried out to determine the marker signals

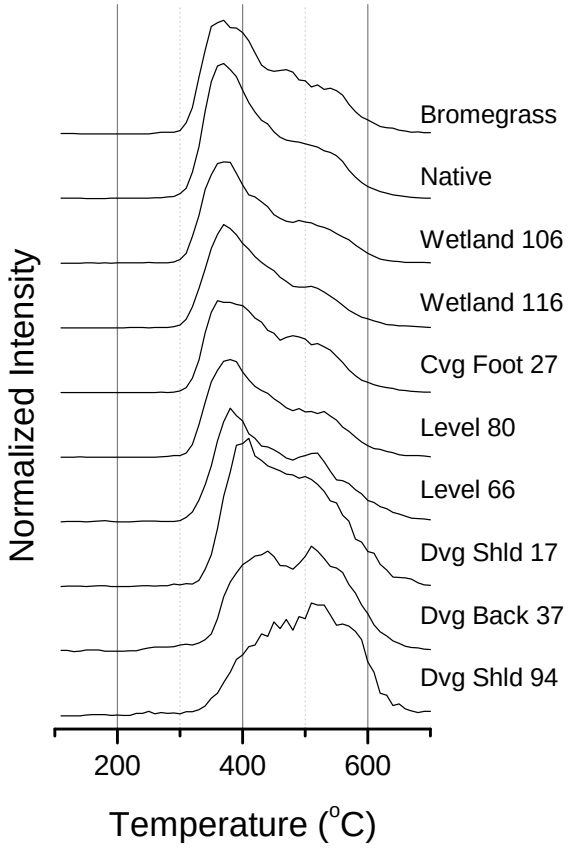

Fig. 5.10. **Pyrolysis thermograms of carbohydrate compound class from St. Denis soils. Peaks at higher temperatures indicate higher thermal stability.**

that contribute the most to inter-sample variability. For this study, almost all the signals showed significant Wilks'-lambda scores, and so all were included in the ordination analysis. Figure 5.12 shows the NMS ordination for all signals between m/z 55-500. Soils from similar landforms cluster together, indicating similar patterns of marker signals in the organic matter from these locations. For this analysis, data for the compound classes defined by Schulten (1996) were included for the joint plot analysis (i.e., included in the second matrix for the ordination analysis). The vectors showed correlations between lower molecular weight classes of carbohydrates, phenols/lignin monomers and alkylaromatics with the divergent positions, and correlations between higher molecular weight classes of lipids, sterols and lignin dimers with the higher TOC-containing soils from level and depressional landscape positions.

Because most m/z biomarkers had significant Wilks' lambda scores, identification of most

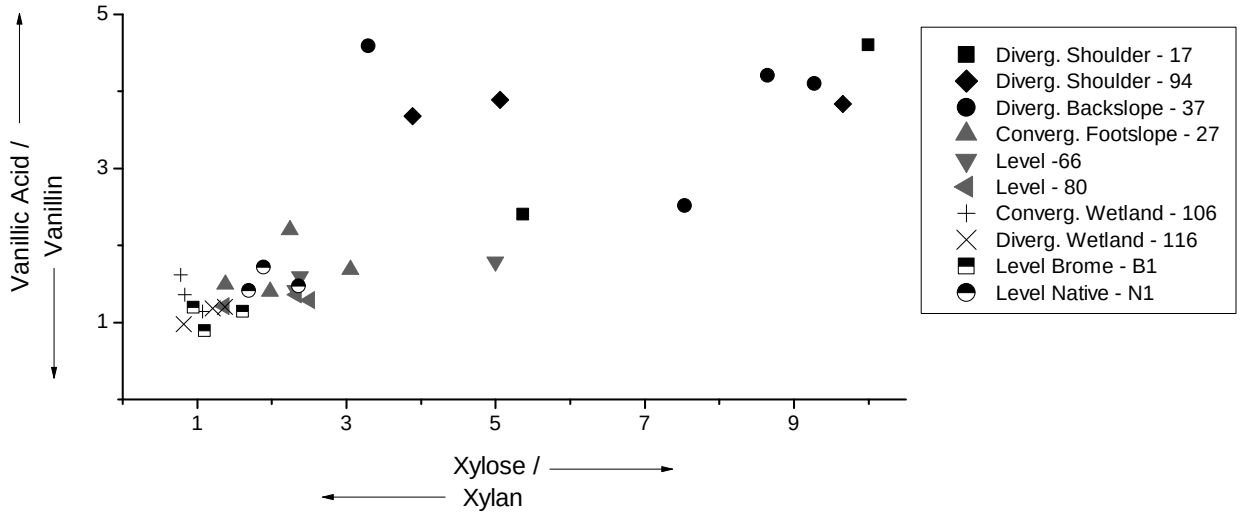

Fig. 5.11. **Fungal depolymerization of carbohydrates and lignins demonstrated using *m/z* signals extracted from Py-FIMS analysis. Increasing ratios of product:substrate shows increasing fungal alteration at shoulder slope positions. Carbohydrates on X-axis as xylose (*m/z* 132):xylan (*m/z* 114), plotted against lignin monomers on Y-axis as vanillic acid (*m/z* 168):vanillin (*m/z* 152).**

significant biomarkers was arbitrarily limited to the top 100 *m/z* signals. An ANOVA was performed on each *m/z*, and are categorized in Table 5.2 based on their abundance in divergent positions or in level/wetland positions. While ANOVA (Table 5.1) and ordination plots (Figure 5.12) showed that the N-containing compound class did not differ between landscape positions or cultivation regime, many individual N-containing compounds were identified in the top 100 significant *m/*z signals using Wilks' lambda feature selection. Low molecular weight heterocyclic-N compounds are proportionately higher in divergent positions, whereas higher molecular weight heterocyclic N compounds, in particular, a homologous family of indoles, dominate the level/wetland positions. In addition, ranges of *m/z* tentatively identified as homologous series' of aromatic and aliphatic amides were present in the level/wetland soils.

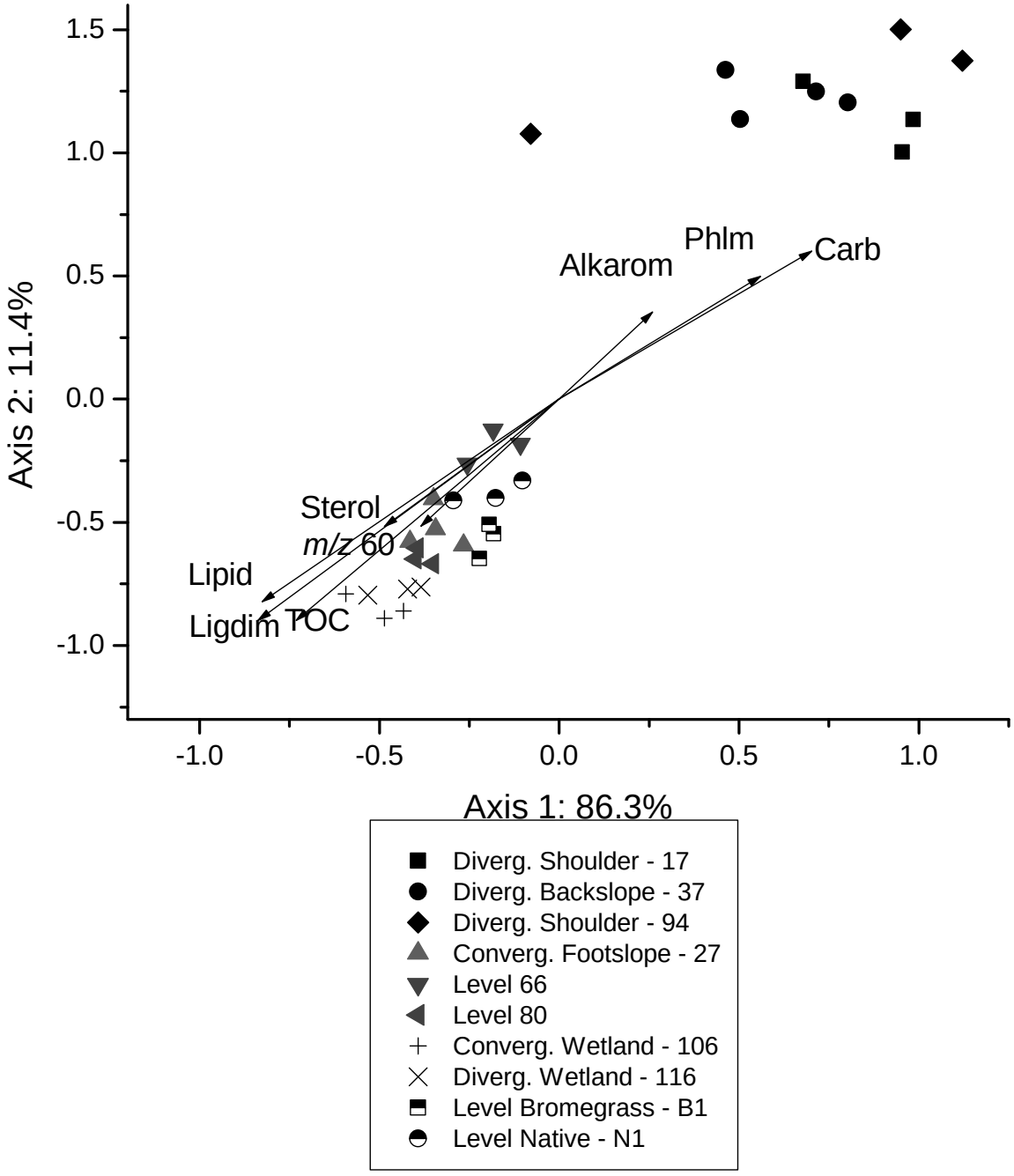

Fig. 5.12. Non-metric multidimensional scaling analysis of *m/z* 55-500 from pyrolysis-field ionization mass spectra of St. Denis soils obtained across landscape elements. Vectors correspond to compound classes which correlate with ordination at $r^2 > 0.40$. Compound class identifications are: Carb, carbohydrate; Phlm, phenols and lignin monomers; Alkarom, alkylaromatic; Ligdim, lignin dimers; TOC, total organic carbon. Signal at *m/z* 60 is pyrolytic degradation product of carbohydrates.

Table 5.2. List and tentative identifications of 100 most significant m/z signals (by Wilks' lambda feature selection scores) observed in Py-FIMS spectra of St. Denis soils.

Enriched in divergent positions			**Enriched in convergent/level/wetland positions**					
Class	m/z	**Assignment**	**Class**	m/z	**Assignment**	**Class**	m/z	**Assignment**
Carbohydrates	58	butene	*N-Containing*	139	subst-pyrrole	*N-Containing*	209	c13-nitrile
	60†	acetic acid		151	subst-pyridone	*aliphatics*	223	c14-nitrile
	68	furan		201	c6-indole		251	c17-nitrile
	72	butanone		243	c9-indole		265	c18-nitrile
	82	c1-furan		245			293	c20-nitrile
	96	c2-furan		257	c10-indole		241	c16-alkylamine
Phenols, lignin	94	phenol		271	c11-indole		255	c17-alkylamine
monomers	156	2OH-guaiacol		285	c12-indole		269	c18-alkylamine
	164†	p-OH cinnamic		299	c13-indole		283	c19-alkylamine
	180	c1-phthalic		313	c14-indole		269	c18-alkylamine
Alkylaromatics	78	benzene		327	c15-indole		297	c20-alkylamine
	92	toluene		333			311	c21-alkylamine
	120	c3-alkbenz		355	c18-indole		381	c26-alkylamine
	170	c3-naphthalene	*Benzoic*	247	c9-benzamide		225	c15-allylamine
Peptide	58		*amides*	261	c10-benzamide		239	c16-allylamine
	70			275	c11-benzamide		267	c18-allylamine
	99†			289	c12-benzamide		295	c20-allylamine
N-containing	67	pyrrole		303	c13-benzamide		309	c21-allylamine
	79	pyridine		317	c14-benzamide		323	c22-allylamine
	80	pyrazine		331	c15-benzamide		339	c23-allylamine
	81	c1-pyrrole					351	c24-allylamine
	93	aniline					379	c26-allylamine
	95	OH-pyridine						
	103	benzonitrile						
	117	indole						
	131	c1-indole						

(continued on next page)

Table 5.2 - continued

Enriched in divergent positions			**Enriched in convergent/level/wetland positions**					
Class	***m/z***	**Assignment**	**Class**	***m/z***	**Assignment**	**Class**	***m/z***	**Assignment**
			Phthalic	165	phthalamide	*Aliphatic*	142	c10-alkane
			amides	235	c5-phthalamide	*lipids*	268	c19-alkane
				249	c6-phthalamide		282	c20-alkane
				263	c7-phthalamide		310	c22-alkane
				277	c8-phthalamide		266	c19-alkene
				291	c9-phthalamide		280	c20-alkene
				319	c11-phthalamide		294	c21-alkene
				347	c13-phthalamide		308	c22-alkene
			Benzoic/	248	c9-benzoic		242	c15-fatty acid
			Phthalic	262	c10-benzoic		256	c16-fatty acid
			esters	276	c11-benzoic		284	c18-fatty acid
				304	c13-benzoic		300	
				264	c7-phthalic			
				278	c8-phthalic			
				292	c9-phthalic			

†enriched in level/wetland positions

5.4 Discussion

In this study, a multi-analytical approach coupled with a multivariate statistical analysis was undertaken to evaluate the influence of landscape-position and land use on the composition of soil organic C and N. Evidence presented here shows that SOM composition is controlled principally by landscape position in hummocky terrain through processes arising from water redistribution and tillage erosion. Management has only a comparatively slight effect.

5.4.1 Landscape position impacts carbohydrates, lignins and lipids

Comparison of the ordination diagrams for the C XANES, N XANES and Py-FIMS data show similar clustering patterns. Soils from divergent positions cluster together, and are separated from convergent, level and wetland positions; uncultivated grassland soils cluster with their level positional counterparts.

Pyrolysis results show a relative enrichment of normally labile compounds such as carbohydrates and low-molecular weight aromatics at the divergent positions (Figure 5.12). Tillage operations in agricultural hummocky landscapes results in translocation of material from the upslope divergent to the downslope depressional positions (Pennock and Dejong, 1987; Lobb et al., 1995; Pennock, 2003). Over many growing seasons, tillage operations at divergent positions expose and incorporate deeper subsoil material into the topsoil (Lobb et al., 1995; Papiernik et al., 2005). Evidence for the long-term stabilization of carbohydrates and lignins in subsoils has been shown to occur (Guggenberger et al., 1994), and the data presented here supports tillage-induced incorporation of subsoil organic matter at the divergent positions.

Pyrolysis results contrast with the C-XANES data (Figure 5.5), where the vectors for carbohydrate-hydroxyl and substituted aromatic carbon show enrichment in the convergent and wetland soils. This is because XANES responds to all carbohydrate-type C atoms in a sample, regardless of the molecule in which it is found, whereas Py-FIMS is sensitive to individual biomarkers for sugar monomers and sugar degradation products. The Py-FIMS

carbohydrate compound class comprises the summed and averaged m/z signals assigned to individual carbohydrates (see Appendix C). These signals collectively represent sugar monomers, and pyrolysis transformation products arising from the degradation of sugar precursors (Schnitzer and Schulten, 1992; Gregorich et al., 1996; Schulten, 1996). The signal for $m/z = 60$, however, is identified as acetic acid, which is a thermal breakdown product of carbohydrates (Schnitzer and Schulten, 1992; Dinel et al., 1998). In this experiment, the vector representing the individual response of $m/z = 60$ trends toward the level and wetland soils, which is opposite to the direction of the composite carbohydrate compound class (Figure 5.12). This indicates that carbohydrates in the convergent/depressional positions are degrading more completely through the pyrolysis process, and conversely, carbohydrates at the divergent positions are fragmenting into larger monomeric units. In addition, thermograms for the carbohydrate compound class showed higher temperatures for both principal volatilization peak and for the initial onset of volatilization, indicating that carbohydrates were more thermally stable at the divergent positions than at the convergent and wetland positions (Figure 5.10). Higher thermal stability has been correlated with higher resistance to biodegradation (Leinweber et al., 2009), and increased physical protection of OM by the solid phase.

A similar pattern is seen in the distribution of lignin compounds across the landscape. Py-FIMS shows increases of monomeric lignins at the divergent positions, and increases of dimeric lignins at the depressional/convergent/level positions (Figure 5.12). Again, a spatial pattern of stabilization is revealed that depends on landscape position, with more 'labile' compounds enriched at divergent positions. As with the carbohydrate data, a discrepancy exists between the C XANES and Py-FIMS data for lignins. The C XANES signal for substituted aromatic compounds has an increasing trend toward the level and downslope positions (Figure 5.5). The signal for substituted aromatic compounds includes phenol components as well as an aniline (Arom-NH_2) component, whereas the Py-FIMS signal for lignins is divided into lignin monomers and lignin dimers (Schulten, 1996).

Older organic matter is expected to have undergone microbial transformations. The extent of carbohydrate and lignin degradation can be investigated using carbohydrate depolymerization (Leinweber et al., 2008b) and lignin oxidation parameters (Feng et al., 2008). Figure 5.11 plots the ratio of product:substrate m/z biomarkers for hemicelluose (a carbohydrate) on the X-axis and vanillin (a lignin) on the Y-axis, with higher values indicating increased microbial transformation. This suggests that carbohydrates and lignins have undergone more degradation at the divergent positions. Xylanase is a fungal enzyme responsible for the depolymerization of hemicellulose (xylan) to xylose (Hrmova et al., 1989), and fungal peroxidases carry out vanillin oxidation to vanillic acid (Kirk and Farrell, 1987; Lewis and Yamamoto, 1990; Otto and Simpson, 2006). This implies a possible fungal link between the transformation and stabilization of carbohydrates and lignins at different landscape positions.

Pyrolysis (Figure 5.12) and C XANES (Figure 5.5) data show the retention of higher molecular weight lipid products (i.e., lipids, suberins, lignin dimers) at the convergent and depressional locations. Moisture transfer regimes would favour higher plant production in depressional positions, resulting in higher input of fresh plant-based OM in the depressions. Divergent positions, however, are influenced by re-incorporated subsoil material through tillage, and by lower inputs of fresh material and thus contains material that has undergone comparatively more microbial transformation.

Mechanisms of OM stabilization apparently are different between landscape positions. Divergent positions may be stabilizing polar molecules through interactions with iron and calcium cations, and represent long-term stabilized SOM (Anderson, 1988; Mikutta et al., 2006; Christl and Kretzschmar, 2007; Kleber et al., 2007; Marschner et al., 2008; von Lützow et al., 2008). As well, clay content was higher in the carbonate-rich divergent samples (#37 and #94, Figure 5.1), indicating possible carbonate-induced clay flocculation (Birkeland, 1999), and enhanced stabilization of lower molecular weight polar molecules. At convergent/level/wetland positions, lipids predominate, and are selectively enriched because of metabolism of uncomplexed compounds (Sollins et al., 1996; von Lützow et al., 2006, 2008).

These compounds represent SOM stabilized in the medium term, because although they are somewhat recalcitrant, recent evidence has shown that lipid-type materials are not persistent over long terms in soils (Guggenberger et al., 1994; Gleixner et al., 1999).

5.4.2 N-bonded aromatics

Nitrogen XANES detected nitroaromatic and N-bonded aromatic (anilide) compounds (see Appendix A). This is an interesting finding because these types of compounds are rarely discussed within the context of SON, and are only now starting to gain attention in the soils community (e.g., Olk, 2008b). The ecological function and formation of these compounds is still largely unclear, and they have only been detected in labeled experiments (Thorn and Mikita, 2000), model systems (Azhar et al., 1986) or using a specialized form of ^{13}C-NMR (Schmidt-Rohr and Mao, 2002; Schmidt-Rohr et al., 2004). The present study is a step forward, showing that N XANES offers a corroborating technique which reveals N-bonded aromatic moiety in whole soils.

In environmental samples, the generation of these compounds has been associated with nitrification processes in acid soils (Stevenson et al., 1970; Azhar et al., 1989; Stevenson, 1994), or with flooded/anaerobic soils under rice cropping (Schmidt-Rohr et al., 2004; Olk et al., 2006). Previous studies provided evidence for the incorporation of nitrite (NO_2^-) into aromatic and phenolic structures (Thorn and Mikita, 2000), representing one possible route of N incorporation into organic matter (Palm and Sanchez, 1991) and a potential pathway for N_2O production in soils (VanCleemput and Samater, 1996; Thorn and Mikita, 2000; Venterea, 2007). In this experiment, the soils which exhibited the strongest signals for N-bonded aromatics were calcareous soils from dry, upper landscape positions, which do not fit the traditional criteria for the observation of these compounds. Instead, other phenomena must be responsible for the generation and incorporation of these N-containing moieties into soil organic matter. Davidson et al. (2003) hypothesized that nitrate can be reduced by iron to nitrite, and incorporated abiotically into aromatic structures. This has been debated by

several other research groups who have not observed the generation of N-bonded aromatics in controlled systems (Colman et al., 2007, 2008; Schmidt and Matzner, 2009). This idea may still have merit, however, if constituents other than iron are involved in a redox mechanism coupled with nitrate/nitrite. This warrants further investigation.

Other hypotheses involve the incorporation of nitrite with phenolic lignins (Stevenson et al., 1970; Schmidt-Rohr et al., 2004; Olk et al., 2006). Nitrite is generated as an intermediate compound in the microbial transformations of ammonium and nitrate through nitrification and denitrification. Smith et al. (1997) showed an accumulation of nitrite resulting from nitrification, where excess ammonium inhibited nitrite oxidizers, and Müller et al. (2006) used ^{15}N tracers to show that denitrification contributed significantly to nitrite content in grassland soils. Many studies have demonstrated loss or immobilization of inorganic N, which was attributed to abiotic processes (Smith and Chalk, 1979, 1980; Olk, 2008b). This hypothesis may have merit for the present study if we consider that for inorganic N to accumulate in soil, inputs into the inorganic pool through mineralization or fertilization would have to exceed the rates of microbial/plant uptake or of loss through nitrification/denitrification. This most likely occurs at divergent slope positions, if microbial activity is reduced due to low amounts of labile substrates (which has been demonstrated in this study) and low water availability (Pennock et al., 1992), but where N inputs through fertilizer application would be similar across the entire landscape. Indeed, considering that monomeric lignins are enriched in divergent soils, it could be argued that under these conditions N is being abiotically immobilized as N-bonded aromatic compounds. Schmidt-Rohr et al. (2004) detected anilide-N in mobile humic acids in rice soil, suggesting a possible short term storage pool of inorganic N. The divergent soils in this experiment all show lower C_{org}:N (see Figure 5.1).

5.4.3 N-containing compounds - cultivation and landscape effects

Whereas landscape position controls the majority of the variability in SOM composition, heterocyclic-N, as detected by N XANES is also influenced by cultivation. Heterocyclic

N-containing pyridine and pyrrole vectors do not show a clear correlation with soils from specific slope positions, but do show a decrease in the wetland and the native soil (Figure 5.3). A recent study by Leinweber et al. (2009) demonstrated that cultivation increased the relative contribution of heterocyclic N to SOM, and data presented here supports this long term shift in OM composition. Although the bromegrass soil has remained uncultivated for 20 yr, the organic matter composition continues to reflect a similar pattern to the continuously cultivated soils. This shows that cultivation effects may remain in reclaimed landscapes at the time frame of decades. Why would N-XANES be particularly sensitive to detecting cultivation effects? XANES is inherently surface sensitive, because it relies on the penetration depth of soft X-rays (Stöhr, 1992). Soil has been cultivated for a short time (57+ yr, Leinweber et al., 2009) as compared to pedological development since the last glaciation (*ca.* 10,000 yr, Christiansen, 1979). It is possible that organic matter changes over the short term are limited to surface modifications, which would enhance their detection using XANES.

Pyrolysis data for heterocyclic-N does not show a cultivation effect. Moreover, the N-containing compound class also does not show a significant trend for landscape position (Figure 5.12). Wilks' lambda scores, however, flagged many m/z signals corresponding to individual heterocyclic-N-containing compounds (Table 5.2). A pattern emerged from this data which was landscape controlled; low molecular weight, heterocyclic compounds were enriched at divergent positions and higher molecular weight, polysubstituted compounds (especially a homologous series tentatively identified as indoles) were enriched in the depressional positions. Mahieu et al. (2000) used ^{15}N NMR to suggest heterocyclic-N as a product of long-term microbial turnover in soils. The presence of low molecular weight heterocyclic-N at the divergent position supports the evidence presented above for the enhanced microbial transformation of carbohydrates and lignins. Conversely, the depressional positions are enriched by a family of predominantly indole compounds, which may be derived from release of plant-based alkaloids (Heldt, 1997) and, similar to the lipid-type compounds described above, may be early-stage degradation components of plant material.

Molecular signals corresponding to organic aliphatic and aromatic amides were also detected in downslope soils (Table 5.2). These compounds are not generally considered in the evaluation of organic N (Schulten and Schnitzer, 1998), and their detection in this study raises questions surrounding the production and persistence of aliphatic amines and amides in soil. Moreover, feature selection using Wilks' lambda scores shows that these compounds may be highly influenced by landscape position; however, information pertaining to their role in N cycling and storage remains scarce. It is also possible that these compounds arise as artefacts of a reaction between interlayer ammonium and lipids catalyzed by the pyrolysis process (Nierop and Van Bergen, 2002). Nitrogen XANES amide/sigma signals which correspond with amine N found in amino acids and amino sugars, are not consistent with Py-FIMS data. These signals increase in the divergent positions and decrease toward the wetland. In the deconvolution of the N- XANES spectra, this particular region was fitted with a single Lorentzian curve (Figure 5.4B). It is possible, however, that there is overlap of nitrate-N in this region which is not resolvable.

5.5 Conclusions

The toposequence investigated in the present study provides evidence for a transition of OM stability from a passive, stabilized, pool prevalent at the divergent positions, to a newer, active pool predominating at depressional positions. According to von Lützow et al. (2008), the passive pool is characterized by compounds which have been stabilized through interactions with mineral surfaces and polyvalent cations (Anderson et al., 1981; Six et al., 2004; Mikutta et al., 2006). These include polar compounds normally considered as labile (carbohydrates, monomeric lignins and phenols, single-ring N-heterocycles), but which may be stabilized by polyvalent cations present at divergent positions from tillage incorporation of iron and calcium carbonates. Conversely, an active pool at the depressional landscape positions consists of fresh, lipid-type plant materials, and is characterized by

selective preservation of chemically recalcitrant molecules.

An important finding in this study was the detection of nitroaromatic and N-bonded aromatic compounds, particularly in upper slope soils. N-bonded aromatics have been detected in other studies on anaerobic and acidic soils (Stevenson et al., 1970; Olk et al., 2006); this study detected the same compounds in calcareous, upper slope soils, suggesting that these compounds may be widespread in the soil system. By showing the presence of N-bonded aromatics, the data presented here indicates that this class of compounds may constitute a significant portion of soil organic N, and warrants consideration as a portion of soil 'unknown-N'.

This is the first report of the application of multivariate statistics with C and N *K*-edge XANES. This data treatment combined with multivariate analysis of Py-FIMS data provided a sensitive tool for the study of soil organic matter composition in whole soils. This novel ordination approach shows the sensitivity of XANES to changes in SOM composition, particularly in the organic N-containing compounds, and that these changes are driven primarily by landscape-scale processes. Moreover, multivariate ordination of N XANES data also revealed cultivation effects.

The next steps are to explore the microbial participation in the stabilization and cycling of SOM across landscapes. In particular, elucidation of microbial and fungal participation in the generation of N-bonded aromatics is essential to understanding the role of this organic N pool in soil systems. Indeed, continued application and integration of multi-analytical research is essential to understanding the stability, pools and fates of SOM, particularly with respect to N-bonded aromatics and organic amines in agricultural soil systems.

Chapter 6

Profiling rhizosphere chemistry: Evidence from carbon and nitrogen *K*-edge XANES and from pyrolysis-FIMS[†]

Abstract

The rhizosphere is region of complex interactions among plants, soil and microbiota, and by its very nature, presents many technical challenges to the analyst. Whereas previous studies have generally focused on root exudation in artificial systems, we compared whole-soil samples from bulk and rhizosphere soils developed under field pea (*Pisum sativum* L.). Synchrotron-based C and N *K*-edge X-ray absorption near edge structure (XANES) spectroscopy and pyrolysis field-ionization mass-spectrometry (Py-FIMS) were used to investigate plant effects on the organic chemistry of rhizosphere in a growth chamber experiment. Soil type appeared to play a significant role in development of the rhizosphere. Indeed, the C and N *K*-edge XANES analyses revealed patterns of rhizosphere development that were strongly influenced by soil type. Relative to the bulk soil, pea rhizospheres developed on a clay soil showed increases in heterocyclic N compounds, proteins and carboxylates. Pea rhizospheres developed on a sandy clay loam soil showed increased nitroaromatic compounds, and reduced aromatics, whereas proteins,

[†]This work has been published in Gillespie, A.W., F.L. Walley, R.E. Farrell, P. Leinweber, A. Schlichting, K.U. Eckhardt, T.Z. Regier, and R.I.R. Blyth. 2009. Profiling rhizosphere chemistry: Evidence from carbon and nitrogen *K*-edge XANES and from pyrolysis-FIMS. Soil Sci. Soc. Am. J. 73:2002-2012. Minor modifications have been made for consistency in formatting.

carbohydrates and carboxylic compounds remained unchanged relative to the bulk soils. Pyrolysis-MS results showed that rhizosphere processes promote selective enrichment of lipid compounds (alkanes, alkenes, alkylamides, alkylaromatics, and alkyl/benzoic/phthalic esters) with a concomitant depletion of carbohydrates, proteins and phenols/lignins. These results suggest enhanced decomposition of labile organic matter at a molecular level in the rhizosphere; presumably as a result of enhanced microbial activity. The presence of nitroaromatic and alkylamide compounds in the rhizosphere indicates a unique cycling of N in this region. Synchrotron-based analysis of whole soils offers useful, corroborating information regarding the organic chemistry in the rhizosphere when compared to established pyrolytic techniques.

6.1 Introduction

Lorenz Hiltner, realizing the importance of plant roots and their effect on soil, coined the term "rhizosphere" (root sphere) at the turn of the last century (Hiltner, 1904). Loosely defined, the rhizosphere is the volume of soil that is directly affected by the presence and/or activity of plant roots (Katznelson, 1965; Curl and Truelove, 1986; Jones et al., 2004) and exists because of rhizodeposition processes. The rhizosphere is an area of elevated nutrient availability reflecting (i) the release of carbonaceous and nitrogenous compounds; (ii) the deposition of necrotic tissue through root turnover; (iii) the interaction of root exudates with the organic-mineral soil surfaces; and (iv) the translocation of water and dissolved constituents toward the root (Curl and Truelove, 1986; Jones and Darrah, 1994; Crowley and Rengel, 1999; Badalucco and Nannipieri, 2007; Uren, 2007). As a result, this region is characterized by a larger microbial activity, diversity and function compared to the bulk soil (Curl and Truelove, 1986; Grayston et al., 1998; Brimecombe et al., 2007). Moreover, plants contribute the raw organic precursors that over time become humic materials and which,

in turn, can have a profound impact on the chemical and biochemical functioning of soils (Hempfling et al., 1991; Gregorich et al., 1996).

Root exudates consist of a variety of compounds including, among others, sugars, amino and organic acids, polyphenols and sterols (Curl and Truelove, 1986; Uren, 2007). In non-sterile environments, microbial activity also contributes to the suite of compounds present in the rhizosphere through the release of microbial metabolites, the turnover of plant derived compounds and the transformation of previously existing humic substances (Lynch, 1990; Kuzyakov, 2002; Brimecombe et al., 2007). Identification of rhizosphere compounds is challenging because of the complex mixtures present and the need to extract these compounds from the soil matrix. Further complicating matters is the fact that, for sampling purposes, rhizosphere soil is only 'operationally' defined by the method used to collect the sample. Techniques used to isolate and quantify rhizosphere compounds typically involve wet chemical methods that employ ion exchange resins and solvent extractions from artificial systems (e.g., hydroponic or sand cultures) (Badalucco and Kuikman, 2001; Fan et al., 2001; Neumann and Römheld, 2007). These techniques are usually targeted to specific, low molecular weight compounds, which are expected to be present in a sample; however, this approach may ignore important compounds not included in the method development process (Leinweber et al., 2008a; Schlichting and Leinweber, 2009). The development of techniques that facilitate investigations of whole soils, with little pretreatment or bias toward specific compounds or compound classes, affords the opportunity to gain a better understanding of the rhizosphere. Indeed, the use of techniques such as N and C K-edge XANES can eliminate artifacts that may be produced during compound extraction and recovery.

Recently, synchrotron-based X-ray Absorption Near Edge Structure (XANES) analysis has been used to probe the speciation of N in environmental samples (Vairavamurthy and Wang, 2002; Abe and Watanabe, 2004; Jokic et al., 2004a; Leinweber et al., 2007). The applicability of C K-edge XANES to soil investigations also has been demonstrated (Jokic et al., 2003; Solomon et al., 2005; Kinyangi et al., 2006; Christl and Kretzschmar, 2007). XANES is

a purportedly non-destructive technique (Vairavamurthy and Wang, 2002) that targets individual elements based on their electron binding energies, and is thus able to determine the chemical properties of specific substance classes in a mixture. However, the validity of this technique toward characterizing organic compounds in a heterogeneous and complex medium such as soil has not been attempted. Pyrolysis coupled with mass spectrometry provides a suite of applications whereby complex organic samples are thermally decomposed in the absence of oxygen and the masses of the volatilized decomposition products are determined. These techniques continue to be widely supported for investigation of organic compounds in soil (Sorge et al., 1994; Schnitzer and Schulten, 1995; Schnitzer et al., 2006). Pyrolysis field-ionization mass-spectrometry (Py-FIMS), in particular, uses soft electric field ionization to minimize fragmentation of the pyrolyzed molecules and, in principle, yield the molecular masses of the decomposition products with little fragmentation. Futhermore, unlike with flash pyrolysis, the thermal decomposition products are resolved by employing a temperature ramp, with the temperature-resolved data providing diagnostic information complementary to the measured mass. This technique has been successfully applied to humic substances (Haider and Schulten, 1985), dissolved organic matter (DOM) (Kuzyakov et al., 2003; Melnitchouck et al., 2005), organic-mineral particle-size and aggregate fractions (Leinweber and Schulten, 1999; Schulten and Leinweber, 2000) and whole soil samples (Sorge et al., 1994; Schnitzer and Schulten, 1995; Schulten and Sorge, 1995; Wilcken et al., 1997; Schnitzer et al., 2006).

Whereas data obtained using XANES analysis provide information regarding functional groups and the local bonding environment of the element in question, pyrolysis mass spectrometry yield complementary information about the molecules and polymeric monomers of an organic sample. To date, however, these complementary techniques have not been applied to studies of the rhizosphere. The objectives of the present study were (i) to characterize bulk and rhizosphere soils developed under field pea (*Pisum sativum* L.) using N and C K-edge XANES and Py-FIMS, (ii) to assess the influence of soil type on rhizosphere development of field pea, and ultimately, (iii) to compare and contrast the information provided by these

two techniques.

6.2 Materials and Methods

6.2.1 Soils, growth conditions and recovery of rhizosphere samples

The soils were a clay, Orthic Black Chernozem (Vertic Cryoboroll) collected from Melfort (Saskatchewan) and a sandy clay loam, Dark Brown Chernozem (Typic Haploboroll) from Elstow (Saskatchewan). Both soils are smectite-dominated borolls (Dasog, 1986; Hardie, 2008). Bulk (i.e., unplanted) soils were maintained at 5°C. Field pea (*Pisum sativum* L.) was planted into 0.7 kg of soil (in 15-cm pots) maintained at 60% of moisture holding capacity and kept in a controlled growth chamber with a diurnal photoperiod of 16-h, 22°C /8-h, 18°C. Supplemental nutrients added were 30 $\mu g \cdot g^{-1}$ P as $Ca(H_2PO_4) \cdot H_2O$, 50 $\mu g \cdot g^{-1}$ S as K_2SO_4 + micronutrients, 200 $\mu g \cdot g^{-1}$ K as K_2SO_4 + KCl, 0.6 $\mu g \cdot g^{-1}$ Mo as $NaMoO_4 \cdot H_2O$, 1.5 $\mu g \cdot g^{-1}$ B as H_3BO_4, 5 $\mu g \cdot g^{-1}$ Mn as $MnSO_4 \cdot H_2O$, 4 $\mu g \cdot g^{-1}$ Zn as $ZnSO_4 \cdot 7H_2O$ and 0.6 $\mu g \cdot g^{-1}$ Cu as $CuSO_4 \cdot 5H_2O$. Plants were harvested at 28 days after planting. Plants were grown in non-sterile soil, and visual inspection showed limited nodulation on all plants; no differences were observed between the two soil types. Rhizosphere soil was collected by carefully removing the plant and soil from the pot, gently shaking the root mass to remove any loosely adhering soil, and recovering any soil remaining adhered to the root by manual separation. Gloves were worn to prevent contamination, and care was taken to exclude root material from the soil sample. Basic characteristics of the bulk and rhizosphere soils are presented in Table 6.1. The C and N contents were determined using a Vario EL elemental analyzer (Elementar Analysensysteme GmbH, Hanau, Germany) and the textures were determined using a laser scattering particle size analyzer (Horiba LA-950, Irvine, California).

Table 6.1. Chemical and physical characteristics of the Melfort and Elstow soils.

Sample ID†	Total C	Org‡ C	Total N	C:N§	TII/ OrgC	Sand	Silt	Clay
	——————g·kg^{-1}——————				cts×10^6 · g^{-1}¶	——————%——————		
Mel-B	27.30	22.99	2.65	10.3	295.9	5.8	10.2	84.0
Mel-R	45.40	37.88	3.87	11.7	158.5			
Els-B	28.42	26.31	2.56	11.1	127.9	49.9	16.0	34.1
Els-R	42.07	35.11	3.47	12.1	322.0			

†Mel: Melfort clay; Els: Elstow sandy clay loam; B: bulk soil; R: rhizosphere soil
‡Org = organic
§C:N = ratio of total C to total N
¶Ratio of total ion intensity (TII) to organic carbon (OC); ion counts×10^6·g^{-1}OC

6.2.2 C and N *K*-edge XANES

Bulk and rhizosphere soils were air-dried, ball-milled, and a *ca.* 1 mg subsample was pressed onto freshly scraped indium metal (Sigma-Aldrich, Mississauga, ON, Canada), and affixed to a steel sample disc using double-sided conductive carbon tape (SGE, Toronto, ON, Canada). Carbon and N *K*-edge XANES spectra were collected using the Spherical Grating Monochromator (SGM) beamline 11ID-1 at the Canadian Light Source (CLS), Saskatoon, SK, Canada. This beamline delivers 10^{11} photons s^{-1} at the N *K*-edge with a resolving power (E/ΔE) better than 10,000 (Regier et al., 2007a,b). The exit slit was set at 50 μm and fluorescence yield (FLY) data and total electron yield (TEY) were collected simultaneously. Whereas a two stage microchannel plate detector was used to collect FLY data, TEY was determined by measuring the drain current from the sample. TEY and fluorescence yield are competitive processes, and their relative yields heavily favor electron emission over fluorescence emission as a function of decreasing atomic number (Stöhr, 1992). Thus, although both FLY and TEY were satisfactory at the N *K*-edge, only TEY data were satisfactory at the C *K*-edge. For calibration at the C *K*-edge, a solid-state absorption spectrum for glutaric acid (dicarboxylic acid) was measured. The C 1s$\rightarrow \pi^*_{C=O}$ transition

has an energy of 288.6 eV (Kim et al., 2003). Carbon spectra were normalized to the incident flux by using a blank spectrum obtained from a freshly sputtered gold surface to account for attenuation of the photon beam by C on the optical components. Carbon features were assigned based on a review of the literature (Urquhart and Ade, 2002; Hardie et al., 2007).

For calibration at the N K-edge, an absorption spectrum for N_2 was measured using a photoionization chamber mounted upstream of the solid state X-ray absorption chamber (Regier et al., 2007a). The vibrational manifold of the N 1s$\rightarrow \pi^*$ transition has an energy of 400.8 eV for the $\nu = 0$ peak (Sodhi and Brion, 1984; Schwarzkopf et al., 1999). This was then calibrated to a secondary solid-state standard (6-hydroxyquinoline) that was used for routine calibration. Nitrogen spectra were normalized to the incident flux using an in-line Au mesh which was refreshed by evaporation in situ prior to data collection. Assignment of the N spectral features to N functions was based on published analysis of reference compounds (Leinweber et al., 2007). Data processing was performed using the aXis 2000 (Hitchcock et al., 2005) and WinXAS (Ressler, 1998) software packages. Data for N and C edges were averaged from a minimum of two scans, and background corrected by a linear regression fit through the pre-edge region followed by normalization to an edge step of one.

6.2.3 Pyrolysis field-ionization mass-spectrometry(Py-FIMS)

Soils were dried, milled with a mortar and pestle, transferred to quartz capsules and pyrolysed at temperatures ranging from 110°C to 700°C in steps of 20°C in the direct inlet of a Finnigan MAT 900 mass spectrometer (Finnigan MAT, Bremen, Germany). Over the full temperature range, 91 scans were recorded for masses ranging from 15 to 900 m/z; ion intensities were normalised on a sample weight basis (i.e., ion counts per mg soil). These were combined to produce a single thermogram of total ion intensity (TII), and a single summed and averaged mass spectrum. A detailed description of the Py-FIMS method and the statistical treatment of TII and weight normalization is given by Sorge et al. (1993a).

6.2.4 Statistics - multivariate feature selection

The Py-FIMS analyses resulted in complicated, multidimensional data sets that were simplified using Wilks' lambda feature selection. The Wilks' lambda scores (F-statistics comparing the variance within reps to the overall variance) were calculated for each individual m/z normalized to TII. Variables for which the Wilks' lambda score was significant ($p \leq 0.05$) were retained and (i) visualized using principal component analysis (PCA) and (ii) subjected to analysis of variance (ANOVA) to determine significant treatment effects. Principal component analysis (PCA) was performed using MINITAB (ver. 12.1); ANOVA and Wilks' lambda calculations were performed using SPSS (ver. 14.0).

6.3 Results and Discussion

6.3.1 X-ray Absorption Near Edge Structure (XANES)

Carbon K-edge spectra for the rhizosphere-bulk soil pairs are presented in Figure 6.1. The dominant features of the C K-edge spectra included: (1) a normalization artefact, likely quinone @ 283.7 eV; (2) aromatic C @ 285.2 eV; (3) C≡C @ 285.7 eV; (4) N-substituted aromatic @ 286.8 eV; (5) phenolic @ 287.1 eV; (6) aliphatic @ 287.5 eV; (7) carbonyl (ketone, carboxylic, amide) @ *ca.* 288.6 eV; (8) carbohydrate hydroxyl @ 289.6; and (9) carbonate @ 290.5 eV.

Aromatic functionalities (@ 285.2 eV) decreased in the rhizosphere developed in the Elstow soil, but remained unchanged in the Melfort soils. Carboxylic functionalities (@ 288.7 eV), on the other hand, increased in the rhizosphere developed in the Melfort soil, but remained unchanged in the Elstow soil. The line drawn in Figure 6.1 for feature 7 approximates the region of energies covered by carbonyl functionalities. This peak will shift depending on the chemical nature of the adjoining molecule. Although these spectra were calibrated to the carboxylic peak for glutaric acid @ 288.6 eV, we see that this peak has shifted slightly to

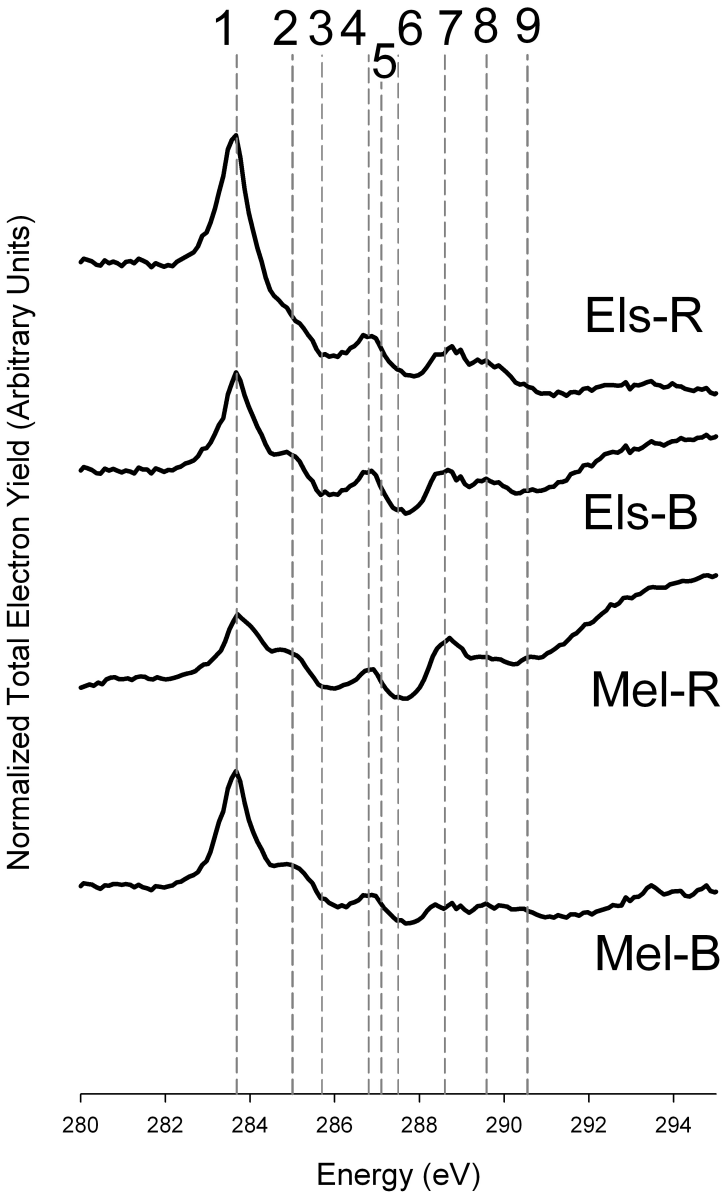

Fig. 6.1. **Carbon *K*-edge XANES spectra from the Elstow and Melfort bulk and rhizosphere soils. Features numbered as: (1) 283.7 eV, quinone; (2) 285.2 eV, aromatic; (3) 285.7 eV, C≡C ; (4) 286.8 eV, N-substituted aromatic; (5) 287.1 eV, phenolic; (6) 287.5 eV, aliphatic; (7) 288.7 eV, carbonyl (ketone, carboxylic, amide); (8) 289.6 eV, carbohydrate hydroxyl; and (9) 290.5 eV, carbonate.**

288.7 eV, indicating that carboxylic acid groups may be bonded to non-aliphatic structures. The carbonyl peak region also resolved into amide-C (@ 288.4 eV) in both the Elstow and Melfort soils, but with the bulk soils exhibiting a slightly greater amide-C signal. Carbon functionalities for carbohydrates and substituted (i.e., phenolic and N-substituted) benzene compounds were present in all the soils and showed little or no rhizosphere effect. Very weak aliphatic and triple-bonded C signals also were observed (@ 287.5 eV), and were slightly stronger in the bulk soils. Weak carbonate signals also were detected (@ 288.6 eV), which was expected given that both the Elstow and Melfort soils developed from calcareous parent materials. The strong initial peak in all the spectra (@ 283.7 eV) is believed to originate from residual C in the beamline that was not removed using the normalization process. This feature appears in scans of whole soils where carbon content is low (*ca.* 5%). Data collection at the C *K*-edge of soils must measure small changes in absorbance over a large background, whereas scans of reference materials with high levels of C typically mask this feature. In addition, C-XANES spectra of whole soils are further complicated by a convolution with second-order oxygen *K*-edge features starting from 270 eV (i.e., half the oxygen *K*-edge occurring at 540 eV). Soil minerals contain large quantities of oxygen in crystal lattices, and so will produce an extended X-ray absorption fine-structure (EXAFS) spectrum which will overlap with the C *K*-edge. Organic C amounts are small compared to oxygen in minerals, and so the spectra presented here, which have not been adjusted to account for this superposition, appear to drop in intensity across the C *K*-edge because they are following a descending background produced by this second-order oxygen EXAFS.

Nitrogen *K*-edge spectra for the rhizosphere-bulk soil pairs are presented in Figure 6.2. The dominant features of the N *K*-edge spectra include: (1) aromatic N in 6-membered rings (pyridines, pyrazines) @ 398.7 eV, (2) amino acid decomposition products @ 399.0 eV, (3) nitrilic and aromatic N in 5-membered rings (pyrazolic) @ 400.0 eV, (4) amide (protein) @ 401.2 eV, (5) inorganic nitrate @ 401.7 eV, (6) N with unpaired electrons in 5-membered rings (pyrrolic) @ 402.5 eV, (7) an unknown feature @ 402.9 eV, (8) nitroaromatic @ 403.5

eV, (9) inorganic nitrite @ 405.8 eV, and (10) alkyl-N and the 1s→ σ^* transition @ 406.2 eV. In soil, contributions to each functional family can come from well-defined compounds (e.g., nucleotides, amino acids and proteins) together with more complex, poorly defined transformation products of humification pathways. Thus, XANES data analysis provides information about compound families regardless of what individual components from each family are present.

Protein/amide-N is widely reported as being the most dominant form of organic N in soils (Stevenson, 1982; Knicker et al., 1993). As seen in Figure 6.2, both the bulk and rhizosphere soils produced spectra with a strong feature (@ 401.2 eV) corresponding to this N-functionality. As well, spectra for the Melfort soils indicated an increase in protein/amide-N in the rhizosphere soil compared to the bulk soil.

Leinweber et al. (2007) reported that reference spectra for a variety of amino acid, protein, and amino sugar standards showed the effects of beam-induced damage (corresponding to the peak at 399.0 eV; Figure 6.2). This feature occurs near the pyridinic peak and, given that protein/amide-N is the dominant form of organic-N in soils, is of concern. Each scan reported here was taken at a fresh spot on the sample. However since each scan requires 7 to 8 min to complete, it is still unclear how much the sample at the incident spot has been damaged by beam exposure during the time it takes to scan through the pre-edge region. A few of the XANES features corresponding to ring-bound heterocyclic N functions (e.g., features 1 and 3) are coincident with other functionalities. For example, there is little resolution between the peaks corresponding to the pyridines/pyrazines and the amino acid decomposition products (features 1 and 2; @ 398.7 and 399.0 eV, respectively), making it difficult to judge their individual contributions to the organic N pool. As well, pyrazolic-N (feature 3) occurs at the same energy resonance (400.0 eV) as nitrile-N. Aliphatic nitriles and pyrazoles have been detected in soils using pyrolysis techniques , and the co-occurrence of these two features in XANES spectra renders it difficult to differentiate them based on this analysis alone. Of the N-heterocycles, only feature 6 (pyrrolic-N; @ 402.5 eV) occurs without known interferences.

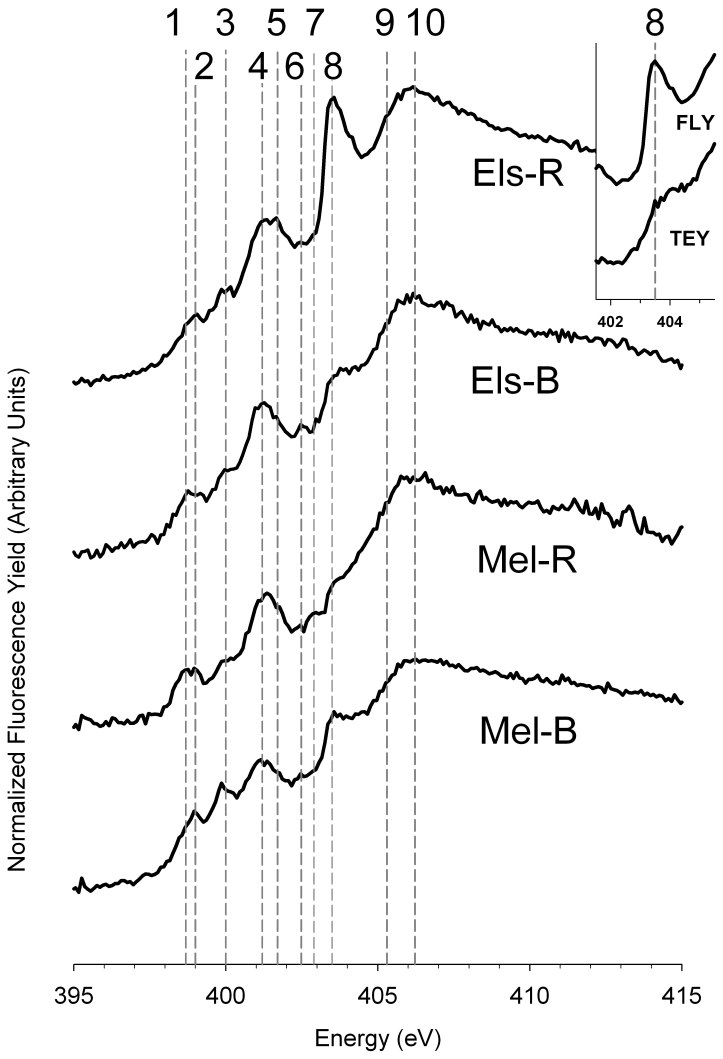

Fig. 6.2. **Nitrogen *K*-edge XANES spectra from the Elstow bulk and rhizosphere soils. Features numbered as: (1) 398.7 eV: aromatic N in 6-membered rings (pyridines, pyrazines); (2) 399.0 eV: amino acid decomposition products; (3) 400.0 eV: nitrilic & aromatic N in 5-membered rings (pyrazolic); (4) 401.2 eV: amide (protein); (5) 401.7 eV: inorganic nitrate - peak 1; (6) 402.5 eV: N with unpaired electrons in 5-membered rings (pyrrollic); (7) 402.9 eV: unknown feature; (8) 403.5 eV: nitroaromatic; (9) 405.8 eV: inorganic nitrate - peak 2; and (10) 406.2 eV: alkyl-N and the 1s$\rightarrow \sigma$* feature. Inset shows fluorescence yield (FLY) and total electron yield (TEY) spectra from the Elstow rhizosphere soil, illustrating suppression of nitroaromatic peak in the surface-sensitive TEY compared to bulk-sensitive FLY.**

Relative to the bulk soil, spectra for the Elstow rhizosphere show decreased signals for features 1 and 3, and no change in feature 2. Whereas this may reflect degradation or transformation of the N-heterocycles, it also may reflect increased stability of nitrile compounds. Rhizosphere development in the Melfort soil was accompanied by an increased signal for feature 1, a decrease for feature 3, and no change in feature 6. This indicates an increase in pyridine-based compounds found in nucleotides, which may reflect an increase in microbial numbers in the clay soil (Brimecombe et al., 2007). Alternatively, this increase may also support the hypothesis of pyridinic N creation via abiotic Maillard humification pathways (Jokic et al., 2004c). Indeed, favourable conditions for Maillard pathway reactions would be provided in the rhizosphere, where elevated levels of precursor compounds (sugars, amino acids and polyphenols) are released in root exudates (Uren, 2007).

Feature 10 occurs within the 1s$\rightarrow \sigma^*$ character region of the spectrum. Thus, although this corresponds to the spectral resonance for the -NH_2 functionality in amino acids, amino sugars, and aliphatic amines, 1s$\rightarrow \sigma^*$ transitions for many other compounds also occur in this region. In general, the intensity of this feature was slightly greater in the rhizospheres in both the Elstow and Melfort soils, relative to their respective bulk soils. It is likely that amino sugar/acid and amine levels are elevated in the rhizosphere soils, though this is by no means certain at this time.

Field pea grown in the Elstow (sandy clay loam) soil produced a rhizosphere exhibiting a very strong nitroaromatic functionality (@ 403.5 eV; Figure 2, feature 8); however, this feature was absent in the spectrum for the Melfort (clay) soil. Nitroaromatic compounds are rarely discussed in the context of soil organic matter (SOM), and their formation through nitrite/nitrate incorporation into organic materials has recently been questioned (Colman et al., 2007). Nevertheless, evidence does exist for the incorporation of nitrite (NO_2^-) into aromatic and phenolic structures (Verhaegen et al., 1988; Azhar et al., 1989; Thorn and Mikita, 2000), and Palm and Sanchez, (Palm and Sanchez, 1991) suggested that this represents one possible route of N incorporation into SOM. Our results provide possible corroborating

evidence for this process. Features 5 and 9 correspond to inorganic nitrate, and are slightly increased in the Elstow rhizosphere (Elst-R), which is the sample where we see strong nitroaromatic functionality. Other evidence of N substitution into aromatic structures comes from rice-cropped soils, where amide-N is incorporated into lignin structures under anaerobic conditions (Schmidt-Rohr et al., 2004; Olk et al., 2006). While aromatic amides have not been investigated using XANES, these other studies show possible pathways for aromatic N-substitution exist under environmental conditions. These XANES results suggest that soil type exerts a differential control over the development of nitroaromatic compounds in the rhizosphere developed from a common plant species.

The spectra shown in Figure 6.2 are composites of four scans obtained from a single mounted soil sample. In the Elst-R spectrum, the nitroaromatic peak, which is strongly expressed in the composite spectrum, was quite variable in the individual scans, as were features 5 and 9 for nitrate (data not shown). This suggests strong localized, microscale formation and consumption of nitroaromatic compounds in the Elstow rhizosphere. However, why this feature was absent in spectra for the Melfort rhizosphere soil, and was weakly expressed in spectra for the Melfort bulk soil, is not yet known. This nitroaromatic feature was also suppressed in the TEY scan (Figure 6.2, inset). Total electron yield has an estimated penetration depth of <10 nm, whereas fluorescence yield has an estimated penetration depth of 70-100 nm (Katsikini et al., 1997; Frazer et al., 2003); this indicates that nitroaromatic formation is occurring primarily below the surface layer, implying that this formation mechanism is strongly coupled to the mineral phase.

6.3.2 Py-FI mass spectra

The mass spectra and thermograms of total ion intensity from the Py-FIMS analyses of the rhizosphere and bulk soil pairs are presented in Figure 6.3. Although all four soils exhibited bimodal thermograms with an onset temperature of *ca.* 300 °C, the TII distributions differed between soils. The Elstow samples yielded thermograms with volatilization peaks at *ca.* 400

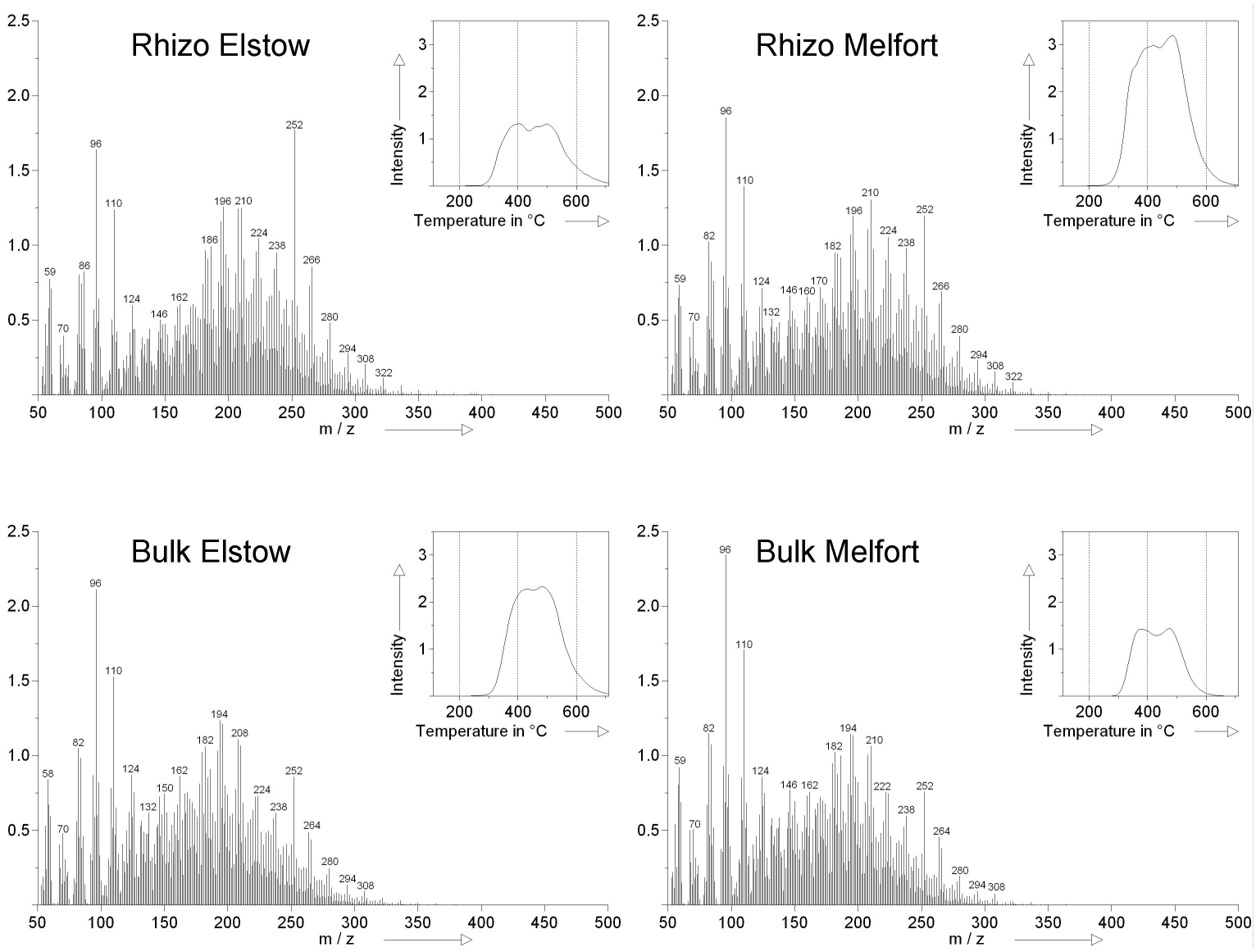

Fig. 6.3. Summed and averaged pyrolysis field ionization mass spectra and thermograms of total ion intensity (TII, upper right) of bulk and rhizosphere soils.

°C and 500 °C for the rhizosphere soil, and at *ca.* 425 °C and 500 °C for the bulk soil. The Melfort rhizosphere soil also exhibited volatilization peaks at *ca.* 400 °C and 500 °C, but with a small, poorly defined peak at *ca.* 350 °C. The Melfort bulk soil, on the other hand, exhibited only two volatilization peaks at *ca.* 350 °C and 500 °C.

A shift to higher volatilization temperatures indicates an increase in stability of the organic compounds. Thus, the data indicate that the Elstow rhizosphere was slightly enriched in labile organic compounds. The data also indicate enhanced stability of organic compounds in the Melfort rhizosphere-a phenomenon that may be related to the higher clay content of the Melfort soil.

The ratio of total ion intensity (TII) to organic carbon (OC) reveals trends in the distribution of molecular masses that were volatilized. That is, because each pyrolysis fragment results in a single ion, the production of small molecular fragments yields more ions by weight than does the production of large molecular fragments. As seen in Table 6.1, the Melfort rhizosphere was characterized by a lower TII:OC ratio than its bulk soil counterpart. This indicates that higher molecular weight fragments are conserved in the Melfort rhizosphere, signifying the presence of a suite of compounds that are more stable. This trend was reversed in the Elstow soils.

Visual inspection of the mass spectra (Figure 6.3) reveals few differences between bulk soils, rhizosphere soils, and rhizosphere/bulk pairs. Thus, a multivariate statistical feature selection approach was used to obtain a more detailed analysis of the effects of soil type and rhizosphere development on soil organic compounds.

Feature selection yielded 144 masses with significant ($p \leq 0.05$) Wilks' lambda scores that were subsequently subjected to principal component analysis (PCA). Figure 6.4 illustrates the first two principal components, with PC1 representing 84% ($p \leq 0.001$) and PC2 representing 7.0% ($p = 0.014$) of the total variability within the feature selected data. The PCA plot shows a clear separation between the bulk and rhizosphere pairs along PC1. In addition, bulk soils cluster closer together, whereas the individual rhizosphere soils separate along

both PC1 and PC2. These results suggest that the rhizodeposits of the field peas grown and subsequent turnover processes dominate the organic chemistry of the rhizosphere, although differences inherent in the soil may also contribute to the degree to which rhizosphere differences are expressed. This implies the importance of short term C and N cycling in the rhizosphere. These may be transient effects, reflecting rhizodeposit-influenced development of specific microbial communities, whereas similarities in bulk soils may be due to longer term humification mechanisms. There is also a significant interaction between rhizosphere development and soil type, indicated by separation along PC2. Differences in clay content between the two soils may promote organic matter protection in the heavier textured soil. This interaction with the mineral phase will alter substrate accessibility and, in turn, affect microbial community structure and function. Rhizosphere development also may be altered directly by changes in plant rhizodeposition patterns in response to soil texture and other textually mediated properties, such as porosity and pore-size distribution (Vetterlein et al., 2007), and water retention and movement.

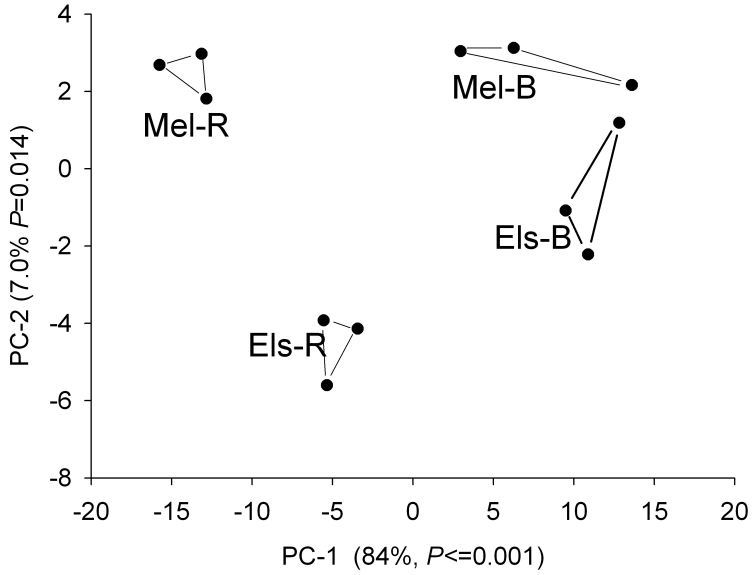

Fig. 6.4. Principal component analysis of feature-selected m/z from pyrolysis-field ionization mass spectra of bulk and rhizosphere soils.

In general, there is a separation point at $m/z = 200$ which distinguishes between rhizosphere and bulk soils. That is, rhizosphere soils yield a greater number of molecular markers with $m/z > 200$, whereas bulk soils yield a greater number of markers with $m/z < 200$. Marker masses were tentatively assigned as pyrolysis products from organic soil polymers such as proteins, carbohydrates and humic substances; or as other free, low molecular weight compounds such as alkanes, alkenes, sterols and fatty acids (Schulten and Leinweber, 1999). Masses selected as having high discriminating power-according to their Wilks' lambda score-and for which the ANOVA showed a significant enrichment in the rhizosphere soils are listed in Table 6.3. Present are masses corresponding to homologous alkanes (m/z 212-324; C_{15}-C_{23}), alkenes (m/z 210-336; C_{15}-C_{24}) and dialkyl esters (m/z 244-286; C_{13}-C_{16}). These masses are consistent with larger, more stable monomeric compounds such as those derived from plant waxes. These can be preserved in organic matter and selectively enriched by faster cycling of more labile organic matter (Lichtfouse et al., 1998). In addition, alkanes in the range of C_{16}-C_{23} have been identified in root material (Jandl et al., 2007), and their selective enrichment in rhizosphere soil may be through direct deposition into the rhizosphere through root exudation, rhizodeposition and turnover of fine roots .

Rhizosphere soils also contained a greater number of homologous sequences corresponding to aromatic signals; with masses corresponding to alkylaromatics (m/z 232-302; C_{11}-C_{16}), benzoate esters (m/z 234-318; C_8-C_{14}) and phthalate esters (m/z 208-292; C_3-C_9). Alkylaromatics are known to form the backbone of humic substances (Schulten et al., 1991). Their selective enrichment may be explained as a result of microbial degradation of other, more labile, components within SOM, and not from plant deposition (Melnitchouck et al., 2005). The two homologous m/z series tentatively assigned to benzoate and phthalate esters, however, have not (except for diethyl phthalate, a common plasticizer) been reported for soils based on Py-FIMS studies. Our hypothesis is that enrichment may occur either through selective enrichment through degradation of labile SOM constituents (as for alkylaromatics), or through microbially altered aromatic acids released as root exudates. The rhizosphere

Table 6.2. Compound groups, *m/z* and tentative identification using Py-FIMS of substances enriched in rhizosphere soil. Boldface *m/z* are enriched in Melfort rhizospheres only, and italicized *m/z* are enriched in Elstow only. All other *m/z* are enriched in rhizosphere soils generated on both Melfort and Elstow soils.

Class	*m/z*	#C	Class	*m/z*	#C	Assignment
Alkanes	212	c15	Alkyl/benzoic	234	c8	tetramethylphenanthrene
	226	c16	esters	248	c9	
	240	c17		276	c11	
	254	c18		**290**	c12	
	268	c19		**318**	c14	
	282	c20	Alkylphthalates	**208**	c3	sinapylaldehyde
	296	c21		**222**	c4	ethylphthalate,flavone
	324	c23		236	c5	
Alkanamine	227	c15		250	c6	
	255	c17		**264**	c7	abcissic acid
	269	c18		278	c8	linolenic acid
Alkenes	210	c15:1		292	c9	allyl-isoflavone
	224	c16:1	Alkyl diesters	244	c13	Tetrahydroxystilbene
	238	c17:1		258	c14	
	252	c18:1		272	c15	naphthoflavone
	266	c19:1		286	c16	kaempferol,luteolin
	280	c20:1	Fatty Acids	**214**	c13	
	294	c21:1		**242**	c15	
	322	c23:1		**270**	c17	
	336	c24:1		**284**	c18	
Allylamine	239	c16:1	Sterols	**386**		cholesterol
	253	c17:1		**388**		
	267	c18:1		**390**		ethylcholestapenaene
	281	c19:1		**392**		ethylcholestatetraene
	295	c20:1		**394**		ethylcholestatriene
	323	c22:1		**396**		ergosterol
Alkyl	232	c11	Other	*57*		Peptide
Aromatic	246	c12		86		Carbohydrate
	260	c13		87		Peptide
	274	c14		251		
	288	c15		*261*		
	302	c16		*265*		octadecanenitrile
				359		N-containing

soils also include two homologous sequences of amides/amines linked to alkyl (*m/z* 227, 255, 269) and allyl (*m/z* 239-323) straight chains. Organic aliphatic N-containing compounds are rarely discussed in the context of soil organic N . However, the data presented here suggests that potentially significant N transformations may be occurring in the rhizosphere, where N is being attached or substituted onto existing aliphatic soil lipids. However, it is also possible that this may be an artefact of the pyrolysis method itself. Flash pyrolysis of alkanols and alkanoic acids in the presence of clay have resulted in the formation of aliphatic nitriles (Nierop and Van Bergen, 2002). These authors suggest that clay minerals catalyze the reaction of alkanols and alkanoic acids, with clay interlayer-bound ammonium. Although the flash pyrolysis system differs from temperature-controlled Py-FIMS used in this study, and the endpoint compound in our study was an amide/amine (compared to nitrile), there exists the possibility that other side reactions are occurring in this soil system that produce these *m/z* signals.

In addition to the above-described compounds assigned in the rhizosphere soils, the Melfort soil included two additional classes of compounds: (i) saturated fatty acids (*m/z* 214-284; C_{13}-C_{18}), which except for C_{18}, are likely methylated even-chained bacterial fatty acids and (ii) sterols [*m/z* 386 (cholesterol), *m/z* 388, *m/z* 390 (ethylcholestapenaene), *m/z* 392 (ethylcholestatetraene), *m/z* 394 (ethylcholestatriene) and *m/z* 396 (ergosterol)]. Although ergosterol and C_{26} (cerotic) fatty acid can not be differentiated based on the nominal mass alone, this presumptive assignment was made based on the presence of other members of the sterol series (i.e., *m/z* 386-394) and an absence of other fatty acids in this mass range. Whereas most sterols are likely released from plant roots (Uren, 2007), ergosterol is also a fungal metabolite (Djajakirana et al., 1996). The enrichment of both fatty acids and sterols in the Melfort rhizosphere suggests their selective protection and preservation in the clay soil (Schulten and Schnitzer, 1990; Bull et al., 2000; Jandl et al., 2004).

Other compounds that were selected, but did not fall into any of the above-mentioned classes are *m/z* 86 (carbohydrate), *m/z* 87 (peptide) and odd-numbered signals (*m/z* 57,

261, 269, 359) enriched only in the Elstow rhizosphere, which may indicate still unidentified N-containing compounds.

Masses selected as being significantly depleted in the rhizosphere soils are listed in Table 6.3. These masses denote marker signals for carbohydrates (*m/z* 72, 82, 96, 98, 100, 102, 110, 112, 114, 126, 128, 132, 142, 144, 162), proteins/peptides (*m/z* 73, 97, 101, 120, 129, 135), phenols and lignin monomers (*m/z* 94, 108, 122, 124, 136, 138, 150, 152, 154, 164, 166, 168, 178, 180), N-containing compounds (*m/z* 67, 79, 80, 81, 93, 95, 103, 107, 109, 117, 119, 121, 123, 125, 131, 137, 139, 143, 145, 151, 153, 159, 161, 167, 171, 175), alkylaromatics (*m/z* 78, 104, 106, 118, 130, 134, 172, 190, 192,) nitriles (*m/z* 55, 147, 163), and unassigned *m/z* (146, 177, 179). These *m/z* signals represent predominantly monomers of biological macromolecules (including carbohydrates, proteins, lignins and humic substances) and the more labile components of SOM. One possible explanation for the depletion of these compounds in the rhizosphere may be the result of depolymerization and enhanced mineralization/cycling of native organic materials by an elevated microfloral population. This process is driven by elevated substrate availability and the priming effects of organic compounds released in root exudates (Kuzyakov, 2002), which affords higher microbial numbers and accelerated organic matter cycling in the rhizosphere. Many rhizosphere-depleted signals reported here correspond to low molecular weight compounds known to be released in root exudates (e.g., salicylic, *p*-hydroxycinnamic, phthalic, vanillic and caffeic acids; *m/z* 138, 164, 166, 168, 180 respectively) (Uren, 2007). These *m/z* also are marker signals for phenols and lignin monomers (Schulten and Leinweber, 1999). While these compounds are certainly released into the rhizosphere in root exudates (Uren, 2007), it is likely that they are rapidly assimilated by the microbial population. This observed decrease in abundance of these compounds in the rhizosphere may be through degradation of phenols and lignin monomers from native organic material by the microbial population.

Soil texture appears to influence the degradation of labile organic compounds, with the Melfort (clay) rhizosphere exhibiting greater depletion (i.e., elevated mineralization) of these

Table 6.3. Compound groups, *m/z* and tentative identification using Py-FIMS of substances depleted in rhizosphere soil. Boldface *m/z* are depleted in Melfort rhizospheres only, and italicized *m/z* are depleted in Elstow only. All other *m/z* are depleted in rhizosphere soils generated on both Melfort and Elstow soils.

Class	*m/z*	Assignment	Class	*m/z*	Assignment
Carbohydrate	**72**	butanone	N-cont.	67	pyrrole
	82	c1-furan	compounds	**79**	pyridine
	96	c2-furan		**80**	pyrazine
	98	OH-methylfuran		81	c1-pyrrole
	100	pentanedione		**93**	c1-pyridine
	102	OH-ketobutanal		95	c2-pyrrole
	110	c1-furaldehyde		**103**	benzonitrile
	112			**107**	c2-pyridine
	113	c1-aminofuranone		**109**	c3-pyrrole
	114			**117**	indole
	126	levoglucosenone		**119**	indoline
	128			121	c3-pyridine
	132	anhydropentose		**123**	c4-pyrrole
	133			*125*	chitin fragment
	142			**131**	c1-indole
	144	dianhydrohexose		*137*	chitin fragment
	162			*139*	chitin fragment
Alkylaromatic	**78**	benzene		**143**	c1-quinoline
	104	styrene		145	c2-indole
	106	xylene		*151*	chitin fragment
	118	c1-styrene		153	OH-acetoxypyridine
	130	c2-indene		**159**	acetylindole
	134	benzofuranone		**161**	indolecarboxylic acid
	172	dehydroshikimic		167	acetylmuramic frag
Phenols/lignin	**94**	phenol		*171*	c3-quinoline
monomers	**108**	cresol		*175*	indoleacetic acid
	122	c2-phenol	Peptide	73	propionamide
	124	guaiacol		**97**	furfurylamine
	136	c3-phenol		**101**	formylhydroxyglycine
	138	salicylic acid		**120**	acetophenone
	150	vinylguaiacol		**129**	quinoline
	152	OH-toluic acid		**135**	aminoacetophenone
	154	syringic acid	Nitriles	55	propanenitrile
	164	p-OH cinnamic		147	ethoxybenzonitrile
	166	phthalic acid		163	dimethoxybenzonitrile
	168	c1-syringic acid	Other	**146**	
	178	coniferyl aldehyde		177	
	180	conifery alcohol		179	

compounds than the sandy clay loam Elstow rhizosphere. Clay content influences microbial populations by offering higher surface areas for colonization, protection from predation (Brimecombe et al., 2007) and control of microbial species composition (Ulrich and Becker, 2006). Marker signals for chitin (m/z 125, 137, 139, 151) (Vanderkaaden et al., 1984), a fungal cell wall component composed of conjugated acetylated amino sugars, however, shows preferential degradation in the Elstow rhizosphere but not for Melfort.

Typically, evaluation of Py-FIMS data involves grouping the m/z markers into compound classes (e.g., carbohydrates, phenols, peptides, etc.) and treating these classes as a unit. However, similarities in the relative abundance between the bulk and rhizosphere samples rendered this evaluation unsuitable for the present study. Nevertheless, the soils did show unique lipid characteristics based on their individual thermal volatilization curves (Figure 6.5, top). Thermograms for the rhizosphere soils showed a distinct release of volatile material in the 300-350°C range; this feature was not observed in the thermograms for the bulk soils (Figure 6.5, top). Because this peak is produced by a compound (or group of compounds) which is (are) released at a comparatively low temperature, it indicates that a thermolabile lipids are being released into the rhizosphere. Thermograms for masses 252 and 254 (corresponding to C_{18} alkene and alkane) have been plotted separately in Figure 6.5 (bottom), to show the contribution of these two compounds to the overall thermogram. These compounds have been observed in lipid extracts from agricultural soils (Bull et al., 2000; Jandl et al., 2007), and are likely released as plant waxes from the roots. These compounds degrade more slowly than carbohydrates and proteins (Baldock et al., 1992), and so are seen here to accumulate in the rhizosphere.

The rhizosphere is the region of soil around the plant root that is most affected by rhizodeposition, thus it is to be expected that an analysis of rhizosphere soil would find an increase in compounds typically associated with root exudates. However, this was not the case in the present study. Indeed, the major trend observed in the development of the rhizosphere was one where native labile compounds were decreased relative to more

recalcitrant structures. Similar observations have been observed in decomposition studies using ^{13}C-NMR, where compounds are degraded in the order proteins/carbohydrates > aromatics > aliphatics (Baldock et al., 1992). This suggests that what we are seeing in the rhizosphere is enhanced decomposition of labile organics as a result of the priming effects of root exudates on microbial numbers and activity.

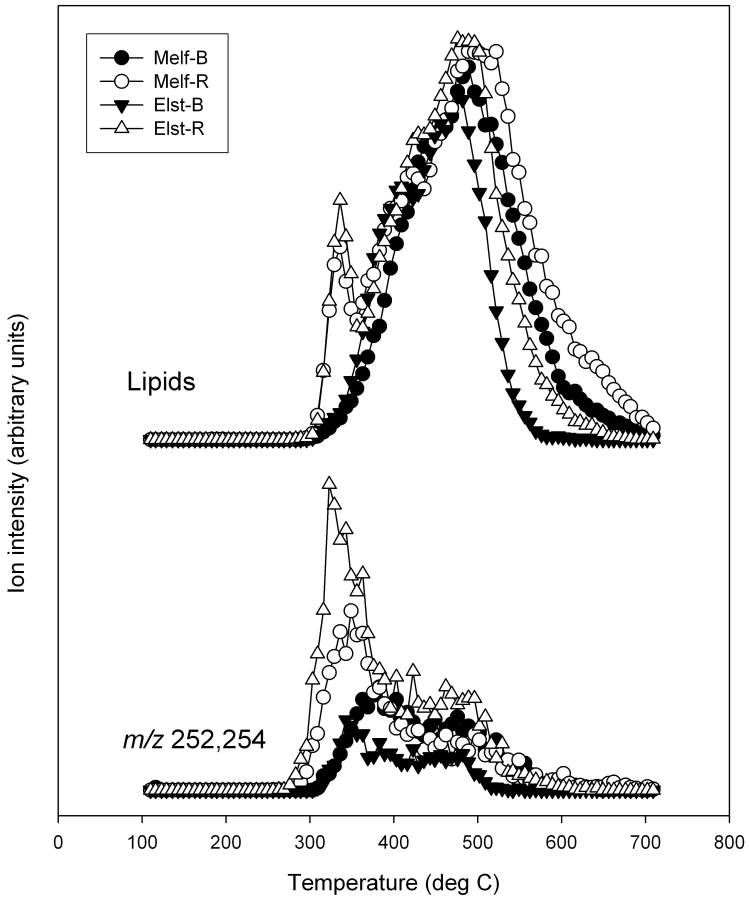

Fig. 6.5. Thermogram for the volatilization of total lipid compounds (top) and for *m/z* 252 and 254 (C_{18} alkene and C_{18} alkane) alone (bottom). Rhizosphere soils show enrichment of these compounds.

6.4 Synthesis

X-ray absorption spectroscopy (XANES) and Py-FIMS results show agreement between some trends observed in overall rhizosphere chemistry. Increases in amine groups in the rhizosphere compared to bulk are seen in both the N-XANES and Py-FIMS data for both soils. Both techniques show increases in carboxylic acids in the Melfort rhizosphere, and decreases in aromatic C and heterocyclic compounds in the Elstow rhizosphere. Otherwise, comparisons of trends observed with these techniques disagree. With carbohydrates, both rhizosphere soils show depletion in Py-FIMS data; however, no C-XANES spectra show any carbohydrate differences. With protein signals, XANES and Py-FIMS remained constant between Elstow bulk and rhizosphere soils; however protein increases were seen using N-XANES and decreases using Py-FIMS for the Melfort site. Aromatic and aliphatic compounds pose a challenge to data interpretation using these techniques. Aliphatic lipid-type compounds in both rhizospheres show increases using Py-FIMS, with no differences observable using XANES. There are also differences between aromatic-type compounds with XANES showing a decrease in aromatic carbon in C-XANES spectra for Elstow rhizosphere soil only, whereas Py-FIMS data show decreases in low molecular weight phenols and alkylaromatics and an increase in high molecular weight aromatics in the Melfort rhizospheres. The observed presence of nitroaromatic compounds in XANES spectra of both bulk soils and greatly enriched in the Elstow rhizosphere represents development and cycling of a class of N-containing compounds not yet investigated with Py-FIMS and only slightly addressed using Curie-point pyrolysis GC-MS and ^{15}N-NMR (Thorn and Mikita, 2000). Their detection in the soil and rhizosphere samples under study shows the applicability of using N-XANES to investigate nitroaromatic cycling, and it suggests an as-yet unknown pedo-ecological meaning of these compounds.

How does one resolve this overall discrepancy between the two techniques used in this study? We must look at the scale at which these two techniques operate. Whereas pyrolysis techniques offer molecular-level characterization, XANES offers finer characterization of bond- and element-specific speciation. For example, resonances corresponding to aromatic

functionalities in the XANES spectra reflect contributions from all aromatic C, regardless of the molecule in which it resides. This includes C in phenols, heterocycles and amino acids that are not bonded directly to oxygen or N. Consequently, a shift in the proportion of any of these compound classes (e.g., an increase in alkylaromatics or a decrease in phenols) will influence the 'amount' of aromatic C detected. Carboxylic acids are another example; i.e., benzoic and aliphatic acids contribute jointly to the carboxylic signal, and separately to the aromatic or aliphatic signals. Pyrolysis mass-spectrometric techniques thus depend on thermal depolymerization and classification into compound classes, whereas XANES analysis resolves elemental functionality.

These analytical differences are useful as complimentary approaches to analyzing intact environmental samples such as soils. In this study, data obtained using Py-FIMS implies that the rhizosphere is characterized by the rapid cycling of organic materials and is fuelled by the process of root exudation. We also see evidence of enhanced depolymerization of the more labile macromolecules, and preservation of recalcitrant organics with aliphatic functions. These processes appeared to be influenced by soil type, and were shown to be accelerated in the rhizosphere of field pea developed in a clay soil (as opposed to the rhizosphere developed in a sandy clay loam). X-ray absorption (XANES) spectra also show the influence of texture on the cycling and transformation of C and N in the rhizosphere-including the depletion of heterocyclic, aromatic, and nitroaromatic functionalities, and enrichment of carboxylic functionalities. The information provided by XANES analyses, however, is at the sub-molecular level. The link between the methods lies in the fact that XANES analysis is species-specific, thus allowing for differentiation between pools based on bond-type, whereas Py-FIMS differentiates based on molecular/polymeric characteristics. Finally, other aspects of the analyses also permit novel investigations of SOM; e.g., XANES allows for the detection of nitroaromatic compounds in soils, even though this is not yet developed in Py-FIMS. Further development of the two techniques in tandem will provide the integration of signals that are representative of pools of agronomic significance.

6.5 Conclusions

Characterization of bond- and element-specific speciation through C and N XANES and molecular-level characterization coupled with multivariate statistical methods of pyrolysis techniques are useful, complementary techniques for investigating the functionality of organic matter C and N. These techniques are applicable to whole soils, allowing for direct measurement of these environmental samples with minimal workup.

New evidence showing development of nitroaromatic compounds using XANES analysis, and aliphatic amine compounds using Py-FIMS indicates unique N cycling in some soils-warranting further investigation. These are also compounds and compound classes that have not, as yet, been investigated in great detail. Other evidence obtained using these techniques shows the rhizosphere to be a region of elevated nutrient cycling and mineralization of native organic material. Whereas labile compounds are preferentially degraded in the rhizosphere, the more stable aliphatic soil- and plant-derived compounds become enriched in the rhizosphere. As well, the evidence suggests that organic chemical development in the rhizosphere is influenced by soil type.

Use of XANES for soil studies will require further refinement of the data evaluation process and in improvements to beamline components to minimize beam-induced damage and maximize detection limits. This study also demonstrates the need to continue soil and rhizosphere research to spatial and imaging techniques such as Scanning Transmission X-ray Microscopy (STXM) (Myneni, 2002; Schumacher et al., 2005; Kinyangi et al., 2006; Lehmann et al., 2008) and to further explore unique cycling of aliphatic amine and nitroaromatic compounds in soils.

Chapter 7

Glomalin-related soil protein contains thioredoxin, non-mycorrhizal-related heat-stable proteins, lipids and humic materials: Evidence from XANES, Py-FIMS and proteomics

Abstract

Glomalin is reportedly a stable and persistent protein produced in copious quantities by arbuscular mycorrhizal fungi (AMF) and may be an important pool of organic N in soil. Glomalin-related soil protein (GRSP), however, is only operationally defined by its extraction method, and has been only poorly characterized at best. Synchrotron-based X-ray absorption near-edge structure (XANES) spectroscopy and pyrolysis field-ionization mass-spectrometry (Py-FIMS) revealed that GRSP contains a consortium of proteins and proteinaceous material along with many impurities. Employing proteomic techniques, we found that glomalin itself may be a thioredoxin-containing protein; however, no homologies with mycorrhizal proteins or DNA were detected. Proteomics techniques further revealed that this fraction contains large amounts of soil-related heat-stable proteins and proteins of non-mycorrhizal origin. Results of this research show that the current extraction procedure that defines GRSP produces a broad mixture of proteinaceous compounds and thereby overestimates glomalin

stocks when quantified using the Bradford assay. Results also showed no evidence for glomalin as a discrete protein originating from AMF. The structural nature of glomalin has yet to be conclusively determined; it is unlikely that the chemical structure of glomalin can be elucidated from the mixture extracted as GRSP.

7.1 Introduction

It is widely accepted that amino acid-, peptide- and protein-N comprise the largest fraction of identifiable organic N-containing compounds in soils, with estimates ranging from 30 to 45% of total soil N (Stevenson, 1982; Schulten and Schnitzer, 1998; Stevenson and Cole, 1999; Kögel-Knabner, 2006). Characterizing the protein content in soil has mainly focused on wet chemical hydrolysis and chromatographic separation of individual amino acids (Bremner, 1965; Schnitzer and Khan, 1972; Stevenson, 1982, 1994), or on studies assaying enzyme activities (Skujins, 1967; Boyd and Mortland, 1990; Tabatabai, 1994; Badalucco and Nannipieri, 2007). Despite the importance and magnitude of the protein fraction, investigations of whole proteins have proceeded slowly (Bastida et al., 2009).

Wright and Upadhyaya (1996) discovered an abundant and persistent extracellular protein produced by arbuscular mycorrhizal fungi (AMF), which was named 'glomalin', after the source organism genus 'Glomales'. Glomalin is reportedly a non-water soluble, highly persistent glycoproteinaceous substance (Wright et al., 1998; Bolliger et al., 2008) produced in mycorrhizal fungal cell walls, and remains in soil after hyphal death (Driver et al., 2005). Glomalin has been linked to aggregate stability (Wright and Upadhyaya, 1998; Rillig, 2004; Wilson et al., 2009), long-term C and N storage (Wright and Upadhyaya, 1996; Rillig et al., 2001; Lovelock et al., 2004; Treseder and Turner, 2007) and responds to land use changes (Rillig et al., 2003). The role of glomalin in the ecosystem is still unclear (Treseder and Turner, 2007); however, the hypothetical role has evolved from that of an active secretion to enhance soil aggregation (Wright et al., 1996; Rillig and Steinberg, 2002), to a hydrophobin that

modifies water acquisition (Rillig, 2005), and finally, to a current hypothesis that glomalin is specifically related to fungal metabolism, and that its role as a persistent soil protein is fortuitous (Purin and Rillig, 2007).

Glomalin was first discovered through the development of an enzyme-linked immunoreactive assay (ELISA) with antibodies generated against AMF spores (Wright et al., 1987, 1996). An extraction method meant to optimize glomalin recovery was then evaluated, with the accepted protocol involving a harsh extraction of soil by autoclaving in a sodium citrate buffer. Glomalin is thus operationally defined, and instead of referring to this substance as 'glomalin', researchers now use the broader term 'glomalin-related soil protein' (GRSP), and reserving the term 'glomalin' for the purified protein or gene product (Rosier et al., 2006).

Since many laboratories are not equipped to carry out the ELISA assay, many studies measure GRSP using the colourimetric Bradford total protein assay (Bradford, 1976; Rosier et al., 2006). Critical assessments of using the Bradford assay to quantify GRSP have shown cross-reactivity with non-AMF proteins added before autoclaving, and with other non-proteinaceous materials added to the GRSP extract (Whiffen et al., 2007; Roberts and Jones, 2008). This can result in an overestimation of GRSP stocks. Since the composition of GRSP (and the structure of individual proteins within this material) remains unknown, and since GRSP is reported to be a significant pool of C and N, there is a pressing need to clarify the composition of the extracted material, and ultimately, to clarify the structure of the glomalin molecule itself.

Synchrotron-based soft X-ray absorption near-edge structure (XANES) spectroscopy at the N and C K-edges is a novel and sensitive tool for the characterization of the chemical bonding environment of specific elements in environmental samples (Stöhr, 1992; Myneni, 2002; Leinweber et al., 2007). XANES has been used successfully in soil and sediment analyses, and here we explore the suitability of N and C K-edge XANES for elucidating the composition of GRSP extracts at the atomic scale.

Pyrolysis field ionization mass spectrometry (Py-FIMS) is a technique where samples are

decomposed into constituent monomers by heating in the absence of oxygen. The mass/charge (m/z) of the monomers are then measured using mass spectrometry, and assigned to specific molecules or compound classes (Schulten, 1996). Py-FIMS provides a molecular-scale m/z fingerprint of complex samples, and has been applied to the characterization of soils, sediments and humic substances (Haider and Schulten, 1985; Sorge et al., 1993a; Schnitzer and Schulten, 1995).

XANES and Py-FIMS supply detailed information on the monomeric and atomic content of the whole GRSP extract, which may be useful in refining quantification assays and in understanding the composition of this operationally defined soil fraction. Characterizing discrete proteins remaining in the autoclaved extract, including glomalin (the protein), requires application of a protein-specific approach. Proteomics consists of a suite of techniques specific to the separation, characterization and identification of proteins. These techniques include electrophoretic separation of protein mixtures followed by peptide sequencing through tandem mass spectrometry (MS) and identification using bioinformatics.

MS-based proteomics is used to identify target proteins based on peptide sequence database matches. It is also used as a screening method for multiple proteins in complex samples. The application of this so-called 'metaproteomics' to soils and soil extracts has been limited to dissolved proteins (Schulze et al., 2005) and contaminated settings (Benndorf et al., 2007). Soil proteomics studies suffer from low protein concentrations and are challenged by the cleanup steps needed to remove interfering substances that cause gel streaking (Bastida et al., 2009).

The goal of this study was to gain a comprehensive assessment of GRSP structures at the atomic, monomeric, and molecular scales using XANES, Py-FIMS and proteomics techniques. The proteomics section also describes a GRSP purification protocol allowing electrophoresis of larger GRSP quantities.

7.2 Materials and Methods

7.2.1 Source materials and reagents

Bovine serum albumin (CAS#: 9048-46-8) and acid phosphatase (CAS#: 9001-77-8) were obtained from Sigma-Aldrich (Mississauga, ON), and were used as reference proteins. Reference humic substances were Pahokee Peat humic and fulvic acids, both of which were obtained from the International Humic Substances Society (St. Paul, MN). Soils were obtained from the St Denis National Wildlife Area (SDNWA), as described in Section 5.2.1. Sodium citrate, sodium hydroxide, hydrochloric acid, EDTA and sodium dodecyl sulphate (SDS) were purchased from BDH/VWR (Mississauga, ON). Tris base, glycine, sodium thiosulphate ($Na_2S_2O_3$), sodium carbonate (Na_2CO_3), sucrose, phenol (Tris buffered), ammonium acetate (NH_4CH_2COOH), potassium ferricyanide [$K_3Fe(CN)_6$], ammonium bicarbonate (Ambic - NH_4HCO_3), silver nitrate ($AgNO_3$) and iodoacetamide (ICH_2CONH_2) were purchased from Sigma-Aldrich (Mississauga, ON). All solvents were high purity grade, and were obtained from BDH/VWR (Mississauga, ON). Bradford reagent and dithiothreitol (DTT) were purchased from BioRad (Mississauga, ON).

7.2.2 Extraction and purification of glomalin-related soil protein

Total glomalin extractions on soils obtained from the SDNWA followed the protocol detailed in Wright and Upadhyaya (1996). Soil (1g) was treated with 8 mL of 50 μM sodium citrate at pH=8, and autoclaved using the liquid cycle for 60 min at 121 °C. Immediately after autoclaving, samples were centrifuged at 5000 × g for 15 min and decanted. The extraction process was repeated until the liquid fraction was straw-coloured, and the supernatants from all extraction cycles were combined. Glomalin extract was then purified according to Wright et al. (1998). Briefly, after centrifugation at 5000 × g for 10 min, the GRSP extract was precipitated by titration to a pH of 2.1 with 0.1 M HCl. After incubation in ice for 60 min, tubes were centrifuged at 5000 × g for 10 min and decanted. The pellet was

resolubilized using 0.1 M NaOH until it was completely reconstituted. Samples were then transferred to dialysis tubing (Spectra/Por membrane, Spectrum, Gardena CA - molecular weight cutoff: 3500 Da) and purified against deionized H_2O for 60 h with constant mixing, changing the water every 12 h. After dialysis, samples were diluted to 40 mL, assayed for total protein content using the Bradford assay (Bradford, 1976; Wright and Upadhyaya, 1996), transferred to multiple centrifuge tubes and frozen at -20 °C. Material required for Py-FIMS and proteomics analyses was freeze-dried in volumes outlined below.

7.2.3 C and N *K*-edge XANES

Glomalin was reconstituted in deionized H_2O, and *ca.* 10 μL was deposited on Au-coated silicon for C K-edge analysis. Gold-coated silicon was prepared by evaporating a gold nugget at *ca.* 650 °C onto 5 mm × 5 mm silicon wafers under vacuum. Glomalin was deposited on copper foil for N K-edge analysis, where blank Cu foil was shown to have no residual N-contamination. Samples were affixed to a steel sample disc using double-sided conductive carbon tape (SGE, Toronto, ON). Carbon and N K-edge XANES spectra were collected using the Spherical Grating Monochromator (SGM) beamline 11ID-1 at the Canadian Light Source (CLS), Saskatoon, SK, and calibration and normalization of spectra at the C and N K-edges was carried out as described in Section 5.2.2.

7.2.4 Py-FIMS

Freeze-dried glomalin residue was transferred to quartz capsules and pyrolyzed at temperatures ranging from 50 °C to 650 °C in steps of 10 °C in the direct inlet of a Finnigan MAT 95 mass spectrometer (Finnigan MAT, Bremen, Germany). Over the full temperature range, 61 scans were recorded for masses ranging from 15 to 900 m/z; ion intensities were normalized on a sample weight basis (i.e., ion counts per mg glomalin). These were combined to produce a single thermogram of total ion intensity (TII), and a single summed and averaged mass spectrum. A detailed description of the Py-FIMS method and the statistical treatment of

TII and weight normalization is given by Sorge et al. (1993a). Molecular assignments for individual m/z biomarkers are based on previous evaluations of synthetic and natural systems (Hempfling et al., 1991; Gregorich et al., 1996; Schulten, 1996), and are compiled in Appendix C

7.2.4.1 Py-FIMS data handling

The Py-FIMS data were subjected to Wilks' lambda feature selection followed by non-metric multidimensional scaling (NMS) ordination. Wilks' lambda scores are F-statistics comparing the variance within treatments to the overall variance and were calculated using SPSS (ver. 16.0) for each individual m/z normalized to TII. Wilks' lambda scores identified 150 m/z which contributed significantly ($p \leq 0.05$) to the overall variance in the data, and were subjected to NMS ordinations using PC-ORD (ver. 5.10) with Sorenson (Bray-Curtis) distance measures.

7.2.5 Proteomics

7.2.5.1 SDS-PAGE

Extracts of GRSP containing *ca.* 10 μg Bradford reactive material were freeze dried, and redissolved in 20 μL pre-incubation buffer containing 20 mM sodium citrate and 1 mM EDTA at a pH of 9.3, and incubated overnight at 4 °C (Wright and Upadhyaya, 1996). Following incubation, 200 μL of a solution containing 3% SDS and 1% DTT dissolved in pre-incubation buffer was added, and samples were boiled for 8 min at 100 °C to denature proteins. After cooling, 30 μL aliquots were transferred to microcentrifuge tubes containing 10 μL of a 4× sample buffer (140 mL H_2O, 1.52 g Tris base, 20 mL glycerol, 2.0 g SDS, 1 mg bromophenol blue, brought to pH 6.8 with 1 M HCl) and centrifuged briefly (*ca.* 10 s).

For sodium dodecyl sulfate polyacrylamide gel electrophoresis (SDS-PAGE), 40 μL samples were transferred to a precast polyacrylamide gel containing 12.5% Tris (12+2, 45 μL, Bio-Rad Criterion, Mississauga, ON), in electrophoresis buffer containing 0.025 M Tris, 0.192 M

glycine and 0.1% SDS, pH=8.3. The molecular weight marker lane was filled with 2 μL of a commercial recombinant protein standard ranging from 10-250 kDa (Kaleidoscope Precision Plus Protein Standard - Bio-Rad, Mississauga, ON). Electrophoresis program was set to 80 V, 30 mA and 2 W for 10 min, followed by 150 V, 70 mA and 14 W for 1 h 40 min. Following electrophoresis, gels were removed from the plastic housing, rinsed with deionized H_2O and fixed by immersing overnight in an aqueous solution of 50% methanol, 12% acetic acid and 0.05% formaldehyde.

Protein bands on the gels were visualized by the silver staining method using a Hoefer Processor Plus Automated Gel Stainer (Amersham Biosciences, GE Healthcare, Baie d'Urfé, QC). Gels were first washed three times with fresh 35% ethanol for 20 min. Gels were then immersed for 3 min in a sensitization solution containing 0.02% sodium thiosulphate (0.158 g $Na_2S_2O_3$ in 500 mL H_2O). After the sensitization solution was pumped out, a total of three rinses with dionized H_2O for 5 min each followed. A silver staining solution containing 0.2% silver nitrate and 0.076% formaldehyde (0.8 g $AgNO_3$, 304 μL formaldehyde in 400 mL H_2O) was then added, and allowed to react with the gel for 25 min. Following staining, three more rinses with dionized water, each for 2 min, followed. Finally, gels were developed using a solution containing 6% sodium carbonate, 0.05% formaldehyde and 0.0004% sodium thiosulphate (24 g Na_2CO_3, 200 μL formaldehyde, 8 mL sensitizing solution in 392 mL H_2O). Gel development times varied, ranging from 30 s to 4 min depending on the concentration of proteins in the bands. When protein bands were visible, the gel was transferred immediately to a stop solution containing 50% methanol and 12% acetic acid. Gels were then stored in 10% methanol/1% acetic acid at 4 °C.

7.2.5.2 Deglycosylation

Deglycosylation of GRSP extracts was carried out using a GlycoProfile II, enzymatic in-solution *N*-deglycosylation kit (Sigma-Aldrich, Mississauga, ON). This kit uses peptide-*N*-glycosidase F from *Elizabethkingia meningoseptica* to enzymatically cleave the glycan

from the protein domain. Freeze-dried GRSP subsamples containing *ca.* 10 μg Bradford reactive protein were redissolved in 40 μL deionized H_2O, and deglycosylated according to the manufacturer's instructions accompanying the kit. After deglycosylation, mixtures were analyzed by SDS-PAGE as described above.

7.2.5.3 GRSP Cleanup

Evaluation of GRSP purification methods was carried out by redissolving 1 mg Bradford reactive GRSP into 500 μL 0.1 *M* NaOH (Benndorf et al., 2007) and 0.2 mg, 1 mg and 2 mg freeze-dried GRSP into 500 μL 'dense SDS' solution (2% SDS + 30% sucrose + 0.1 *M* Tris buffer, pH=8, Faurobert et al., 2007). Proteins were extracted from humic materials by vortexing with 500 μL Tris-buffered phenol (pH=8). Protein in the aqueous phase partitioned into the phenol phase by incubating the mixture for 10 min on ice, followed by centrifugation at 5000 $\times$ g for 5 min. Phenol was recovered, precipitated with 5$\times$ volume (2.5 ml) 0.1 *M* NH_4-acetate in cold methanol (-20 °C) and pelleted by centrifugation at 2000 $\times$ g for 20 min. The pellet was resolubilized in 0.1 *M* NH_4-acetate in cold methanol and rinsed a second time by vortexing, followed by centrifugation at 2000 $\times$ g for 20 min. The final pellet wash was performed with cold acetone (-20 °C), centrifuged at 2000 $\times$ g for 20 min, decanted, and evaporated to dryness under N_2. The extraction cycle was repeated on the same material three times, and phenol fractions from each cycle were analyzed separately by SDS-PAGE as outlined above.

7.2.5.4 Digest, LC-ESI-MS/MS, bioinformatics

After electrophoresis, bands of interest were excised and subjected to an automated digest with trypsin using the MassPrep system (Micromass, Manchester, UK). Gels were destained using two 15 min cycles of a 50 μL, 1:1 solution of 30 m*M* potassium ferricyanide and 100 m*M* sodium thiosulphate (prepared fresh). The destaining agent was removed by rinsing for 5 min with 75 μl distilled water followed by 5 min with 50 μL aceotnitrile (ACN) admixed

with the water. Following aspiration of the water and ACN, 75 μL 100 mM Ambic was added for 5 min, after which 50 μL ACN was added. After 5 min, all remaining liquid was aspirated. Gel fragments were dehydrated by dispensing 50 μL ACN, waiting 5 min, aspirating 45 μL of ACN, and dehydrating a second time with 75 μL ACN for 5 min, followed by complete removal of all liquid. A surfactant solution was then prepared by dissolving 1 mg PPS-silent surfactant {3-[3-(1,1-Bishexyloxyethyl)pyridine-1-yl]propane-1-sulfonate, Protein Discovery, Knoxville TN}, in 500 μL 50 mM Ambic. Each well received 10 μL surfactant solution, and was allowed to sit for 18 min. Gel fragments were then washed with 50 μL ACN, and aspirated after 5 min. Gels were then reduced by adding 50 μL of 10 mM DTT in 0.1 mM Ambic, and allowed to sit for 30 min. The alkylation step followed, where 50 μL 55 mM iodoacetamide in 100 mM Ambic was added and allowed to sit for 45 min, after which 100 μL ACN was added, allowed to sit for 5 min, and all liquid aspirated. Gels were then washed with 50 μL Ambic for 10 min followed by the addition of 50 μL ACN, and all liquid aspirated after 5 min. This was followed by two dehydration steps of 50 μL ACN each for 5 min, followed by complete aspiration.

Trypsin was prepared by dissolving all contents (20 μg) of porcine trypsin (sequencing grade, Promega, Madison, WI, USA) into 200 μL 50 mM acetic acid. After dispensation of 100 μL 0.1 mM Ambic to each sample vial, 25 μL trypsin solution was added, and allowed to sit covered for 30 min. Samples were then incubated on a heating block at 37 °C for 4.5 h. After cooling, peptide fragments were extracted three times for 30 min with 30 μL 1% formic acid/2% ACN. The extraction solutions were combined in a cooled PCR plate. Gel fragments were then extracted two more times for 20 min with 50 μL of 75% ACN and 1% trifluoroacetic acid, and combined with the above extracts in the cooled PCR plate. Samples were then evaporated in a vacuum centrifuge (model DNA 120; Thermo Savant, Colin Drive, NY).

Liquid chromatography-electrospray ionization-tandem mass-spectrometry (LC-ESI-MS/MS) analysis using data-dependent acquisition was performed as described in Aryal and Ross

(2010), with the exception that samples were reconstituted in 0.1% aqueous trifluoroacetic acid. The MS/MS data were searched against the NCBInr database using MASCOT (v. 2.2), with carbamidomethylation of cysteine as the fixed modification and oxidized methionine and glucosylation/glycation as variable modifications. Low abundance of peptides of interest meant that no useable identifications were obtained using the automated system. Instead, peptide data were subjected to *de-novo* sequencing using PEAKS (v. 2.2) software with the same parameters as above, and subjected to BLAST (Basic Local Alignment Research Tool) with a Scoring Parameters Matrix set to PAM30, to find homologies to peptide sequences (Sheoran et al., 2009).

7.3 Results

7.3.1 XANES

Normalized total electron yield spectra for C K-edge XANES of GRSP extracts, reference glycoproteins and humic substances are presented in Figure 7.1. Overall, the C K-edge XANES spectra for GRSP were very similar. The 1s$\rightarrow$ $\pi^*_{C=O}$ (carbonyl) peak between 288-289 eV dominates all spectra. All spectra also show strong, slightly asymmetrical aromatic peaks (at 285 eV), and small variations in the substituted aromatic (at 286.8 eV) and aliphatic (at 287.5 eV) peaks. Scans of GRSP can resolve two types of carbonyl peaks, with carboxylic features (C-**C**=O) occurring at 288.6 eV and with varying amounts of amide features (N-**C**=O) at 288.1 eV. The presence of the N-containing amide bond causes a shift of the C=O peak toward lower energies (Gordon et al., 2003; Stewart-Ornstein et al., 2007; Zubavichus et al., 2008). Reference glycoproteins only show a dominant amide peak (at 288.1 eV), whereas humic substances show a peak closer to the carboxylic acid value of 288.6 eV. While this indicates that GRSP contains large amounts of proteinaceous material, it also suggests that the GRSP extraction protocol releases large quantities of carboxylic acids.

Reference glycoproteins and GRSP extracts show asymmetry on the higher-energy side of

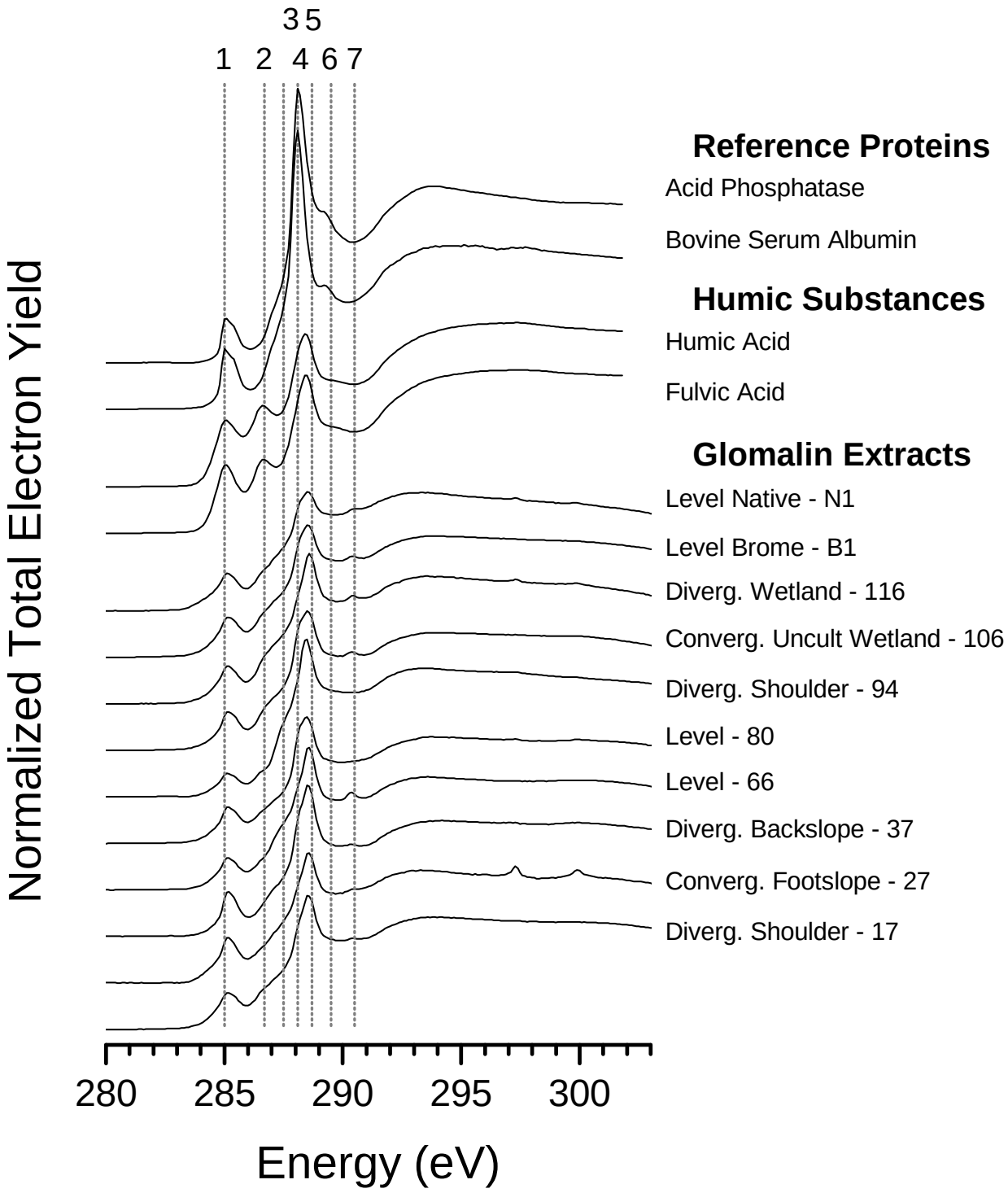

Fig. 7.1. Carbon *K*-edge XANES scans of reference glycoproteins, International Humic Substances Society Pahokee peat humic substances, and glomalin-related soil protein extracts obtained from the transect at St. Denis, SK. Features numbered as: (1) 285 eV, aromatic; (2) 286.8 eV, N-substituted aromatic; (3) 287.5 eV, aliphatic; (4) 288.1, amide; (5) 288.6 eV, carbonyl; (6) 289.5 eV, carbohydrate-OH; (7) 290.5 eV, carbonate.

the 1s$\rightarrow \pi^*_{C_{arom}}$ (aromatic) peak at 285 eV. This indicates the presence of heterocyclic-N, which may be evidence for the presence of histidine in the protein structure, or may arise from the co-extraction of heterocyclic-N in humic substances. Humic compounds do not show this same aromatic peak shape, showing that humic substances contain less aromatic N-containing heterocycles than the reference proteins. Peaks corresponding to substituted aromatic compounds (at 286.8 eV) and aliphatics (at 287.5 eV) show slight variability between the reference proteins and GRSP samples, but show no discernible pattern. Humic substances, however, show strong peaks in the substituted aromatic region (at 286.8 eV) but not in the aliphatic region (at 287.5 eV).

Normalized total electron yield spectra for N K-edge XANES are shown in Figure 7.2. Reference proteins have dominant features corresponding to amide-N (at 401.1 eV), and show other smaller peaks corresponding to heterocyclic pyridines (at 398.7 eV) and pyrazoles and/or nitriles (at 399.9 eV). Low-lying 1s$\rightarrow \sigma^*$ orbitals also produce features at 406 and 412 eV, which are characteristic of amide bonds in proteins (Zubavichus et al., 2008). The presence of these distinct σ^* features in the GRSP extracts and to a lesser extent in humic substances also indicates amide (i.e., proteinaceous material) content in these operationally-defined fractions. Heterocyclic features are different in humic substances, showing mostly pyridinic, with very little contribution from pyrazoles and/or nitriles. GRSP spectra show dominant peaks for amide-N and heterocyclic-N, but these peaks differ in shape and intensity between GRSP extracts, suggesting differences in the composition of this proteinaceous substance.

7.3.2 Py-FIMS

Selected Py-FIMS spectra, and accompanying thermograms, for GRSP are shown in Figure 7.3. The Py-FIMS data for glomalin showed abundant protein/peptide signals (m/z 58, 59, 70, 73, 84), but few signals for carbohydrates (m/z 84, 96, 110). These data also show that GRSP contains many non-proteinaceous substances, including potassium salts (m/z 39 K^+, 113 K_2Cl^+), fatty acids (m/z 256, 280, 308, 312, 396, 410), and phenols/lignin monomers

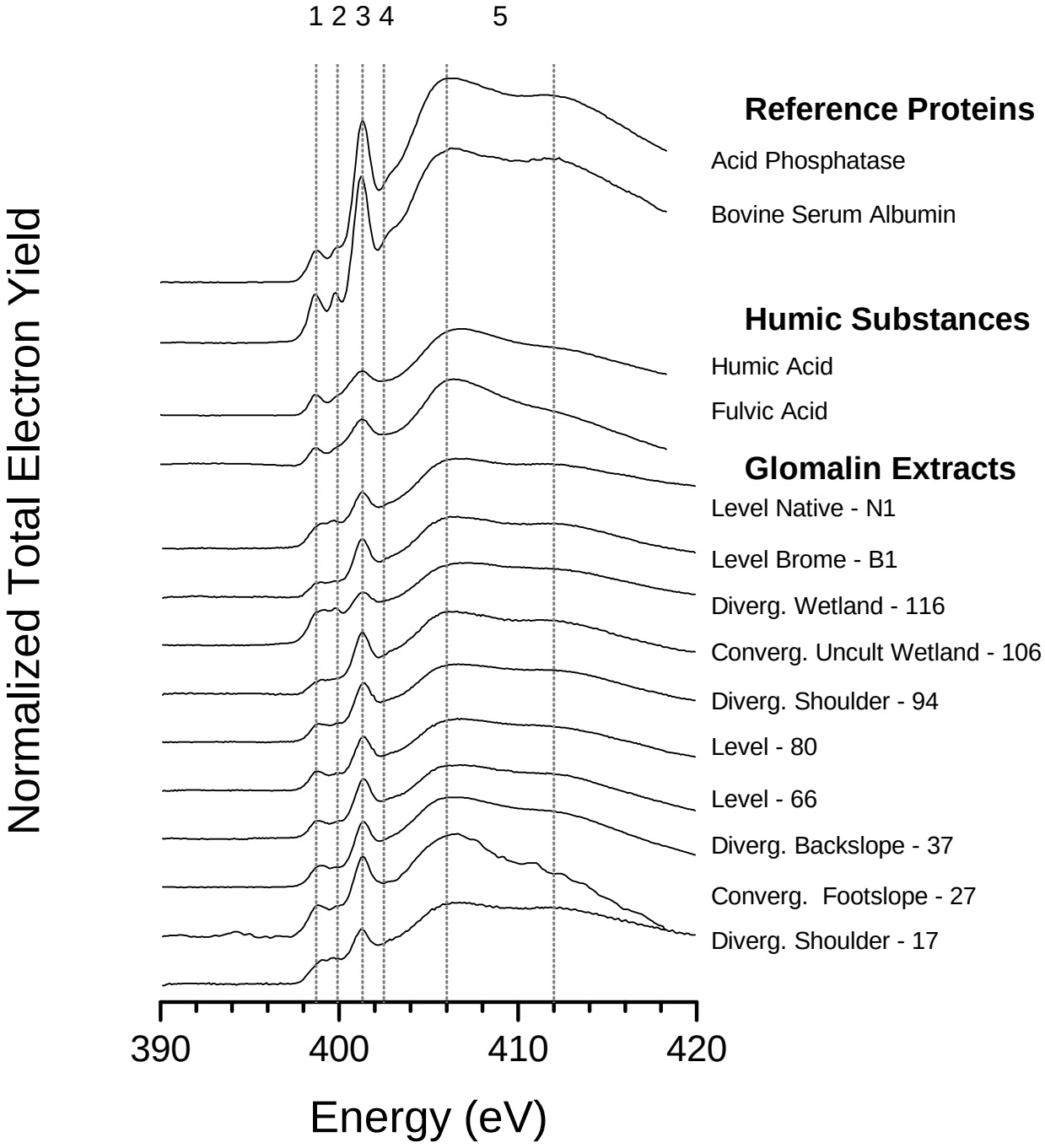

Fig. 7.2. Nitrogen *K*-edge XANES scans of reference proteins, International Humic Substances Society Pahokee peat humic substances, and glomalin-related soil protein extracts obtained from the transect at St. Denis, SK. Features numbered as: (1) 398.7 eV: aromatic N in 6-membered rings (pyridines, pyrazines); (2) 399.9 eV: nitrilic & aromatic N in 5-membered rings (pyrazolic); (3) 401.1 eV: amide (protein); (4) 402.5 eV: N with unpaired electrons in 5-membered rings (pyrrolic); and (5) 406/412 eV: alkyl-N and the 1s$\rightarrow \sigma^*$ feature characteristic of proteins.

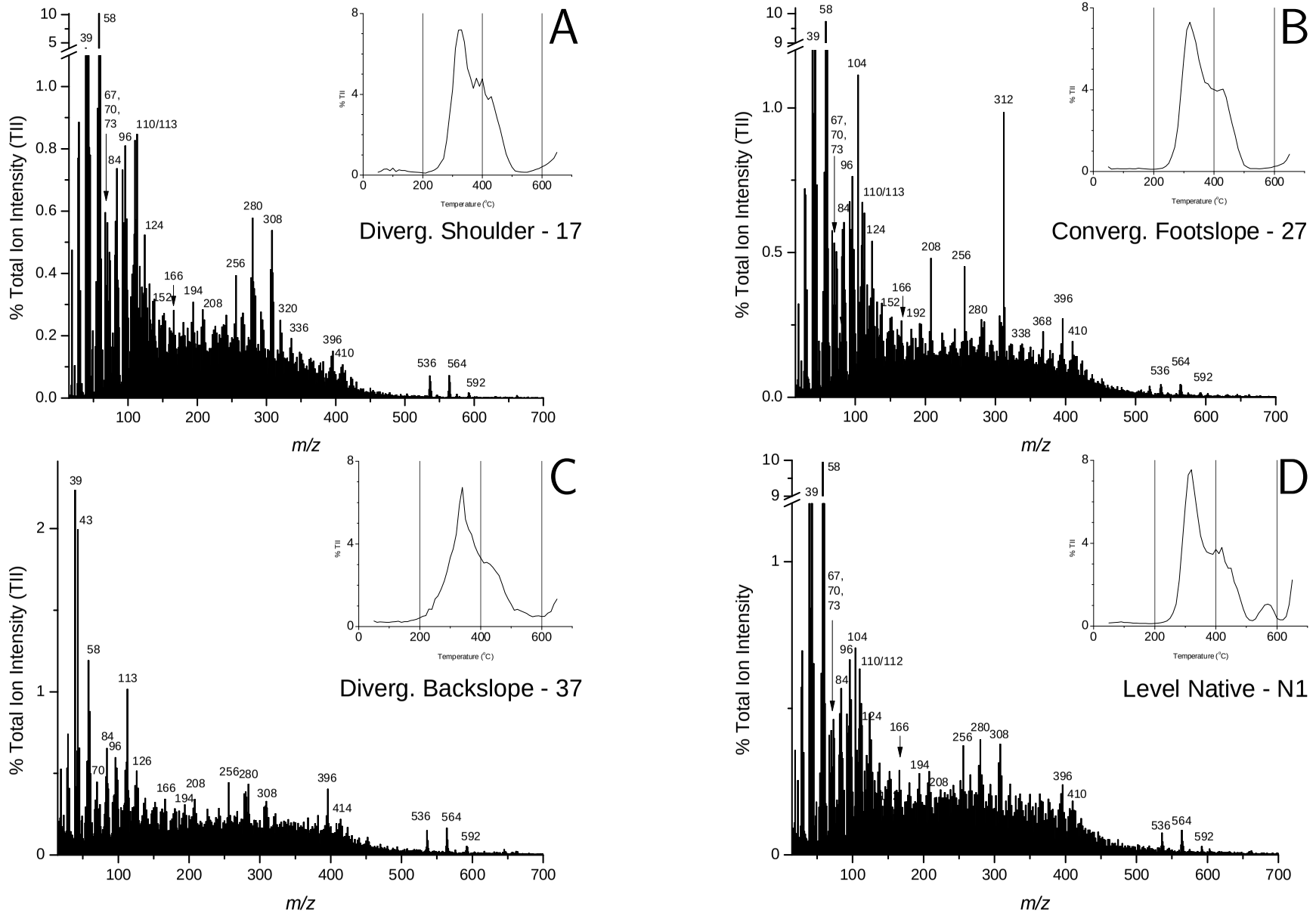

Fig. 7.3. **Summed and averaged pyrolysis field ionization mass spectra and thermograms of total ion intensity (TII, upper right) of selected glomalin-related soil protein extracts obtained from soils from the St Denis National Wildlife Area.**

(m/z 124, 152, 166, 194, 208). There are also signals for very high molecular weight waxes (m/z 536, 564, 592). Thermograms for Py-FIMS spectra (inset Figures 7.3) show strong initial volatilization peaks at *ca.* 325 °C, with smaller secondary peaks at *ca.* 400 to 450 °C. Onset and peak of volatilization temperature is related to stability and biodegradability of organic matter, (Schulten and Leinweber, 1999). These temperatures for thermogram onset are lower than for soils and humic substances (Schulten and Leinweber, 1999), indicating a highly labile substance. This is expected because GRSP is organic material already extracted from the solid phase, and would requires less energy to volatilize pyrolysis products.

Because of the similarity of spectra between GRSP extracts, multivariate feature selection using Wilks' lambda scores was used in conjunction with non-metric multidimensional scaling (NMS) to determine the m/z signals which contributed most to the variation between the spectra. Before the multivariate ordination was carried out, visual inspection of the raw spectra revealed problems with two samples: level - 80 and divergent shoulder - 94 (data not shown). These samples apparently degraded completely in the pyrolysis inlet, producing a continuum of low molecular weight compounds, possibly due to potassium salts which remained in the samples; potassium facilitates catalytic cracking of organic molecules (Pant and Kunzru, 1999). These samples were excluded from subsequent analyses. Wilks' lambda scores filtered 150 m/z which contributed significantly ($p \leq 0.05$) to the overall variance in the data. When only these m/z signals were selected for NMS ordination, the algorithm was unable to find an adequate solution, and clustering was not observed between the different GRSP extracts (Figure 7.4). This indicates that the combination of m/z signals from GRSP extracts showed no discriminating patterns, and that the GRSP are similar in composition.

7.3.3 Proteomics

Figure 7.5 shows SDS-PAGE of proteins in total glomalin-related soil protein (Tot-GRSP) extracts which were denatured and separated without further modifications. A group of two to four bands was apparent in the molecular weight range of *ca.* 55 to 65 kDa. Identification

of several excised bands from the gel pictured in Figure 7.5 was carried out using LC-ESI-MS/MS on tryptic-digested peptides. Database searches on these peptides yielded no hits except for keratin, a common background protein in proteomics analysis, and for the trypsin enzyme used in the digest. This indicates that target protein levels were too low, or that they were not represented in the database.

Knowledge that this material is glycoproteinaceous (Wright et al., 1998) led to the decision

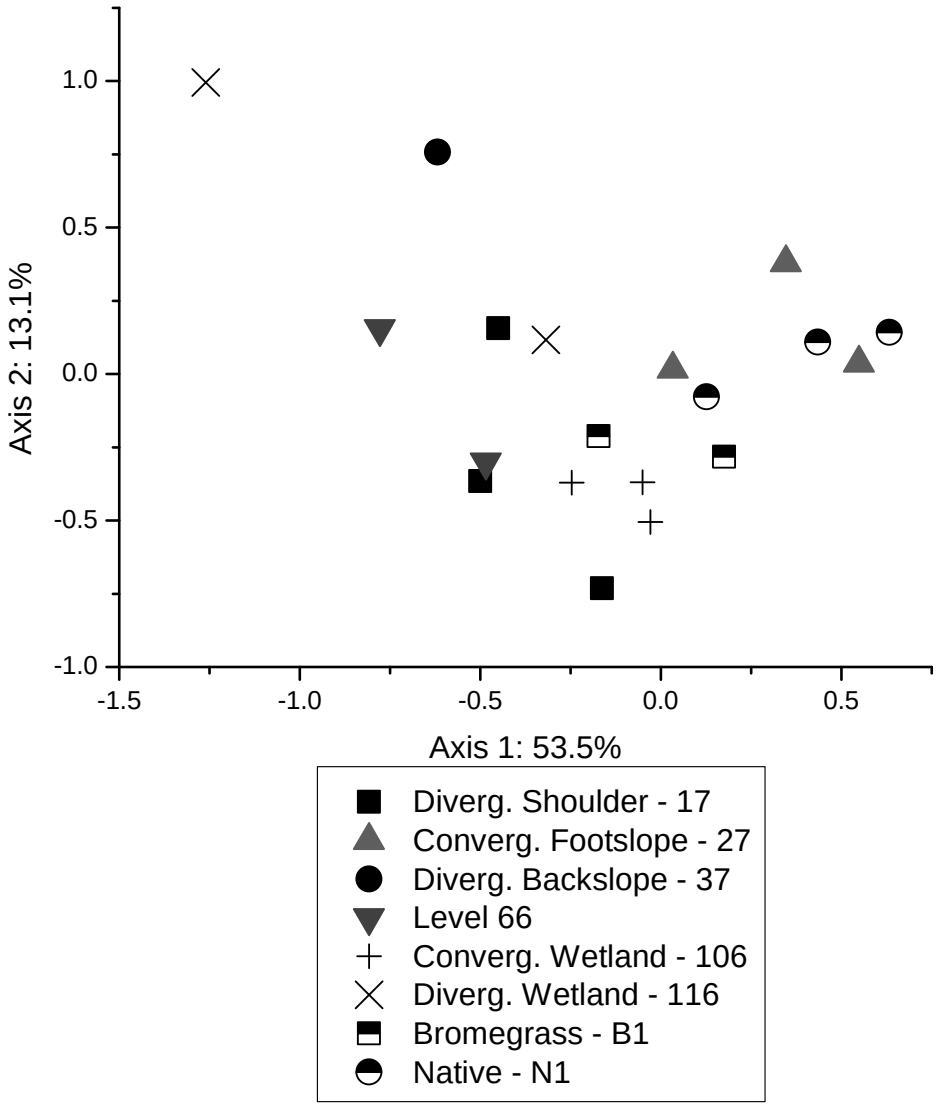

Fig. 7.4. Non-metric multidimensional scaling (NMS) ordination of pyrolysis-field ionization mass spectra of glomalin-related soil protein extracts. NMS performed on 150 m/z signals with $p \leq 0.05$ as determined using Wilks' lambda feature selection.

to enzymatically deglycosylate GRSP. The aim was to (i) better resolve protein domains on the gel by removing oligosaccharides and, (ii) improve chances of characterizing the protein domain by removing the glycan chain(s). A different banding pattern with multiple proteins occurring from *ca.* 25 to 30 kDa emerged in the deglycosylated treatments which were not seen in the denatured protein treatments (Figure 7.6). This suggests that GRSP comprises several base proteins, which are glycosylated with different oligosaccharide units. Database searches on excised protein bands from these deglycosylated proteins, however, yielded the same inconclusive pattern of keratin and trypsin hits as obtained from the non-deglycosylated gel.

Only a small amount of Bradford reactive material could be applied to the gel to avoid unacceptable streaking. Since unsuccessful database searches were likely related to inadequate amounts of protein in the bands, a phenol-based cleanup and a purification method were

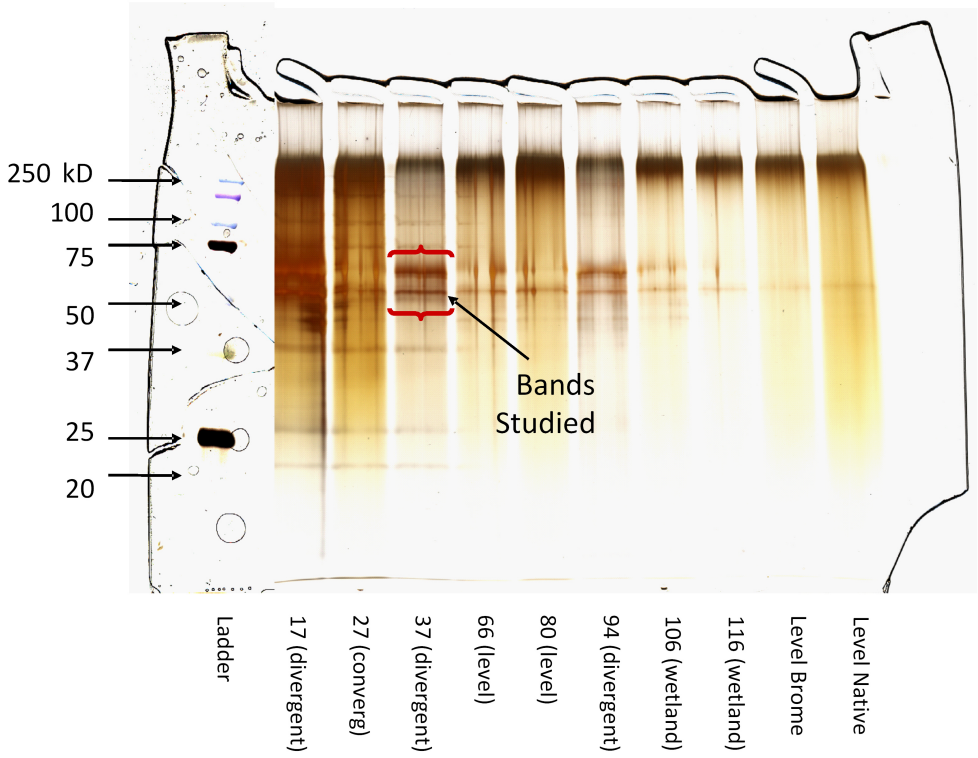

Fig. 7.5. SDS-PAGE of GRSP extracts from the St Denis transect. Gel stained with colloidal silver.

developed and tested. Figures 7.7 and 7.8 show the results of the phenol extraction of GRSP from the NaOH and dense-SDS aqueous phases. The NaOH-phenol partitioning method was the most effective in removing humic substances from the GRSP extract; interestingly, the protein recoveries occurred mostly in the second cycle. Dense SDS was not as effective at separating proteins from humic substances in GRSP.

Sequencing of tryptic peptides using LC-ESI-MS/MS from bands A, B and C excised from the phenol:NaOH cleanup gels indicated in Figures 7.7 and 7.8 was possible. Although the main hits were from background keratin, GRSP peptides were present in quantities high enough to yield *de-novo* sequences which could then be identified manually through comparison using BLAST to protein and nucleotide databases.

The results from the BLAST searches are shown in Tables 7.1 to 7.3. Many sequences reported in this study matched thermophilic organisms and proteins from thermophiles.

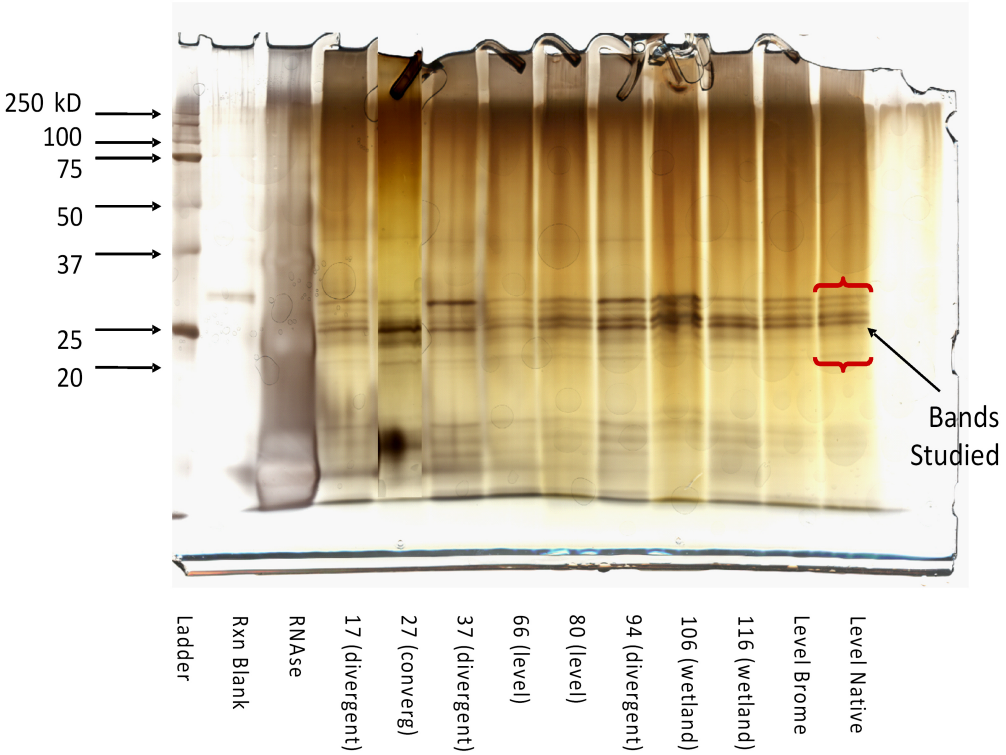

Fig. 7.6. SDS-PAGE of glomalin related soil protein after deglycosylation and denaturing using PGNase enzyme and N-deglycosylation kit protocol.

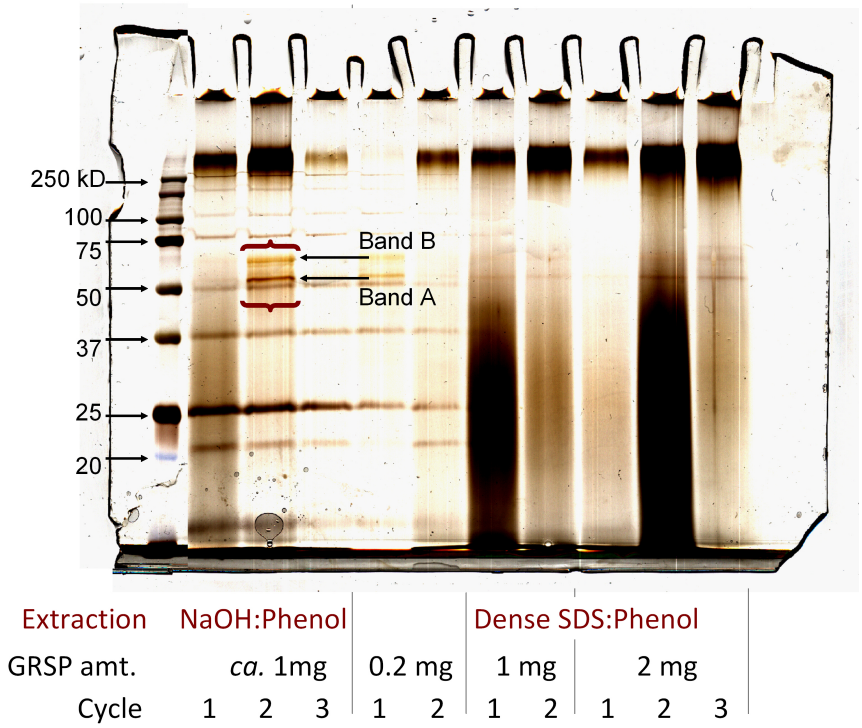

Fig. 7.7. 1-D SDS PAGE of glomalin related soil protein (GRSP) purification optimization. Gel developed by silver staining. GRSP extracted in 2nd cycle of purification process using 0.1M NaOH. Tryptic digests and proteomics carried out on indicated band (above 50 kD).

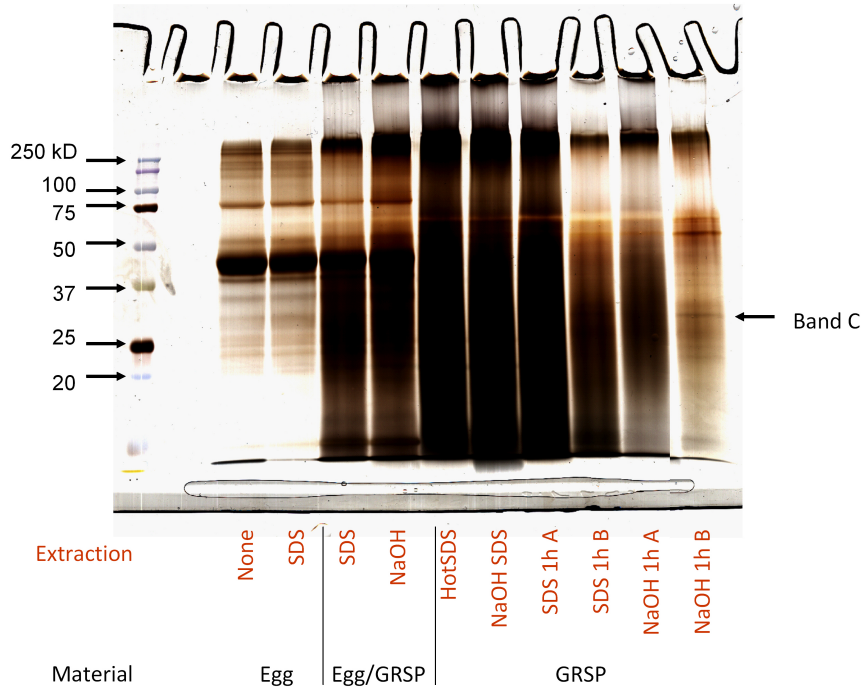

Fig. 7.8. 1-D SDS PAGE of glomalin related soil protein (GRSP) purification optimization. Gel developed by silver staining. Tryptic digests and proteomics carried out on indicated band (above 50 kD).

While the quality of de-novo sequences varies, as do the BLAST scores, it appears that the extraction/autoclaving process selected for a range of heat-stable proteins and organisms. In addition, we also report multiple hits for proteins derived from soil bacteria and non-mycorrhizal fungi (Tables 7.1 to 7.3), which may persist through the extraction process. Most importantly, none of these hits were from AMF, of which a 2-D proteomic profile for *G. intraradices* exists (Dumas-Gaudot et al., 2004), indicating that the accepted GRSP extraction method may not be selecting for the material of interest.

7.4 Discussion

7.4.1 XANES and Py-FIMS

X-ray absorption spectroscopy and Py-FIMS were useful techniques in determining the overall chemical structure of GRSP at the atomic and molecular scale. This information is useful toward determining the kinds of materials released by the extraction protocol, thus providing assessments of the bulk composition of GRSP.

The XANES spectra of GRSP were similar, but not identical. Slight differences in the N-XANES spectra at energies below the amide peak (Figure 7.2), and differences in the shape and intensity of peaks in the C-XANES spectra (Figure 7.1), suggest differences in the composition of this proteinaceous substance. These spectral differences lead to a contention that GRSP is a family (or mixture) of proteins, mixed with a range of co-extracted non-proteinaceous substances, which may include compounds formed by the heat and pressures of the autoclaving procedure.

Table 7.1. Basic Local Alignment Search Tool (BLAST) results of *de-novo* sequences from excised band A in Figure 7.7

Peptide	*de-novo* score	BLAST score†	BLAST E-value‡	Assignment
Thioredoxin				
LLNDKNPGTAPK	46.14	28.6	75	Thioredoxin
NNLDQNPGTAPK	54.53	34.1	1.6	Thioredoxin
LAPLLDELADEYQGK	51.23	41.4	0.011	Thioredoxin
EDAPLLDELADEYQGK	98.74	40.9	0.015	Thioredoxin
Thermophilic				
NPTLLFK	86.21	25.7	420	*Thermococcus sp.*
ELTDVALR	59.80	25.2	644	*Thermomicrobium roseum*
VGSGQPLNDR	63.71	27.4	148	Thermoresistant gluconokinase
DLSKFLNAAK	60.50	26.9	247	Putative heat shock protein PS1 (2nd hit)
		26.9	247	*Thermoanaerobacter sp.*
DLSQFLNAAK	99.57	28.2	103	*Pyrobaculum arsenaticum*
TLLTPGPGNDPK	19.37	29.5	43	*Sphaerobacter thermophilus*
Y(OxM)KA(OxM)TDAQAR	67.13	31.6	9.6	Ubiquitin activating enzyme - Arabidopsis
APADLDSLLAEAR	12.24	31.2	13	*Lachancea thermotolerans* (2nd hit)
T(OxH)EGRSQFLNAAK	99.11	27.8	137	*Streptococcus pyogenes*
MANAYLSSNPLVAD(OxM)K	11.85	30.8	17	*Meiothermus silvanus* (2nd hit)
MNFQENGELVD(CamC)DKNK	72.49	30.8	17	Putative flap endonuclease - *Sulfolobus sp*
LDLVYWGNTK	91.56	26.9	248	Ferrochelatase - *Thermomonospora curvata*
L(OxH)DADNGEPR	32.34	28.6	77	Ferredoxin Fe-S binding domain-containing

(continued on next page)

Table 7.1 - continued

Peptide	*de-novo* score	BLAST score†	BLAST E-value‡	Assignment
Fungi, Soil Bacteria				
LATVLSPR	87.04	26.9	99	Polysaccharide biosynthesis - Bacillus cereus
VT(OxM)QNLAGTR	92.57	28.2	102	*Gibberella zeae*
LEPELAGTYR	77.82	29.5	42	Aminodeoxychorismate lyase - many spp
ESVKADLDVAR	44.29	29.1	57	kinesin related - *Nectria haematococca*
EGTLLKEKGTK	66.22	29.1	57	*Chryseobacterium gleum*
LSALEEAGLQQLR	89.44	31.6	9.7	*Ustilago maydis*
VDPHLDSGLMVVLK	77.21	28.2	102	Transcript regulator CysB - *Pseudomonas spp.*
LPMTLLYGGGGPDNK	25.41	28.2	101	Choline kinase - *Ajellomyces dermatitidis*
LAPGAPMNGGMHTAGTVPLPR	6.39	35.0	0.91	*Aspergillus flavus*
LGEHPEKEAEGRVDLAD(OxM)AK	58.29	35.0	0.91	*Methylobacterium extorquens*
EPTHGQNGRLG(GluK)NDLTGTNK	62.51	28.6	75	*Geobacillus sp.*
NVSP(GluN)LV(GluN)NAARPDLTKLLNGGMR	67.50	32.0	7.0	Cytidylyltransferase - *Thioalkalivibrio sp.*
High de-novo scores, no matches				
VVTVSLPR	99.95			
AAGTDSPGR	82.52			
(OxH)GALYHSK	99.86			
SDLTSPGLR	69.16			
SSANDLEG(OxH)K	92.71			
SPAGLLVYNAK	71.40			
SYEGLDNDLMLLK	90.32			
AKLTFDGSLMVVLK	89.16			

†BLAST - Basic Local Alignment Search Tool

‡E-value - Expectation value. The lower the E value, the more significant the score

Table 7.2. Basic Local Alignment Search Tool (BLAST) results of *de-novo* sequences from excised band B in Figure 7.7

Peptide	*de-novo* score	BLAST score[†]	BLAST E-value[‡]	Assignment
Thioredoxin				
LNLDKNPGTAPK	98.80	32.5	6.0	Thioredoxin
Thermophilic				
YEELEV(OxH)AK	95.35	28.6	85.0	*Thiomicrospira crunogena*
NQYEDELNKR	50.67	30.8	20.0	*Roseobacter sp.*
Fungi, Soil Bacteria				
LATVLSPR	87.53	26.9	193	Polysacch. biosynth. prot - *Bacillus cereus*
FVNDAAPNVK	47.78	32	8.1	Blotch Fungus (*Phaeosphaeria nodorum*)
S(OxH)PGLASPSSGGGSGGGSNR	31.07	35.0	0.98	*Chlamydomonas reinhardtii*
(GluQ)LKGPYSS(OxM)TGGPTDGKPPR	26.42	31.6	9.9	*Herpetosiphon aurantiacus*
High de-novo scores, no matches				
VVTVSLPR	87.93			
SSANDLEG(OxH)K	99.99			
VVHQELNSR	99.37			
AQYEELAGAR	82.43			
STSSFSSSGER	55.06			
HVGEDQNNKR	79.71			
SKAEAESLYKSK	49.24			

[†]BLAST - Basic Local Alignment Search Tool

[‡]E-value - Expectation value. The lower the E value, the more significant the score

Table 7.3. Basic Local Alignment Search Tool (BLAST) results of *de-novo* sequences from excised band C in Figure 7.8

Peptide	*de-novo* score	BLAST score[†]	BLAST E-value[‡]	Assignment
Thioredoxin				
None				
Thermophilic				
YEKLAGAGLGTAK	28.29	29.9	35	*Acetobacter pasteurianus*
NQYEDELNKR	28.46	30.8	19.0	*Tetrahymena thermophila*
VGGGADALADMGAPK	19.27	29.9	35.0	*Deinococcus deserti*
GPPYADMHTDELMNPEK	35.36	32.0	7.7	Fe-S oxidoreductase - *Campylobacterales*
Fungi, Soil Bacteria				
APVDADLNVAR	37.80	33.3	3.4	*Penicillium marneffei*
LDDLEDAMLPVK	69.60	32.0	7.9	*Pseudomonas aeruginosa*
EEFSSGSAGLAFNGER	12.35	35.0	1.0	*Myxococcus xanthus*
(GluH)HPEQEAEGRVDL(OxM)DAAK	64.07	32.9	4.3	*Rhodopseudomonas palustris*
WNCDCC(OxW)(OxM)CDPPCYR	100.00	29.9	35	*Mycobacterium kansasii*
High de-novo scores, no matches				
S(OxH)YEQLLAK	65.52			
VT(OxM)QNLAGTR	91.83			
LPLDRAT(OxM)EK	99.47			
TLDGSLFLGLR	60.15			
YEELAGKTAGR	96.13			

[†]BLAST - Basic Local Alignment Search Tool

[‡]E-value - Expectation value. The lower the E value, the more significant the score

It was expected that glomalin, which is thought to be a glycoprotein, would show significant amounts of the carbohydrate signal at 289.5 eV in the C-XANES spectra of GRSP, similar to the signal observed in the spectra of glycoprotein standards (Figure 7.1). However, this was not the case. Indeed, this peak was absent from all of the GRSP scans; moreover, the Py-FIMS data also showed weak signals for carbohydrates. Low carbohydrate and aliphatic levels also were reported by Schindler et al. (2007), who used ^{13}C-NMR to characterize GRSP from soils with varying amounts of organic matter content. Proteinaceous material was abundant, with high amide-N signals in the N-XANES and C-XANES scans (Figures 7.1 and 7.2), and abundant peptide *m/z* in the Py-FIMS data (see Section 7.3.2). This showed that GRSP indeed contains proteinaceous material, but this did not support the contention that glomalin is a glycosylated protein. Instead, it supported the possibility that GRSP is a heterogeneous mixture of many proteins, of which only a portion may be glycosylated.

The NMR study published by Schindler et al. (2007) found that GRSP was predominantly aromatic, with significant carboxylic functionality. The C-XANES data supports this relationship (see Figure 7.1) insofar as it shows that GRSP is highly carboxylic and aromatic in nature. However, because molar absorptivity differs between functional groups, it is not possible to calculate percent contributions of each compound class. In addition, the NMR spectra were recorded using direct polarization (DP), whereas soil and environmental studies commonly use cross-polarization (CP) to increase sensitivity (Silverstein et al., 2005). Aromatic compounds have a higher response factor in DP (Xing et al., 1999), thus potentially leading to the assumption of lower carboxylate quantities. Nevertheless, carboxylic acids apparently are present in large amounts in GRSP, which is also seen in the abundant signals for fatty acids in the Py-FIMS data (see Section 7.3.2).

Many phenolic compounds also were detected in GRSP using Py-FIMS, and to a lesser extent, C-XANES. Polyphenols may be derived from co-extracted lignins and humic substances. Heterocyclic-N also was detected in GRSP in the form of pyridines and pyrroles through N-XANES. These varying spectral features may arise from the presence of histidine in protein

structures or from DNA nucleotides co-extracted with GRSP. They may also arise as the result of Maillard reaction products formed by heating the soil through the autoclaving extraction procedure (Jokic et al., 2004b), or through beam damage of the peptide and protein-N (Leinweber et al., 2007). Polyphenols and substituted heterocyclic-N may be problematic when using the Bradford total protein assay because of cross reactivity with the Coomassie dye (Whiffen et al., 2007). Like saponified fatty acids, any co-extracted polyphenols, N-heterocycles and nucleotides in GRSP may confound quantitative determinations.

Glomalin-related soil protein has been correlated with soil aggregation, arguably as a result of GRSP hydrophobicity (Wright and Upadhyaya, 1998; Rillig, 2004; Rillig and Mummey, 2006; Wilson et al., 2009). Soil lipids, however, also have been associated with aggregate and mechanical stability. Hempfling et al. (1990) found that fatty acids, aliphatic polymers, lignins and carbohydrates were important in aggregate stability, and Piccolo and Mbagwu (1999) found aggregate stability improved with the addition of hydrophobic humic materials. In the present study, GRSP was co-extracted with many hydrophobic compounds, including fatty acids, heavier plant waxes and lignins. These various clues to the influences over soil aggregation require further research into how fungi, humic materials and organic matter contribute to soil aggregation.

7.4.2 Proteomics

X-ray absorption and Py-FIMS have proven useful in describing the bulk chemical composition of GRSP, showing that it contains a range of materials which can be broadly classified as proteinaceous. These techniques, however, were not as effective in elucidating the individual proteins. Thus, proteomics, which comprises a suite of techniques based on gel electrophoresis, mass spectrometry and bioinformatics were used to ascertain protein-specific identifications and information regarding protein homology.

In the present study, a gel pattern consisting of 2 to 4 bands between 55 and 65 kDa was observed in the GRSP extract. Chen et al. (2009) observed this same gel pattern for

extracts of total GRSP extracted using 50 mM Na-citrate, pH = 8. Wright et al. (1996, 1998), and Wright and Upadhyaya (1996), however, observed patterns consisting of two higher molecular weight bands between 90 and 100 kDa for GRSP extracted from soil and from AMF fungal hyphae using the 'easily extractable' glomalin (E-GRSP) method (20 mM Na-citrate, pH = 7, Wright and Upadhyaya, 1996). Furthermore, Bolliger et al. (2008) used the E-GRSP method and showed a slightly different pattern of five to six bands between 60 and 90 kDa. Differences in molecular weight ranges between the various studies suggest that varying extractant concentration and/or pH causes different proteins to be released. Alternatively, similar proteins may be released and modified, perhaps by changes to the glycan domain. Since the purpose of the present study was to examine the composition of GRSP using proteomics, the Tot-GRSP method was selected because it releases more proteinaceous material compared to the E-GRSP method (Rosier et al., 2006). The same approach was taken by Bolliger et al. (2008)(i.e., E-GRSP was used for immunoblotting and staining, whereas Tot-GRSP was used for LC-ESI-MS/MS), though, SDS-PAGE gels of Tot-GRSP were not provided. Despite using the Tot-GRSP extraction method in the present study, automated sequencing was not successful in identifying any proteins except for background keratin.

Deglycosylation of the GRSP was used to improve gel separation of the proteins by removing glycans, and to increase the chances of bioinformatic identification by removing the glycosylation variable. The glycan domain was characterized by Wright et al. (1998) who used capillary electrophoresis to study N-linked oligosaccharides cleaved by peptide-N-glycosidase F from AMF extracts and from GRSP extracts from soils. Results from the AMF extracts showed that a single oligosaccharide was released, while soil GRSP extract results showed multiple oligosaccharides, of which the largest component was that observed in the AMF samples. This indicates that GRSP extracted from soils includes multiple glycoproteins, or glycoproteins other than glomalin.

The focus of the present study was the protein domain. Gel electrophoresis of deglycosy-

lated GRSP (Figure 7.6) showed a series of 5 to 6 bands at lower molecular weights than those observed in the glycosylated gels (Figure 7.5). As well, there were more visible bands after deglycosylation. Because glycoproteins may contain a range of glycan sizes and/or multiple glycan chains (Nelson and Cox, 2005), evidence presented in this study, like that reported by Wright et al. (1998), suggests that the glycan domains on these proteins are highly variable, indicating further heterogeneity in GRSP composition. Despite deglycosylation, database searches on excised bands, like the glycosylated automated searches, also yielded no hits.

Lack of success with the automated searches was attributed to low protein concentrations in the gel. Increasing the overall amount of GRSP resulted in excessive streaking, thus, a cleanup method was required to allow electrophoresis of higher levels of protein material without streaking. Previously published methods for SDS-PAGE of GRSP were thus unsuitable for proteomics analysis because of low protein abundance and because crude GRSP extracts contain humic substances that react with silver stain and cause streaking (Bastida et al., 2009). In this research cleanup techniques using phenol partitioning were evaluated for their ability to reduce streaking and allow increased amounts of GRSP to be applied to the gel. A comparison was made between aqueous phases of a 'dense SDS' buffer and 0.1 M NaOH. Although Chen et al. (2009) advocated an extraction system based on SDS for possible characterization of the soil metaproteome, the results presented here show 0.1 M NaOH to be the most effective aqueous phase for isolating GRSP (Figures 7.7 and 7.8).

Database searches were successful on protein bands excised from gels where GRSP was first cleaned, but only after the generation of *de-novo* peptide sequences. Normally, the MASCOT database searching algorithm exports peptide information of the best match in the database, whereas *de-novo* sequencing uses fragmentation patterns from the raw MS/MS data to generate peptide sequences which can then be directly compared using BLAST to peptide and nucleotide databases (Sheoran et al., 2007; Bastida et al., 2009). BLAST database hits with the highest scores and coverage were for thioredoxin (Tables 7.1 and 7.2). Thioredoxin hits were obtained from bands A and B; however no evidence for thioredoxin

presence was found in band C (Table 7.3). Thioredoxins are small proteins of about 12 kD, which does not match the migration distance of the bands from which the identification was made (*ca.* 50 kD). Also, thioredoxins are not glycoproteins themselves, which does not match the existing evidence for glomalin structure. These hits may instead reflect the presence of larger proteins that contain a thioredoxin domain. Examples of these proteins include thioredoxin reductases (TrxR, Kern et al., 2003), oligosaccharyltransferases (Schulz et al., 2009), and protein disulfide isomerases (PDI, Wilkinson and Gilbert, 2004).

The presence of a thioredoxin in GRSP is a new piece of information in the puzzle of glomalin structure, and may help point a new direction for GRSP characterization. Evidence in the literature shows that glomalin (the protein) is a putative homolog of Hsp60 (Gadkar and Rillig, 2006). Heat shock proteins are molecular chaperones responsible for protein re-folding by catalyzing disulfide bond formation in the event of heat stress damage (Nelson and Cox, 2005), and several of these protein families contain thioredoxin domains (Raia et al., 1995; Scharf et al., 1998; Harada et al., 2001; Lee et al., 2009). A particular class of heat stable chaperone is the PDI, which contains a thioredoxin-like domain, and is found in all organisms (Wilkinson and Gilbert, 2004). It is possible then, that this particular protein is a PDI present in soil that has been extracted in the GRSP fraction.

Despite the contention that glomalin is a protein of mycorrhizal origin, there were no database hits from any excised bands from AMF sequences. The database searches instead yielded many hits for thermophilic proteins and from non-mycorrhizal soil-based organisms. Bolliger et al. (2008) also reported limited success with their database searches, and found only homologies with some free living soil bacteria. Of particular interest is the lack of AMF-related protein hits in the results of the proteomic database search. This indicates that the proteinaceous material in GRSP is either not of AMF origin or, represents only a small part of the overall protein content. While Gadkar and Rillig (2006) previously reported homology between glomalin and heat shock protein 60 (Hsp60), no homologies between any proteins isolated in the present study matched sequences in Hsp60, despite the inclusion of

the sequence for Hsp60 isolated from *G. intraradices* in the database search.

Confirmed results using BLAST searches depend on the completeness of the databases. Development of soil metaproteomics has revealed that much of the protein profiled from soils is not identifiable (Schulze et al., 2005; Benndorf et al., 2007; Bolliger et al., 2008; Bastida et al., 2009). In this study, several peptides with high *de-novo* scores yielded poor hits from the BLAST database (see Tables 7.1 to 7.3), indicating that these peptides are likely from proteins not yet sequenced, and may be important in the characterization of glomalin.

Most of the evidence presented shows that glomalin (the protein) as a product of AMF is either not present, or is poorly represented in the GRSP mixture. The current methods of isolation and detection of glomalin rely on two major components. The first is isolation and extraction through autoclaving, and the second is through detection, either by the Bradford total protein assay or by ELISA. Autoclaving of soil samples is meant to denature heat-sensitive proteins, and to use heat and citrate complexation to extract physically bound hydrophobic proteins. This is complicated somewhat by the adoption of easily extractable and total extractable glomalin protocols which modify the autoclaving time and number of autoclave cycles (Wright and Upadhyaya, 1998; Janos et al., 2008), and the introduction of alterative complexation agents such as sodium pyrophosphate and borate (Wright et al., 2006). We see that SDS-PAGE banding patterns occur at different protein molecular weights when using the easily extractable glomalin as compared to total extractable. This indicates that either different proteins are being extracted, or that similar proteins undergo modifications in the more intensive total-GRSP extraction process. Also, the extraction process apparently does not remove all non-glomalin-related protein, as Whiffen et al. (2007) demonstrated in experiments where proteins spiked into soils were recovered after autoclaving.

Secondly, the methods of detection may not be adequately specific for glomalin. Certainly, it has been demonstrated that the Bradford total protein assay is not specific enough to quantify glomalin in GRSP extracts of soils. The ELISA method should, however, be reactive only to proteins present in AMF. The combination of autoclaving and AMF-specific detection

thus is the rationale for the use of this method in identifying and quantifying glomalin. The glomalin-reactive antibody usee in the ELISA test is named MAb32B11, and was developed against spores of *G. intraradices* (Wright et al., 1987, 1996). However, the binding site of this antibody is still unknown. Presumably the antibody is reactive to any of a number of proteins present in *G. intraradices* spores, and the question raised in this study is whether glomalin is truly an AMF-specific protein, or whether it is more widely conserved. If, indeed, glomalin is a widely conserved protein, then efforts to understand C and N cycling and soil aggregation will have to refocus on non-mycorrhizal organisms.

7.5 Conclusions

X-ray absorption spectroscopy and Py-FIMS revealed that GRSP is a rich mixture of proteinaceous, humic, lipid and inorganic substances. Protein-specific characterization of GRSP using MS- and PAGE-based proteomics showed no evidence for glomalin as a discrete protein originating from AMF.

Chemical analysis of GRSP showed little carbohydrate, despite previous reports that glomalin is a glycoprotein. Other results show that humic substances comprise a small fraction of GRSP, and that lipids and fatty acids are predominant non-proteinaceous co-extractants. We speculate that these may include compounds formed by the heat and pressures of the autoclaving procedure, and that they may contribute to overestimations of glomalin when the Bradford assay is used.

A purification method described in this research was required for proteomic analysis of GRSP. Proteins tentatively identified using proteomics consisted of a thioredoxin, proteins from thermophilic organisms, proteins from non-mycorrhizal soil organisms, and proteins for which no database hits were registered despite high confidence values associated with de-novo sequences. Immediately clear is the lack of AMF-related protein hits in the results of the proteomic database search. This indicates that the proteinaceous material in GRSP is either

not of AMF origin or that AMF-derived proteins represent only a small part of the overall protein content. This indicates that the current depth of information in the NCBInr database is insufficient for characterization of GRSP or soil-related protein profiles, a concern which has been raised elsewhere (Bastida et al., 2009). Indeed, linking glomalin to an AMF origin has been based on its reactivity to an enzyme-linked antibody generated against mycorrhizal spores (Wright et al., 1996). This raises the need to understand the specific mechanism of the glomalin-reactive antibody MAb31B11, and the protein sites to which it binds.

Based on evidence presented here, we propose three areas for further GRSP research. First, extensive proteomics fingerprinting should be carried out using a controlled system using AMF hyphae cultivated on RiT-DNA carrot roots (Dumas-Gaudot et al., 2004). This information would be very useful for building the current database set, thus improving the search quality in the bioinformatics stages. Secondly, a critical assessment of a range of extraction conditions similar to that undertaken by Chen et al. (2009) should be explored specifically for characterizing GRSP, and refined by developing cleanup techniques that allow for the concentration of large amounts of glomalin so that 2-D methodologies can be used. After these fundamental issues are addressed, a new approach to quantifying glomalin may be developed together with the targeted development of ELISA antibodies against known proteins.

Chapter 8

Synthesis and overall conclusions

A strong analytical basis for determining the forms and structures within which soil organic N is bound is imperative for understanding the cycling, storage and reactivity of N in the biosphere. Soil organic matter is a complex medium, challenging to the organic and inorganic chemist. Applying advanced molecular techniques to the characterization of soil organic N provides useful assessments of this complex medium.

The research that comprises this dissertation sought to incorporate state-of-the-art methodologies to the analysis of soil organic matter in whole soils and in operationally-defined soil extracts. In the past, soil chemists have integrated many techniques from the fields of materials sciences and biochemistry. Indeed, for this dissertation, synchrotron-based soft X-ray absorption spectroscopy, a technique from the field of fundamental materials science research, and proteomics, common in biochemistry, were adopted to answer questions related to SON chemistry. These techniques were incorporated with established methodologies in pyrolysis field-ionization mass-spectrometry to provide a multi-faceted analytical framework for SON characterization.

8.1 Methodological development

Synchrotron-based XANES spectroscopy at the N K-edge is a relatively new technique for application to soils. My involvement in the early development of applying N-XANES to soils produced a reference compound library (Leinweber et al., 2007). Previous to the

development of this library, interpretation of N XANES spectra relied on very few reference compounds (e.g., Myneni, 2002; Vairavamurthy and Wang, 2002). Our work included many heterocyclic-N containing compounds, inorganic N-containing salts, in addition to amino acids, sugars and DNA biomolecules. This early work provided the basis for interpretation of N-XANES spectra obtained from the various environmental samples investigated in this dissertation. In the developmental phase, several synchrotron methodological questions were addressed, including development of simplified calibration methods and an assessment of beam damage to peptides. These studies formed the groundwork needed to run better experiments and to interpret the synchrotron data obtained for field soils.

In Chapter 3, we demonstrated that N_2 gas, generated through beamline decomposition of common solid-state ammonium-containing salts, could be used to provide a rapid assessment of beamline energy offset. Soft X-ray beamlines at energies corresponding to the N K-edge are normally calibrated using the vibrational structure found in spectra of gas phase N_2 (Schwarzkopf et al., 1999; Yates et al., 2000). This requires the installation of a gas cell in the beamline. Because our protocol uses solid state materials, it can be easily measured during an experiment using whole soils (or other non-gaseous samples) without disrupting the normal stream of sample throughput.

The main finding from the study in Chapter 4, which assessed beam damage to peptide compounds, was that amino acid, peptide and protein-N were sensitive to degradation under soft X-ray irradiation, but that these effects are compound-specific. This is to say that some amino acids investigated, notably those containing S (i.e., methionine) were especially susceptible, and may be degraded before the completion of a single XANES scan. Other peptidic compounds were not as susceptible, and should not pose problems for beam degradation provided that beamline flux is closely monitored by optimizing the exit slit size, and that no more than one scan is recorded at a single incident spot.

These methodological experiments provided baseline experience in synchrotron beamline operation and in processing and interpretation of data. These techniques were then applied

to the study of whole soils and soil extracts.

8.2 Studies of whole soils and soil extracts

Three studies were conceived and structured to follow a spatial gradient from the landscape scale, to the rhizosphere scale, and ending with an assessment of an operationally-defined protein extract. This study structure was designed to apply N K-edge XANES to a range of sample types (including soil and soil extracts). Carbon K-edge XANES also was incorporated to achieve greater insight into organic N characterization of soils. Some time was spent developing experimental and signal processing protocols needed to overcome challenges inherent in C XANES experiments, most notably the need to mount samples on a C-free substrate, and the proper normalization of spectra. Because these techniques are new to soils, a corroboratory technique was needed. Pyrolysis field ionization mass spectrometry (Py-FIMS) was selected because it is a well developed technique for characterizing complex samples including soils and humic compounds (e.g., Sorge et al., 1993b; Schulten, 1996; Schlichting and Leinweber, 2009).

Soil properties may vary extensively across hummocky landscapes and from different management practices. Chapter 5 in this dissertation examined soils obtained from various locations in a hummocky landscape, including soils from adjacent wetland, bromegrass and uncultivated prairie grassland areas. XANES and Py-FIMS were successful in showing differences in SON composition in this study. Landscape position was the most important factor in determining SON composition, though differences from management practice were observed in the N XANES data. Lipid-type compounds were predominant in the convergent, level and wetland (i.e., water receiving) landscape positions; more polar carbohydrates, monomeric lignins and single ring heterocyclic-N compounds were predominant in the divergent (water shedding) slope positions. Nitrogen XANES also detected N-bonded aromatic compounds such as nitroaromatics and anilides at the divergent slope positions; this is an

interesting result, as these compounds are not commonly discussed in the literature.

Chapter 6 focused on comparing SOM in rhizosphere and bulk soils. Field pea (*Pisum sativum*) was planted on two soils, and rhizosphere soils were compared to unplanted bulk soils. Rhizospheres were depleted in 'labile' polar compounds such as carbohydrates and peptides, and were enriched in hydrophobic lipids, sterols and aromatic compounds. It was also found that soil type influenced the chemistry in the rhizosphere. Nitrogen-bonded aromatics also were detected in this experiment.

Several common themes were observed in the results of the landscape-scale and rhizosphere studies. The first was the presence of N-bonded aromatics. These compounds have been observed in other experiments, primarily in acid (Stevenson, 1994) or anaerobic soils (Schmidt-Rohr et al., 2004). Detecting the presence of this type of organic N in calcareous, rhizosphere, and topographically diverse soils suggests that N-bonded aromatics may be widespread, although the abundance and biological significance remains obscure. Nitrogen K-edge XANES may also have a particular affinity for detecting N-bonded aromatics over other spectroscopic methods. Certainly, strong delocalized π^* character of N-bonded aromatics means that peaks are sharper and easier to resolve in the overall spectral shape (Stöhr, 1992). Nitrogen-15 NMR may not have the requisite sensitivity or resolution to detect these compounds in unlabelled soils.

Secondly, several patterns of stabilization and enrichment of organic molecules were seen. Studies of whole soils obtained from diverse landscape positions showed enrichment of lipid-type organic matter components at lower landscape positions. Lipid-type compounds also were enriched in rhizosphere soils. Both of these soils experience fresh input of plant material, and are characterized by selective enrichment of recalcitrant materials (Marschner et al., 2008; von Lützow et al., 2008). Soils which would experience lower inputs of plant material, such as in knoll landscape positions and in bulk (i.e., non-rhizosphere) soils, were enriched in more 'labile' compounds such as carbohydrates, peptides and monomeric lignins. Marschner et al. (2008) and von Lützow et al. (2008) have suggested that recalcitrance is

not necessarily a controlling factor on the persistence of a compound in soil. In their review papers, these authors cite several studies where carbohydrates and peptides form part of a much older pool of organic C than do lipids and complex lignins. These authors suggest that persistence is more likely controlled by specific interactions between organic molecules and clay surfaces and cations, thereby sterically limiting microbial access for biodegradation.

Thirdly, both studies showed that N-containing compounds were sensitive to landscape-related controls, management practices or rhizosphere processes. These included heterocyclic N-containing compounds, proteins and N-bonded aromatics (described above). Also tentatively identified were organic aromatic and aliphatic amines and amides. These compounds are not widely discussed in the literature, and their tentative identification in these two studies indicates that their presence, cycling, abundance, and roles in the terrestrial ecosystem should be further investigated.

Soils in both studies also showed high protein content, which agrees with the accepted view that protein-N comprises the largest fraction of organic N-containing compounds in soil (Bremner, 1965; Stevenson, 1994; Schulten and Schnitzer, 1998; Olk, 2008b). Despite this widespread acceptance, identification of individual proteins is still in its infancy (Bastida et al., 2009). Chapter 7 in this dissertation was conceived to address this gap in the knowledge base, and focused on the operationally defined soil extract termed 'glomalin-related soil protein' (GRSP), thought to be an AMF-derived glycoprotein. Glomalin research is important because this material is purportedly widespread and persistent, and has been implicated in soil aggregate stability and carbon sequestration (Wright and Upadhyaya, 1998; Rillig and Mummey, 2006; Treseder and Turner, 2007). The operationally derived extract, however, has not been properly characterized and the goal of this study was to investigate the applicability XANES to this task.

The GRSP extracts were obtained from the landscape study soils above. Indeed, XANES and Py-FIMS were useful in describing the bulk GRSP mixture and the composition of the non-proteinaceous materials. But despite strong differences observed between the SOM

components in the whole soil, no patterns of differences were found between GRSP extracts. This implies that GRSP is either uniform across soils, or that the extraction method favours the production/extraction of similar substances. There also was a lack of specificity in defining the proteinaceous component, which prompted a move to adopt proteomics as a third technique to characterize GRSP.

Considerable time was spent adapting existing proteomics methodologies for use with GRSP. Quantities of GRSP were too low in initial trials to obtain successful database hits. Increasing protein concentrations for gel separation required the development of a cleaning protocol, because co-extracted humic substances interfered with the silver staining process, causing streaking. After implementation of the cleanup protocol, several proteins were identifiable. Interestingly, despite the body of literature connecting GRSP to an AMF fungal origin, no database hits from any of the excised bands corresponded to AMF proteins (or genetic products thereof). Instead, the most significant hits were for thioredoxin, and for a range of heat stable and non-AMF soil microbial proteins.

Database completeness is the main limitation in proteomic studies of soils (Bastida et al., 2009). It is likely that the absence of links between AMF and GRSP are because the protein sequences are not present in the database. These results, however, still support the notion that GRSP is proteinaceous and is heat-stable in nature. Since GRSP has been correlated with many agronomic parameters, it may simply be that proteins (and/or non-proteinaceous co-extractants) extracted using the GRSP protocol, which still play a strong agronomic role, are derived from a species pool which is more diverse than AMF alone.

8.3 Analytical considerations

The studies in this dissertation showed that XANES spectroscopy is highly suitable for the study of soils and soil extracts. These techniques provide atomic-level speciation in whole samples, with little preparation required. In addition, XANES is isotope independent,

meaning that studies do not rely on ^{15}N or ^{13}C content.

Because XANES operates at the atomic scale, it should be understood that similar functional groups may appear in a variety of molecules. For example, amide-type N occurs predominantly in proteins, and also occurs in acetylated amino sugars (i.e., chitin). In this example, amide-N may be present in multiple pools of relevance to soil N cycling. The combination of XANES with another technique such as Py-FIMS adds the molecular dimension to the interpretation of SON structures.

Proteomics operates at the whole protein level. This technique uses enzyme digestion to disassemble proteins in a predictable fashion. These peptide fragments are sequenced using tandem mass spectrometry, and the sequences compared to databases for identification. While this technique is very powerful and allows the analysis of complex samples, identifications are limited by database completeness. Proteins derived from soil microorganisms, in particular, are not yet well represented in the available commercial databases (Bastida et al., 2009), which limits environmental proteomics studies.

Improvements in data handling, data quality, and analytical approaches were incorporated throughout the course of this dissertation project. Chapters in this dissertation were presented topically, not chronologically; Chapter 6 was written (and published) before Chapters 5 and 7, and the refinement in data quality is evident. This is particularly apparent when considering the progress in handling C K-edge XANES data, and in the application of multivariate ordination statistics and curve fitting to C and N K-edge XANES data. Handling of C K-edge XANES data is challenging for several reasons. Samples must be prepared on a C-free substrate. This is not trivial, as most adhesives are C-based, and exposure to the atmosphere for extended periods may deposit C on the substrate. This problem was solved by building an *in vacuo* Au evaporation system, which deposited Au onto silicon wafers. Soil slurry and liquid samples were then deposited on the clean Au surface immediately prior to analysis and transferred to the beamline endstation very quickly, thereby removing potential substrate C contamination.

Residual carbon contamination is inherent with the beamline optics, and attenuates the beam before it reaches the sample. Consequently, the C K-edge spectra are convolutions of sample C signal and beamline C signal. This required the development of a double normalization procedure which requires the collection of three spectra - sample, substrate, and upstream I_o from a fresh Au mesh. This was followed by a normalization procedure where substrate spectra were scaled to, and subtracted from, the sample spectra, and finally normalized to the upstream I_o spectra. All of these improvements were developed after the publication of material in Chapter 6, and were included in the generation of spectra for Chapters 5 and 7.

8.4 Summary of findings

The key findings in this dissertation were: (1) Synchrotron-based XANES is a new technique for application to soils. Methodological questions addressed, included simplified calibration methods and an assessment of beam damage to peptides. These studies formed the groundwork needed to interpret synchrotron data obtained from field soils. (2) Synchrotron studies of whole soils obtained from diverse landscape positions showed enrichment of lipid-type molecular organic matter components at lower landscape positions. Cultivation increased heterocyclic-N content, which was observed only in the N XANES data. A second study conducted at the rhizosphere scale showed enrichment of lipid-type components in the rhizosphere. Py-FIMS techniques were used to corroborate these findings. (3) A unique pool of organic N was observed in these whole soil studies. Results obtained using XANES showed the detection of oxidized N-bonded aromatic compounds, which are rarely considered in treatments of soil organic matter. These compounds were detected in soils from upslope and level positions and in some rhizosphere soils. (4) XANES and Py-FIMS revealed that GRSP contains a consortium of proteins along with many impurities. Proteomic techniques were employed, suggesting that glomalin itself may be a thioredoxin-containing chaperone.

This fraction also contains large amounts of soil-related heat-stable proteins and proteins of non-mycorrhizal origin.

8.5 Future work

This dissertation presented information pertaining to the composition of SON. Since soil biota are responsible for processing the majority of C and fixed N in the biosphere, the next steps would be to begin exploring the dynamic link between microbial metabolism and SOM composition. Superimposing investigations of both microbial diversity and SOM composition will provide deeper understanding of how land management alterations may affect large-scale C and N cycling, pool size and storage.

Nitrogen-bonded aromatics, which were detected in the landscape and rhizosphere studies, may represent unique components of the organic N cycle. Currently, Py-FIMS methodology does not have a library of biomarkers corresponding to possible N-bonded aromatic precursors. These should be explored and incorporated into the Py-FIMS evaluation protocol. Since these compounds are apparent in a wide range of soils, the focus on this pool should be to further investigate its production, kinetics, modification and biological significance in a wide range of soils and agronomic conditions.

Investigations into GRSP would continue with fundamental additions to the proteomic databases. This would be accomplished through extensive proteomic (including 2-D gel electrophoresis) characterization of multiple AMF species grown gnotobiotically with transformed RiT-DNA carrot roots (Dumas-Gaudot et al., 2004).

Finally, continued refinement and development of XANES at a fundamental level, combined with progressive improvements and upgrades to beamline components, will help increase sensitivity, throughput and data quality for improved applications of XANES to the study of soils.

Chapter 9

References

Abe, T., N. Maie, and A. Watanabe, 2005. Investigation of humic acid N with X-ray photoelectron spectroscopy: Effect of acid hydrolysis and comparison with N-15 cross polarization/magic angle spinning nuclear magnetic resonance spectroscopy. Org. Geochem. 36:1490–1497.

Abe, T. and A. Watanabe, 2004. X-ray photoelectron spectroscopy of nitrogen functional groups in soil humic acids. Soil Sci. 169:35–43.

Adachi, J. I. and N. Kosugi, 1995. Renner-Teller effect and Rydberg-valence mixing in the N and O K-edge photoabsorption spectra of N_2O. J. Chem. Phys. 102:7369–7376.

Aldrich, S., 1980. Nitrogen in relation to food, environment, and energy. Agricultural Experiment Station, College of Agriculture, University of Illinois at Urbana-Champaign, Urbana-Champaign, Il.

Anderson, D. W., 1988. The effect of parent material and soil development on nutrient cycling in temperate ecosystems. Biogeochemistry 5:71–97.

Anderson, D. W., S. Saggar, J. R. Bettany, and J. W. B. Stewart, 1981. Particle-size fractions and their use in studies of soil organic-matter. 1. The nature and distribution of forms of carbon, nitrogen, and sulfur. Soil Sci. Soc. Am. J. 45:767–772.

Anderson, D. W. and J. J. Schoenau, 2008. Soil humus fractions. p. 675–680. *In* M. Carter and E. G. Gregorich (ed.) Soil sampling and methods of analysis, 2nd ed. CRC Press, Boca Raton, FL.

Aryal, U. K. and A. R. S. Ross, 2010. Enrichment and analysis of phosphopeptides under different experimental conditions using titanium dioxide affinity chromatography and mass spectrometry. Rapid Commun. Mass Spectrom. 24:219–231.

Ascone, I., W. Meyer-Klaucke, and L. Murphy, 2003. Experimental aspects of biological X-ray absorption spectroscopy. J. Synch. Rad. 10:16–22.

Azhar, E., R. Verhe, M. Proot, P. Sandra, and W. Verstraete, 1986. Binding of nitrite-N on polyphenols during nitrification. Plant Soil. 94:369–382.

Azhar, E. S., R. Verhe, M. Proot, P. Sandra, and W. Verstraete, 1989. Fixation of nitrite nitrogen during the humification of alpha-naphthol in soil suspensions. J. Agric. Food Chem. 37:262–266.

Badalucco, L. and P. Kuikman, 2001. Mineralization and immobilization in the rhizosphere. p. 159–196. *In* R. Pinton, Z. Varanini, and P. Nannipieri (ed.) The rhizosphere: Biochemistry and organic substances at the soil-plant interface. Marcel Dekker, New York, NY.

Badalucco, L. and P. Nannipieri, 2007. Nutrient transformations in the rhizosphere. p. 111–133. *In* R. Pinton, Z. Varanini, and P. Nannipieri (ed.) The rhizosphere: Biochemistry and organic substances at the soil-plant interface, 2nd ed. Marcel Dekker, New York, NY.

Baldock, J. A., J. M. Oades, A. G. Waters, X. Peng, A. M. Vassallo, and M. A. Wilson, 1992. Aspects of the chemical-structure of soil organic materials as revealed by solid-state C-13 NMR-spectroscopy. Biogeochemistry 16:1–42.

Balesdent, J. and A. Mariotti, 1996. Measurement of soil organic matter turnover using ^{13}C natural abundance. p. 83–111. *In* T. Boutton and S.-i. Yamasaki (ed.) Mass spectrometry of soils. Marcel Dekker, Inc., New York, NY.

Bastida, F., J. L. Moreno, C. Nicolas, T. Hernandez, and C. Garcia, 2009. Soil metaproteomics: a review of an emerging environmental science. Significance, methodology and perspectives. Eur. J. Soil Sci. 60:845–859.

Bedard-Haughn, A., A. L. Matson, and D. J. Pennock, 2006. Land use effects on gross nitrogen mineralization, nitrification, and N_2O emissions in ephemeral wetlands. Soil Biol. Biochem. 38:3398–3406.

Benndorf, D., G. U. Balcke, H. Harms, and M. von Bergen, 2007. Functional metaproteome analysis of protein extracts from contaminated soil and groundwater. ISME J. 1:224–234.

Birkeland, P., 1999. Soils and Geomorphology. Oxford Univ. Press, New York, NY.

Bolliger, A., A. Nalla, J. Magid, A. de Neergaard, A. D. Nalla, and T. C. Bog-Hansen, 2008. Re-examining the glomalin-purity of glomalin-related soil protein fractions through immunochemical, lectin-affinity and soil labelling experiments. Soil Biol. Biochem. 40:887–893.

Boon, J. J. and J. W. De Leeuw, 1987. Amino-acid-sequence information in proteins and complex proteinaceous material revealed by pyrolysis capillary gas-chromatography low and high-resolution mass-spectrometry. J. Anal. Appl. Pyrolysis 11:313–327.

Boyd, S. and M. Mortland, 1990. Enzyme interactions with clays and clay-organic matter complexes. p. 1–28. *In* J.-M. Bollag and G. Stotzky (ed.) Soil Biochemistry, Vol. 6. Marcel Dekker, New York, NY.

Bozack, M. J., Y. Zhou, and S. D. Worley, 1994. Structural modifications in the amino-acid lysine induced by soft-X-ray irradiation. J. Chem. Phys. 100:8392–8398.

Bradford, M., 1976. A rapid and sensitive method for the quantitation of microgram quantities of protein utilizing the principle of protein-dye binding. Anal. Biochem. 72:248–254.

Bremner, J. M., 1965. Organic nitrogen in soils. p. 93–149. *In* W. Bartholomew and F. Clark (ed.) Soil nitrogen. American Society of Agronomy, Madison, WI.

Breuer, L., J. A. Huisman, T. Keller, and H. G. Frede, 2006. Impact of a conversion from cropland to grassland on C and N storage and related soil properties: Analysis of a 60-year chronosequence. Geoderma 133:6–18.

Briggs, D., 1998. Surface analysis of polymers by XPS and static SIMS. Cambridge Solid State Science Series. Cambridge University Press, Cambridge, UK.

Brimecombe, M., F. De Leij, and J. M. Lynch, 2007. Rhizodeposition and microbial populations. p. 73–110. *In* R. Pinton, Z. Varanini, and P. Nannipieri (ed.) The rhizosphere: Biochemistry and organic substances at the soil plant interface, 2nd ed. Marcel Dekker, New York, NY.

Bull, I. D., P. F. van Bergen, C. J. Nott, P. R. Poulton, and R. P. Evershed, 2000. Organic geochemical studies of soils from the Rothamsted classical experiments - V. The fate of lipids in different long-term experiments. Org. Geochem. 31:389–408.

Burdon, J., 2001. Are the traditional concepts of the structures of humic substances realistic? Soil Sci. 166:752–769.

Catroux, G. and M. Schnitzer, 1987. Chemical, spectroscopic, and biological characteristics of the organic-matter in particle-size fractions separated from an aquoll. Soil Sci. Soc. Am. J. 51:1200–1207.

Chantigny, M. H., D. A. Angers, K. Kaiser, and K. Kalbitz, 2008. Extraction and characterization of dissolved organic matter. p. 617–635. *In* M. Carter and E. G. Gregorich (ed.) Soil sampling and methods of analysis, 2nd ed. CRC Press, Boca Raton, FL.

Chen, S. N., M. C. Rillig, and W. Wang, 2009. Improving soil protein extraction for metaproteome analysis and glomalin-related soil protein detection. Proteomics 9:4970–4973.

Christiansen, E. A., 1979. Wisconsinan deglaciation of southern Saskatchewan and adjacent areas. Can. J. Earth Sci. 16:913–938.

Christl, I. and R. Kretzschmar, 2007. C-1s NEXAFS spectroscopy reveals chemical fractionation of humic acid by cation-induced coagulation. Environ. Sci. Technol. 41:1915–1920.

Cody, G. D., J. Brandes, C. Jacobsen, and S. Wirick, 2009. Soft X-ray induced chemical modification of polysaccharides in vascular plant cell walls. J. Electron Spectrosc. Relat. Phenom. 170:57–64.

Coffey, T., S. G. Urquhart, and H. Ade, 2002. Characterization of the effects of soft X-ray irradiation on polymers. J. Electron Spectrosc. Relat. Phenom. 122:65–78.

Colman, B. P., N. Fierer, and J. P. Schimel, 2007. Abiotic nitrate incorporation in soil: is it real? Biogeochemistry 84:161–169.

Colman, B. P., N. Fierer, and J. P. Schimel, 2008. Abiotic nitrate incorporation, anaerobic microsites, and the ferrous wheel. Biogeochemistry 91:223–227.

Crews, T. E. and M. B. Peoples, 2004. Legume versus fertilizer sources of nitrogen: ecological tradeoffs and human needs. Agric. Ecosyst. Environ. 102:279–297.

Crowley, D. E. and Z. Rengel, 1999. Biology and chemistry of nutrient availability in the rhizosphere. p. 1–40. *In* Z. Rengel (ed.) Mineral nutrition of crops: Fundamental mechanisms and implications. Haworth Press, New York, NY.

Curl, E. A. and B. Truelove, 1986. The rhizosphere. Springer-Verlag, Berlin, Germany.

Dasog, G., 1986. Properties, genesis and classification of clay soils in Saskatchewan. Ph.D. diss. University of Saskatchewan, Saskatoon, SK, Canada.

Davidson, E. A., J. Chorover, and D. B. Dail, 2003. A mechanism of abiotic immobilization of nitrate in forest ecosystems: The ferrous wheel hypothesis. Glob. Change Biol. 9:228–236.

DiCosty, R. J., D. P. Weliky, S. J. Anderson, and E. A. Paul, 2003. N-15-CPMAS nuclear magnetic resonance spectroscopy and biological stability of soil organic nitrogen in whole soil and particle-size fractions. Org. Geochem. 34:1635–1650.

Dinel, H., M. Schnitzer, and H. R. Schulten, 1998. Chemical and spectroscopic characterization of colloidal fractions separated from liquid hog manures. Soil Sci. 163:665–673.

Djajakirana, G., R. G. Joergensen, and B. Meyer, 1996. Ergosterol and microbial biomass relationship in soil. Biol. Fert. Soils 22:299–304.

Driver, J. D., W. E. Holben, and M. C. Rillig, 2005. Characterization of glomalin as a hyphal wall component of arbuscular mycorrhizal fungi. Soil Biol. Biochem. 37:101–106.

Dumas-Gaudot, E., B. Valot, G. Bestel-Corre, G. Recorbet, M. St-Arnaud, B. Fontaine, M. Dieu, M. Raes, R. S. Saravanan, and S. Gianinazzi, 2004. Proteomics as a way to identify extra-radicular fungal proteins from *Glomus intraradices*-RiT-DNA carrot root mycorrhizas. FEMS Microbiol. Ecol. 48:401–411.

Elder, F. R., A. M. Gurewitsch, R. V. Langmuir, and H. C. Pollock, 1947. Radiation from electrons in a synchrotron. Phys. Rev. 71:829–830.

Fan, T. W. M., A. N. Lane, M. Shenker, J. P. Bartley, D. Crowley, and R. M. Higashi, 2001. Comprehensive chemical profiling of gramineous plant root exudates using high-resolution NMR and MS. Phytochemistry 57:209–221.

Fani, R. and M. Fondi, 2009. Origin and evolution of metabolic pathways. Phys. Life Rev. 6:23–52.

Faurobert, M., E. Pelpoir, and J. Chab, 2007. Phenol extraction of proteins for proteomic studies of recalcitrant plant tissues. p. 9–14. *In* H. Thiellement, M. Zivy, C. Damerval, and V. Mchin (ed.) Plant proteomics: Methods and protocols, Vol. 335 of Methods in Molecular Biology. Humana Press, Totowa, NJ.

Feng, X., A. J. Simpson, K. P. Wilson, D. Dudley Williams, and M. J. Simpson, 2008. Increased cuticular carbon sequestration and lignin oxidation in response to soil warming. Nature Geoscience 1:836–839.

Frazer, B. H., B. Gilbert, B. R. Sonderegger, and G. De Stasio, 2003. The probing depth of total electron yield in the sub-keV range: TEY-XAS and X-PEEM. Surf. Sci. 537:161–167.

Gadkar, V. and M. C. Rillig, 2006. The arbuscular mycorrhizal fungal protein glomalin is a putative homolog of heat shock protein 60. FEMS Microbiol. Lett. 263:93–101.

Galloway, J. N., J. D. Aber, J. W. Erisman, S. P. Seitzinger, R. W. Howarth, E. B. Cowling, and B. J. Cosby, 2003. The nitrogen cascade. BioScience 53:341–356.

Galloway, J. N. and E. B. Cowling, 2002. Reactive nitrogen and the world: 200 years of change. Ambio 31:64–71.

Gejo, T., Y. Takata, T. Hatsui, M. Nagasono, H. Oji, N. Kosugi, and E. Shigemasa, 2003. Angle-resolved photoion spectroscopy of NO_2 and SO_2. Chem. Phys. 289:15–29.

Ginder-Vogel, M. and D. L. Sparks, 2010. The impacts of X-ray absorption spectroscopy on understanding soil processes and reaction mechanisms. p. 1–26. *In* B. Singh and M. Grfe (ed.) Synchrotron-based techniques in soils and sediments, Vol. 34 of Developments in soil science. Elsevier, New York, NY.

Gleixner, G., R. Bol, and J. Balesdent, 1999. Molecular insight into soil carbon turnover. Rapid Commun. Mass Spectrom. 13:1278–1283.

Gordon, M. L., G. Cooper, C. Morin, T. Araki, C. C. Turci, K. Kaznatcheev, and A. P. Hitchcock, 2003. Inner-shell excitation spectroscopy of the peptide bond: Comparison of the C 1s, N 1s, and O 1s spectra of glycine, glycyl-glycine, and glycyl-glycyl-glycine. J. Phys. Chem. A 107:6144–6159.

Grayston, S., S. Wang, C. Campbell, and A. Edwards, 1998. Selective influence of plant species on microbial diversity in the rhizosphere. Soil Biol. Biochem. 30:369–378.

Gregoratti, L., T. O. Mentes, A. Locatelli, and M. Kiskinova, 2009. Beam-induced effects in soft X-ray photoelectron emission microscopy experiments. J. Electron Spectrosc. Relat. Phenom. 170:13–18.

Gregorich, E. G. and D. W. Anderson, 1985. Effects of cultivation and erosion on soils of 4 toposequences in the Canadian prairies. Geoderma 36:343–354.

Gregorich, E. G. and M. H. Beare, 2008. Physically uncomplexed organic matter. p. 607–616. *In* M. Carter and E. G. Gregorich (ed.) Soil sampling and methods of analysis, 2nd ed. CRC Press, Boca Raton, FL.

Gregorich, E. G., C. M. Monreal, M. Schnitzer, and H. R. Schulten, 1996. Transformation of plant residues into soil organic matter: Chemical characterization of plant tissue, isolated soil fractions, and whole soils. Soil Sci. 161:680–693.

Guggenberger, G., W. Zech, and H. R. Schulten, 1994. Formation and mobilization pathways of dissolved organic-matter - evidence from chemical structural studies of organic-matter fractions in acid forest floor solutions. Org. Geochem. 21:51–66.

Haider, K. and H. R. Schulten, 1985. Pyrolysis field-ionization mass-spectrometry of lignins, soil humic compounds and whole soil. J. Anal. Appl. Pyrolysis 8:317–331.

Harada, T., E. Kurimoto, K. Tokuhiro, O. Asami, T. Sakai, D. Nohara, and K. Kato, 2001. Disulfide bond formation in refolding of thermophilic fungal protein disulfide isomerase. J. Biosci. Bioeng. 91:596–598.

Hardie, A., 2008. Pathways of abiotic humification as catalyzed by mineral colloids. Ph.D. diss. University of Saskatchewan, Saskatoon, SK, Canada.

Hardie, A., J. Dynes, L. M. Kozak, and P. M. Huang, 2007. Influence of polyphenols on the integrated polyphenol-Maillard reaction humification pathway as catalyzed by birnessite. Ann. Environ. Sci. 1:91–110.

Heldt, H.-W., 1997. Plant biochemistry and molecular biology. Oxford University Press, New York, NY.

Hempfling, R., H. R. Schulten, and R. Horn, 1990. Relevance of humus composition to the physical/mechanical stability of agricultural soils: a study by direct pyrolysis-mass spectrometry. J. Anal. Appl. Pyrolysis 17:275–281.

Hempfling, R., N. Simmleit, and H.-R. Schulten, 1991. Characterization and chemodynamics of plant constituents during maturation, senescence and humus genesis in spruce ecosystems. Biogeochemistry 13:27–60.

Hiltner, L., 1904. Über neuere Erfahrungen und Probleme auf dem Gebiet der Bodenbakteriologie und unter besonderer Berücksichtigung der Gründüngung und Brache. Arb. Dtsch. Landwirtsch. Ges. 98:59–78.

Hitchcock, A. P., C. Morin, X. Zhang, T. Araki, J. J. Dynes, H. Stover, J. L. Brash, J. R. Lawrence, and G. G. Leppard, 2005. Soft X-ray spectromicroscopy of biological and synthetic polymer systems. J. Electron Spectrosc. Relat. Phenom. 144-147:259–269.

Holgado, J. P., F. Yubero, A. Cordon, F. Gracia, A. R. Gonzalez-Elipe, and J. Avila, 2003. Molecular nitrogen implanted in Al_2O_3 by low energy N-2(+) ion bombardment. Solid State Commun. 128:235–238.

Hrbek, J., 2002. Surface reactions studied by synchrotron based photoelectron spectroscopy. p. 573–604. *In* T. K. Sham (ed.) Chemical applications of synchrotron radiation, Vol. 12A. World Scientific, River Edge, NJ.

Hrmova, M., P. Biely, and M. Vrsanska, 1989. Cellulose-degrading and xylan-degrading enzymes of *Aspergillus-terreus* and *Aspergillus-niger*. Enzyme Microb. Technol. 11:610–616.

Jackson, L. E., M. Burger, and T. R. Cavagnaro, 2008. Roots nitrogen transformations, and ecosystem services. Annu. Rev. Plant Biol. 59:341–363.

Jandl, G., P. Leinweber, and H. R. Schulten, 2007. Origin and fate of soil lipids in a Phaeozem under rye and maize monoculture in Central Germany. Biol. Fert. Soils 43:321–332.

Jandl, G., P. Leinweber, H. R. Schulten, and K. Eusterhues, 2004. The concentrations of fatty acids in organo-mineral particle-size fractions of a Chernozem. Eur. J. Soil Sci. 55:459–469.

Janos, D. P., S. Garamszegi, and B. Beltran, 2008. Glomalin extraction and measurement. Soil Biol. Biochem. 40:728–739.

Jokic, A., J. N. Cutler, D. W. Anderson, and F. L. Walley, 2004a. Detection of heterocyclic N compounds in whole soils using N-XANES spectroscopy. Can. J. Soil Sci. 84:291–293.

Jokic, A., J. N. Cutler, E. Ponomarenko, G. van der Kamp, and D. W. Anderson, 2003. Organic carbon and sulphur compounds in wetland soils: Insights on structure and transformation processes using K-edge XANES and NMR spectroscopy. Geochim. Cosmochim. Acta 67:2585–2597.

Jokic, A., H. R. Schulten, J. N. Cutler, M. Schnitzer, and P. M. Huang, 2004b. A significant abiotic pathway for the formation of unknown nitrogen in nature. Geophys. Res. Lett. 31.

Jokic, A., M. C. Wang, C. Liu, A. I. Frenkel, and P. M. Huang, 2004c. Integration of the polyphenol and Maillard reactions into a unified abiotic pathway for humification in nature: the role of delta-MnO_2. Org. Geochem. 35:747–762.

Jones, D. L. and P. R. Darrah, 1994. Role of root derived organic acids in the mobilization of nutrients from the rhizosphere. Plant Soil. 166:247–257.

Jones, D. L., A. Hodge, and Y. Kuzyakov, 2004. Plant and mycorrhizal regulation of rhizodeposition. New Phytol. 163:459–480.

Junk, G. and H. Svec, 1958. The absolute abundance of hte nitrogen isotopes in the atmosphere and compressed gas from various sources. Geochim. Cosmochim. Acta 14:234–243.

Kade, A., D. V. Vyalikh, S. Danzenbacher, K. Kurnmer, A. Bluher, M. Mertig, A. Lanzara, A. Scholl, A. Doran, and S. L. Molodtsov, 2007. X-ray absorption microscopy of bacterial surface protein layers: X-ray damage. J. Phys. Chem. B 111:13491–13498.

Katsikini, M., E. C. Paloura, M. Fieber-Erdmann, J. Kalomiros, T. D. Moustakas, H. Amano, and I. Akasaki, 1997. N K-edge X-ray-absorption study of heteroepitaxial GaN films. Phys. Rev. B 56:13380–13386.

Katznelson, H., 1965. Nature and importance of the rhizosphere. p. 187–209. *In* K. Baker and W. Snyder (ed.) Ecology of soil-borne plant pathogens: Prelude to biological control. University of California Press, Los Angeles, CA.

Kelemen, S. R., M. Afeworki, M. L. Gorbaty, P. J. Kwiatek, M. S. Solum, J. Z. Hu, and R. J. Pugmire, 2002. XPS and N-15 NMR study of nitrogen forms in carbonaceous solids. Energy Fuels 16:1507–1515.

Kern, R., A. Malki, A. Holmgren, and G. Richarme, 2003. Chaperone properties of *Escherichia coli* thioredoxin and thioredoxin reductase. Biochem. J. 371:965–972.

Kim, J. S., M. Ree, S. W. Lee, W. Oh, S. Baek, B. Lee, T. J. Shin, K. J. Kim, B. Kim, and J. Luning, 2003. NEXAFS spectroscopy study of the surface properties of zinc glutarate and its reactivity with carbon dioxide and propylene oxide. J. Catal. 218:386–395.

Kinyangi, J., D. Solomon, B. I. Liang, M. Lerotic, S. Wirick, and J. Lehmann, 2006. Nanoscale biogeocomplexity of the organomineral assemblage in soil: Application of STXM microscopy and C 1s-NEXAFS spectroscopy. Soil Sci. Soc. Am. J. 70:1708–1718.

Kirk, K. and R. Farrell, 1987. Enzymatic "combustion": The microbial degradation of lignin. Annu. Rev. Microbiol. 41:465–505.

Kleber, M., P. Sollins, and R. Sutton, 2007. A conceptual model of organo-mineral interactions in soils: self-assembly of organic molecular fragments into zonal structures on mineral surfaces. Biogeochemistry 85:9–24.

Knicker, H., R. Fründ, and H. D. Lüdemann, 1993. The chemical nature of nitrogen in native soil organic-matter. Naturwissenschaften 80:219–221.

Knicker, H., F. J. Gonzalez-Vila, O. Polvillo, J. A. Gonzalez, and G. Almendros, 2005. Fire-induced transformation of C- and N-forms in different organic soil fractions from a Dystric Cambisol under a Mediterranean pine forest (*Pinus pinaster*). Soil Biol. Biochem. 37:701–718.

Knicker, H., P. G. Hatcher, and A. W. Scaroni, 1996. A solid-state N-15 NMR spectroscopic investigation of the origin of nitrogen structures in coal. Int. J. Coal Geol. 32:255–278.

Knicker, H. and H. D. Lüdemann, 1995. N-15 and C-13 CPMAS and solution NMR studies of N-15 enriched plant material during 600 days of microbial degradation. Org. Geochem. 23:329–341.

Knicker, H. and J. O. Skjemstad, 2000. Nature of organic carbon and nitrogen in physically protected organic matter of some Australian soils as revealed by solid-state C-13 and N-15 NMR spectroscopy. Aust. J. Soil Res. 38:113–127.

Kögel-Knabner, I., 1997. C-13 and N-15 NMR spectroscopy as a tool in soil organic matter studies. Geoderma 80:243–270.

Kögel-Knabner, I., 2000. Analytical approaches for characterizing soil organic matter. Org. Geochem. 31:609–625.

Kögel-Knabner, I., 2006. Chemical structure of organic N and organic P in soil. p. 23–48. *In* P. Nannipieri and K. Smalla (ed.) Nucleic acids and proteins in soil, Vol. 8 of Soil Biology. Springer-Verlag, Berlin, Germany.

Kowalenko, C., 1978. Organic nitrogen, phosphorus and sulfur in soils. p. 95–136. *In* M. Schnitzer and S. Khan (ed.) Soil Organic Matter, Vol. 8. Elsevier Scientific, New York, NY.

Kroetsch, D. and C. Wang, 2008. Particle size distribution. p. 713–725. *In* M. Carter and E. G. Gregorich (ed.) Soil sampling and methods of analysis, 2nd ed. CRC Press, Boca Raton, FL.

Kuzyakov, Y., 2002. Review: Factors affecting rhizosphere priming effects. J. Plant Nutr. Soil Sci. 165:382–396.

Kuzyakov, Y., P. Leinweber, D. Sapronov, and K. U. Eckhardt, 2003. Qualitative assessment of rhizodeposits in non-sterile soil by analytical pyrolysis. J. Plant Nutr. Soil Sci. 166:719–723.

Ladd, J. and R. Jackson, 1982. Biochemistry of ammonification. p. 173–228. *In* F. Stevenson (ed.) Nitrogen in agricultural soils. American society for agronomy, Madison, WI.

Landi, A., A. R. Mermut, and D. W. Anderson, 2004. Carbon distribution in a hummocky landscape from Saskatchewan, Canada. Soil Sci. Soc. Am. J. 68:175–184.

Lee, J. R., S. S. Lee, H. H. Jang, Y. M. Lee, J. H. Park, S. C. Park, J. C. Moon, S. K. Park, S. Y. Kim, S. Y. Lee, H. B. Chae, Y. J. Jung, W. Y. Kim, M. R. Shin, G. W. Cheong, M. G. Kim, K. R. Kang, K. O. Lee, and D. J. Yun, 2009. Heat-shock dependent oligomeric status alters the function of a plant-specific thioredoxin-like protein, AtTDX. Proc. Natl. Acad. Sci. U.S.A. 106:5978–5983.

Lehmann, J., B. Q. Liang, D. Solomon, M. Lerotic, F. Luizao, J. Kinyangi, T. Schafer, S. Wirick, and C. Jacobsen, 2005. Near-edge X-ray absorption fine structure (NEXAFS) spectroscopy for mapping nano-scale distribution of organic carbon forms in soil: Application to black carbon particles. Global Biogeochem. Cycles 19:GB1013.

Lehmann, J., D. Solomon, J. Kinyangi, L. Dathe, S. Wirick, and C. Jacobsen, 2008. Spatial complexity of soil organic matter forms at nanometre scales. Nature Geoscience 1:238–242.

Leinweber, P., K.-U. Eckhardt, H. Fischer, and Y. Kuzyakov, 2008a. A new rapid micromethod for the molecular-chemical characterization of rhizodeposits by field-ionization mass spectrometry. Rapid Commun. Mass Spectrom. 22:1230–1234.

Leinweber, P., G. Jandl, C. Baum, K.-U. Eckhardt, and E. Kandeler, 2008b. Stability and composition of soil organic matter control respiration and soil enzyme activities. Soil Biology and Biochemistry 40:1496–1505.

Leinweber, P., J. Kruse, F. L. Walley, A. Gillespie, K. U. Eckhardt, R. I. R. Blyth, and T. Regier, 2007. Nitrogen K-edge XANES - An overview of reference compounds used to identify 'unknown' organic nitrogen in environmental samples. J. Synch. Rad. 14:500–511.

Leinweber, P. and H. R. Schulten, 1998. Nonhydrolyzable organic nitrogen in soil size separates from long-term agricultural experiments. Soil Sci. Soc. Am. J. 62:383–393.

Leinweber, P. and H. R. Schulten, 1999. Advances in analytical pyrolysis of soil organic matter. J. Anal. Appl. Pyrolysis 49:359–383.

Leinweber, P., F. Walley, J. Kruse, G. Jandl, K. U. Eckhardt, R. I. R. Blyth, and T. Regier, 2009. Cultivation affects soil organic nitrogen: Pyrolysis-mass spectrometry and nitrogen K-edge XANES spectroscopy evidence. Soil Sci. Soc. Am. J. 73:82–92.

Lewis, N. and E. Yamamoto, 1990. Lignin: Occurrence, biogenesis and biodegradation. Annu. Rev. Plant Physiol. Plant Mol. Biol. 41:455–496.

Lichtfouse, E., P. Wehrung, and P. Albrecht, 1998. Plant wax n-alkanes trapped in soil humin by noncovalent bonds. Naturwissenschaften 85:449–452.

Lobb, D. A., R. G. Kachanoski, and M. H. Miller, 1995. Tillage translocation and tillage erosion on shoulder slope landscape positions measured using Cs-137 as a tracer. Can. J. Soil Sci. 75:211–218.

Lovelock, C. E., S. F. Wright, D. A. Clark, and R. W. Ruess, 2004. Soil stocks of glomalin produced by arbuscular mycorrhizal fungi across a tropical rain forest landscape. J. Ecol. 92:278–287.

Lynch, J. M., 1990. Microbial metabolites. p. 177–206. *In* J. M. Lynch (ed.) The rhizosphere. John Wiley & Sons, Chichester, UK.

Ma, W. K., A. Bedard-Haughn, S. D. Siciliano, and R. E. Farrell, 2008. Relationship between nitrifier and denitrifier community composition and abundance in predicting nitrous oxide emissions from ephemeral wetland soils. Soil Biol. Biochem. 40:1114–1123.

Mahieu, N., D. C. Olk, and E. Randall, 2000. Accumulation of heterocyclic nitrogen in humified organic matter: A ^{15}N-NMR study of lowland rice soils. Eur. J. Soil Sci. 51:379–389.

Maron, P. A., L. Ranjard, C. Mougel, and P. Lemanceau, 2007. Metaproteomics: A new approach for studying functional microbial ecology. Microbial Ecology 53:486–493.

Marschner, B., S. Brodowski, A. Dreves, G. Gleixner, A. Gude, P. M. Grootes, U. Hamer, A. Heim, G. Jandl, R. Ji, K. Kaiser, K. Kalbitz, C. Kramer, P. Leinweber, J. Rethemeyer, A. Schaeffer, M. W. I. Schmidt, L. Schwark, and G. L. B. Wiesenberg, 2008. How relevant is recalcitrance for the stabilization of organic matter in soils? J. Plant Nutr. Soil Sci. 171:91–110.

Marschner, H., 1995. Mineral nutrition of higher plants. 2nd ed. Academic Press, London, UK.

Masciandaro, G., C. Macci, S. Doni, B. E. Maserti, A. C. B. Leo, B. Ceccanti, and E. Wellington, 2008. Comparison of extraction methods for recovery of extracellular beta-glucosidase in two different forest soils. Soil Biol. Biochem. 40:2156–2161.

McCune, B., J. Grace, and D. Urban, 2002. Analysis of Ecological Communities. MjM Software Design, Gleneden Beach, OR.

Melnitchouck, A., P. Leinweber, K. U. Eckhardt, and R. Beese, 2005. Qualitative differences between day- and night-time rhizodeposition in maize (*Zea mays* L.) as investigated by pyrolysis-field ionization mass spectrometry. Soil Biol. Biochem. 37:155–162.

Mikutta, R., M. Kleber, M. S. Torn, and R. Jahn, 2006. Stabilization of soil organic matter: Association with minerals or chemical recalcitrance? Biogeochemistry 77:25–56.

Müller, C., R. J. Stevens, and R. J. Laughlin, 2006. Sources of nitrite in a permanent grassland soil. Eur. J. Soil Sci. 57:337–343.

Mulvaney, R. L. and S. A. Khan, 2001. Diffusion methods to determine different forms of nitrogen in soil hydrolysates. Soil Sci. Soc. Am. J. 65:1284–1292.

Myneni, S., 2002. Soft X-ray spectroscopy and spectromicrosopy studies of organic molecules in the environment. p. 485–579. *In* P. Fenter, M. Rivers, N. Sturchio, and S. Sutton (ed.) Applications of synchrotron radiation in low-temperature geochemistry and environmental science, Vol. 49 of Reviews in Mineralogy and Geochemistry. The Mineralogical Society of America, Washington, DC.

Myrold, D. and P. Bottomley, 2008. Nitrogen mineralization and immobilization. p. 157–172. *In* J. Schepers and W. Raun (ed.) Nitrogen in agricultural systems. American Society for Agronomy, Crop Science Society of America, Soil Science Society of America, Madison, WI.

Nannipieri, P. and E. A. Paul, 2009. The chemical and functional characterization of soil N and its biotic components. Soil Biol. Biochem. 41:2357–2369.

Näsholm, T., K. Kielland, and U. Ganeteg, 2009. Uptake of organic nitrogen by plants. New Phytol. 182:31–48.

Nelson, D. and M. Cox, 2005. Principles of biochemistry. 4th ed. W.H. Freeman and Co., New York, NY.

Neumann, G. and V. Römheld, 2007. The release of root exudates as affected by the plant's physiological status. p. 23–72. *In* R. Pinton, Z. Varanini, and P. Nannipieri (ed.) The rhizosphere - biochemistry and organic substances at the soil-plant interface, 2nd ed. Marcel Dekker, New York, NY.

Nichols, K. A. and S. F. Wright, 2006. Carbon and nitrogen in operationally defined soil organic matter pools. Biol. Fert. Soils 43:215–220.

Nierop, K. and P. Van Bergen, 2002. Clay and ammonium catalyzed reactions of alkanols, alkanoic acids and esters under flash pyrolytic conditions. J. Anal. Appl. Pyrolysis 63:197–208.

Nordberg, R., R. G. Albridge, T. Bergmark, U. Ericson, J. Hedman, C. Nordling, K. Siegbahn, and B. J. Lindberg, 1968. Molecular spectroscopy by means of ESCA - charge distribution in nitrogen compounds. Arkiv for Kemi 28:257.

Ogunseitan, O., 2006. Soil proteomics: extraction and analysis of proteins from soils. p. 96–115. *In* P. Nannipieri and K. Smalla (ed.) Nucleic acids and proteins in soil, Vol. 8 of Soil Biology. Springer-Verlag, Berlin, Germany.

Olk, D. C., 2006. A chemical fractionation for structure-function relations of soil organic matter in nutrient cycling. Soil Sci. Soc. Am. J. 70:1013–1022.

Olk, D. C., 2008a. Organic forms of nitrogen. p. 667–680. *In* M. Carter and E. G. Gregorich (ed.) Soil sampling and methods of analysis, 2nd ed. CRC Press, Boca Raton, FL.

Olk, D. C., 2008b. Organic forms of soil nitrogen. p. 57–100. *In* J. Schepers and W. Raun (ed.) Nitrogen in agricultural systems. American Society for Agronomy, Crop Science Society of America, Soil Science Society of America, Madison, WI.

Olk, D. C., K. G. Cassman, K. Schmidt-Rohr, M. M. Anders, J. D. Mao, and J. L. Deenik, 2006. Chemical stabilization of soil organic nitrogen by phenolic lignin residues in anaerobic agroecosystems. Soil Biol. Biochem. 38:3303–3312.

Otto, A. and M. J. Simpson, 2006. Evaluation of CuO oxidation parameters for determining the source and stage of lignin degradation in soil. Biogeochemistry 80:121–142.

Palm, C. A. and P. A. Sanchez, 1991. Nitrogen release from the leaves of some tropical legumes as affected by their lignin and polyphenolic contents. Soil Biol. Biochem. 23:83–88.

Pant, K. K. and D. Kunzru, 1999. Noncatalytic and catalytic pyrolysis of toluene. Can. J. Chem. Eng. 77:150–155.

Papiernik, S. K., M. J. Lindstrom, J. A. Schumacher, A. Farenhorst, K. D. Stephens, T. E. Schumacher, and D. A. Lobb, 2005. Variation in soil properties and crop yield across an eroded prairie landscape. J. Soil Water Conserv. 60:388–395.

Paungfoo-Lonhienne, C., T. G. A. Lonhienne, D. Rentsch, N. Robinson, M. Christie, R. I. Webb, H. K. Gamage, B. J. Carroll, P. M. Schenk, and S. Schmidt, 2008. Plants can use protein as a nitrogen source without assistance from other organisms. Proc. Natl. Acad. Sci. U.S.A. 105:4524–4529.

Peatman, W. B., 1997. Gratings, mirrors and slits - beamline design for soft X-ray synchrotron radiation sources. Gordon and Breach Science Publishers, Amsterdam, Netherlands.

Pennock, D. J., 2003. Multi-site assessment of cultivation-induced soil change using revised landform segmentation procedures. Can. J. Soil Sci. 83:565–580.

Pennock, D. J., D. W. Anderson, and E. Dejong, 1994. Landscape-scale changes in indicators of soil quality due to cultivation in Saskatchewan, Canada. Geoderma 64:1–19.

Pennock, D. J. and M. D. Corre, 2001. Development and application of landform segmentation procedures. Soil Tillage Res. 58:151–162.

Pennock, D. J. and E. Dejong, 1987. The influence of slope curvature on soil-erosion and deposition in hummock terrain. Soil Sci. 144:209–217.

Pennock, D. J. and E. Dejong, 1990. Spatial pattern of soil redistribution in Boroll landscapes, southern Saskatchewan, Canada. Soil Sci. 150:867–873.

Pennock, D. J., C. Vankessel, R. E. Farrell, and R. A. Sutherland, 1992. Landscape-scale variations in denitrification. Soil Sci. Soc. Am. J. 56:770–776.

Pennock, D. J., B. J. Zebarth, and E. De Jong, 1987. Landform classification and soil distribution in hummocky terrain, Saskatchewan, Canada. Geoderma 40:297–315.

Petravic, M., Q. Gao, D. Llewellyn, P. N. K. Deenapanray, D. Macdonald, and C. Crotti, 2006. Broadening of vibrational levels in X-ray absorption spectroscopy of molecular nitrogen in compound semiconductors. Chem. Phys. Lett. 425:262–266.

Piccolo, A. and J. S. C. Mbagwu, 1999. Role of hydrophobic components of soil organic matter in soil aggregate stability. Soil Sci. Soc. Am. J. 63:1801–1810.

Plekan, O., V. Feyer, R. Richter, M. Coreno, M. de Simone, K. C. Prince, and V. Carravetta, 2007. Photoemission and the shape of amino acids. Chem. Phys. Lett. 442:429–433.

Posgate, J., 1998. Nitrogen fixation. Cambridge University Press, Cambridge, UK.

Preston, C. M., 1996a. Applications of NMR to soil organic matter analysis: History and prospects. Soil Sci. 161:144–166.

Preston, C. M., 1996b. Applications of NMR to soil organic matter analysis: History and prospects (vol 161, pg 144, 1996). Soil Sci. 161:232–232.

Preston, C. M., 2001. Carbon-13 solid-state NMR of soil organic matter - using the technique effectively. Can. J. Soil Sci. 81:255–270.

Purin, S. and M. C. Rillig, 2007. The arbuscular mycorrhizal fungal protein glomalin: Limitations, progress, and a new hypothesis for its function. Pedobiologia 51:123–130.

Raia, C. A., S. D'Auria, A. Guagliardi, S. Bartolucci, M. De Rosa, and M. Rossi, 1995. Characterization of redox proteins from extreme thermophilic archaebacteria: studies on alcohol dehydrogenase and thioredoxins. Biosens. Bioelectron. 10:135–140.

Ratner, B. D. and D. G. Castner, 2009. Electron spectroscopy for chemical analysis. *In* J. Vickerman and I. Gilmore (ed.) Surface analysis - The principal techniques, 2nd ed. John Wiley & Sons, West Sussex, UK.

Ravel, B. and M. Newville, 2005. ATHENA, ARTEMIS, HEPHAESTUS: Data analysis for X-ray absorption spectroscopy using IFEFFIT. J. Synch. Rad. 12:537–541.

Regier, T., J. Krochak, T. K. Sham, Y. F. Hu, J. Thompson, and R. I. R. Blyth, 2007a. Performance and capabilities of the Canadian Dragon: The SGM beamline at the Canadian Light Source. Nucl. Instrum. Methods Phys. Res. Sect. A-Accel. Spectrom. Dect. Assoc. Equip. 582:93–95.

Regier, T., J. Paulsen, G. Wright, I. Coulthard, K. Tan, T. K. Sham, and R. I. R. Blyth, 2007b. Commissioning of the Spherical Grating Monochromator soft X-ray spectroscopy beamline at the Canadian Light Source. AIP Conf. Proc. 879:473–476.

Remmers, G., M. Domke, A. Puschmann, T. Mandel, G. Kaindl, E. Hudson, and D. A. Shirley, 1993. High-resolution inner-shell photoionization of NO. Chem. Phys. Lett. 214:241–249.

Rennenberg, H., M. Dannenmann, A. Gessler, J. Kreuzwieser, J. Simon, and H. Papen, 2009. Nitrogen balance in forest soils: nutritional limitation of plants under climate change stresses. Plant Biol. 11:4–23.

Ressler, T., 1998. WinXAS: A program for X-ray absorption spectroscopy data analysis under MS-Windows. J. Synch. Rad. 5:118–122.

Rillig, M. C., 2004. Arbuscular mycorrhizae, glomalin, and soil aggregation. Can. J. Soil Sci. 84:355–363.

Rillig, M. C., 2005. A connection between fungal hydrophobins and soil water repellency? Pedobiologia 49:395–399.

Rillig, M. C. and D. L. Mummey, 2006. Mycorrhizas and soil structure. New Phytol. 171:41–53.

Rillig, M. C., P. W. Ramsey, S. Morris, and E. A. Paul, 2003. Glomalin, an arbuscular-mycorrhizal fungal soil protein, responds to land-use change. Plant Soil. 253:293–299.

Rillig, M. C. and P. D. Steinberg, 2002. Glomalin production by an arbuscular mycorrhizal fungus: a mechanism of habitat modification? Soil Biol. Biochem. 34:1371–1374.

Rillig, M. C., S. F. Wright, K. A. Nichols, W. F. Schmidt, and M. S. Torn, 2001. Large contribution of arbuscular mycorrhizal fungi to soil carbon pools in tropical forest soils. Plant Soil. 233:167–177.

Roberts, P. and D. L. Jones, 2008. Critical evaluation of methods for determining total protein in soil solution. Soil Biol. Biochem. 40:1485–1495.

Robertson, G. P. and P. M. Vitousek, 2009. Nitrogen in agriculture: Balancing the cost of an essential resource. Annu. Rev. Environ. Resour. 34:97–125.

Rodrigues, F., G. M. do Nascimento, and P. S. Santos, 2007. Studies of ionic liquid solutions by soft X-ray absorption spectroscopy. J. Electron Spectrosc. Relat. Phenom. 155:148–154.

Rosier, C. L., A. T. Hoye, and M. C. Rillig, 2006. Glomalin-related soil protein: Assessment of current detection and quantification tools. Soil Biol. Biochem. 38:2205–2211.

Rovezzi, M., F. D'Acapito, A. Navarro-Quezada, B. Faina, T. Li, A. Bonanni, F. Filippone, A. A. Bonapasta, and T. Dietl, 2009. Local structure of (Ga,Fe)N and (Ga,Fe)N:Si investigated by X-ray absorption fine structure spectroscopy. Phys. Rev. B 79:9.

Ruck, B. J., A. Koo, U. D. Lanke, F. Budde, S. Granville, H. J. Trodahl, A. Bittar, J. B. Metson, V. J. Kennedy, and A. Markwitz, 2004. Quantitative study of molecular N-2 trapped in disordered GaN:O films. Phys. Rev. B 70:235202.1–5.

Schäfer, T., P. Michel, F. Claret, T. Beetz, S. Wirick, and C. Jacobsen, 2009. Radiation sensitivity of natural organic matter: Clay mineral association effects in the Callovo-Oxfordian argillite. J. Electron Spectrosc. Relat. Phenom. 170:49–56.

Scharf, C., S. Riethdorf, H. Ernst, S. Engelmann, U. Volker, and M. Hecker, 1998. Thioredoxin is an essential protein induced by multiple stresses in bacillus subtilis. J. Bacteriol. 180:1869–1877.

Schimel, J. P. and J. Bennett, 2004. Nitrogen mineralization: Challenges of a changing paradigm. Ecology 85:591–602.

Schindler, D. W., P. J. Dillon, and H. Schreier, 2006. A review of anthropogenic sources of nitrogen and their effects on Canadian aquatic ecosystems. Biogeochemistry 79:25–44.

Schindler, F. V., E. J. Mercer, and J. A. Rice, 2007. Chemical characteristics of glomalin-related soil protein (GRSP) extracted from soils of varying organic matter content. Soil Biol. Biochem. 39:320–329.

Schlichting, A. and P. Leinweber, 2009. New evidence for the molecular-chemical diversity of potato plant rhizodeposits obtained by pyrolysis-field ionisation mass spectrometry. Phytochem. Anal. 20:1–13.

Schmidt, B. H. M. and E. Matzner, 2009. Abiotic reaction of nitrite with dissolved organic carbon? Testing the ferrous wheel hypothesis. Biogeochemistry 93:291–296.

Schmidt-Rohr, K. and J. D. Mao, 2002. Selective observation of nitrogen-bonded carbons in solid-state NMR by saturation-pulse induced dipolar exchange with recoupling. Chem. Phys. Lett. 359:403411.

Schmidt-Rohr, K., J. D. Mao, and D. C. Olk, 2004. Nitrogen-bonded aromatics in soil organic matter and their implications for a yield decline in intensive rice cropping. Proc. Natl. Acad. Sci. U.S.A. 101:6351–6354.

Schnitzer, M., 2001. The *in situ* analysis of organic matter in soils. Can. J. Soil Sci. 89:249–254.

Schnitzer, M. and S. Khan, 1972. Humic substances in the environment. Marcel Dekker, New York, NY.

Schnitzer, M., D. F. E. McArthur, H. R. Schulten, L. M. Kozak, and P. M. Huang, 2006. Long-term cultivation effects on the quantity and quality of organic matter in selected Canadian prairie soils. Geoderma 130:141–156.

Schnitzer, M. and H. R. Schulten, 1992. The analysis of soil organic-matter by pyrolysis field-ionization mass-spectrometry. Soil Sci. Soc. Am. J. 56:1811–1817.

Schnitzer, M. and H. R. Schulten, 1995. Analysis of organic matter in soil, extracts, and whole soils by pyrolysis mass spectrometry. Adv. Agron. 55:167–217.

Schulten, H. R., 1996. Direct pyrolysis-mass spectrometry of soils: A novel tool in agriculture, ecology, forestry, and soil science. p. 373–436. *In* T. Boutton and S.-i. Yamasaki (ed.) Mass spectrometry of soils. Marcel Dekker, Inc., New York, NY.

Schulten, H. R. and P. Leinweber, 1999. Thermal stability and composition of mineral-bound organic matter in density fractions of soil. Eur. J. Soil Sci. 50:237–248.

Schulten, H. R. and P. Leinweber, 2000. New insights into organic-mineral particles: composition, properties and models of molecular structure. Biol. Fert. Soils 30:399–432.

Schulten, H. R., B. Plage, and M. Schnitzer, 1991. A chemical-structure for humic substances. Naturwissenschaften 78:311–312.

Schulten, H. R. and M. Schnitzer, 1990. Aliphatics in soil organic-matter in fine-clay fractions. Soil Sci. Soc. Am. J. 54:98–105.

Schulten, H. R. and M. Schnitzer, 1998. The chemistry of soil organic nitrogen: A review. Biol. Fert. Soils 26:1–15.

Schulten, H. R. and C. Sorge, 1995. Pyrolysis methylation mass spectrometry of whole soils. Eur. J. Soil Sci. 46:567–579.

Schulten, H. R., C. Sorge, and M. Schnitzer, 1995. Structural studies on soil-nitrogen by Curie-point pyrolysis - gas-chromatography mass-spectrometry with nitrogen-selective detection. Biol. Fert. Soils 20:174–184.

Schulten, H. R., C. SorgeLewin, and M. Schnitzer, 1997. Structure of "unknown" soil nitrogen investigated by analytical pyrolysis. Biol. Fert. Soils 24:249–254.

Schulz, B. L., C. U. Stirnimann, J. P. A. Grimshaw, M. S. Brozzo, F. Fritsch, E. Mohorko, G. Capitani, R. Glockshuber, M. G. Grutter, and M. Aebi, 2009. Oxidoreductase activity of oligosaccharyltransferase subunits Ost3p and Ost6p defines site-specific glycosylation efficiency. Proc. Natl. Acad. Sci. U.S.A. 106:11061–11066.

Schulze, W. X., G. Gleixner, K. Kaiser, G. Guggenberger, M. Mann, and E. D. Schulze, 2005. A proteomic fingerprint of dissolved organic carbon and of soil particles. Oecologia 142:335–343.

Schumacher, M., I. Christl, A. C. Scheinost, C. Jacobsen, and R. Kretzschmar, 2005. Chemical heterogeneity of organic soil colloids investigated by scanning transmission X-ray microscopy and C-1s NEXAFS microspectroscopy. Environ. Sci. Technol. 39:9094–9100.

Schwarzkopf, O., M. Borchert, F. Eggenstein, U. Flechsig, C. Kalus, H. Lammert, U. Menthel, M. Pietsch, G. Reichardt, P. Rotter, F. Senf, T. Zeschke, and W. B. Peatman, 1999. The BESSY constant length Rowland circle monochromator. J. Electron Spectrosc. Relat. Phenom. 103:997–1001.

Sham, T. K. and M. Rivers, 2002. A brief overview of synchrotron radiation. p. 117–147. *In* P. Fenter, M. Rivers, N. Sturchio, and S. Sutton (ed.) Applications of synchrotron radiation in low-temperature geochemistry and environmental science, Vol. 49 of Reviews in Mineralogy and Geochemistry. The Mineralogical Society of America, Washington, DC.

Sheoran, I. S., A. R. S. Ross, D. J. H. Olson, and V. K. Sawhney, 2007. Proteomic analysis of tomato (*Lycopersicon esculentum*) pollen. J. Exp. Bot. 58:3525–3535.

Sheoran, I. S., A. R. S. Ross, D. J. H. Olson, and V. K. Sawhney, 2009. Differential expression of proteins in the wild type and 7B-1 male-sterile mutant anthers of tomato (*Solanum lycopersicum*): A proteomic analysis. J. Proteomics 71:624–636.

Siegbahn, K., 1990. From X-ray to electron-spectroscopy and new trends. J. Electron Spectrosc. Relat. Phenom. 51:11–36.

Siegbahn, K., C. Nordling, A. Fahlman, R. Nordberg, K. Hamrin, J. Hedman, G. Johansson, T. Bergmark, S.-E. Karlsson, I. Lindgren, and B. Lindberg, 1967. ESCA - atomic, molecular and solid-state structure studied by means of electron spectroscopy, Vol. 20, Series IV of Nova Acta Regiae Societatis Scientiarum Upsaliensis. Almqvist & Wiksells Boktryckeri AB, Uppsala, Sweden.

Silverstein, R., F. Webster, and D. Kiemle, 2005. Spectrometric identification of organic compounds. 7th ed. John Wiley & Sons, Hoboken, NJ.

Simpson, A., 2001. Multidimensional solution state NMR of humic substances: A practical guide and review. Soil Sci. 166:795–809.

Simpson, A. J., G. X. Song, E. Smith, B. Lam, E. H. Novotny, and M. H. B. Hayes, 2007. Unraveling the structural components of soil humin by use of solution-state nuclear magnetic resonance spectroscopy. Environ. Sci. Technol. 41:876–883.

Simpson, M. J. and C. M. Preston, 2008. Soil organic matter analysis by solid-state ^{13}C nuclear magnetic resonance spectroscopy. p. 681–692. *In* M. Carter and E. G. Gregorich (ed.) Soil sampling and methods of analysis, 2nd ed. CRC Press, Boca Raton, FL.

Six, J., H. Bossuyt, S. Degryze, and K. Denef, 2004. A history of research on the link between (micro)aggregates, soil biota, and soil organic matter dynamics. Soil Tillage Res. 79:7–31.

Skujins, J., 1967. Enzymes in soil. p. 371–414. *In* A. McLaren and G. Peterson (ed.) Soil Biochemistry. Marcel Dekker, New York, NY.

Smernik, R. J. and J. A. Baldock, 2005. Does solid-state N-15 NMR spectroscopy detect all soil organic nitrogen? Biogeochemistry 75:507–528.

Smernik, R. J., D. C. Olk, and N. Mahieu, 2004. Quantitative solid-state C-13 NMR spectroscopy of organic matter fractions in lowland rice soils. Eur. J. Soil Sci. 55:367–379.

Smil, V., 2001. Enriching the Earth: Fritz Haber, Carl Bosch, and the transformation of world food production. The MIT Press, Cambridge, MA.

Smith, C. J. and P. M. Chalk, 1979. Mineralization of nitrite fixed by soil organic-matter. Soil Biol. Biochem. 11:515–519.

Smith, C. J. and P. M. Chalk, 1980. Fixation and loss of nitrogen during transformations of nitrite in soils. Soil Sci. Soc. Am. J. 44:288–291.

Smith, R. V., R. M. Doyle, L. C. Burns, and R. J. Stevens, 1997. A model for nitrite accumulation in soils. Soil Biol. Biochem. 29:1241–1247.

Sodhi, R. N. S. and C. E. Brion, 1984. Reference energies for inner shell electron energy-loss spectroscopy. J. Electron Spectrosc. Relat. Phenom. 34:363–372.

Solaiman, Z., M. Kashem, and M. I., 2007. Environmental proteomics: Extraction and identification of protein in soil. p. 156–166. *In* A. Varma and R. Oelmuller (ed.) Advanced techniques in soil microbiology. Springer-Verlag, Berlin, Germany.

Sollins, P., P. Homann, and B. A. Caldwell, 1996. Stabilization and destabilization of soil organic matter: Mechanisms and controls. Geoderma 74:65–105.

Solomon, D., J. Lehmann, J. Kinyangi, B. Q. Liang, and T. Schafer, 2005. Carbon K-edge NEXAFS and FTIR-ATR spectroscopic investigation of organic carbon speciation in soils. Soil Sci. Soc. Am. J. 69:107–119.

Sorge, C., R. Muller, P. Leinweber, and H. R. Schulten, 1993a. Pyrolysis mass-spectrometry of whole soils, soil particle-size fractions, litter materials and humic substances - statistical evaluation of sample weight, residue, volatilized matter and total ion intensity. Fresenius J. Anal. Chem. 346:697–703.

Sorge, C., M. Schnitzer, P. Leinweber, and H. R. Schulten, 1994. Molecular-chemical characterization of organic-matter in whole soil and particle-size fractions of a spodosol by pyrolysis field-ionization mass-spectrometry. Soil Sci. 158:189–203.

Sorge, C., M. Schnitzer, and H. R. Schulten, 1993b. In-source pyrolysis-field ionization mass-spectrometry and Curie-point pyrolysis gas-chromatography mass-spectrometry of amino-acids in humic substances and soils. Biol. Fert. Soils 16:100–110.

Stevenson, F., 1982. Organic forms of nitrogen. p. 67–122. *In* F. Stevenson (ed.) Nitrogen in agricultural soils. American society for agronomy, Madison, WI.

Stevenson, F., 1994. Humus chemistry: Genesis, composition, reactions. 2nd ed. John Wiley & Sons, Inc., Toronto, ON.

Stevenson, F., 1996. Nitrogen - organic forms. p. 1185–1200. *In* D. L. Sparks (ed.) Methods of soil analysis. Part 3. Chemical methods, 2nd ed. Soil Science Society of America, Madison, WI.

Stevenson, F. and M. Cole, 1999. Cycles of soil: Carbon, nitrogen, phosphorus, sulfur, micronutrients. 2nd ed. John Wiley & Sons, Inc., Toronto, ON.

Stevenson, F., R. M. Harrison, W. R., and R. A. Leeper, 1970. Nitrosation of soil organic matter. 3. Nature of gases produced by reaction of nitrite with lignins, humic substances, and phenolic constituents under neutral and slightly acidic conditions. Soil Sci. Soc. Am. Proc. 34:430–435.

Stewart-Ornstein, J., A. P. Hitchcock, D. H. Cruz, P. Henklein, J. Overhage, K. Hilpert, J. D. Hale, and R. E. W. Hancock, 2007. Using intrinsic X-ray absorption spectral differences to identify and map peptides and proteins. J. Phys. Chem. B 111:7691–7699.

Stöhr, J., 1992. NEXAFS spectroscopy, Vol. 25 of Springer Ser. Surf. Sci. Springer, New York, NY.

Sylvia, D., P. Hartel, J. Furhrmann, and D. Zuberer, 2005. Principles and applications of soil microbiology. Pearson Prentice Hall, New Jersey, NJ.

Tabatabai, M., 1994. Soil Enzymes. p. 775833. *In* R. Weaver, J. Angle, and P. Bottomley (ed.) Methods of soil analysis: microbiological and biochemical properties. Part 2, SSSA Book Ser., 2nd ed. Soil Science Society of America, Madison, WI.

Thorn, K. A. and M. A. Mikita, 2000. Nitrite fixation by humic substances: Nitrogen-15 nuclear magnetic resonance evidence for potential intermediates in chemodenitrification. Soil Sci. Soc. Am. J. 64:568–582.

Treseder, K. K. and K. M. Turner, 2007. Glomalin in ecosystems. Soil Sci. Soc. Am. J. 71:1257–1266.

Ulrich, A. and R. Becker, 2006. Soil parent material is a key determinant of the bacterial community structure in arable soils. FEMS Microbiol. Ecol. 56:430–443.

Uren, N. C., 2007. Types, amounts, and possible functions of compounds released into the rhizosphere by soil-grown plants. p. 1–21. *In* R. Pinton, Z. Varanini, and P. Nannipieri (ed.) The rhizosphere: Biochemistry and organic substances at the soil-plant interface, 2nd ed. Marcel Dekker, New York, NY.

Urquhart, S. G. and H. Ade, 2002. Trends in the carbonyl core (C 1s, O 1s) → pi*c=o transition in the near-edge X-ray absorption fine structure spectra of organic molecules. J. Phys. Chem. B 106:8531–8538.

Vairavamurthy, A. and S. Wang, 2002. Organic nitrogen in geomacromolecules: Insights on speciation and transformation with K-edge XANES spectroscopy. Environ. Sci. Technol. 36:3050–3056.

van Kessel, C., D. J. Pennock, and R. E. Farrell, 1993. Seasonal-variations in denitrification and nitrous-oxide evolution at the landscape scale. Soil Sci. Soc. Am. J. 57:988–995.

VanCleemput, O. and A. H. Samater, 1996. Nitrite in soils: Accumulation and role in the formation of gaseous N compounds. Fert. Res. 45:81–89.

Vanderkaaden, A., J. J. Boon, J. W. Deleeuw, F. Delange, P. J. W. Schuyl, H. R. Schulten, and U. Bahr, 1984. Comparison of analytical pyrolysis techniques in the characterization of chitin. Anal. Chem. 56:2160–2165.

Venterea, R. T., 2007. Nitrite-driven nitrous oxide production under aerobic soil conditions: kinetics and biochemical controls. Glob. Change Biol. 13:1798–1809.

Verhaegen, K., O. Vancleemput, and W. Verstraete, 1988. Nitrification mediated nitrosation of organics and effects on soil microbial biomass. Biol. Waste 26:235–245.

Verity, G. E. and D. W. Anderson, 1990. Soil-erosion effects on soil quality and yield. Can. J. Soil Sci. 70:471–484.

Vetterlein, D., K. Szegedi, F. Stange, and R. Jahn, 2007. Impact of soil texture on temporal and spatial development of osmoticpotential gradients between bulk soil and rhizosphere. J. Plant Nutr. Soil Sci. 170:347–356.

Vinogradov, A. S. and V. N. Akimov, 1998. X-ray absorption study of the spectrum of free electronic states in a KNO_3 crystal. Opt. Spectrosc. 85:53–59.

Vitousek, P. M., J. D. Aber, R. W. Howarth, G. E. Likens, P. A. Matson, D. W. Schindler, W. H. Schlesinger, and D. G. Tilman, 1997. Human alteration of the global nitrogen cycle: Sources and consequences. Ecol. Appl. 7:737–750.

von Lützow, M., I. Kögel-Knabner, K. Ekschmitt, E. Matzner, G. Guggenberger, B. Marschner, and H. Flessa, 2006. Stabilization of organic matter in temperate soils: mechanisms and their relevance under different soil conditions - a review. Eur. J. Soil Sci. 57:426–445.

von Lützow, M., I. Kögel-Knabner, B. Ludwig, E. Matzner, H. Flessa, K. Ekschmitt, G. Guggenberger, B. Marschner, and K. Kalbitz, 2008. Stabilization mechanisms of organic matter in four temperate soils: Development and application of a conceptual model. J. Plant Nutr. Soil Sci. 171:111–124.

Voroney, R. and D. Derry, 2008. Origin and distribution of nitrogen in soils. p. 1–30. *In* J. Schepers and W. Raun (ed.) Nitrogen in agricultural systems. American Society for Agronomy, Crop Science Society of America, Soil Science Society of America, Madison, WI.

Walley, F. L., C. van Kessel, and D. J. Pennock, 1996. Landscape-scale variability of N mineralization in forest soils. Soil Biol. Biochem. 28:383–391.

Wang, D. L. and D. W. Anderson, 1998. Direct measurement of organic carbon content in soils by the Leco CR-12 Carbon Analyzer. Commun. Soil Sci. Plant Anal. 29:15–21.

Wang, J., C. Morin, L. Li, A. P. Hitchcock, A. Scholl, and A. Doran, 2009. Radiation damage in soft X-ray microscopy. J. Electron Spectrosc. Relat. Phenom. 170:25–36.

Whiffen, L. K., D. J. Midgley, and P. A. McGee, 2007. Polyphenolic compounds interfere with quantification of protein in soil extracts using the Bradford method. Soil Biol. Biochem. 39:691–694.

Wilcken, H., C. Sorge, and H. R. Schulten, 1997. Molecular composition and chemometric differentiation and classification of soil organic matter in Podzol B-horizons. Geoderma 76:193–219.

Wilkinson, B. and H. F. Gilbert, 2004. Protein disulfide isomerase. Biochimica et Biophysica Acta (BBA) - Proteins & Proteomics 1699:35–44.

Wilks, R. G., J. B. MacNaughton, H. B. Kraatz, T. Regier, R. I. R. Blyth, and A. Moewes, 2009. Comparative theoretical and experimental study of the radiation-induced decomposition of glycine. J. Phys. Chem. A 113:5360–5366.

Wilson, G. W. T., C. W. Rice, M. C. Rillig, A. Springer, and D. C. Hartnett, 2009. Soil aggregation and carbon sequestration are tightly correlated with the abundance of arbuscular mycorrhizal fungi: results from long-term field experiments. Ecol. Lett. 12:452–461.

Winick, H., 1994. Synchrotron radiation sources: a primer. World Scientific, River Edge, NJ.

Wright, S. F., M. Franke-Snyder, J. B. Morton, and A. Upadhyaya, 1996. Time-course study and partial characterization of a protein on hyphae of arbuscular mycorrhizal fungi during active colonization of roots. Plant Soil. 181:193–203.

Wright, S. F., J. B. Morton, and J. E. Sworobuk, 1987. Identification of a vesicular-arbuscular mycorrhizal fungus by using monoclonal-antibodies in an enzyme-linked-immunosorbent-assay. Appl. Environ. Microbiol. 53:2222–2225.

Wright, S. F., K. A. Nichols, and W. F. Schmidt, 2006. Comparison of efficacy of three extractants to solubilize glomalin on hyphae and in soil. Chemosphere 64:1219–1224.

Wright, S. F. and A. Upadhyaya, 1996. Extraction of an abundant and unusual protein from soil and comparison with hyphal protein of arbuscular mycorrhizal fungi. Soil Sci. 161:575–585.

Wright, S. F. and A. Upadhyaya, 1998. A survey of soils for aggregate stability and glomalin, a glycoprotein produced by hyphae of arbuscular mycorrhizal fungi. Plant Soil. 198:97–107.

Wright, S. F., A. Upadhyaya, and J. S. Buyer, 1998. Comparison of N-linked oligosaccharides of glomalin from arbuscular mycorrhizal fungi and soils by capillary electrophoresis. Soil Biol. Biochem. 30:1853–1857.

Xavier, L. J. C., I. J. Xavier, and J. J. Germida, 2000. Potential of spore protein profiles as identification tools for arbuscular mycorrhizal fungi. Mycologia 92:1210–1213.

Xing, B., J. D. Mao, W.-G. Hu, K. Schmidt-Rohr, G. Davies, and E. Ghabbour, 1999. Evaluation of different solid-state ^{13}C NMR techniques for characterizing humic acids. p. 49–61. *In* E. Ghabbour and G. Davies (ed.) Understanding humic substances: Advanced methods, properties and applications. Royal Society of Chemistry, Cambridge, UK.

Yates, B. W., Y. F. Hu, K. H. Tan, G. Retzlaff, R. G. Cavell, T. K. Sham, and G. M. Bancroft, 2000. First results from the Canadian SGM beamline at SRC. J. Synch. Rad. 7:296–300.

Yates, T. T., B. C. Si, R. E. Farrell, and D. J. Pennock, 2006. Probability distribution and spatial dependence of nitrous oxide emission: Temporal change in hummocky terrain. Soil Sci. Soc. Am. J. 70:753–762.

Zhang, W. H., V. Carravetta, O. Plekan, V. Feyer, R. Richter, M. Coreno, and K. C. Prince, 2009. Electronic structure of aromatic amino acids studied by soft x-ray spectroscopy. J. Chem. Phys. 131:11.

Zubavichus, Y., O. Fuchs, L. Weinhardt, C. Heske, E. Umbach, J. D. Denlinger, and M. Grunze, 2004a. Soft X-ray-induced decomposition of amino acids: An XPS, mass spectrometry, and NEXAFS study. Radiat. Res. 161:346–358.

Zubavichus, Y., A. Shaporenko, M. Grunze, and M. Zharnikov, 2005a. Innershell absorption spectroscopy of amino acids at all relevant absorption edges. J. Phys. Chem. A 109:6998–7000.

Zubavichus, Y., A. Shaporenko, M. Grunze, and M. Zharnikov, 2008. Is X-ray absorption spectroscopy sensitive to the amino acid composition of functional proteins? J. Phys. Chem. B 112:4478–4480.

Zubavichus, Y., A. Shaporenko, M. Grunze, and M. Zharnikov, 2009. NEXAFS spectroscopy of biological molecules: From amino acids to functional proteins. Nucl. Instrum. Methods Phys. Res. Sect. A-Accel. Spectrom. Dect. Assoc. Equip. 603:111–114.

Zubavichus, Y., M. Zharnikov, A. Shaporenko, O. Fuchs, L. Weinhardt, C. Heske, E. Umbach, J. D. Denlinger, and M. Grunze, 2004b. Soft X-ray induced decomposition of phenylalanine and tyrosine: A comparative study. J. Phys. Chem. A 108:4557–4565.

Zubavichus, Y., M. Zharnikov, Y. J. Yang, O. Fuchs, C. Heske, E. Umbach, G. Tzvetkov, F. P. Netzer, and M. Grunze, 2005b. Surface chemistry of ultrathin films of histidine on gold as probed by high-resolution synchrotron photoemission. J. Phys. Chem. B 109:884–891.

Chapter 10

Appendices

Appendix A

Structures of organic N-containing molecules identified in soils

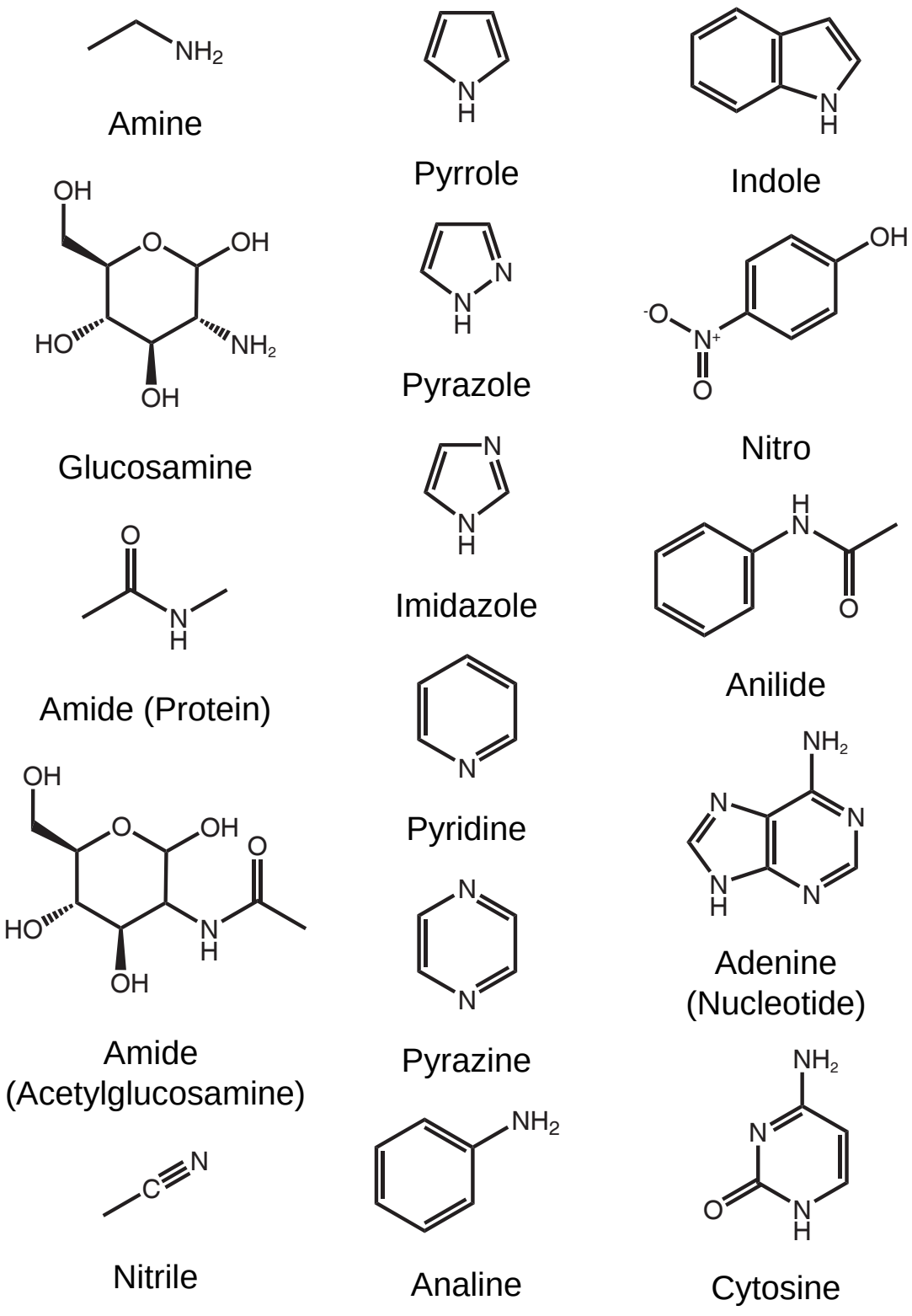

Fig. A.1. Structures of organic nitrogen-containing molecules identified in soils, as identified using wet chemical methods, ^{15}N-Nuclear Magnetic Resonance, and Pyrolysis Field-Ionization Mass-Spectrometry.

Appendix B

Permission to reprint content

Permission Granted

Frances Katz
Director of Publications
ASA-SSSA-CSSA

-----Original Message-----
From: Adam Gillespie [mailto:a.gillespie@usask.ca]
Sent: Tuesday, November 17, 2009 2:49 PM
To: Frances Katz
Subject: Request to Reprint Content

Contact Info	
Name	Adam Gillespie
Institution	University of Saskatchewan
Department	Soil Science
Line 1	51 Campus Drive
City	Saskatoon
State/Prov.	SK
Postal Code	S7N 5A8
Country	CAN
Phone	(306) 966-2386
Fax	(306) 966-6881
EMail	a.gillespie@usask.ca

Original Work	
Original Format	Book
Title of Work	Nitrogen in Agricultural Soils
Author Name	F. Stevenson
Year	1982
Editors	F. Stevenson
Chapter Title	Organic Forms of Soil Nitrogen

Page Number(s)	67-122
Series/Special Publication	#22
Published By	ASA
Text I would like to reproduce	Chapter 3, table 1, page 68

Reprinted Material
The work will be reproduced/used in the following format(s):

Title	Characterizing soil organic nitrogen using advanced molecular analytical techniques
Publisher	Dissertation
Publisher's Location	Saskatoon
Quantity	6
Publication Date	Jan 2010
Publisher Type	Non-profit Publisher

Appendix C

Marker signals in Py-FIMS of aquatic and terrestrial humic substances, soil fractions and whole soils

Table C.1. Marker signals in Pyrolysis Field Ionization Mass Spectrometry (Py-FIMS). Compiled from Schulten (1996) and Gregorich et al. (1996)

Identification	m/z
Carbohydrates	60, 72, 82, 84, 96, 98, 110, 112, 114, 126, 132, 144, 162
Phenols & lignin monomers	110, 124, 138, 140, 152, 154, 166, 168, 178, 180, 182, 194, 196, 208, 210, 212
$n\mathrm{C}_0$-$n\mathrm{C}_6$ phenols	94, 108, 122, 136, 150, 164
Lignin dimers	246, 260, 270, 272, 274, 284, 286, 296, 298, 300, 310, 312, 314, 316, 326, 328, 330, 340, 342, 356
Lipids	
nC_{10}-nC_{30} fatty acids	256, 270, 284, 298, 312, 326, 340, 354, 368, 382, 396, 410, 424, 438, 452, 466, 480, 494, 508
nC_{10}-nC_{20} diesters	202, 216, 230, 244, 258, 272, 286, 300, 314, 328, 342
nC_{37}-nC_{61} monoesters	550, 564, 578, 592, 606, 620, 634, 648, 662, 676, 690, 704, 718, 732, 746
nC_{14}-nC_{28} alkanes	198, 212, 226, 240, 254, 268, 282, 296, 310, 324, 338, 352, 366, 380, 394
nC_{14}-nC_{28} alkenes	196, 210, 224, 238, 252, 266, 280, 294, 308, 322, 336, 350, 364, 378, 392
Alkylaromatics	92, 106, 120, 134, 148, **162,** 170, 176, 184, 190, 192, 198, 204, 206, 218, 220, 232, 234, 246, 260, 274, 288, 302, 316, 330, 344, 358, 372, 386
N-containing compounds	59, 67, 79, 81, 95, 103, 109, 111, 123, 125, 137, 139, 153, 161, 167, 181, 183, 195, 203, 233, 245, 255, 257, 271, 285, 333, 359, 363, 393
Sterols	372, 386, 388, 390, 392, 394, 396, 398, 400, 402, 408, 410, 412, 414, 416, 426, 430
Peptides	57, 70, 73, 74, 75, 84, 87, 91, 97, 99, 115, 120, 129, 135
Suberin	432, 446, 460, 474, 488, 502, 516, 530

Appendix D

X-ray photoemission spectroscopy C 1s assignments

Table D.1. C 1s binding energies for X-ray photoemission spectroscopy assignments. Reference is saturated C 1s=285 eV. Calculated from values in Briggs (1998)

Function	min (eV)	max (eV)	**mean (eV)**
C–C (reference)	—	—	**285.00**
C–O–C	286.13	286.75	**286.45**
C–OH	286.47	286.76	**286.55**
C–O–C=O	286.12	286.98	**286.64**
C=O	287.81	287.97	**287.9**
O–C–O	287.83	288.06	**287.93**
O–C–**C**=O	288.64	289.23	**288.99**
HO–C=O (carboxylic)	289.18	289.33	**289.26**
O–(C–O)–O	289.3	289.34	**289.32**
–(C=O)–O–(C=O)–	289.36	289.46	**289.41**
–O–(C=O)–O–	290.35	290.44	**290.4**
C–NO_2	—	—	**285.76**
C–N<	285.56	286.41	**285.94**
C–$\overset{+}{N}\equiv$	285.99	286.22	**286.11**
C–C≡N	286.35	286.46	**286.41**
C≡N	286.73	286.75	**286.74**
C–ONO_2	—	—	**287.62**
N–C–O	—	—	**287.78**
N–C=O	287.97	288.59	**288.11**
(C=O)–N–(C=O)	288.49	288.61	**288.55**
N–(C=O)–N	—	—	**288.84**
N–(C=O)–O	—	—	**289.6**
C=C	284.76	284.69	**284.73**
Arom	284.8	284.44	**284.66**
C–S	285.21	285.52	**285.37**